EFFECT OF UNCERTAINTY IN WIND ON WIND-HYDRO

HYBRID SYSTEM

A THESIS SUBMITTED TO
THE GRADUATE SCHOOL OF NATURAL AND APPLIED SCIENCES
OF
MIDDLE EAST TECHNICAL UNIVERSITY

BY

ONUR GÜNDOĞDU

IN PARTIAL FULFILLMENT OF THE REQUIREMENTS
FOR
THE DEGREE OF MASTER OF SCIENCE
IN
CIVIL ENGINEERING

APRIL 2025

Approval of the thesis:

EFFECT OF UNCERTAINTY IN WIND ON WIND-HYDRO HYBRID SYSTEMS

submitted by **ONUR GÜNDOĞDU** in partial fulfillment of the requirements for the degree of **Master of Science** i**n Civil Engineering, Middle East Technical University** by,

Prof. Dr. Naci Emre Altun
Dean, **Graduate School of Natural and Applied Sciences** _____

Prof. Dr. Erdem Canbay
Head of the Department, **Civil Engineering** _____

Prof. Dr. Elçin Kentel Erdoğan
Supervisor, **Civil Engineering, METU** _____

Examining Committee Members:

Prof. Dr. Ali Melih Yanmaz
Civil Engineering, METU _____

Prof. Dr. Elçin Kentel Erdoğan
Civil Engineering, METU _____

Prof. Dr. Ceylan Talu Yozgatlıgil
Statistics, METU _____

Assoc. Prof. Dr. Elif Oğuz
Civil Engineering, METU _____

Asst. Prof. Dr. Önder Koçyiğit
Civil Engineering., Gazi University _____

Date: 09.04.2025

I hereby declare that all information in this document has been obtained and presented in accordance with academic rules and ethical conduct. I also declare that, as required by these rules and conduct, I have fully cited and referenced all material and results that are not original to this work.

Name Last name : Onur Gündoğdu

Signature :

ABSTRACT

EFFECT OF UNCERTAINTY IN WIND ON WIND-HYDRO HYBRID SYSTEM

Gündoğdu, Onur
Master of Science, Civil Engineering
Supervisor: Prof. Dr. Elçin Kentel Erdoğan

April 2025, 164 pages

Energy management remains a critical challenge in today's energy sector, where efficient storage and utilization are essential. Historically, fossil fuels have dominated energy production due to their ease of storage compared to renewable sources. However, growing energy demand, heightened awareness of environmental damage from fossil fuels, and the drive for energy independence in nations lacking fossil resources have fueled interest in renewable alternatives. Despite their advantages, renewables like wind and solar face difficulties due to their intermittent and unpredictable nature, complicating storage and grid integration. For instance, wind turbines rely on fluctuating wind speeds, making it hard to estimate energy generation in advance. Pumped-storage hydropower plants have emerged as a leading solution for large-scale renewable energy storage. This thesis extends a prior optimization study that determined the daily operational schedule for a wind-hydro hybrid system (Ercan, 2020). While the previous study neglected wind speed uncertainty, this study integrates it into the optimization model to evaluate its impact on energy storage efficiency and operational decisions. Wind speeds are simulated

using the autocorrelated Latin Hypercube Sampling (aLHS) method to reflect variability and uncertainty accurately. These simulated hourly wind speeds, combined with realized electricity prices, refine the model, deepening understanding of how wind speed and price uncertainties shape system performance. The findings of this thesis demonstrate that electricity price volatility has a greater impact on revenue than wind speed variability; therefore, WHHS operators should explicitly incorporate electricity price uncertainty and forecasting into their operational planning.

Keywords: Renewable Energy, Uncertainty Analysis, Hourly Wind Speed Simulation, Autocorrelated Latin Hypercube Sampling

ÖZ

RÜZGARDAKİ BELİRSİZLİĞİN RÜZGAR-HİDRO HİBRİT SİSTEM ÜZERİNDEKİ ETKİSİ

Gündoğdu, Onur
Yüksek Lisans, İnşaat Mühendisliği
Tez Yöneticisi: Prof. Dr. Elçin Kentel Erdoğan

Nisan 2025, 164 sayfa

Enerji yönetimi, günümüz enerji sektöründe kritik bir zorluk olarak öne çıkmakta olup, enerjinin etkin depolanması ve kullanımı büyük önem taşımaktadır. Tarihsel olarak, fosil yakıtlar, yenilenebilir kaynaklara kıyasla daha kolay depolanabilir olmaları nedeniyle enerji üretiminde baskın rol oynamıştır. Ancak, artan enerji talebi, fosil yakıtların çevreye verdiği zarara dair artan farkındalık ve fosil yakıt kaynaklarına sahip olmayan ülkelerin enerji bağımsızlığına yönelik çabaları, yenilenebilir enerji alternatiflerine ilgiyi artırmıştır. Avantajlarına rağmen, rüzgar ve güneş gibi yenilenebilir kaynaklar, kesintili ve öngörülemez doğaları nedeniyle depolama ve şebeke entegrasyonunda zorluklarla karşılaşmaktadır. Örneğin, rüzgar türbinleri, dalgalanan rüzgar hızlarına bağlıdır ve bu durum üretilecek enerjinin önceden tahminini zorlaştırmaktadır. Pompalı depolamalı hidroelektrik santraller, yenilenebilir enerji sistemlerinde büyük ölçekli enerji depolama için önde gelen bir çözüm olarak ortaya çıkmıştır. Bu tez, bir rüzgar-hidro hibrit sisteminin günlük işletim programını belirleyen önceki bir optimizasyon çalışmasını (Ercan, 2020)

temel almaktadır. Önceki çalışma rüzgar hızı belirsizliğini göz ardı etmişken, bu çalışma, rüzgar hızı belirsizliğini bir optimizasyon modeline entegre ederek enerji depolama verimliliği ve işletim kararları üzerindeki etkisini değerlendirmektedir. Rüzgar hızları, değişkenlik ve belirsizliği doğru bir şekilde yansıtmak için oto-korelasyonlu Latin Hiperküp Örnekleme (aLHS) yöntemiyle simüle edilmiştir. Bu simüle edilmiş saatlik rüzgar hızları, gerçekleşmiş elektrik fiyatlarıyla birleştirilerek model geliştirilmiş; böylece rüzgar hızı ve fiyat belirsizliklerinin sistem performansını nasıl etkilediğine dair daha derin bir anlayış sağlanmıştır. Bu tezin bulguları, geliri üzerinde rüzgâr hızı değişkenliğine kıyasla elektrik fiyatı oynaklığının daha belirleyici olduğunu ortaya koymaktadır; bu nedenle işletmecilerin, operasyonel planlamalarına elektrik fiyatı belirsizliğini ve elektrik fiyat tahminlerini açıkça dâhil etmelidir.

Anahtar Kelimeler: Yenilenebilir Enerji, Belirsizlik Analizi, Saatlik Rüzgar Hızı Simülasyonu, Otokorelasyonlu Latin Hiperküp Örnekleme

To my family and my love

ACKNOWLEDGMENTS

I would like to express my deepest gratitude to my supervisor, Prof. Dr. Elçin Kentel Erdoğan, for her unwavering support, insightful guidance, and invaluable expertise throughout this research. Her mentorship has been instrumental in the successful completion of this thesis.

I also extend my gratitude to Eray Ercan for his foundational work, which this study builds upon. His contributions have been essential to the development of this research.

My heartfelt thanks also go to my girlfriend, Faize Yıldız, for her patience, understanding, and constant support.

I am profoundly thankful to my family, my mother Hakime Gündoğdu, my father Bahar Gündoğdu, my little sister Nezaket Aydoğdu, my dear nephew Koralp Aydoğdu, and my brother Atakan Gündoğdu, for their endless love, encouragement, and belief in me throughout this journey.

I would like to express my appreciation to my coworkers, Anıl Can Yıldırım, Elif Sena Uzunpınar, Hatice Zeynep Turan, Murat Yeğin, and Ruken Dilara Zaf, for their motivation, collaboration, and the positive working environment they have helped foster.

Finally, I would like to express my deepest respect and gratitude to Mustafa Kemal Atatürk, the founder of the Republic of Türkiye. It is thanks to his visionary reforms and unwavering commitment to science, education, and national sovereignty that conducting a study like this has been possible in our country. I remain eternally grateful for the foundations he laid.

TABLE OF CONTENTS

LIST OF TABLES

TABLES

LIST OF FIGURES

FIGURES

LIST OF ABBREVIATIONS

ACF	Autocorrelation Function
ADF	Augmented Dickey-Fuller
ARIMA	Autoregressive Integrated Moving Average
acLHS	autocorrelated conditioned Latin Hypercube Sampling
aLHS	autocorrelated Latin Hypercube Sampling
BPM	Balancing Power Market
CDF	Cumulative Distribution Function
cLHS	conditioned Latin Hypercube Sampling
CVaR	Conditional Value-at-Risk
DAM	Day-Ahead Market
ECDF	Empirical Cumulative Distribution Function
ECMWF	European Centre for Medium-Range Weather Forecasts
EES	Electrical Energy Storage
EMRA	Energy Market Regulatory Authority
EPİAŞ	Energy Markets Operation Inc.
EU	European Union
EUR	Euro
GE	General Electric
HEPP	Hydroelectric Power Plant
IDM	Intraday Market

LHS	Latin Hypercube Sampling
MCP	Market Clearing Price
MS	Meteorological Station
MW	Megawatt
PACF	Partial-Autocorrelation Function
PC	Probabilistic Choice
PFM	Power Futures Market
PIT	Probability Integral Transform
PSD	Power Spectrum Density
PSHP	Pumped Storage Hydropower Plant
RA	Risk Averse
ROW	Rest of the World
RSV	Reference Semivariogram
SSV	Semivariogram of Sampled Hourly Wind Speeds
TEİAŞ	Turkish Electricity Transmission Corporation
TSMS	Turkish State Meteorological Service
USD	United States Dollar
VQE	Variational Quantum Eigensolver
WPP	Wind Power Plant
WHHS	Wind-Hydro Hybrid System
YEKDEM	Renewable Energy Resources Support Mechanism

CHAPTER 1

INTRODUCTION

Human development and population growth have led to a significant increase in energy consumption over time. This rising population is driven by factors such as urbanization, industrial development, and technological have contributed to the steady rise in energy demand. According to the International Energy Agency (IEA), the world's total annual energy consumption increased by 90% between 1980 and 2022 calculated using data given by IEA (2024). Notably, electricity's share of total energy consumption grew from 9% in 1980 to 21% in 2022 according to IEA (2024) data, highlighting the increasing electrification of human activities. Unfortunately, this progress has come at a cost: a substantial increase in CO_2 emissions over the past decades. Electricity and heat production account for the majority of these emissions, making them a major contributor to climate change and global warming (Lamb et al., 2021). CO_2 emissions, primarily from the burning of fossil fuels such as coal, oil, and natural gas, are a significant driver of environmental degradation. Ultimately, urgent action is required to address these challenges and protect the planet. One key international response to this crisis is the Paris Agreement, a legally binding treaty on climate change adopted by 196 Parties at the UN Climate Change Conference (COP21) in Paris on 12 December 2015. The agreement, which entered into force on 4 November 2016, aims to limit global warming to below 2°C, preferably 1.5°C, compared to pre-industrial levels. A major component of this initiative is reducing reliance on fossil fuels for electricity production and transitioning to renewable energy sources. Renewable energy, such as wind, solar, and hydropower, is widely regarded as a sustainable solution to combat climate change and reduce CO_2 emissions. The Paris Agreement encourages nations to adopt clean energy technologies and invest in renewable energy infrastructure to mitigate environmental

damage. By decreasing the use of fossil fuels and embracing renewable energy, humanity can work towards a more sustainable and resilient future.

Uncertainties introduced into future energy revenue predictions of a wind-hydro hybrid system due to future energy price and wind speed estimations are evaluated simultaneously in this study. Although wind speed uncertainty impacts revenue variability, its effect remains less significant than electricity price fluctuations. The study also underscores that robust simulation methods, like the autocorrelated Latin Hypercube Sampling (aLHS), enhance the understanding of wind speed variability's role in system performance. These insights highlight the importance of addressing electricity price uncertainty to improve the operational reliability and financial outcomes of wind-hydro hybrid systems.

CHAPTER 2

LITERATURE REVIEW

In this thesis, an uncertainty analysis is conducted based on a study that developed an optimization model to determine the best daily operational strategy for a Wind-Hydro Hybrid System (WHHS). In the base study by Ercan (2020), an LSTM model was used to forecast hourly electricity prices for the next day, which serves as input to the optimization model. However, for future hourly wind speed, they utilized historic wind speed data from the NASA MERRA-2 database. This approach neglects the uncertainty associated with wind speeds in their operational strategy. In this thesis, wind speed uncertainty is integrated into the optimization model to evaluate its impact on revenue estimation of the WHHS. Hourly wind speeds from 2014 to 2023 are sourced from the Turkish State Meteorological Service (TSMS), as global datasets like NASA MERRA-2 and ERA5 are found inadequate for representing wind speeds in the case study area. Hourly wind speeds are used to generate a set of future hourly wind speed time series using aLHS. This method ensures that simulated data captures critical statistical characteristics such as seasonality, diurnal variations, and autocorrelation. This chapter provides a comprehensive overview of the relevant concepts and previous studies. In Section 2.1, the roles of pumped storage hydropower plants, wind power plants, and the WHHS are explained. Section 2.2 presents an overview of the Turkish Electricity Spot Markets, highlighting their significance in optimizing energy storage and generation strategies. Section 2.3 describes the wind speed simulation process used to incorporate uncertainty into the optimization model. Finally, Section 2.4 describes uncertainty analysis in wind speeds and electricity prices on WHHS.

2.1 Pumped Storage Hydropower Plants, Wind Power Plants, WHHS

Pumped Storage Hydropower Plants (PSHP) are large-scale energy storage systems that transfer water between two reservoirs at different elevations to store and generate electricity. Wind power plants are facilities that produce electricity by converting the kinetic energy of the wind into mechanical power using wind turbines. WHHS are integrated energy systems that combine wind power plants with pumped storage hydropower plants to enhance the reliability and efficiency of renewable energy generation. These systems address the unpredictability of wind power by using excess electricity generated from wind to pump water from a lower reservoir to an upper reservoir. The following sections explain these systems in more detail.

2.1.1 Pumped Storage Hydropower Plants

PSHP are a type of hydroelectric energy storage system designed to help balance electricity supply and demand. These systems work by using electricity to pump water from a lower reservoir to an upper reservoir during times of low energy demand and consequently low electricity price. Later, when demand is at its peak and consequently electricity price is high, the stored water is released back to the lower reservoir, passing through turbines to generate electricity. This process allows PSHPs to serve as large-scale energy storage solutions, enhancing the reliability and stability of the electricity grid.

In 1882, Switzerland established the world's first pumped storage hydropower plant, marking nearly 140 years of development. Significant progress in pumped storage technology began in the 1950s, particularly in Europe, the United States, and Japan (Zhao et al., 2024).

PSHP in Figure 2.1 consists of an upper reservoir, a lower reservoir, a penstock, and a powerhouse equipped with a reversible pump-turbine and motor-generator. Water

flows downward from the upper reservoir through the penstock to generate electricity during peak demand periods (i.e., on peak). Conversely, during off-peak hours, excess electricity is used to pump water back up to the upper reservoir, storing energy for later use

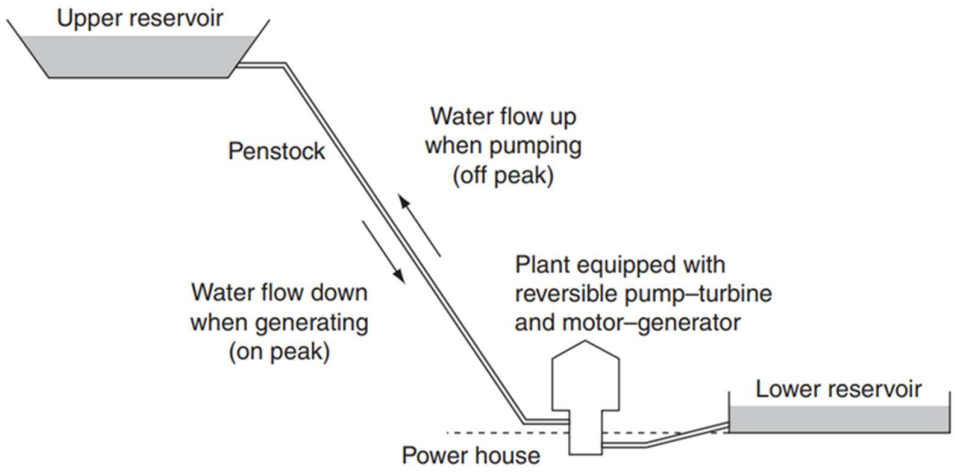

Figure 2.1 Schematic Diagram of Main Building Composition of PSHP (Hino & Lejeune, 2012).

PSHPs account for approximately 96% of the global storage power capacity and 99% of the global storage energy volume (Blakers et al., 2021). Studies by Blakers et al. (2021) and Yang & Jackson (2011) highlight the significance of PSHPs in balancing electricity loads, reducing reliance on fossil fuels, and integrating renewable energy sources like wind and solar into power grids.

There are several types of PSHPs, each designed for different geographical and operational requirements. Open-loop PSHPs interact with natural water bodies such as rivers and lakes, making them easier to construct but often subject to environmental regulations. In contrast, closed-loop PSHPs operate independently of natural water sources, using artificial reservoirs, which significantly reduces environmental impact and water resource dependency (Hunt et al., 2020). Schematic diagrams of open-loop and closed-loop PSHP are shown in Figure 2.2. Other emerging variations include underground PSHPs, where water reservoirs are

constructed in abandoned mines or underground caverns, improving storage efficiency and minimizing land-use concerns (Madlener & Specht, 2020). Seawater PSHPs, demonstrated in Japan's Yanbaru facility, present a promising alternative for coastal regions, utilizing seawater instead of freshwater for energy storage (Luo et al., 2015). These diverse configurations enable PSHPs to be implemented in various landscapes and energy networks. This thesis investigates uncertainty in wind speeds on the operation of a closed-loop PSHP due to its simplicity in modeling.

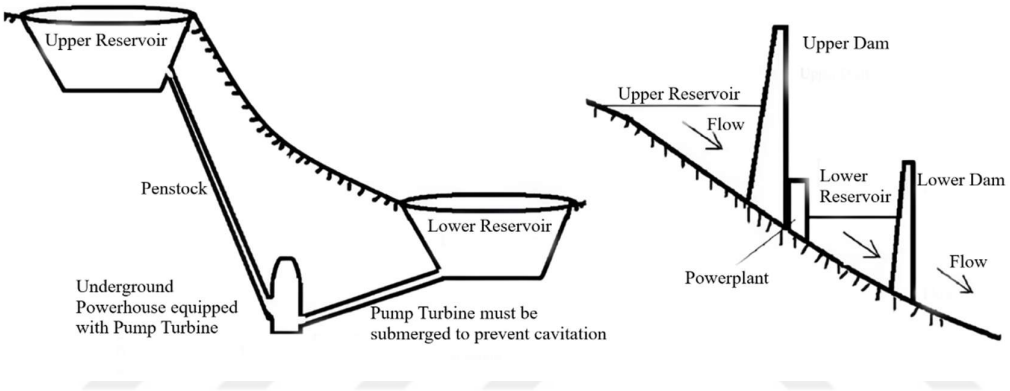

Figure 2.2 Pure PSHP on left and pump back PSHP on right (Deane et al., 2010)

According to IRENA(2024), the global installed power capacity has shown continuous growth from 2000 to 2023, exceeding 140,000 megawatt (MW) in total. As seen in Figure 2.3, Asia has played a dominant role in this expansion, with a significant increase after 2024. This rapid growth is primarily driven by the region's increasing investment in renewable energy sources and grid infrastructure. Europe and North America have also experienced steady growth, though at a comparatively slower rate. The Rest of the World (ROW) and Africa remain minor contributors to the total capacity. With the rising demand for renewable energy integration, the need for greater installed capacity continues to grow. Future projections indicate that as more countries adopt renewable energy, the installed capacity is expected to further increase, especially in regions with strong policy support and infrastructure development.

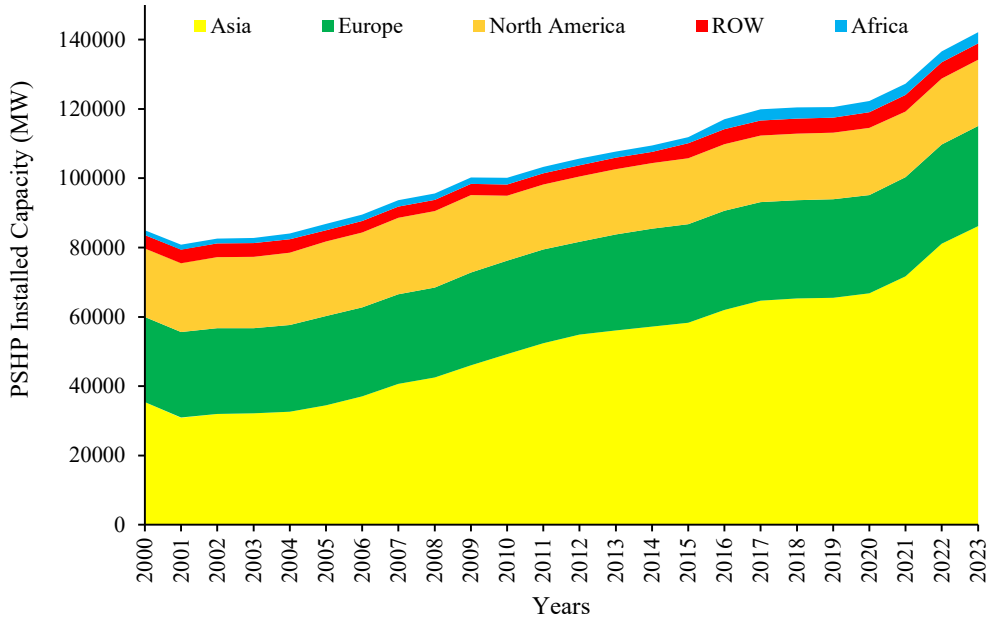

Figure 2.3 PSHP Installed Capacities Trend in the World (based on IRENA (2024) data)

2.1.2 Wind Power Plants

The use of wind energy can be traced back thousands of years, with historical records indicating that multiple ancient civilizations independently discovered and employed it across different parts of the world. However, the first automatically operated wind turbine was developed by Charles Brush in 1888 (Tong, 2010). A wind turbine is a device that converts the kinetic energy of the wind into mechanical energy, which is then transformed into electricity. They are primarily categorized based on their installation location: onshore and offshore. Wind turbines are mainly classified as onshore, which are installed on land and typically have lower installation and maintenance costs, and offshore, which are located in bodies of water, benefiting from stronger and more consistent winds, resulting in higher energy output.

Onshore wind turbines are installed on land and these turbines have seen significant growth in capacity over the years. In the United States, the average capacity of newly

installed onshore wind turbines was 3.4 MW in 2023, reflecting advancements in technology and efficiency (Wiser et al., 2024). Offshore wind turbines are in bodies of water, usually at sea and they benefit from stronger and more consistent wind patterns. These turbines are generally larger than their onshore counterparts. According to the latest data, global installations in 2023 had a capacity-weighted average turbine rating of 9.7 MW, representing a 26% year-over-year increase. The average rotor diameter reached 183.4 meters (a 5% increase), and the average hub height was 124 meters (a 6% increase) (McCoy et al., 2024).

Wind turbines generate electricity by using wind energy to spin their blades, which drive a generator. They produce electricity immediately when wind speeds are adequate. Despite this limitation, Figure 2.4 shows that the global onshore and offshore wind energy installed capacity has been increasing steadily each year. From 2000 to 2023, the onshore wind energy installed capacity grew from 16,896.74 MW to 944,205.12 MW, representing an increase of approximately 5,588%. In the same period, offshore wind energy capacity expanded from 66.95 MW in 2000 to 73,185.40 MW in 2023, reflecting an impressive growth of 109,314% (IRENA, 2024).

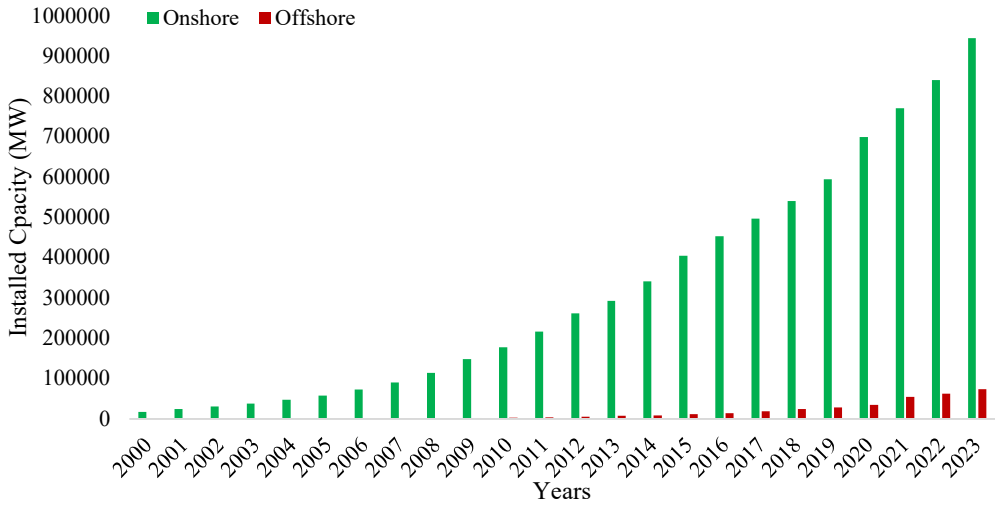

Figure 2.4 Onshore and Offshore Wind Energy Installed Capacities Trend in the World (based on IRENA (2024) data)

the onshore wind energy installed capacity percentages by country in 2023 is given in Figure 2.5 presents. According to IRENA (2024) data, China leads the market with 43% of the total onshore capacity, reflecting its significant investment in renewable energy. The United States follows with 16%, while Germany (6%) and India (5%) are also key contributors. Additionally, Türkiye has achieved a significant position with an onshore wind energy installed capacity of 11,697.16 MW in 2023, marking a remarkable rise from just 19 MW in 2000.

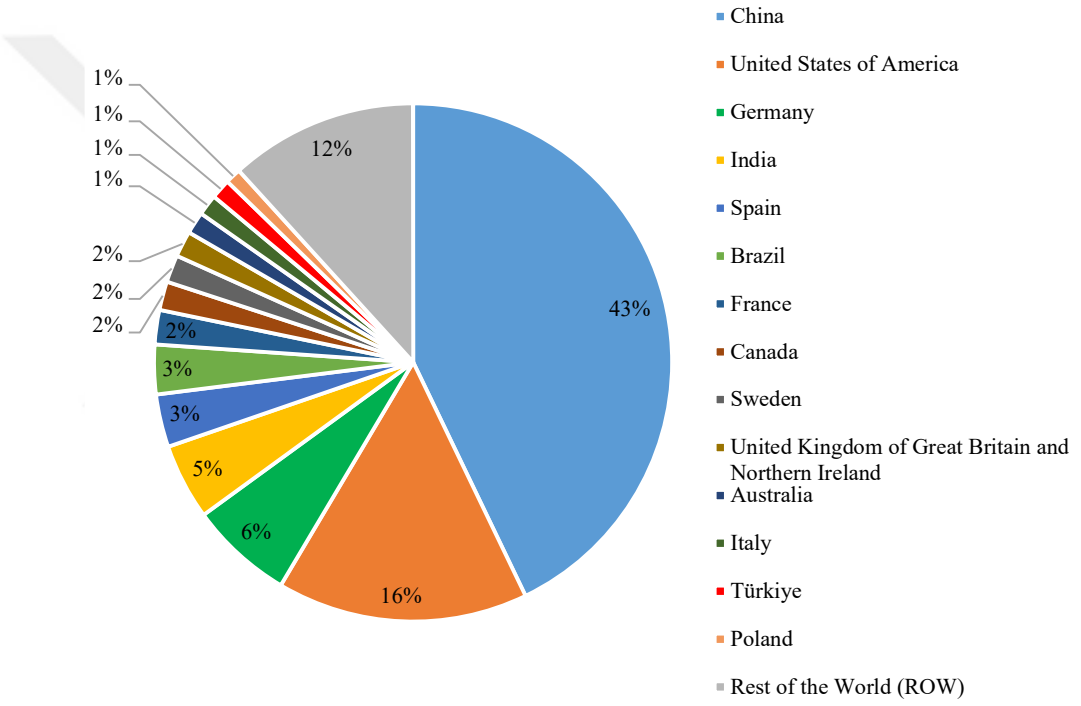

Figure 2.5 Onshore Wind Energy Installed Capacity Percentages of Countries in 2023 (based on IRENA (2024) data)

The offshore wind energy installed capacity percentages by country in 2023 is shown in Figure 2.6. According to IRENA (2024), China holds 51% of the total capacity, followed by the United Kingdom (20%) and Germany (11%). Other contributors include the Netherlands (5%), Denmark (4%), and Belgium (3%), while Chinese Taipei, Vietnam, and France account for smaller shares. The Rest of the World

(ROW) represents 1% of the total capacity. As of 2023, there is no installed offshore wind energy capacity in Türkiye.

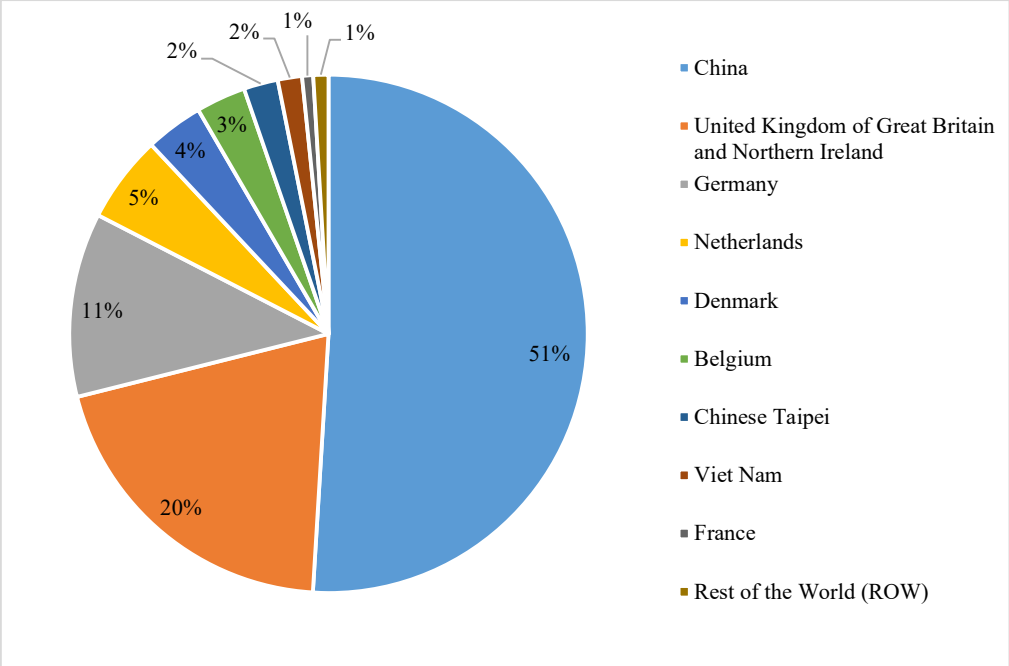

Figure 2.6 Offshore Wind Energy Installed Capacity Percentages of Countries in 2023 (based on IRENA (2024) data)

In this study, onshore wind turbines are considered, thus some of their important characteristics are summarized here. A typical onshore wind turbine has several essential components, as illustrated in Figure 2.7. The rotor includes the blades, which capture the wind's kinetic energy, and the hub, which connects the blades to the main shaft. The nacelle, located at the top of the tower, houses critical mechanical and electrical components, including the gearbox, which adjusts rotational speed, and the generator, which converts mechanical energy into electricity (Bhattacharya, 2019). Supporting these components, the tower provides structural stability, elevating the nacelle to capture higher wind speeds efficiently. The foundation, though not shown in the image, anchors the entire structure to the ground, ensuring

stability against varying wind forces. Energy systems where wind turbines and PSHP are used together are called WHHS. Detailed information about these systems is provided in the following section.

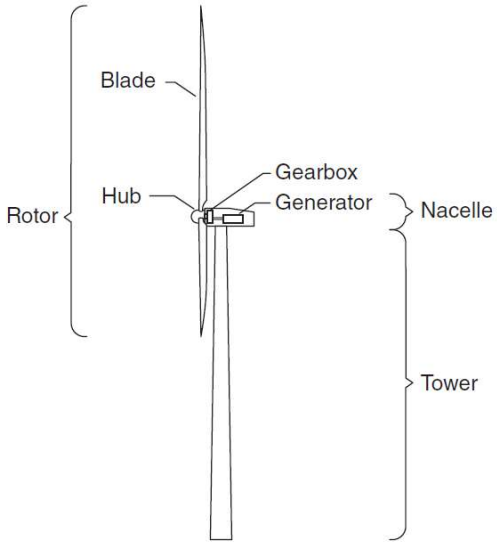

Figure 2.7 Main Components of an Onshore Wind Tower (Bhattacharya, 2019)

2.1.3 Wind-Hydro Hybrid Systems (WHHS)

WHHS combines wind power generation with hydroelectric storage, increasing energy reliability, flexibility, grid stability, and profitability for electricity-generating companies. These systems effectively address the intermittent nature of wind energy by using the storage capacities of hydroelectric power plants. The collaboration between wind and hydro resources enables a continuous energy supply and improves the integration of renewable energy into the power grid. Figure 2.8 shows a typical WHHS. The system includes wind turbines, a pump turbine, penstocks, and both a higher and a lower reservoir.

There are many studies on WHHS in the world while there are a few studies on WHHS in Türkiye and a brief summary of these studies are given in the following paragraphs. These studies highlight the challenges associated with and advantages of WHHS.

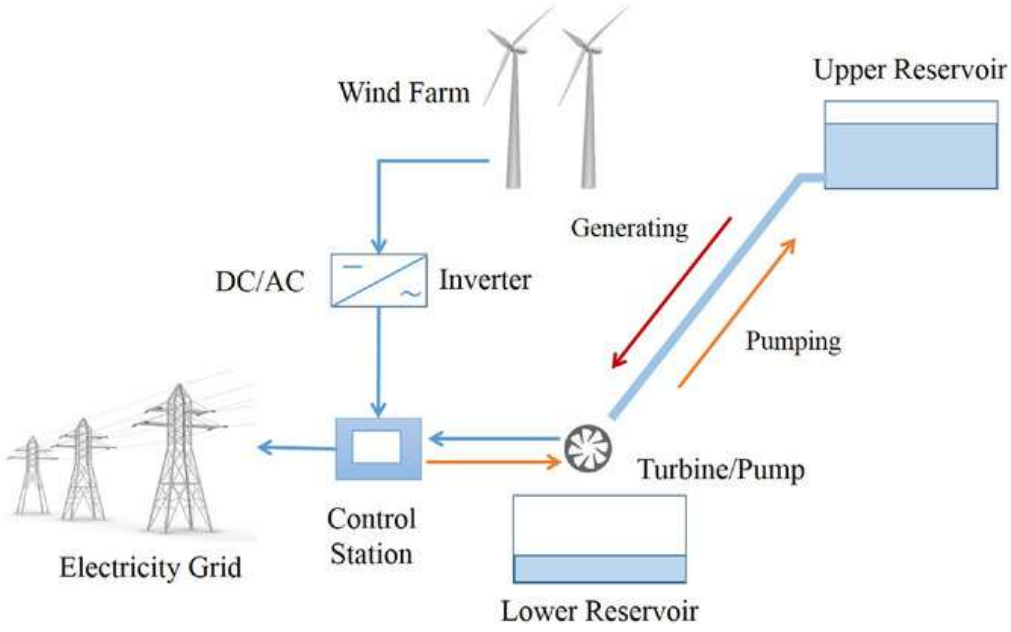

Figure 2.8 Schematic Representation of WHHS (Graça Gomes et al., 2021)

WHHS represents an innovative solution to the challenges posed by wind energy's intermittency. According to Korpaas et al. (2003), integrating energy storage systems with wind power plants increases operational flexibility, allowing producers to align production with market demands. The dynamic programming approach discussed by Korpaas et al. (2003) optimizes energy exchange in the market, emphasizing the role of energy storage in smoothing wind power variations. Their conclusion suggests that WHHS can enhance market participation by mitigating the impact of wind power fluctuations. In this thesis, instead of dynamic programming, a Monte Carlo simulation-based approach is employed to handle wind energy variability.

Castronuovo and Lopes (2004) further explored the operational optimization of WHHS. Their study introduced an hourly-discretized optimization algorithm that balances economic profits with power output fluctuations. The stochastic nature of wind energy was modeled using Monte Carlo simulations, highlighting the importance of wind power forecasting for daily operational strategies. In their conclusion, they emphasized the role of accurate forecasting in maximizing profitability. Similarly, this thesis develops an hourly-resolution simulation framework incorporating an aLHS method to capture the temporal variability of wind power generation for the selected case study, aligning operational decisions with local grid dynamics.

Chen et al. (2009) provided a comprehensive review of electrical energy storage (EES) technologies, including pumped hydroelectric storage, which is central to WHHS. Their work emphasized the importance of Electrical EES in stabilizing power systems, especially with increasing renewable energy penetration. They concluded that PSHP remains the most mature and reliable technology for large-scale applications due to its high efficiency, long operational life, and ability to provide ancillary services.

Díaz-González et al. (2012) reviewed energy storage technologies for wind power applications. They highlighted that WHHS not only addresses power quality issues but also supports grid stability by providing ancillary services such as frequency regulation and voltage control. Their conclusion emphasized that WHHS plays a crucial role in ensuring the long-term operational reliability of power grids by effectively integrating renewable sources. They noted that WHHS could significantly reduce curtailment rates and improve grid responsiveness during peak demand periods.

Ghadikolaei et al. (2012) examined the risk-constrained scheduling of hydro-wind units in short-term electricity markets. Their stochastic programming model accounted for market price and wind power uncertainties, demonstrating that WHHS can enhance profitability while minimizing operational risks. Their conclusions

indicated that risk management frameworks are essential for successful WHHS operations. They also noted that incorporating probabilistic market price forecasts, wind generation uncertainty modeling using autoregressive integrated moving average (ARIMA) processes, and multiple risk tolerance scenarios significantly improve scheduling efficiency. Despite methodological differences, this thesis also shares the common goal of improving the operational efficiency of WHHS by addressing uncertainties in wind power generation. Studies on WHHS in Türkiye are included in the following paragraphs.

Dursun and Alboyacı (2010) investigated the contribution of wind-hydro pumped storage systems in meeting Türkiye's growing electricity demand. The study examined the country's wind and hydropower resources, emphasizing the necessity of integrating these energy sources for a more stable and efficient electricity supply. It highlighted that while Türkiye has substantial wind energy potential, its intermittent nature poses grid stability challenges. Pumped storage hydroelectric plants were proposed as a solution to store surplus wind energy and release it when needed, thus enhancing the reliability of the power system.

Dursun, Alboyacı, and Gökcol (2011) explored an optimal wind-hydro hybrid energy solution for the Marmara region of Türkiye. The study analyzed six different sites with high wind potential and assessed their suitability for WHHS integration. Using long-term wind speed measurements and energy demand data, the researchers developed a model that optimized wind-hydro storage configurations to ensure continuous electricity supply. Their results demonstrated that WHHS could reduce dependency on fossil fuels while improving the efficiency of renewable energy generation in the region.

Köse and Kaya (2013) analyzed the feasibility of using a wind-hydro hybrid system to meet the energy demand of the Konya Water Treatment Plant. The study designed a system that combined a hydroelectric power plant (HEPP) with wind power plants (WPP), using local wind energy measurement data for optimization. The findings showed that integrating wind energy into the existing hydro infrastructure could

significantly reduce electricity costs and reliance on fossil fuels. Additionally, an economic analysis was conducted, revealing a reasonable payback period for the system.

Dinçer and Bozkus (2016) studied the hydraulic challenges associated with WHHS, particularly the occurrence of water hammer effects in pressurized pipelines. Their study focused on the Yahyalı Wind-Hydro Hybrid Plant and used numerical simulations to analyze transient pressure fluctuations caused by sudden flow changes. They found that without proper design considerations, these pressure variations could lead to pipe failures, increasing maintenance costs. Their study recommended installing surge tanks and other protective devices to mitigate these risks, ensuring the safe and efficient operation of WHHS.

Ercan and Kentel (2022) developed an optimization model for the daily operation of WHHS, integrating electricity price forecasting into the decision-making process. Using an LSTM neural network, the study predicted electricity prices in Türkiye's day-ahead market and coupled this with a mixed-integer linear programming model to maximize daily revenue. Their results show that forecasted electricity prices improve the efficiency of the optimization model compared to relying on past prices, leading to increased revenue. However, the LSTM network struggles with sudden fluctuations in electricity prices, particularly during midday hours. As wind turbine capacity increases, the system becomes less dependent on the grid, and revenue growth is primarily driven by wind energy utilization. The results of their study emphasize the importance of jointly optimizing the capacities of pumped storage hydropower and wind turbines for maximum efficiency. While wind turbine capacity does not significantly impact daily operation schedules within the studied range, integrating wind power reduces errors in revenue estimation. However, their study overlooked wind speed uncertainty. Therefore, this thesis aims to incorporate wind speed uncertainty into Ercan and Kentel (2022).

These studies collectively demonstrate that WHHS offers a robust solution for integrating renewable energy into power grids. By combining wind power with

pumped storage, WHHS can mitigate energy supply fluctuations, enhance grid stability, and optimize market operations. In light of these findings, WHHS is utilized in this thesis to store energy generated from wind power and to optimally generate electricity by using the advantages of a pumped-storage hydropower system, with a particular focus on analyzing how wind power uncertainty impacts WHHS's performance in Turkish electricity spot market.

2.2 Turkish Electricity Spot Market

The Turkish electricity spot market is a fundamental mechanism for balancing supply and demand in the country's energy sector. It facilitates short-term electricity trading through organized market platforms, ensuring transparent price formation based on real-time market conditions. This market structure is critical in maintaining grid stability, enhancing competition, and optimizing resource allocation within the energy system.

Eroğlu and Finger (2021) analyze the transformation of Turkey's wholesale electricity market from a state-controlled system to a competitive market-driven model, emphasizing the alignment of regulatory frameworks with European Union (EU) standards. Electricity Market Law No. 4628, enacted in 2001, was a pivotal step in this transition, leading to the establishment of the Energy Market Regulatory Authority (EMRA), which oversees licensing, market transparency, and pricing regulations. The liberalization process was further refined by the Electricity Market Law No. 6446 in 2013, which strengthened competition and ensured third-party access to the grid (Eroğlu & Finger, 2021).

The Turkish electricity spot market consists of several interconnected markets, each serving a distinct role in the country's electricity trade. These markets are Day-Ahead Market (DAM), Intraday Market (IDM), Balancing Power Market (BPM), Power Futures Market (PFM), Renewable Energy Resources Support Mechanism (YEKDEM), Bilateral Contracts Market, and Environmental Markets. However, the

optimization model used in this study is designed solely based on DAM market participation, meaning that real-time adjustments, imbalance corrections, or intraday trading mechanisms are not included in the scope of this work. The study focuses exclusively on bidding in the DAM, where offers are submitted one day in advance, and scheduling decisions are made based on historic hourly electricity price and wind power availability, without incorporating the operational dynamics of other market structures. Other types of electricity markets in Türkiye, such as PFM and YEKDEM, are not considered in this study. However, the details of these markets can be found in the Electricity Market Sector Report (EMRA, 2024).

The DAM was established on December 1, 2011, marking a crucial step toward market liberalization in Türkiye. This platform allows electricity trading one day in advance, where market participants submit bids, and the Market Clearing Price (MCP) is determined based on supply and demand conditions. The introduction of DAM replaced the earlier bilateral contract model, significantly improving price transparency and trading efficiency (EMRA, 2024). In this market, energy sellers submit offers for each hour of the next day, while energy buyers submit their demand, ensuring that generation and consumption are balanced before real-time operations. The market operator sorts these bids and determines the MCP at the intersection of supply and demand curves. The offer period covers 24 hours of the next day, from 00:00 to 24:00, with a submission deadline of 12:30 on the current day. The initial results are announced at 13:30, followed by a 30-minute objection period, after which the final results are declared at 14:00 (Yarıcı, 2018).

The IDM was launched on July 1, 2015, as part of efforts to enhance market flexibility. IDM enables participants to adjust their electricity positions closer to real-time, reducing imbalances between expected and actual electricity generation or consumption. By allowing market participants to fine-tune their trading strategies within the same operational day, IDM has played a crucial role in balancing Türkiye's power grid and ensuring a more responsive market (EMRA, 2024).

The BPM has been operational since 2009 and is managed by TEİAŞ (Turkish Electricity Transmission Corporation). BPM is designed to ensure real-time system balance by managing upward and downward balancing orders to maintain grid frequency stability. Before the introduction of BPM, Türkiye relied on a centrally controlled dispatch system, but the market-based approach has allowed a more efficient and cost-effective allocation of balancing resources (EMRA, 2024).

An example timeline for the Turkish electricity spot markets is shown in Figure 2.9. This timeline shows the market operation schedule for 02.01.2020.

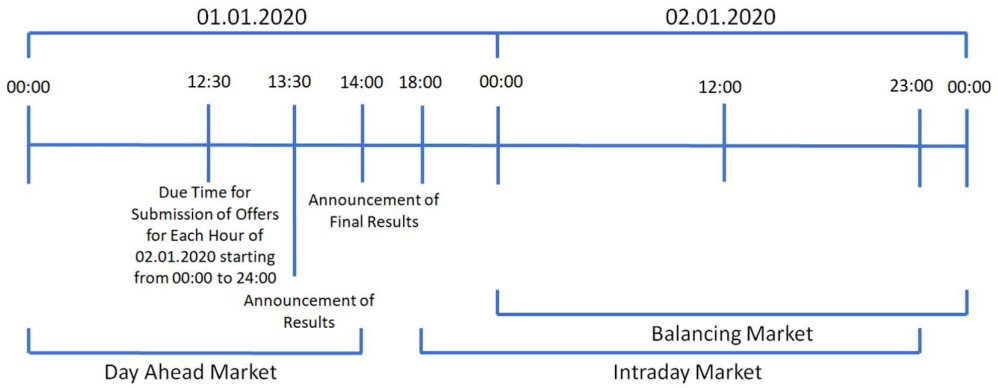

Figure 2.9 Scheduling of Market for 02.01.2020 (Ercan, 2020)

In this thesis, while conducting the optimization study to determine the best operation schedule for WHHS to maximize daily revenue, historic hourly electricity prices and simulated hourly wind speeds (or corresponding wind power generations) are utilized as input data.

2.3 Hourly Wind Speed Simulation

In this study, uncertainty in wind speed on WHHS revenue is quantified by simulating hourly wind speeds. Hourly wind speeds exhibit short-term temporal dependencies. These dependencies arise from local wind generation mechanisms and

long-term trends. Adding temporal dependency to wind speed models is necessary to ensure accurate and reliable results (Brett & Tuller, 1991).

According to Brown et al. (1984), Monte Carlo methods can simplify wind speed simulations by using parameters such as the mean and variance of the distribution. However, this approach underestimates the variance of time-averaged wind speeds by ignoring positive correlations between successive observations. They concluded that long periods of high or low wind speeds, which are common in real data, are often underrepresented when wind speeds are assumed to be temporally uncorrelated.

In this study, hourly wind speeds are sampled from the empirical distribution of the available hourly observed wind speeds. The empirical distribution refers to a distribution constructed from a given sample of data. It is defined as a discrete distribution where each observed data point in the sample is assigned an equal probability of $1/n$, where n is the total number of observations (Borovkov, 1999). Typically, such procedures are carried out using Monte Carlo methods. However, in cases where the data to be sampled is limited, a variant of the Monte Carlo method, known as Latin Hypercube Sampling (LHS), can be preferred. Dutta and Gandomi (2020) describe LHS as "a stratified sampling technique designed to minimize the number of simulations required while effectively quantifying response uncertainty". LHS requires fewer samples to effectively capture the observed data distribution, making it a computationally efficient alternative for scenarios with constrained resources or limited data availability (Janssen, 2013).

Li (2018) used an approach to include autocorrelation when inputting distributions. In his study, the Weibull distribution parameters are estimated from the observed wind speeds, and the generated samples follow the same probability distribution. However, while the generated wind speeds are independent, the actual wind speed time series are often correlated. To address this, the correlation in the simulated samples must match the observed data. Li (2018) iteratively adjusts the power

spectrum density (PSD) of the simulated wind speeds until they match the target PSD.

In a more recent study, Le and Vargas (2024) introduced the autocorrelated conditioned Latin Hypercube Sampling (acLHS) method as an enhancement of the traditional conditioned Latin Hypercube Sampling (cLHS) (Minasny & McBratney, 2006). The acLHS incorporates temporal or spatial autocorrelation into the sampling process by integrating semivariograms as an optimization criterion. This ensures that the sampled data not only preserves the univariate distributions and dependency relationships of the original data but also retains the temporal or spatial autocorrelation structure. They applied acLHS to two case studies: temporal sampling of soil CO_2 efflux data and spatial sampling across the conterminous United States. Their results demonstrated that acLHS provides a more accurate representation of the temporal and spatial variability of the original datasets compared to fixed sampling and traditional cLHS methods. By maintaining the temporal or spatial dependencies, acLHS improves the quality of predictions and reduces uncertainty in geostatistical simulations.

As explained above, one of the most important parameters in autoregressive models is the autocorrelation in the time series. Understanding and representing autocorrelation correctly is crucial for ensuring the effectiveness of the model. Autocorrelation can change for each time series data, and even when examining the same time series data in different regions, different autocorrelation patterns may be observed. Therefore, the autocorrelation of specific time series data in a particular region must be analyzed before building the model. Hence, in this study, while simulating wind speeds using LHS, an optimization procedure is integrated so that autocorrelation of simulated wind speeds can represent the observed wind speeds' autocorrelation.

Building on the concept introduced in Le and Vargas (2024), the Autocorrelated Latin Hypercube Sampling (aLHS) method, focusing solely on simulating a single time series while preserving its autocorrelation structure, is used in the current study.

Unlike the original acLHS method, which emphasizes conditioned sampling to ensure joint representation of multiple variables, this study simplifies acLHS by concentrating solely on the temporal autocorrelation of hourly wind speed data. The semivariance model is used to maintain the autocorrelation structure during simulation, enabling the generation of hourly wind speeds that reflect the temporal variability observed in the original dataset. This approach provides a tailored solution for addressing wind speed uncertainty in the optimization of Wind-Hydro Hybrid Systems. By accurately simulating wind speed time series with preserved autocorrelation, the method enhances the robustness of the operational strategies derived from the optimization model.

Unlike the study by Le and Vargas (2024), which utilized the differential evolution method for optimization, the optimization procedure in this study is conducted using the Powell optimization method. The Powell method has found extensive applications across diverse scientific fields, proving to be a robust optimization tool. For example, Nakanishi et al. (2020) utilized it to enhance quantum-classical hybrid algorithms by optimizing parameterized quantum circuits, achieving efficient cost function minimization. Similarly, Romero et al. (2018) applied the method in the Variational Quantum Eigensolver (VQE) for molecular energy calculations, leveraging the unitary coupled-cluster ansatz. Additionally, Fulton et al. (2018) employed the Powell method in the RadVel toolkit to model radial velocity data, effectively estimating orbital parameters in multi-planet systems.

There are numerous studies on wind speed simulations. In these studies, the first step has generally been to find the distribution of the data. Ramirez and Carta (2005) noted that one of the basic assumptions in statistics, whether wind speeds are dependent or independent, was rarely tested in the studies reviewed. They commented that since wind speeds recorded over short time intervals are usually dependent, using such samples violates the assumptions of estimation methods based on fitted distributions. This means that if the assumption of randomness is not met: (a) common statistical tests will not be valid, (b) uncertainties for commonly used statistics will not be significant, and (c) parameter estimates may not be reliable

(Ramírez & Carta, 2005). However, they concluded that the findings show that using autocorrelated hourly wind speeds does not significantly change the shape of the probability density distribution, although it does invalidate standard tests. In light of this information, in this study, when assigning an empirical distribution to the data for sampling purposes, the distribution is directly assigned without removing autocorrelation.

2.4 Uncertainty Analysis

The uncertainty in annual revenue from wind power generation primarily arises from variability in hourly electricity prices and hourly wind speeds. Consequently, most studies investigating uncertainty in wind power generation or WHHS concentrate their analyses on these two factors. The following paragraphs provide and explain studies that address uncertainty analysis in wind power generation and electricity prices in electricity markets.

The article by Pinson et al. (2009) presents a novel methodology for generating statistical scenarios of short-term wind power production, addressing the critical need for enhanced uncertainty representation in wind energy forecasting. Building on the limitations of traditional point forecasts, which offer only a single expected value, and probabilistic forecasts, which provide uncertainty information on a per-horizon basis but lack insight into temporal interdependence, the authors propose a framework that integrates both predictive distributions and the interdependence structure of forecast errors. This approach transforms non-parametric probabilistic forecasts into a multivariate Gaussian random variable, utilizing a recursively estimated covariance matrix to capture the evolving relationships among prediction errors across forecast horizons. Applied to a multi-MW wind farm in Denmark over a two-year period, the method demonstrates its ability to produce reliable scenarios that respect input predictive distributions while reflecting time-varying error structures, as evidenced by empirical evaluations including Gaussianity tests and Probability Integral Transform (PIT) histograms. This advancement holds significant

potential for optimizing decision-making in applications such as wind-storage system operations and multi-market trading, offering a robust tool for integrating stochastic wind generation into power systems (Pinson et al., 2009).

Pinson et al. (2007) develop a methodology for trading wind power in electricity markets by using short-term probabilistic forecasts to design optimal bidding strategies. They model wind generation as a random variable with predictive distributions and define a piecewise linear loss function that reflects the producer's sensitivity to regulation costs, based on imbalance penalties. Two strategies are proposed: Probabilistic Choice (PC), which minimizes expected regulation costs using quantiles of the wind generation distribution, and Risk Averse (RA), which minimizes worst-case losses through numerical optimization. Applied to a 15-MW wind farm in the Dutch APX market for 2002, PC strategies leveraging annual (PC1) and quarterly (PC2) cost trends achieved performance ratios of 89.14% and 92.1%, respectively, compared to 86.99% for point forecasts. The authors conclude that integrating uncertainty into decision-making significantly enhances forecast value and reduces regulation costs, and that their flexible approach can adapt to producer needs, although it relies on estimating cost trends.

Morales et al. (2010) developed a methodology to optimize bidding strategies for wind power producers across multiple markets, including day-ahead, adjustment, and balancing markets, using a multistage stochastic programming approach. They modeled uncertainties in wind availability and market prices using seasonal ARIMA and autoregressive models, which allowed them to generate simplified scenarios for better tractability. Their linear programming framework aims to maximize expected profit while incorporating risk management through conditional value-at-risk (CVaR), using a weighting factor (β) to balance profit and variability. When applied to a 100-MW wind farm in the Iberian Peninsula, their method demonstrated that including the adjustment market resulted in improved outcomes, reducing profit variability with only a minimal loss in expected profit. They emphasized that the strategy's success depends on the accuracy of scenario generation. In this thesis, a similar study is conducted; however, instead of using the ARIMA model, the aLHS

method is employed to generate different wind speed simulations, and historical electricity prices from the Turkish Electricity Spot Market are utilized to account for uncertainties in electricity prices.

Ma et al. (2013) developed a methodology for generating short-term wind power scenarios to address the uncertainty and variability inherent in wind power forecasts. They proposed using empirical cumulative distribution functions (ECDFs) derived from historical forecast data, offering a nonparametric approach that avoids assumptions of normality. Their approach also incorporated inverse transform sampling with multivariate normal distributions and an exponential covariance structure, dynamically estimating the covariance parameter to match historical fluctuations. Validation with data from the Irish power system demonstrated that their method effectively captures forecast uncertainty and actual variability, significantly improving inputs for stochastic power system operations and decision-making processes. They concluded that accurately modeling wind power uncertainties enhances operational decisions and system reliability in renewable energy integration.

Hosseini-Firouz (2013) proposed an optimal offering strategy for wind power producers in electricity markets, emphasizing risk management. They focused on addressing the uncertainties associated with wind availability, market prices, and balancing energy requirements through stochastic programming methods. Their approach utilized ARIMA techniques to forecast wind speed and electricity market prices, enhancing prediction accuracy. Furthermore, scenario generation was conducted by employing probability distribution functions of forecast errors, which improved the reliability of these scenarios. The method incorporated CVaR to explicitly manage risk aversion, allowing producers to balance profit maximization with financial risk mitigation effectively. Numerical studies demonstrated the effectiveness of this approach in reducing financial risks due to forecasting inaccuracies and improving profitability. Hosseini-Firouz (2013) highlighted the advantage of their strategy, particularly in terms of reducing imbalance costs through optimized risk-aversion levels and improved reserve planning, leading to a

significant enhancement in the economic outcomes for wind power producers operating in competitive electricity markets.

The studies mentioned above emphasize the impact of uncertainties in wind power generation and WHHS operations and underline the importance of understanding these uncertainties. This study aims to investigate the uncertainty in wind power using Monte Carlo simulation, and uncertainty in electricity prices through scenario-based evaluations of historically realized electricity prices for different years.

CHAPTER 3

METHODOLOGY

This study aims to understand and quantify the effect of uncertainty in wind speed on the uncertainty in the annual revenue of WHHS calculated through an optimization model. Figure 3.1 shows the flowchart of the methodology. The two important inputs of the optimization model are hourly wind speed (used in the calculation of hourly wind energy) and hourly electricity prices. In this study, hourly wind speeds for a year are simulated using aLHS. Observed hourly wind speed data at Nilüfer meteorological station (MS18386) between 2014 and 2023 obtained from the Turkish State Meteorological Service are used as inputs to simulate hourly wind speed projections for a year. Then, simulated hourly wind speeds are converted to simulated hourly wind energy and used as input for the optimization model. The second input, hourly electricity prices are obtained from EPİAŞ Transparency Platform (n.d.) between 2012 and 2024. Simulating hourly wind speed time series is described in Section 3.1. Converting hourly wind speeds to hourly wind energy is explained in Section 3.2. The optimization model is summarized in Section 3.3. Finally, the uncertainty analysis is explained in detail in Section 3.4.

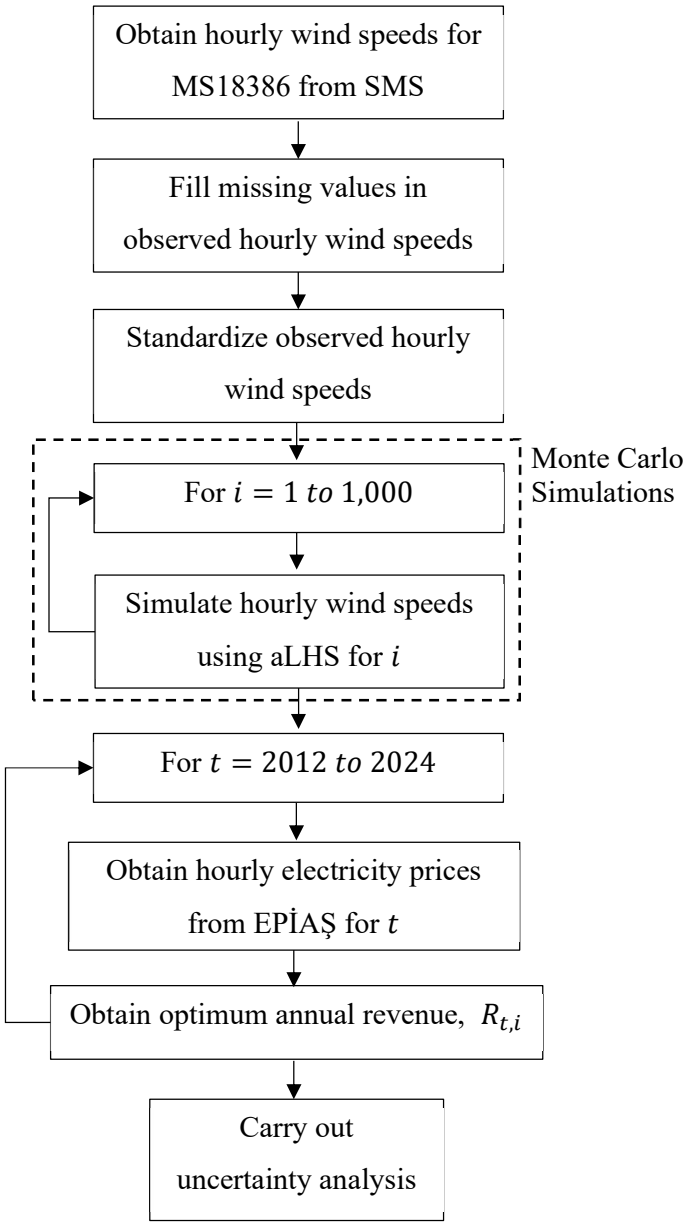

Figure 3.1 Methodology Flowchart

3.1 Hourly Wind Speed Simulation

To understand the effect of uncertainty in wind on the annual revenue of the WHHS, a set of hourly wind speed time series for a year is generated using aLHS. The simulated hourly wind speeds are generated using the methodology explained below, which retains the statistical and temporal characteristics of the observed hourly wind speeds. This process captures diurnal, monthly, and autocorrelation patterns, ensuring the simulated hourly wind speeds reflect the dynamics of observed hourly wind speeds. The algorithm is applied systematically for each month of the year to account diurnal variability in the related month.

The process begins with the preparation of observed hourly wind speeds obtained from MS18386 between 2014 and 2023. There are missing values in MS18386's observations. Hence, missing values are filled using the means of the corresponding hour across the same month in the available years. This imputation method preserves the hourly variability of wind speeds and ensures the dataset is complete for statistical modeling.

3.1.1 Removing Diurnal Variation from Observed Hourly Wind Speeds by Standardization for Each Month

Before applying the aLHS simulation procedure, observed hourly wind speed data needs to be standardized to remove diurnal variations. If these variations are not removed, the aLHS method fails to simulate the data accurately, and the resulting simulated values will not reflect the original diurnal characteristics.

An analysis of diurnal variation of hourly wind speeds at MS18386 over the period from 2014 to 2023, as well as for each month individually, reveals distinct variation patterns (see Section 4.3.1). Consequently, it was determined to remove the diurnal variations for each month separately.

Brown et al. (1984) suggested that diurnal variation in hourly wind speeds should be removed by subtracting the hourly expected values of the data. To remove diurnal variation of hourly wind speeds in each month, observed hourly wind speeds for each month are standardized using Equation (3-1). Hourly statistics, namely mean and standard deviation, are calculated separately for each hour of the day and each month to account for diurnal patterns and monthly variability. This standardization ensures that all subsequent operations are performed on observed hourly wind speeds with uniform statistical properties.

$$Z_{M,D}(t) = \frac{U_{M,D}(t) - \mu_{M,t}}{\sigma_{M,t}} \tag{3-1}$$

where $U_{M,D}(t)$ is the observed wind speed at hour t in D^{th} day of month M, $Z_{M,D}(t)$ is the standardized value of $U_{M,D}(t)$, $\mu_{M,t}$ is the mean of the observed hourly wind speeds in month M for the t^{th} hour, $\sigma_{M,t}$ is the standard deviation of the observed hourly wind speeds in month M for the t^{th} hour. Thus, M = January, February,…, December, D = 1, 2, …, 30 (or 31), and t = 1, 2,…, 24. For example, $\mu_{January,4}$ is the mean of the observed hourly wind speeds at the 4$^{\text{th}}$ hour of each day in all Januarys during observation period (i.e., in this study from 2014 to 2023).

3.1.2 Autocorrelated Latin Hypercube Sampling (aLHS)

After standardizing the observed hourly wind speeds LHS is used to sample hourly wind speeds from the empirical cumulative distribution function of the standardized wind speeds for the corresponding month. Next, the sampled hourly wind speeds are reordered using the Powell optimization method to align their autocorrelation structure with that of the observed standardized hourly wind speeds. This procedure is referred to as aLHS. Finally, the reordered hourly wind speeds are de-standardized to reintroduce the original diurnal and monthly variations present in the observed data.

All standardized hourly wind speeds in the same month of the whole observation duration are gathered into 12 batches. For example, hourly wind speeds in all Januarys in the observation period are grouped together into the January batch. The procedure followed to generate simulated hourly wind speed time series for month which is carried out using all the data in batch M as summarized in Figure 3.2. The details of the procedure are explained in the following sections.

This process is repeated for each month of the year, generating monthly simulated datasets that retain the unique statistical and temporal characteristics of each period. The monthly datasets are then combined into a single dataset, representing simulated hourly wind speeds for a year.

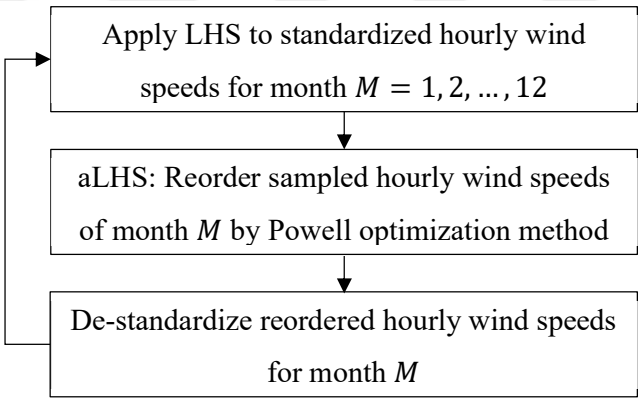

Figure 3.2 Autocorrelated Latin Hypercube Sampling Steps

aLHS process is repeated 1,000 times, resulting in 1,000 simulated hourly wind speed time series for a year. This methodology guarantees that the simulated wind speeds not only represent the statistical distribution of the observed hourly wind speeds but also capture its temporal dependencies and diurnal variations. This approach enables the dataset to be suitable for applications requiring accurate representations of hourly wind speed behavior, particularly for time-sensitive energy storage and generation scheduling in hybrid systems.

3.1.2.1 Latin Hypercube Sampling

In the first step of aLHS, LHS is applied to generate N simulated hourly wind speed time series for month M. For instance, for January, a total number of N ($31 \times 24 = 744$) hourly wind speeds are sampled from the empirical distributions of January's standardized hourly wind speeds.

LHS is a stratified sampling scheme used to reduce the number of simulations in quantifying response uncertainty (Dutta & Gandomi, 2020).

The following steps are used in one dimensional LHS to generate random samples from standardized hourly wind speeds of month M, $Z_{M,D}(t)$ (Dutta & Gandomi, 2020):

- Sort the $Z_{M,D}(t)$ for all D in ascending order, call it the sample space
- Partition the sample space into N ranges of equal probability = $1/N$.
- Select one random sample from each N ranges and generate N samples for a month

After LHS is completed, there are N standardized sampled hourly wind speeds for month M, but these standardized sampled hourly wind speeds do not have any correlation between consecutive hours because they are randomly sampled. In order to capture the autocorrelation structure of the standardized observed hourly wind speed, they should be reordered, as explained in the following subsection.

3.1.2.2 Reordering Sampled Hourly Wind Speeds

The second step is a semivariogram-matching optimization procedure to align the semivariogram of sampled hourly wind speeds (SSV) for month M with the reference semivariogram (RSV) by reordering sampled hourly wind speeds. This is achieved by reordering the sampled hourly values such that the semivariance of the simulated

data approximates the semivariance of the observed wind speeds. The optimization continues until either (i) the change between successive iterations drops below 10^{-6} or (ii) the algorithm reaches the preset maximum of 1,000,000 iterations. Generation of the RSV and SSV is explained in the following section. This reordering process is executed using the optimize.minimize function of the Python Scipy library (Virtanen et al., 2020), employing the Powell optimization method.

Semivariogram Calculations

To do semivariogram-matching optimization, first, an RSV of the standardized observed hourly wind speeds of the observation duration to quantify its autocorrelation at different time lags is generated using Equation (3-2). The semivariogram captures the variance between pairs of data separated by specific time intervals and serves as a key metric for modeling temporal dependencies in data. For the sake of simplicity, the indices in $Z_{M,D}(t)$ is dropped since the RSV is fitted to all the data in the observation period.

$$\gamma(h) = \frac{1}{2N(h)} \sum_{i=1}^{N(h)} [Z(t_i + h) - Z(t_i)]^2 \tag{3-2}$$

where $\gamma(h)$ is the semivariogram value for lag h, $N(h)$ is the total number of data governed by the lag h, $Z(t_i)$ is the value of the variable Z at time t_i and $Z(t_i + h)$ is the value of the variable Z at the time $t_i + h$. When $h = c_1$, $N(h) = N_T - 2 \times c_1$ where $c_1 = 1, 2, 3, \dots, k$; k is the maximum lag and N_T is the total number of data. For example, for lag 4, $h = 4$ and $N(4) = N_T - 8$.

After RSV is generated, SSV of standardized sampled hourly wind speeds for month M is generated using Equation (3-2). In each iteration of aLHS ($M = 1, 2, \dots, 12$), the SSV is generated for the respective month to ensure that the variability in each month is individually treated. When reordering sampled hourly wind speeds of

month M, the error between the RSV and the SSV for that month is minimized using the Powell optimization method.

Powell Optimization Method to Match RSV and SSV

The Powell optimization method minimizes the absolute error between the RSV and SSV using Equation (3-3), ensuring that the autocorrelation structure is preserved in the simulated dataset. This step is critical for capturing the temporal dynamics of wind speed variations over short-term intervals.

$$\mathrm{OF} = \sum_{\mathrm{h}=\Delta\mathrm{t}}^{\mathrm{m}\Delta\mathrm{t}} |\gamma_{\mathrm{s}}(\mathrm{h}) - \gamma_{\mathrm{S}}(\mathrm{h})| \tag{3-3}$$

where OF is the objective function value for comparing the semivariograms of the sampled and the observed data, $\Delta\mathrm{t}$ is the time lag (one hour), $m\Delta t$ is the maximum time lag considered, represented as a multiple of $\Delta\mathrm{t}$, $\gamma_{\mathrm{s}}(\mathrm{h})$ is the empirical semivariogram value at lag h for the sampled data and $\gamma_{\mathrm{S}}(\mathrm{h})$ is empirical semivariogram value at lag h for the observed data.

Maximum Time Lag ($m\Delta t$) Selection for the Objective Function

In aLHS, the maximum time lag is a key parameter. During the simulation process, the goal is to preserve dependency within the maximum time lag, ensuring a realistic generation of wind speed data by minimizing the total semivariance error for lags up to the maximum time lag ($m\Delta t$).

The maximum time lag ($m\Delta t$) is determined by analyzing the partial-autocorrelation function (PACF) of the standardized hourly wind speed observations, to identify the lag at which correlations become small. Autocorrelation analysis is essential for the time series of wind speeds, as hourly wind speeds are dependent on time, similar to

most meteorological data. This implies that a value in the time series can affect future values.

The PACF is based on the relationship between the current observation and past observations, removing the effects of the intermediate lags. It is derived from the Yule-Walker equations (Yule, 1927). The PACF at lag k is the correlation between the original time series, represented with $\overrightarrow{U_t}$ vector and time series lagged k hours, $\overrightarrow{U_{t-k}}$ vector, adjusted for the linear effects of all the intermediate lags $1, 2, \dots, k-1$.

For a time series $\overrightarrow{U_t}$, the PACF at lag k, denoted as ϕ_{kk}, is computed as follows:

$$\phi_{kk} = \text{corr}\left(\overrightarrow{U_t} - P\left(\overrightarrow{U_t}\middle|\overrightarrow{U_{t-1}}, \dots, \overrightarrow{U_{t-k+1}}\right), \overrightarrow{U_{t-k}} - P\left(\overrightarrow{U_{t-k}}\middle|\overrightarrow{U_{t-1}}, \dots, \overrightarrow{U_{t-k+1}}\right)\right) \quad (3\text{-}4)$$

where $P(\overrightarrow{U_t}|\cdot)$ represent the best linear predictor of $\overrightarrow{U_t}$ based on lag k.

The PACF graph of the standardized hourly wind speed observations is plotted to examine the structure of temporal dependence. Based on the visual inspection of the PACF plot, a maximum time lag $m\Delta t$ is selected at this stage.

In addition to PACF analysis, a sensitivity analysis is performed by generating simulated hourly wind speed time series using various maximum time lags (1 to 24 hours) to determine the optimal maximum time lag ($m\Delta t$). For each simulation, the autocorrelation function (ACF) is calculated and compared with the ACF of the observed hourly wind speeds. The absolute differences between the observed and simulated ACFs are plotted across all lags to evaluate how well each simulation preserves the autocorrelation structure. Based on these visual comparisons, the maximum time lag that best aligns with the observed ACF pattern is selected as the optimal $m\Delta t$.

The ACF of observed and simulated hourly wind speeds for a lag of k is calculated as follows:

$$\rho(k) = \frac{\sum_{t=1}^{S-k}(U_t - \bar{U})(U_{t+k} - \bar{U})}{\sum_{t=1}^{S}(U_t - \bar{U})^2} \quad (3\text{-}5)$$

where $\rho(k)$ is autocorrelation at lag *k*, U_t is value at time *t*, $\bar{U}$ is the mean of the time series, *S* is the total number of data points, and k is the lag (time shift).

3.1.2.3 De-standardization of Reordered Hourly Wind Speeds

Once the optimization is completed, de-standardization is performed using Equation (3-6) ensuring the final data reflects the diurnal and seasonal variability of observed hourly wind speeds.

$$U^*_{M,D}(t) = Z^*_{M,D}(t) \times \sigma_{M,t} + \mu_{M,t} \quad (3\text{-}6)$$

where $U^*_{M,D}(t)$ is the simulated wind speed at hour t in D^{th} day of month M, $Z^*_{M,D}(t)$ is the standardized, sampled and reordered wind speed at hour t in D^{th} day of month M, $\mu_{M,t}$ is the mean of the observed hourly wind speeds in month M for the t^{th} hour, $\sigma_{M,t}$ is the standard deviation of the observed hourly wind speeds in month M for the t^{th} hour. Thus, $M =$ January, February,…, December, $D = 1, 2, \ldots, 30$ (or 31), and $t = 1, 2, \ldots, 24$.

3.2 Calculation of Hourly Wind Energy

In generating simulated hourly wind speeds, station-based observed hourly wind speeds at 10 meters are used. However, since the wind turbines are located at higher elevations, the simulated hourly wind speeds have to be extrapolated to the hub height. This is achieved by the power-law expression in this study. The power law is defined by the following equation (Manwell et al., 2009):

$$\frac{U(e)}{U(e_r)} = \left(\frac{e}{e_r}\right)^{\alpha} \tag{3-7}$$

where $U(e)$ is hourly wind speed at height e, $U(e_r)$ is the reference hourly wind speed at the reference height e_r, α is the power-law exponent. Here, $U(e_r)$ is the simulated hourly wind speeds obtained at 10 meters. The power-law exponent changes with many parameters, and these parameters affect the power-law exponent in a complicated manner, so Justus & Mikhail (1976) reduce the simplicity and applicability of the power-law (Manwell et al., 2009). Therefore, an empirical expression proposed by Justus & Mikhail (1976) is used in this study:

$$\alpha = \frac{0.37 - 0.088 \ln\left(U(e_r)\right)}{1 - 0.088 \ln\left(\frac{e_r}{10}\right)} \tag{3-8}$$

where the unit of $U(e_r)$ is m/s, and the unit of e_r is m.

Equation (3-8) is derived from the power law for wind profiles, considering the consistency between the wind speed height variation and Weibull wind speed probability distributions. The constants 0.37 and -0.088 used in Equation (3-8) are specific to a reference height of 10 meters (Justus & Mikhail, 1976). It can be seen from Equation (3-8) that α is a function of the hourly wind speed at the reference height.

Once the simulated hourly wind speeds are adjusted to hub height, they can be used for wind energy calculations. The power generated by a wind turbine varies with wind speed, and each turbine has a unique power curve based on its technical specifications. Using this power curve allows for the assessment of a wind turbine's energy production without the need for detailed technical calculations for each component. In this study, the power curve of the selected General Electric (GE) 2.5 MW wind turbine is sourced from the catalog of wind turbine manufacturers and is employed to calculate wind energy (GE, 2010). Wind energy is determined by multiplying power output by the time interval. The calculated wind energy is

integrated into the optimization model, which seeks to identify the optimal daily operation schedule for the WHHS.

3.3 Daily Revenue Optimization Model

In this study, the daily revenue optimization model used in Ercan (2020) is used. The original optimization model was developed by Cruz et al. (2014) to maximize the daily revenue of the WHHS while operating as a closed-loop system (i.e., all external inflows and outflows to the reservoirs are excluded). Then, it was modified by Ercan (2020), and these modifications are mentioned in Appendix A. The mathematical formulation of the optimization model and associated explanations are given in Appendix A.

The optimization model has eight parameters (Ercan, 2020), which are the maximum energy that can be generated by wind turbines in an hour, the maximum energy that can be generated by the hydro turbine in an hour, the maximum energy that can be bought from the grid in an hour, the maximum energy that can be consumed by the pump in an hour, the minimum energy level in the upper reservoir, the maximum energy level that can be stored in the upper reservoir, the efficiency for the turbine mode and the efficiency for the pump mode (Ercan, 2020). Details of parameters of the daily revenue optimization model are given in Appendix B.

The inputs for the daily revenue optimization model are hourly wind energy generation and hourly electricity price. The optimization model operates on a daily basis, meaning that for each day, it optimizes revenue using hourly wind energy values from 00:00 to 23:00 and the corresponding hourly electricity prices for the same period. Since the optimization model operates on a daily basis, it runs separately for each of the 365 days in a year to determine the optimal revenue for each day. The final annual revenue is obtained by aggregating the results of these 365 daily optimizations. This means that while the optimization model runs for 365

days, it retrieves the required data for each day from the available hourly wind energy and hourly electricity price data for the entire year.

Ercan (2020) estimated hourly electricity prices using an LSTM model and used hourly wind speed data from the NASA MERRA-2 database and did not include uncertainties in wind speed into his study. Here, since the main goal is to analyze the effect of uncertainties in wind speed on annual energy revenue of the WHHS, 1,000 simulated hourly wind speed series for a year are used.

In this study, the optimization model takes hourly wind energy and day-ahead market electricity prices as input variables. Hourly wind energy is derived from simulated hourly wind speeds, which are generated using the aLHS method. Hourly electricity prices of 13 years from 2012 to 2024 are obtained from the EPİAŞ Transparency Platform (n.d.) and are used directly as inputs for the daily revenue optimization model.

3.4 Uncertainty Analysis

Uncertainty in annual revenue is primarily due to uncertainties in hourly electricity prices and uncertainties in hourly wind speeds. In this study, the effect of electricity price uncertainty on the annual revenue is incorporated into the analysis through a scenario-based approach. Each scenario consists of the realized hourly electricity prices (historic and realized are used interchangeably in this study) of the scenario year which are directly obtained from EPİAŞ Transparency Platform (n.d.). In this study, thirteen different scenarios are used to represent electricity prices for each year from 2012 to 2024. On the other hand, uncertainties in wind speed are integrated into the analysis through a Monte Carlo simulation based on aLHS approach. Consequently, the optimization model is run for each of the 1,000 simulated hourly wind speed time series and for each scenario. This approach allows for a comprehensive analysis of the system's performance under various simulated scenarios, capturing the variability in wind speed and electricity prices.

To model the uncertainty in wind speed, hourly wind speed data from 2014 to 2023, obtained from the Turkish State Meteorological Service, are used as the basis for generating simulated wind speeds. aLHS method is applied to capture the statistical properties and temporal dependencies (autocorrelations) of the observed wind speeds, and 1,000 simulated hourly wind speed series for a year are generated.

In this study, the daily revenue optimization model aims to maximize the operating revenue by utilizing hourly electricity prices and simulated hourly wind speed data for each day of a year. For every day, the model determines the optimal operational strategy based on 24-hour data, and the daily revenues are subsequently aggregated to compute the annual optimized revenue.

The model assesses the impact of variations in electricity prices on system performance by employing realized electricity prices for each scenario from 2012 to 2024. For each scenario, the same set of 1,000 simulated hourly wind speed series is used as input. This approach facilitates a detailed examination of how fluctuations in electricity price conditions affect the revenue performance of the system, enabling comprehensive analyses based on the results obtained.

Furthermore, two wind farms with different installed capacities, one being significantly larger than the other, are evaluated in order to quantify the effect of capacity expansion. This methodology elucidates how the outcomes derived from both electricity price scenarios and wind speed simulations vary with different capacity setups, thereby making a significant contribution to literature.

Consequently, within the framework of uncertainty analysis, a total of 26,000 optimized annual WHHS revenue outcomes are obtained by considering 13 different scenarios (i.e., realized electricity prices in years from 2012 to 2024), 1,000 simulated hourly wind speed series per year, and 2 different wind farm installed capacities (i.e., $13 \times 1{,}000 \times 2 = 26{,}000$). This approach provides a deeper understanding of how variability in wind conditions and electricity prices affects the operational strategies and financial performance of the hybrid system, thereby enhancing decision-making under uncertainty.

CHAPTER 4

CASE STUDY AND DATA

A hypothetical WHHS is used as a case study to demonstrate the application of the models developed in this study. The hypothetical WHHS is a wind farm integrated with the existing Uluabat Hydropower Plant, which operates as a closed-loop system. The main goal of this study is to analyze the impact of wind speed uncertainty on energy revenue by simulating hourly wind speeds and incorporating them into an optimization model. Using the simulated hourly wind speeds and historic hourly electricity prices from EPİAŞ for the years 2012 to 2024 (referred to as the scenario years), the optimization model generates an optimum daily schedule for the WHHS to maximize daily revenue for each day of the scenario year.

In this chapter, the details of the case study site (Section 4.1) and the data that serve as inputs for the models are explained. Hourly wind speed data source selection is explained in Section 4.2. Observed hourly wind speeds at MS18386 are analyzed in Section 4.3. Calculation of hourly wind energy from simulated hourly wind speeds is explained in Section 4.4. Finaly, Historic hourly electricity prices are described and analyzed in Section 4.5.

4.1 Location of the WHHS

The Uluabat Hydropower Plant, with its 100 MW installed capacity, is located in the Susurluk Basin on the Orhaneli River in the Marmara Region of Turkey. Water from the Çınarcık Dam reservoir is released to Lake Uluabat to generate electricity. In this study, a hypothetical scenario is considered. The Çınarcık Dam and Lake Uluabat are conceptualized as the upper and lower reservoirs of a pumped storage hydropower plant, respectively. Additionally, it is assumed that wind turbines are located near the hydropower plant site, owned and operated by the same company.

The pumped storage hydropower plant and the wind turbines collectively represent the hypothetical WHHS. Although the Çınarcık Dam and Uluabat Hydropower Plant are located on a river, it is assumed that the hypothetical WHHS operates as a closed-loop system. This means that all natural inflows and outflows to and from the Çınarcık Dam are neglected. The location of the Uluabat Hydropower Plant is shown in Figure 4.1.

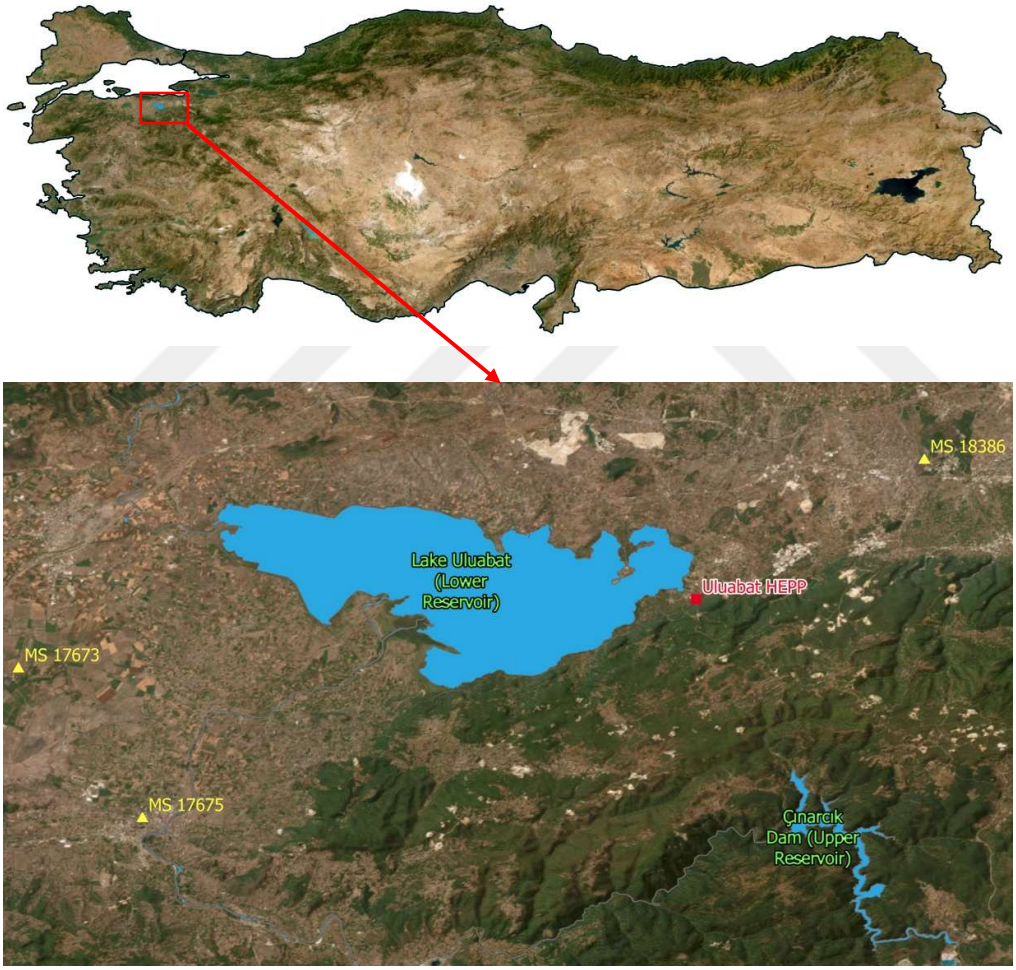

Figure 4.1 Location of the Case Study Site

4.2 Selection of Hourly Wind Speed Data Source

This study is based on a hypothetical scenario, as there is no existing wind farm in the study area. However, the goal is to analyze how the operation of a hydroelectric power plant changes with the addition of a wind farm, particularly considering the uncertainty in hourly wind speeds. To achieve this, a hypothetical wind farm is assumed and placed close to the hydroelectric power plant at a reasonable location.

There is not any meteorological station at or in the close vicinity of the hydroelectric power plant, meaning that no direct wind speed measurements are available for this specific location. However, global meteorological models provide hourly wind speed data for specific locations at various spatial resolutions. One of the most widely used datasets is ERA5, the fifth-generation reanalysis dataset from the European Centre for Medium-Range Weather Forecasts (ECMWF). ERA5 provides global climate and weather data spanning the past eight decades, with records available from 1940 onward. It replaces the previous ERA-Interim reanalysis and offers improved spatial and temporal resolution.

Among reanalysis datasets, ERA5 demonstrates strong performance compared to others, as shown by Olauson (2018). This study highlights that ERA5 outperforms datasets like MERRA-2 in wind energy modeling, though its performance varies depending on the region. Thus, first the performance of ERA5 data in this region is evaluated through comparison of hourly wind speeds from ERA5 with observed hourly wind speeds from three nearby meteorological stations. The results given in

Table 4.1 indicate that ERA5 data aligns well with MS17673, showing a relatively high correlation (0.79) and a positive Nash-Sutcliffe Efficiency (0.52), suggesting reasonable agreement with observed data. However, for MS17675 and MS18386, the correlations are lower (0.58 and 0.62, respectively), and the NSE values are negative (-1.38 and -0.18, respectively), indicating poor performance. In addition, ERA5 underestimates wind speed at all stations, as shown by the negative PBIAS

values. These findings suggest that the ERA5 model's performance is poor in this region, likely due to local geographical and meteorological influences.

The results show that ERA5 model performance varies across stations and is particularly poor for MS17675 and MS18386. Therefore, using ERA5 reanalysis data in this region is not reliable for this study. As a result, the wind farm is assumed to be located near the closest meteorological station (MS18386), with available hourly wind speed measurements. Thus, observed hourly wind speeds from MS18386 are used in this study.

Table 4.1 Comparison of ERA5 Hourly Wind Speeds with Three Nearby Meteorological Stations' Observed Hourly Wind Speeds

	Correlation	RMSE	PBIAS	NSE
MS17673	0.79	1.45	-28.27	0.52
MS17675	0.58	1.89	-60.24	-1.38
MS18386	0.62	1.93	-40.83	-0.18

4.3 Analysis of the MS18386 Hourly Wind Speeds

The observed hourly wind speeds at MS18386 are obtained from the Turkish State Meteorological Service for the years between 2014 and 2023. Within the simulation duration (i.e., 2014-2023) there are 83521 hours with data and 4127 missing hours of wind speed data (see Table 4.2). It is observed that missing values mostly result from short-term measurement gaps (e.g., 2, 3, or 4 hours). However, in the measured data between 2014 and 2023, there are two instances of long-term measurement gaps: the first between June 5, 2018, and August 1, 2018, resulting in a 57-day missing period, and the second between April 28, 2023, and June 22, 2023, lasting 55 days. Due to the presence of missing data, which hindered the correlation analyses, and considering that the amount of missing data is small relative to the overall dataset, it is decided to impute these missing values as explained in Section 3.1. While filling the missing values in the wind speed dataset, the time of day and

month is taken into account. For each missing value, the average wind speed for the same hour of the same month is calculated and used as a replacement. The dataset is grouped by month and hour, and the mean wind speed for each group is determined. Missing values are then substituted with the appropriate group means. Using this approach, the dataset is preprocessed while preserving its daily and seasonal patterns, making it more reliable for future analysis and simulations. The integrity of the data is maintained throughout this process.

Table 4.2 Periods of Received Record and Numbers of Observations at MS18386

SMS Station Name	SMS Station Number	Received Period of Record	Number of Observations	
			Valid	Missing
Nilüfer	MS18386	2014-2023	83521	4127

4.3.1 Stationarity Analysis of MS18386 Hourly Wind Speeds

The stationarity of hourly observed wind speed is evaluated using an R script that applies the Augmented Dickey-Fuller (ADF) test introduced by Dickey & Fuller (1979) across various frequencies (daily, weekly, monthly, yearly), lags (0, 1, 2, 3, 4, 5 and 6 hours), and test types. Four test types are utilized: one assuming stationarity, and three others with distinct model specifications—no constant, constant only, and constant with trend. The first type tests for stationarity directly, while the second excludes a constant term, the third includes a constant to account for a mean level, and the fourth incorporates both a constant and a trend to capture potential linear growth. R script stationarity test is provided in Appendix C. The results across all lags, frequencies (daily, weekly, monthly, yearly), and test types consistently confirm stationarity. The results of the stationary test are provided in Appendix D.

4.3.2 Diurnal Variation and Seasonality Analysis of MS18386 Hourly Wind Speeds

This study utilizes hourly wind speeds at station MS18386 from 2014 to 2023. Figure 4.2 displays the diurnal variation of hourly wind speeds from January 2014 to December 2023 observed at MS18386. As seen in Figure 4.2, there are fluctuations in the expected values of the observed hourly wind speeds. This phenomenon is known as diurnal variation.

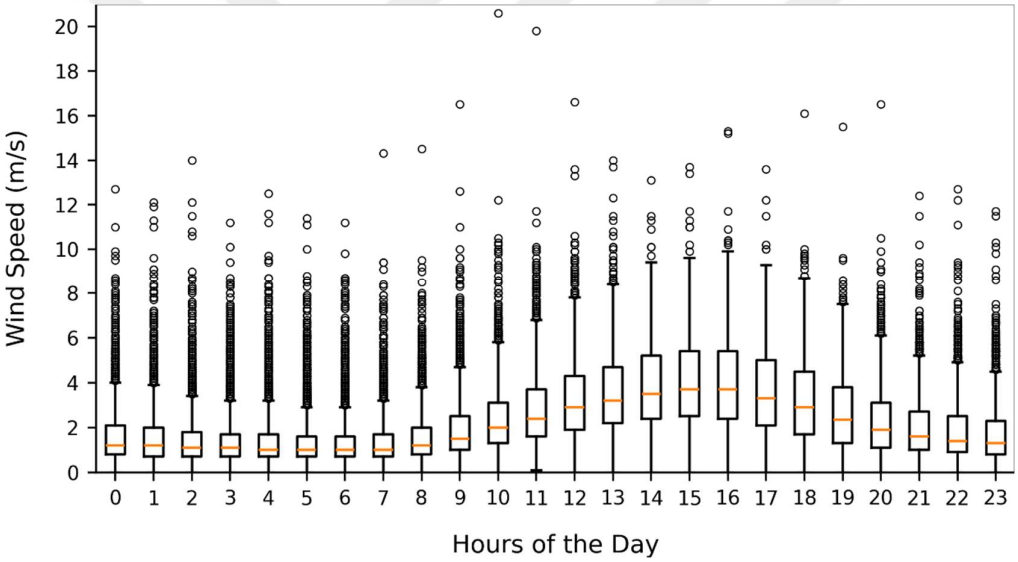

Figure 4.2 Diurnal Variation of Hourly Wind Speeds at MS18386 from 2014 to 2023

Diurnal variation of hourly wind speeds observed in each month at MS18386 between 2014 and 2023 is investigated as well. Diurnal variation of hourly wind speeds at MS18386 for each of the twelve months from 2014 to 2023 is given in Figures 4.3 to 4.14. An examination of Figure 4.3 through Figure 4.14 reveals that diurnal variation exhibits distinct characteristics across different months, providing compelling evidence of seasonality within the data.

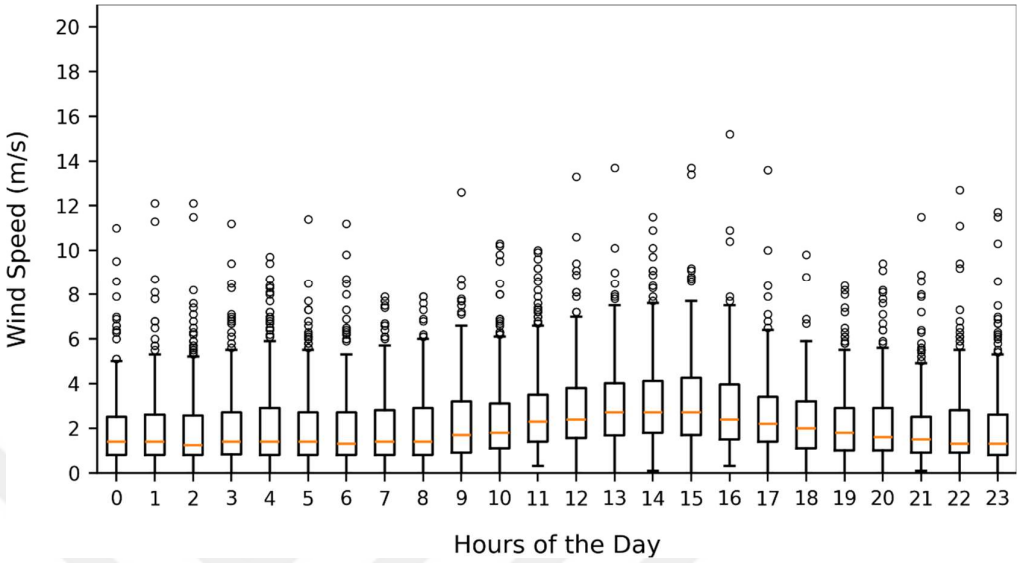

Figure 4.3 Diurnal Variation of Hourly Wind Speeds at MS18386 for all January

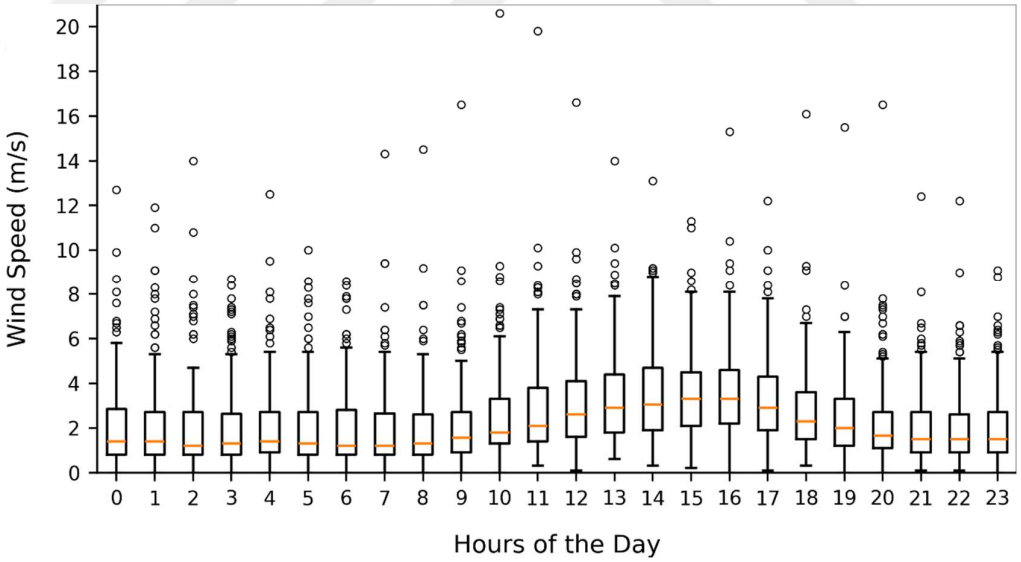

Figure 4.4 Diurnal Variation of Hourly Wind Speeds at MS18386 for all February Months from 2014 to 2023

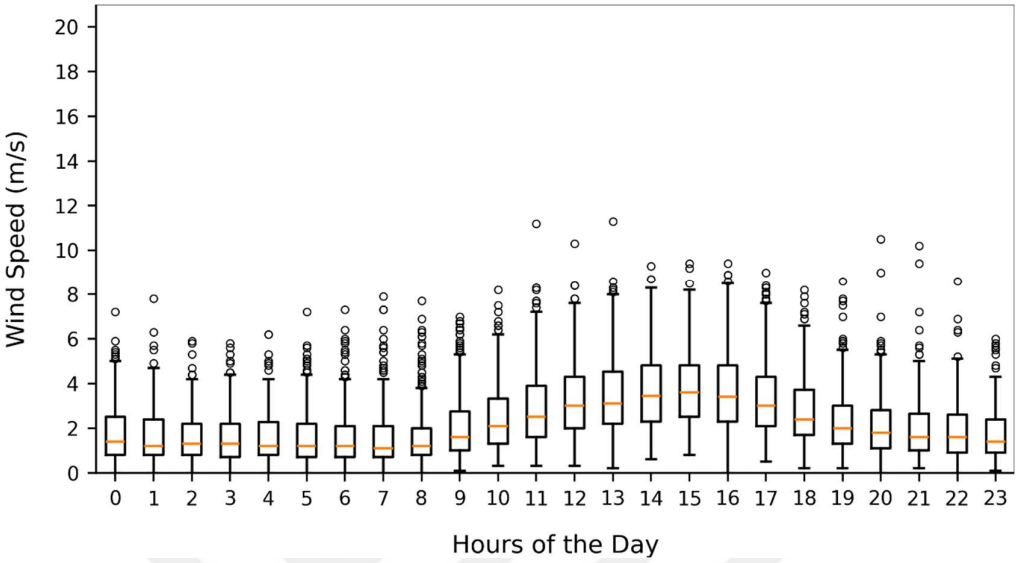

Figure 4.5 Diurnal Variation of Hourly Wind Speeds at MS18386 for all March Months from 2014 to 2023

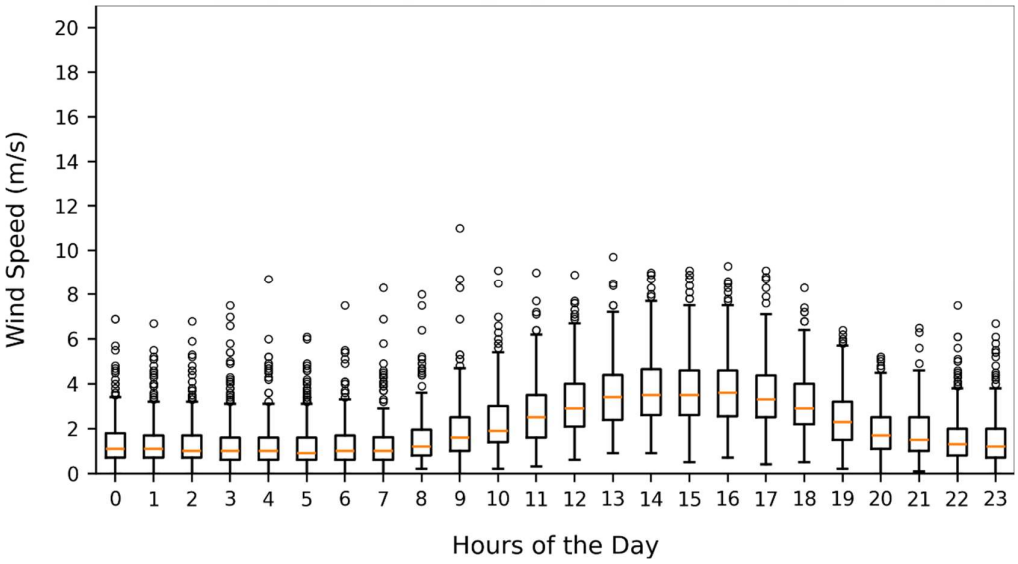

Figure 4.6 Diurnal Variation of Hourly Wind Speeds at MS18386 for all April Months from 2014 to 2023

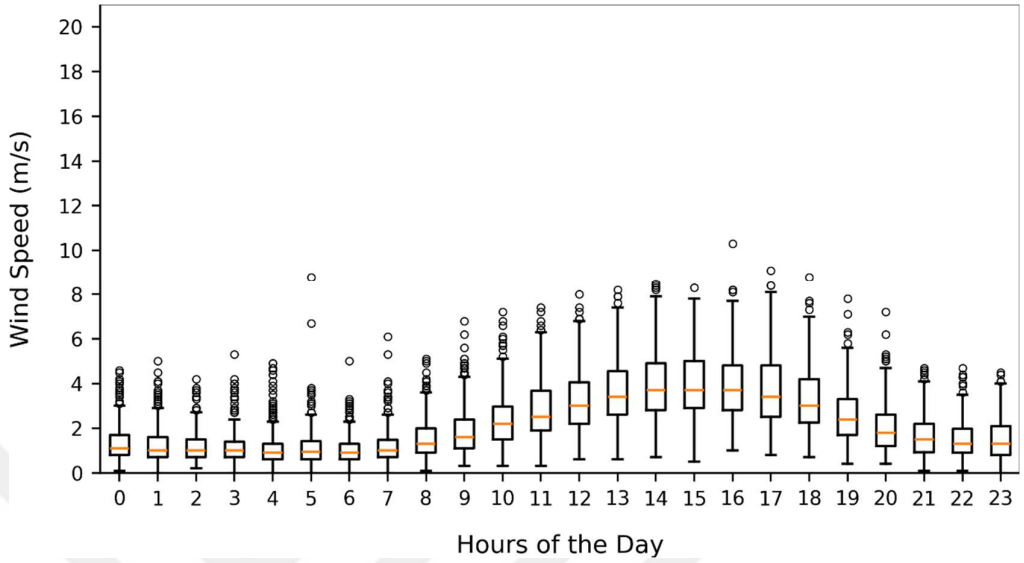

Figure 4.7 Diurnal Variation of Hourly Wind Speeds at MS18386 for all May Months from 2014 to 2023

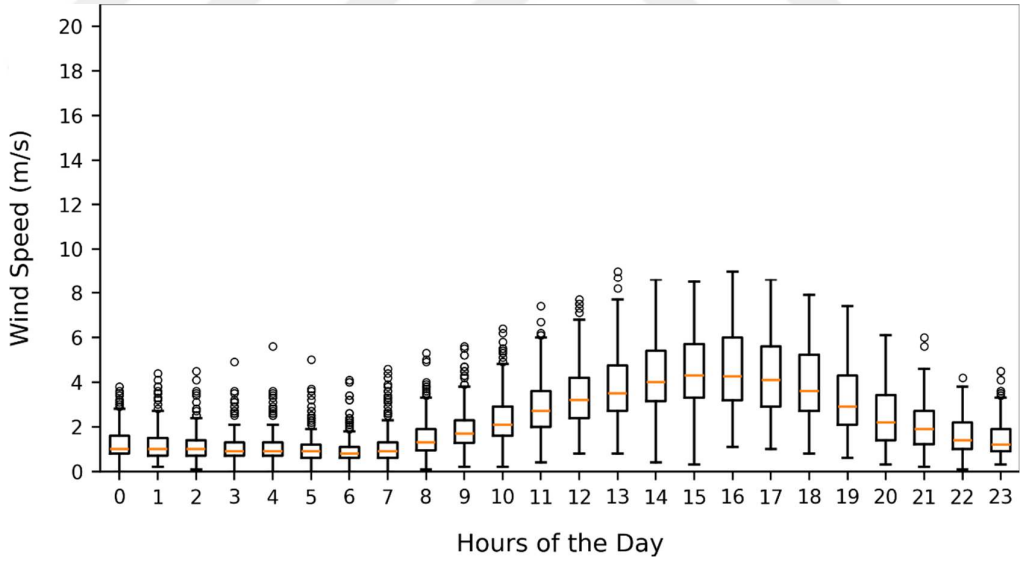

Figure 4.8 Diurnal Variation of Hourly Wind Speeds at MS18386 for all June Months from 2014 to 2023

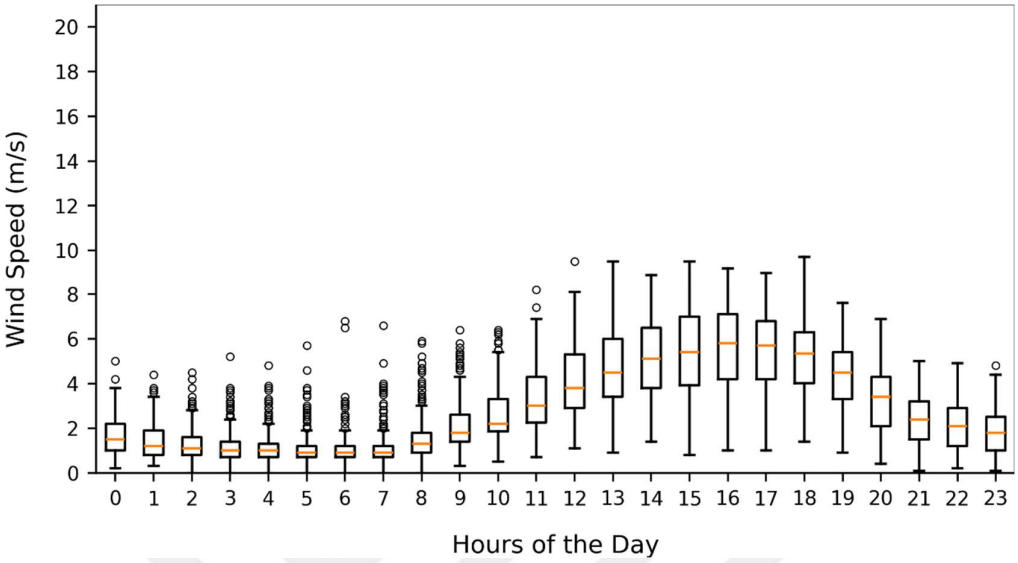

Figure 4.9 Diurnal Variation of Hourly Wind Speeds at MS18386 for all July Months from 2014 to 2023

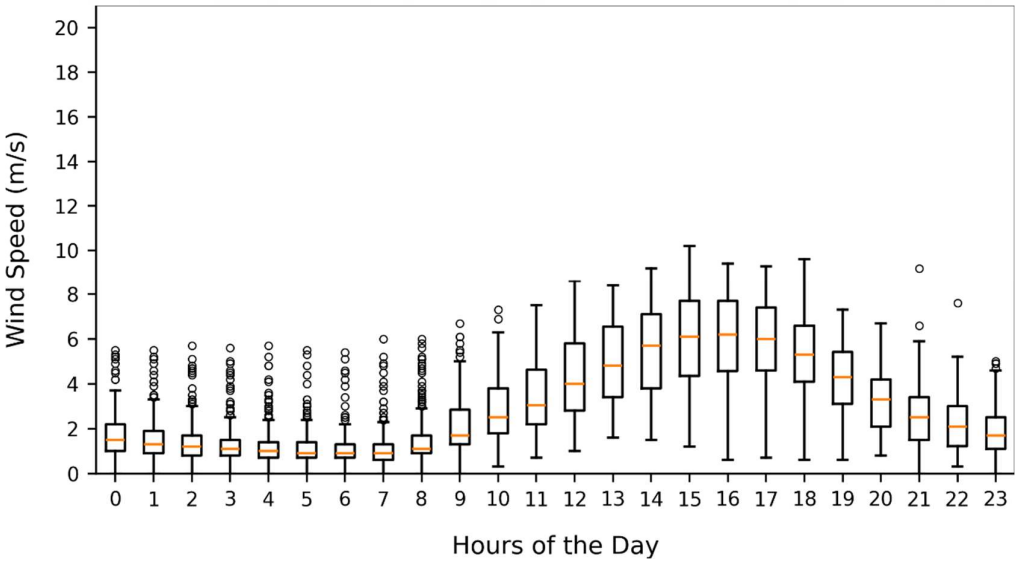

Figure 4.10 Diurnal Variation of Hourly Wind Speeds at MS18386 for all August Months from 2014 to 2023

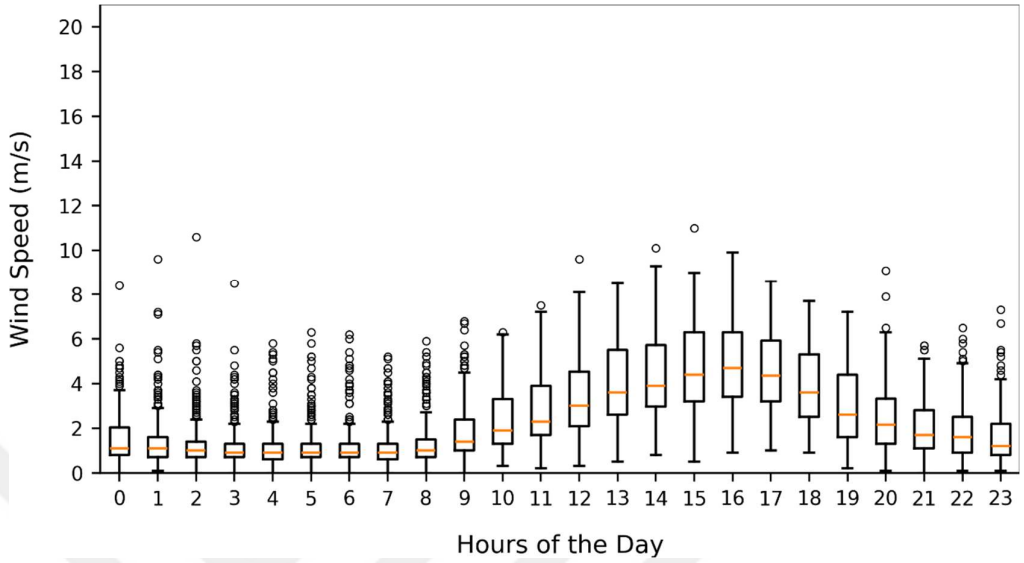

Figure 4.11 Diurnal Variation of Hourly Wind Speeds at MS18386 for all September Months from 2014 to 2023

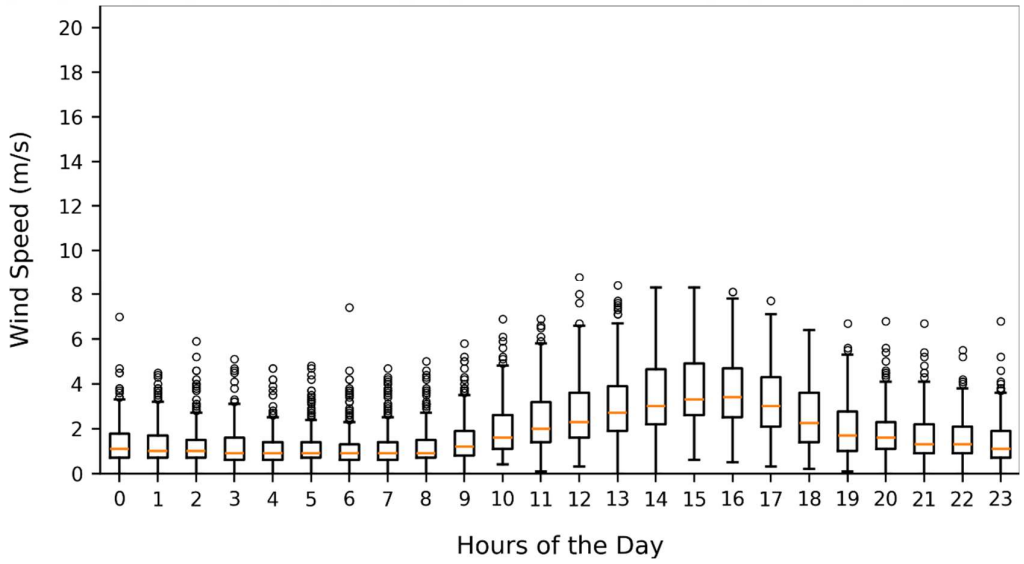

Figure 4.12 Diurnal Variation of Hourly Wind Speeds at MS18386 for all October Months from 2014 to 2023

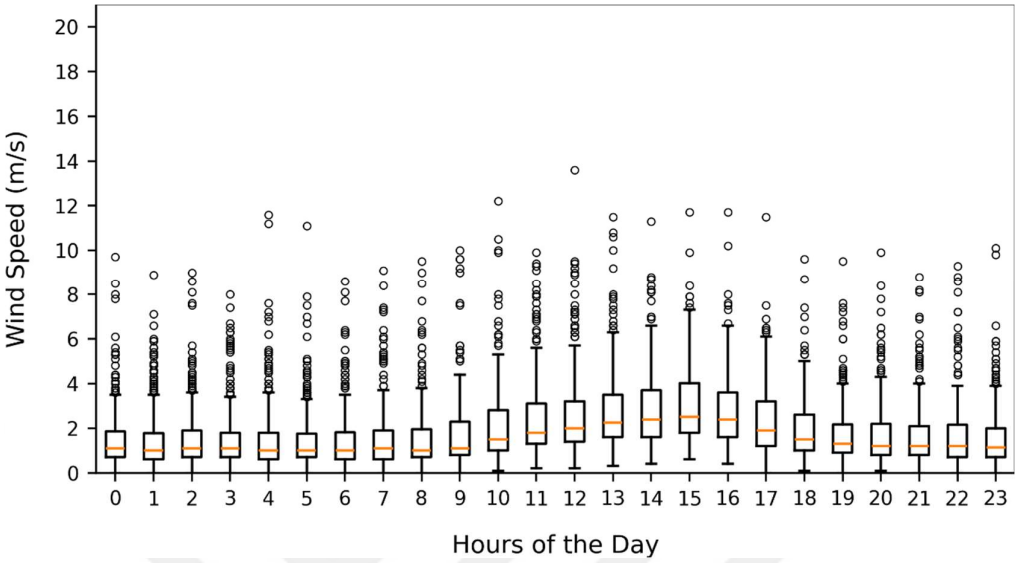

Figure 4.13 Diurnal Variation of Hourly Wind Speeds at MS18386 for all November Months from 2014 to 2023

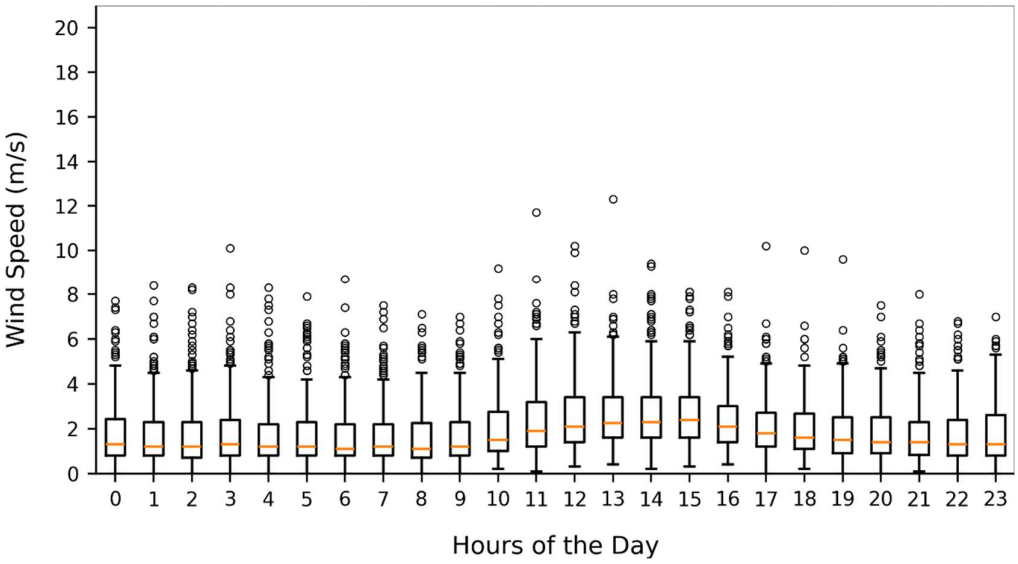

Figure 4.14 Diurnal Variation of Hourly Wind Speeds at MS18386 for all December Months from 2014 to 2023

Monthly average wind speeds are calculated using observed hourly wind speeds at station MS18386 from 2014 to 2023 and are shown in Figure 4.15. As indicated by these averages, there are noticeable differences between the monthly averages, some months demonstrating higher similarity. For example, October, November and December have similar values, as do April and May, while January, February and March also show comparable averages. However, these patterns do not align with the typical seasonal cycles of winter, spring, or summer, as the groupings do not follow the traditional seasonal months. Given these variations, it is not appropriate to divide the data into three-month periods based on conventional seasons. To effectively treat seasonality and ensure a more accurate analysis, we decided to remove diurnal variations for each month separately. This approach takes into account the distinct characteristics of each month, leading to more reliable results.

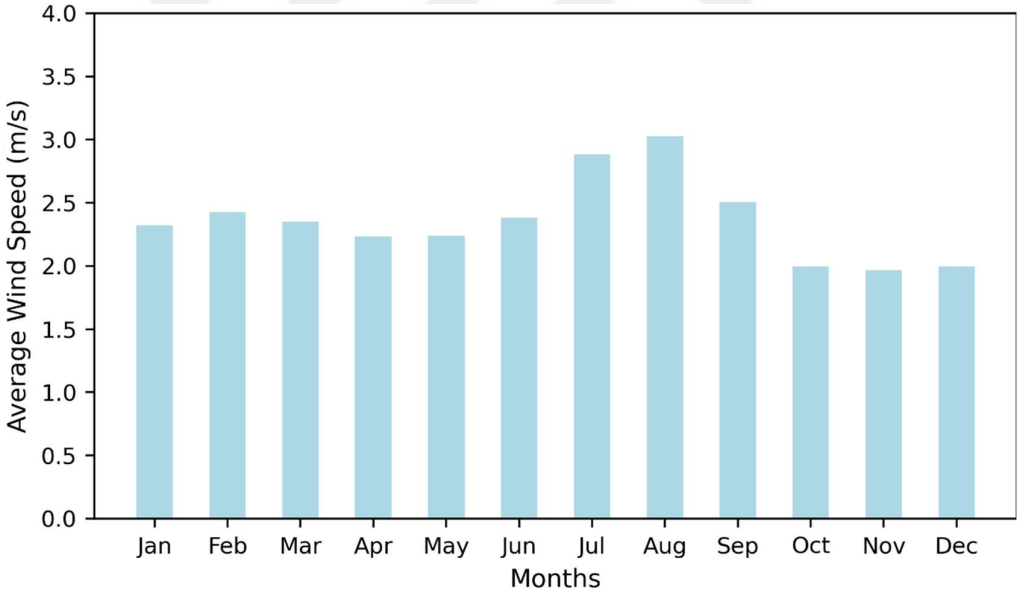

Figure 4.15 Monthly Average MS18386 Wind Speeds between 2014 and 2023

Another approach to analyze seasonal variations is the use of monthly cumulative distribution functions (CDFs) which will help identifying periods of stable or highly variable wind conditions. The shape and steepness of the CDF curves reveal important characteristics such as the consistency of wind speeds and the presence of

extreme values, which impact the efficiency and reliability of wind-based applications. CDFs of hourly wind speeds for each month are given in Figure 4.16.

As shown in Figure 4.16, the CDFs display distinct patterns, reflecting seasonal differences in wind behavior. The positioning and shape of the curves indicate that some months experience higher or lower wind speeds more frequently than others. June and August have CDFs that are positioned further to the right, indicating that wind speeds are generally higher during these months. In contrast, months such as October, November, and December have CDFs positioned further to the left and increase more gradually, suggesting that wind speeds are lower on average. The differences in the slopes of the curves further emphasize the distribution of wind speeds, with some months having more concentrated wind speed values while others exhibit a wider range. These results provide essential insights into seasonal wind speed behavior.

Based on the previous analysis, diurnal variations are removed by subtracting the hourly expected values of data for each month separately, as explained in Section 3.1.1. CDFs of hourly wind speeds for each month after standardization (removal of diurnal variation) are given in Figure 4.17.

As can be seen from Figure 4.17, although these CDFs are in better agreement with each other than those of non-standardized wind speeds but they do not exactly align. Thus, examination of the CDFs indicates that sampling hourly wind speed data in monthly blocks is preferable to better represent monthly variations. For this reason, LHS is applied for each month to generate a simulated hourly wind speed time series for that month, then they are combined to obtain a simulated hourly wind speed time series for a year.

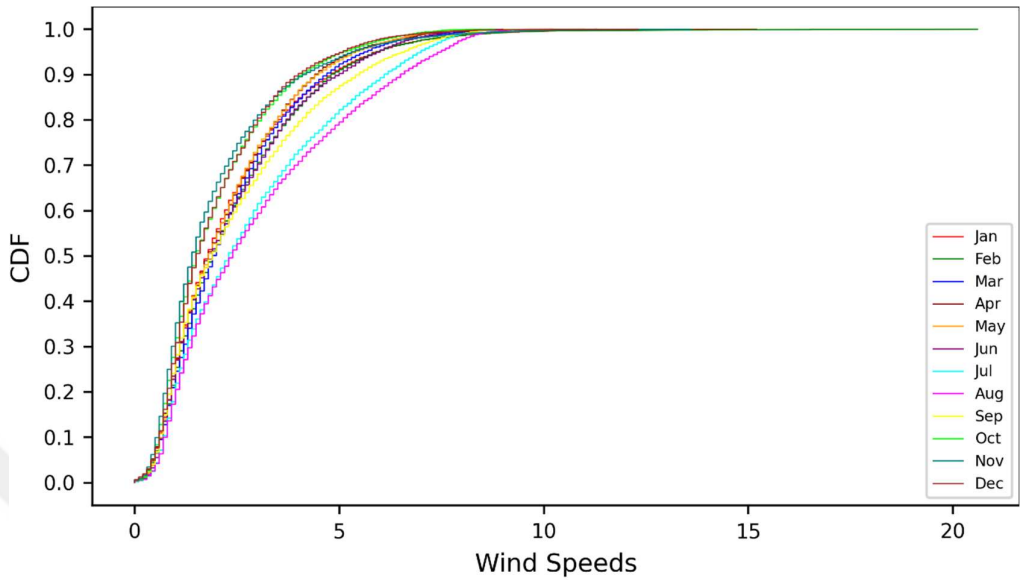

Figure 4.16 CDFs of Hourly Wind Speeds at MS18386 for all Months

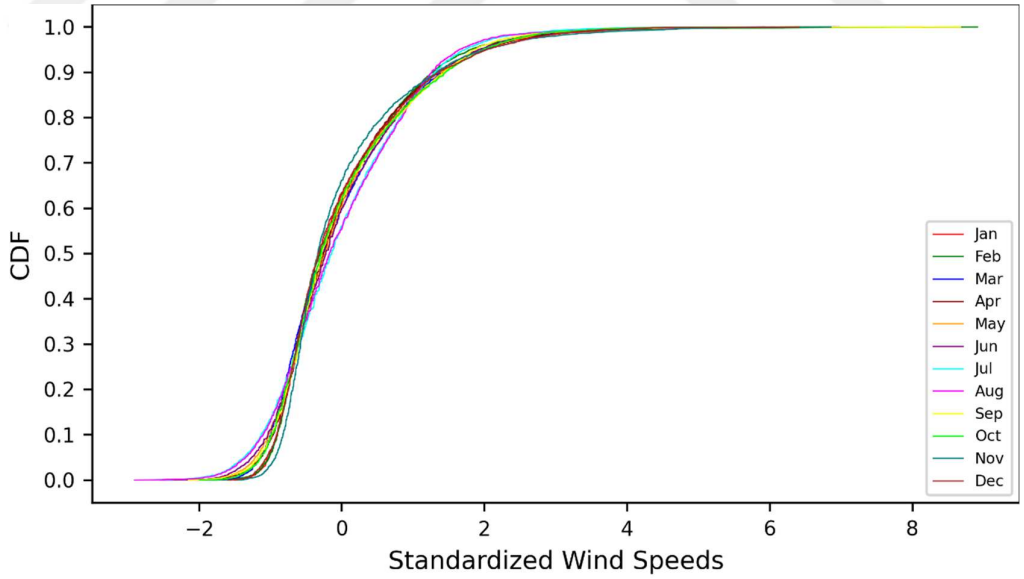

Figure 4.17 CDFs of Standardized Hourly Wind Speeds at MS18386 for all Months

4.4 Wind Turbine Used in the Hypothetical WHSS

Wind energy is one of two inputs for the daily revenue optimization model. Hourly wind speeds are simulated using aLHS for a year, and they need to be converted to hourly wind energy to be used as the input of the optimization model. Thus, first, hourly wind speeds are simulated based on the historical data observed in MS18386 meteorological station between the years 2014 and 2023. MS18386 station records wind speeds at 10 m above ground.

This study assumes a hypothetical WHSS. The wind turbines used in the WHSS are assumed to be 2.5 MW wind turbines manufactured by General Electric. This wind turbine has 85 meters hub height, 3 m/s cut-in speed and 25 m/s cut-out speeds (GE, 2010). Thus, simulated wind speeds are extrapolated to the 85 m hub height from the 10 m observation height using Equation (3-7). Then, to convert simulated hourly wind energy at 85 m hub height to hourly wind energy power curve of the wind turbine acquired from General Electric (2010) is used. The power curve of the 2.5 MW wind turbine is given in Figure 4.18.

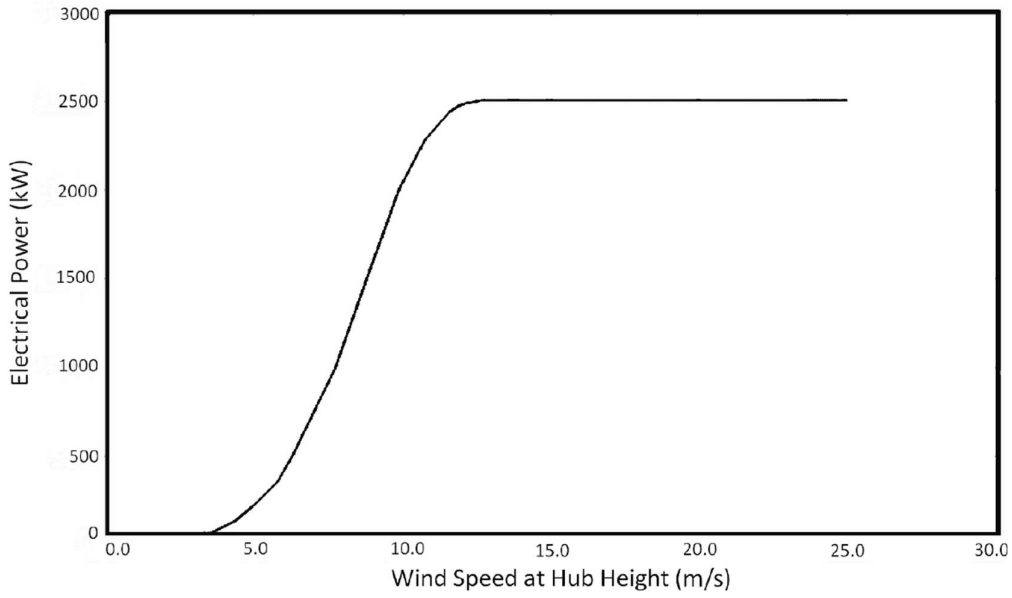

Figure 4.18 GE 2.5 MW Wind Turbine Power Curve (GE, 2010)

Since manually reading wind energy values corresponding to each of the 1,000 simulated hourly wind speeds for a year from the graph is time-consuming, a polynomial function fitted to the power curve presented in Figure 4.18 by Ercan (2020) is used. This function is given in Equation (4.1).

$$f(x) = \begin{cases} 0 & x \leq 3 \\ 0.001x^3 + 0.025x^2 - 0.182x + 0.291 & 3 < x \leq 8.859 \\ 0.003x^3 - 0.168x^2 + 2.83x - 12.511 & 8.859 < x \leq 12.791 \\ 2.5 & x > 12.791 \\ 0 & x > 25 \end{cases} \quad (4.1)$$

4.5 Analysis of the Hourly Electricity Price Data

Hourly electricity prices for the years 2012 to 2024 are obtained from the EPİAŞ Transparency Platform (n.d.). These realized electricity prices are used to generate scenarios for the years 2012 to 2024 to assess the impact of electricity price uncertainty on WHHS operations. Diurnal variation in hourly electricity prices for each year from 2012 to 2024 are given in Figure 4.19 to Figure 4.31. Each year's behavior is examined to better understand the data used. In 2012, electricity prices were highly volatile with sharp spikes between 10:00 and 19:00, and extreme outliers indicated serious imbalances. The year 2013 showed improved stability, with fewer outliers and a more controlled diurnal pattern, while 2014 maintained this structure with a clear increase in prices during the day and a decrease at night, though still with some spread in midday hours. In 2015, the diurnal trend became more distinct, but price volatility increased. The volatility peaked in 2016 with high price spikes between 10:00 and 17:00, reflecting an unstable marked. In contrast, 2017 marked a period of stability with tighter distributions and fewer outliers, and this stability continued into 2018 and 2019, where the diurnal shape of the prices became well-

defined and consistent. Starting in 2020, prices began to rise moderately, and though the diurnal pattern remained, volatility increased, especially in peak hours. In 2021, price levels rose significantly across all hours, and the difference between night and day prices flattened, accompanied by greater uncertainty and price variability. The year 2022 experienced a dramatic price surge, with medians exceeding 2000 TL/MWh and many hours hitting the price cap of 5000 TL/MWh. This trend of extremely high prices continued into 2023, although a slight re-emergence of the diurnal pattern was observed. In 2024, despite the continued high price environment, the hourly structure of the market became more organized again, with daytime prices increasing and nighttime prices decreasing, and fewer extreme outliers than previous years.

To summarize, between 2012 and 2016, the Turkish electricity market experienced significant volatility and instability, with frequent price spikes and irregular diurnal trends. From 2017 to 2019, the system became more stable and predictable, with clear daily cycles and fewer extreme fluctuations. However, starting in 2020, prices began to rise, and by 2022, the market faced a severe shock. While 2023 and 2024 saw continued high prices, the hourly structure of the market started to normalize again. Thus, the scenario years used in this study demonstrate a wide range of hourly electricity price variations which will allow detailed analysis of the effect of variation in electricity prices on energy revenue variation in addition to wind speed variation.

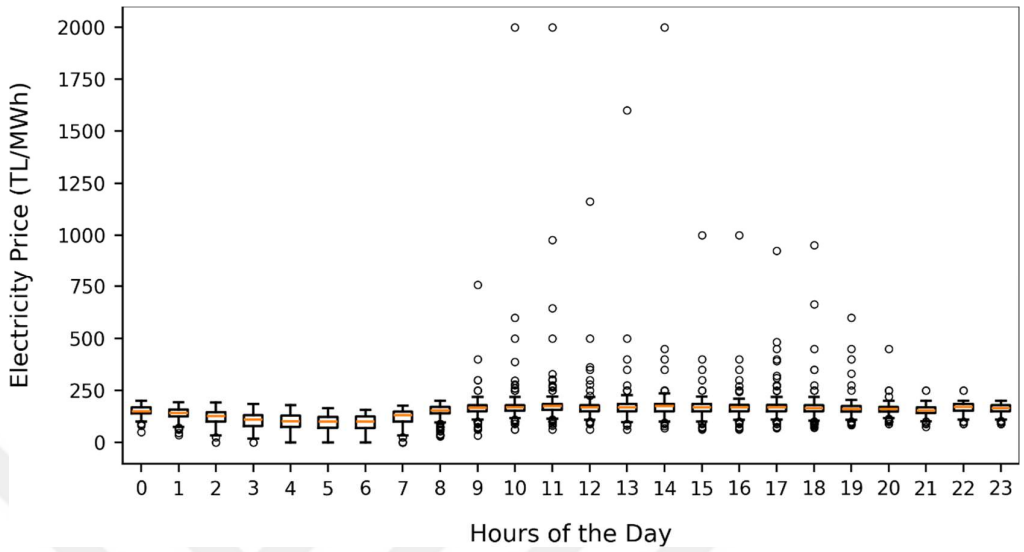

Figure 4.19 Diurnal Variation of Hourly Electricity Prices in 2012

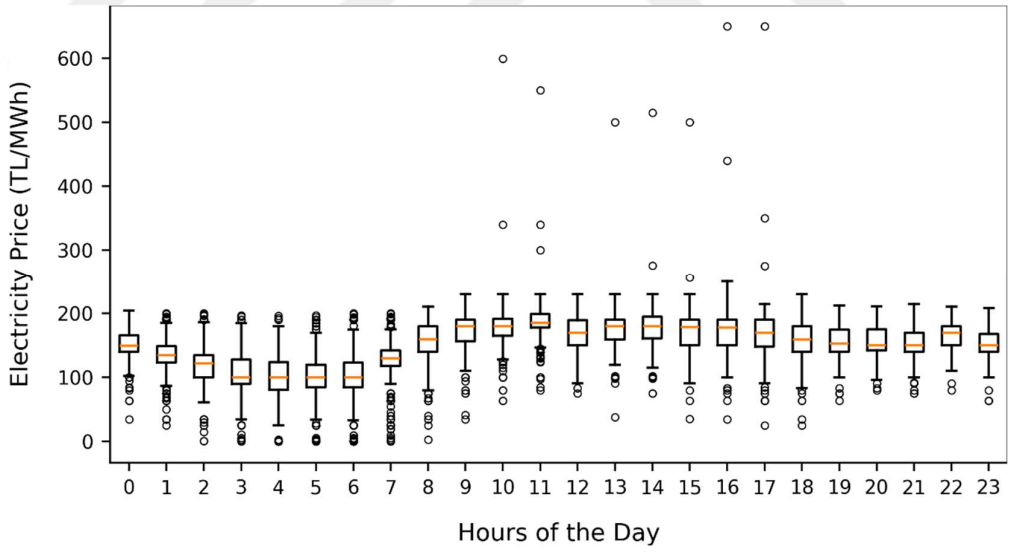

Figure 4.20 Diurnal Variation of Hourly Electricity Prices in 2013

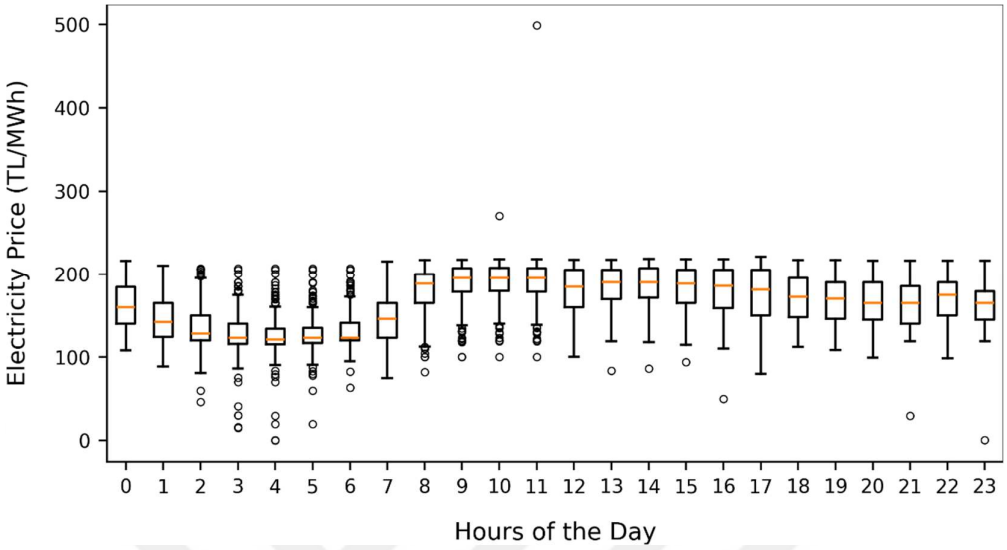

Figure 4.21 Diurnal Variation of Hourly Electricity Prices in 2014

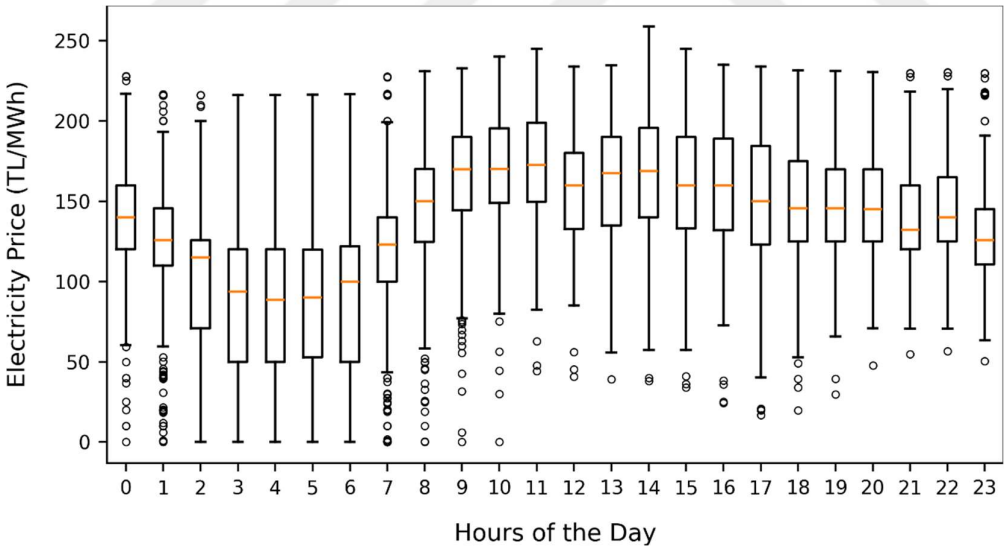

Figure 4.22 Diurnal Variation of Hourly Electricity Prices in 2015

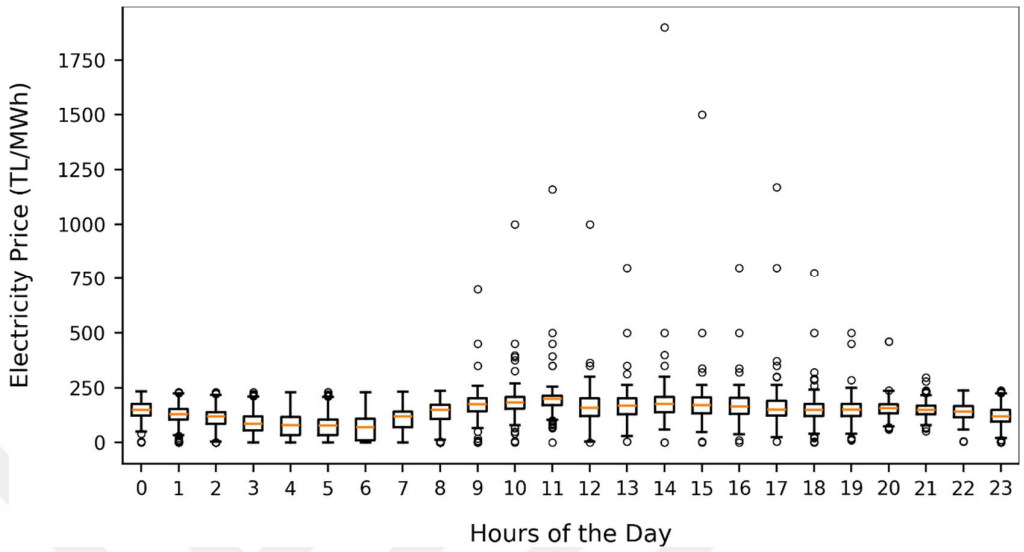

Figure 4.23 Diurnal Variation of Hourly Electricity Prices in 2016

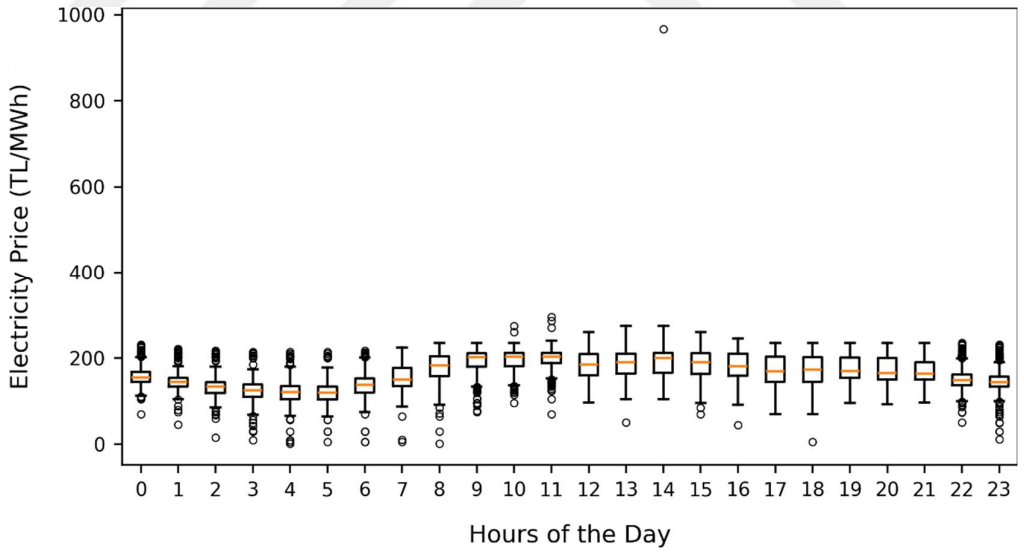

Figure 4.24 Diurnal Variation of Hourly Electricity Prices in 2017

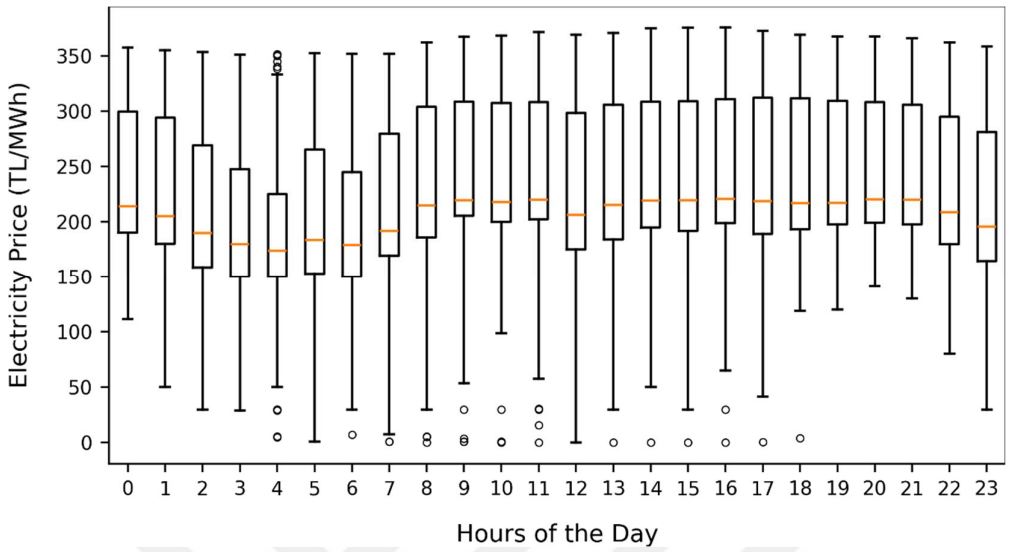

Figure 4.25 Diurnal Variation of Hourly Electricity Prices in 2018

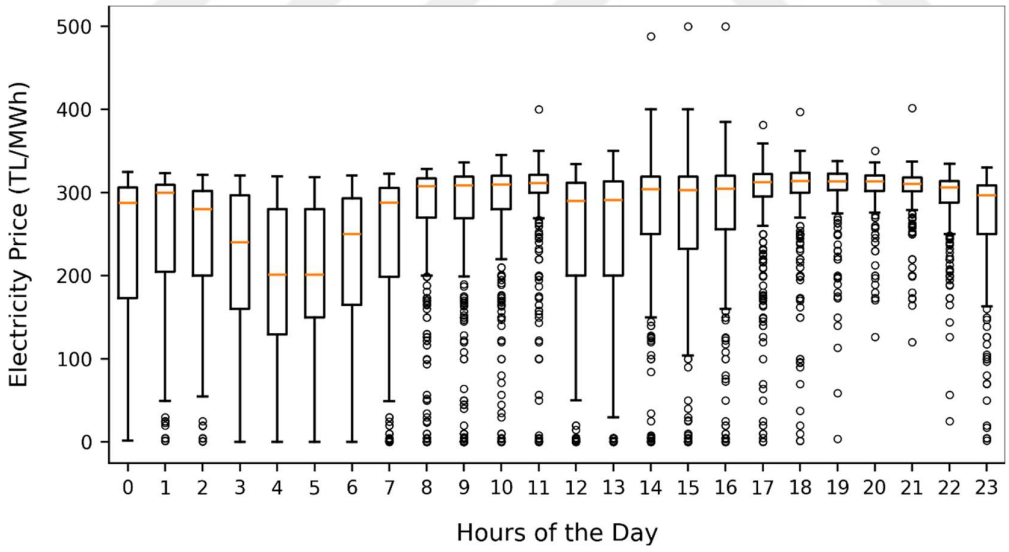

Figure 4.26 Diurnal Variation of Hourly Electricity Prices in 2019

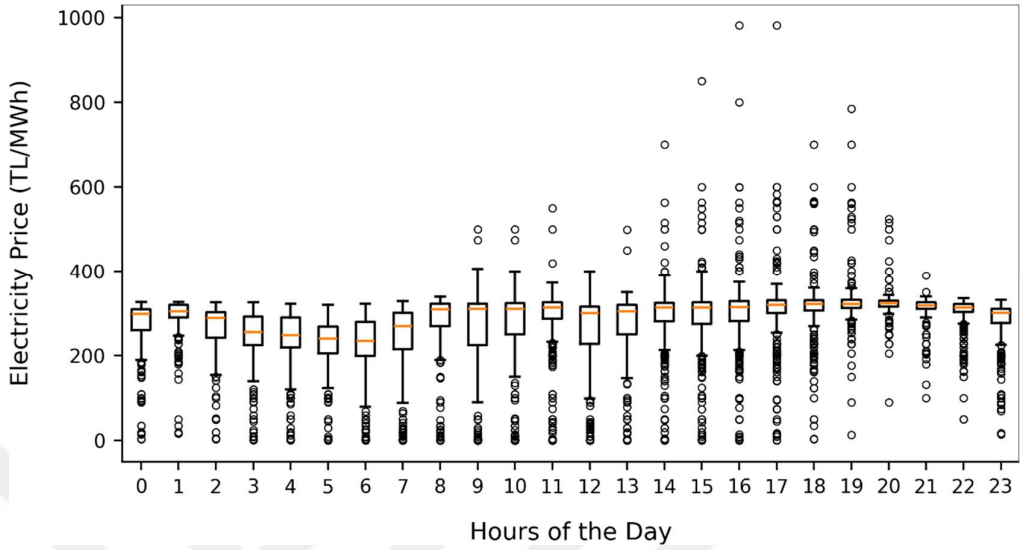

Figure 4.27 Diurnal Variation of Hourly Electricity Prices in 2020

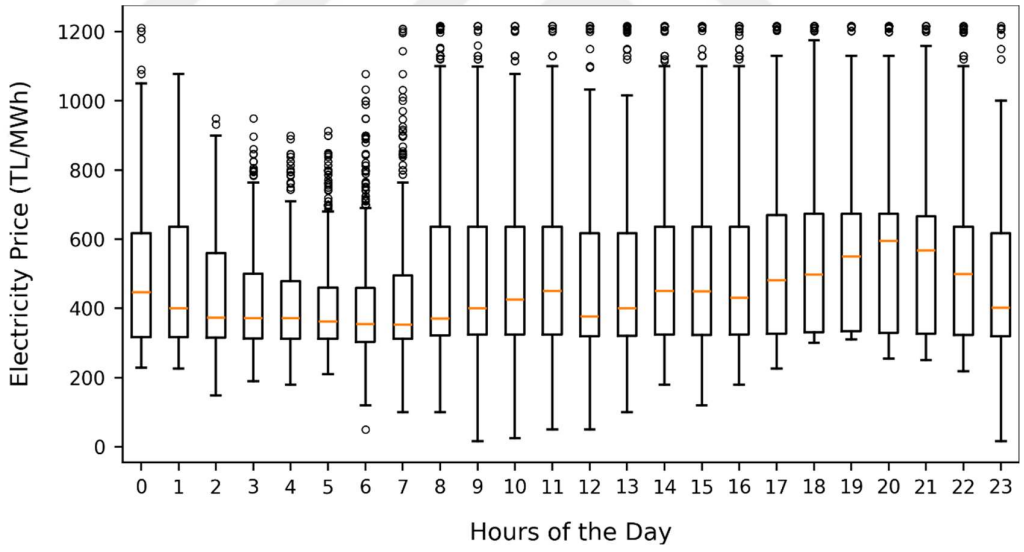

Figure 4.28 Diurnal Variation of Hourly Electricity Prices in 2021

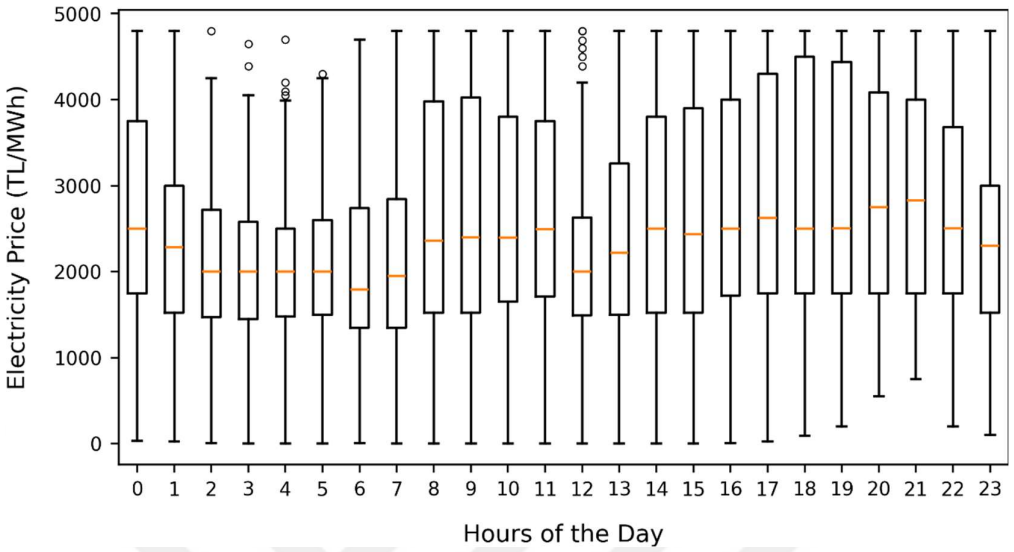

Figure 4.29 Diurnal Variation of Hourly Electricity Prices in 2022

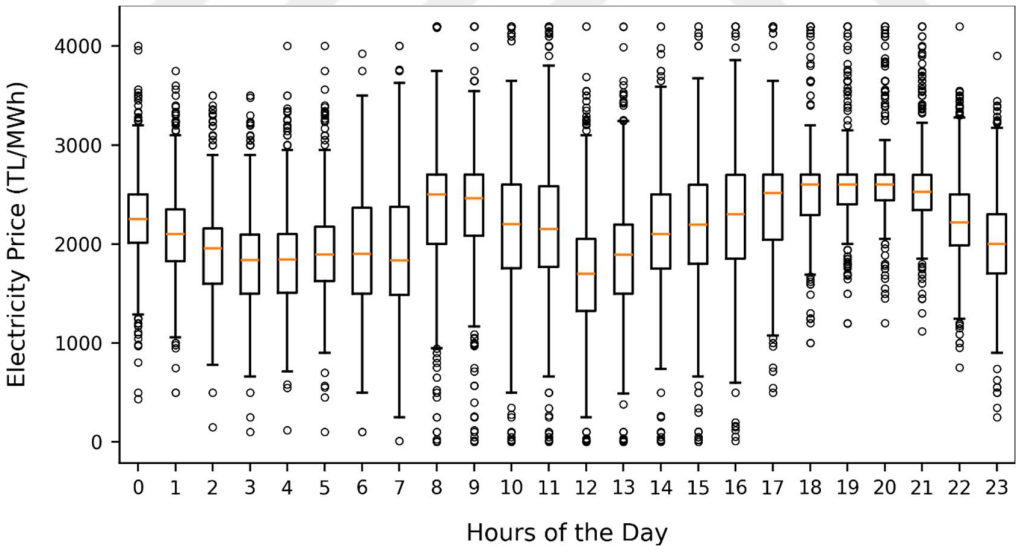

Figure 4.30 Diurnal Variation of Hourly Electricity Prices in 2023

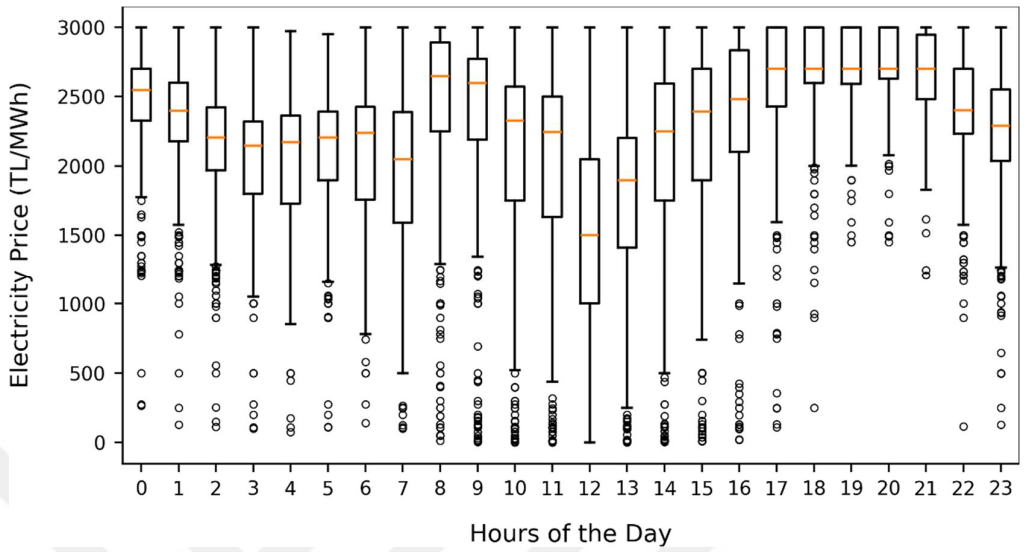

Figure 4.31 Diurnal Variation of Hourly Electricity Prices in 2024

To gain a clearer view of how electricity prices have changed over time, the monthly average values in TL, USD and EUR are computed and illustrated in Figure 4.32. From 2012 to around mid-2021, the electricity prices in TL remained relatively stable, fluctuating between approximately 100 and 400 TL/MWh. During this same period, the prices in USD and EUR also showed minor variation, remaining almost flat and close to each other. Starting in late 2021, a sharp and sustained increase in TL-based prices is observed, peaking in late 2022 to early 2023, where monthly average prices exceeded 3500 TL/MWh. While TL prices surged drastically, the corresponding USD and EUR prices rose only modestly, which confirms that much of the increase in TL terms was driven by currency devaluation rather than just real energy cost hikes. After reaching the peak, TL-based prices began to decrease but remained significantly elevated compared to the pre-2021 period, stabilizing around 2000–2500 TL/MWh in 2023 and 2024. Meanwhile, prices in USD and EUR declined and flattened again, returning closer to pre-crisis levels. Thus, it is decided to carry out the energy revenue calculations in EUR rather than TL, to reflect variations in energy costs rather than currency devaluation.

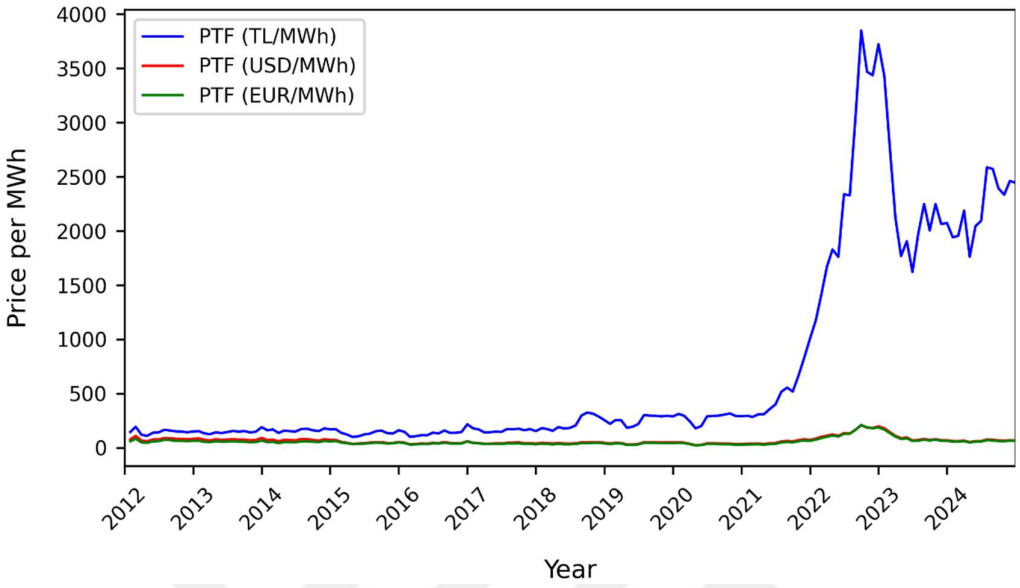

Figure 4.32 Monthly Averaged Electricity Prices

CHAPTER 5

RESULTS AND DISCUSSIONS

In this chapter, the results of hourly wind speed simulation, the optimization model, and uncertainty analysis are presented and discussed. After developing an hourly wind speed simulation method that best represents the original hourly wind speed and obtaining the simulated hourly wind speeds for a year, they are used in the optimization model to evaluate the effect of uncertainty in wind speed and electricity prices on the uncertainty in energy revenue. Effect of uncertainties in hourly wind speeds on energy revenue is quantified through generation of 1,000 hourly wind speed time series using the LHS procedure, while uncertainties in hourly electricity prices are analyzed through a scenario-based approach. Energy revenues are obtained for 13 scenario years, from 2012 to 2024.

5.1 Hourly Wind Speed Simulations

Initially, the need for normalization of observed hourly wind speeds is investigated. In Monte Carlo or LHS simulations, normalization is not necessary since data can be sampled from any distribution (Minasny & McBratney, 2006) while for autoregressive models, data has to be normalized (Poggi et al., 2003). In this study, the decision to normalize or not normalize the observed hourly wind speeds is made by conducting simulations with both approaches and comparing their performances. As seen in Figure 5.1, simulations performed with and without normalization with a maximum time lag of 5 hours generated very similar results. Thus, it is found unnecessary to carry out normalization in this study.

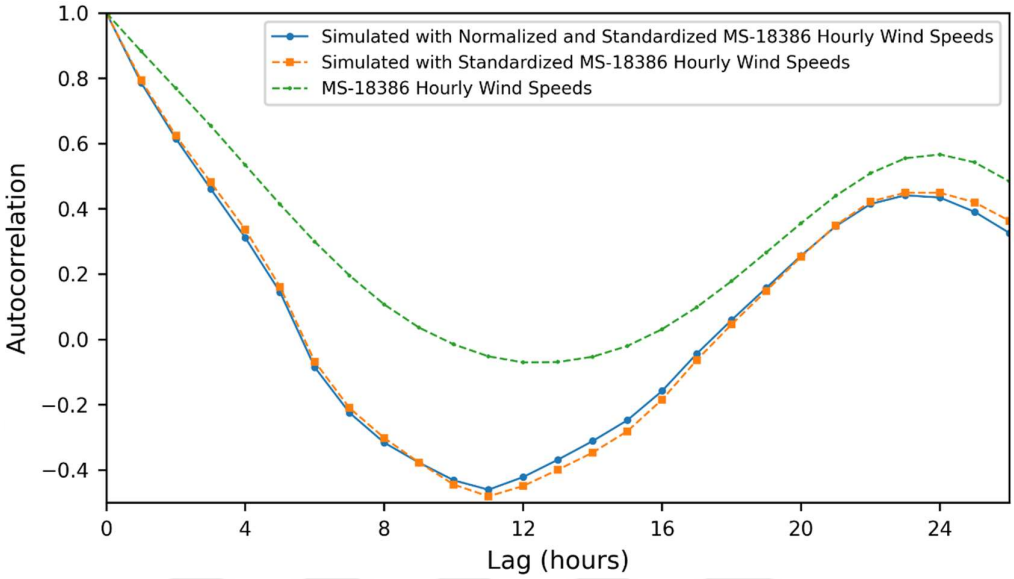

Figure 5.1 ACF of Simulated Hourly Wind Speeds with Normalization and without Normalization of MS18386 Hourly Wind Speeds

5.1.1 Selection of the Maximum Time Lag

The maximum time lag is a key parameter in the hourly wind speed simulation process. The objective function used in minimizing the difference between the semivariograms of the sampled and the observed data (see Equation (3.3)) requires a maximum time lag, which is determined using two approaches in this study. First, the partial autocorrelation function, PACF of standardized observed hourly wind speed is examined to determine the time lag at which the autocorrelation becomes insignificant. Secondly, the aLHS-based hourly wind speed simulation is run with different maximum time lags (e.g., 1, 2, 3, ..., 24 hours), and the ACFs of simulated hourly wind speeds for each maximum time lag are compared with the ACF of observed hourly wind speeds. The results are presented in the following subsections.

5.1.1.1 PACF Analyses for Maximum Time Lag Selection

To select the maximum time lag to be used in the optimization step of aLHS, PACF analysis is conducted. In order to examine the partial autocorrelation behavior of observed hourly wind speeds without diurnal effect, hourly wind speed data is standardized using Equation (3.1). This preprocessing step is crucial for analyzing temporal dependencies, without the interference of repetitive daily patterns.

The maximum time lag for the optimization step of aLHS is determined by analyzing the PACF of standardized hourly wind speed observations, as shown in Figure 5.2. It shows higher than 0.8 partial autocorrelation at 1-hour lag, indicating a strong correlation between wind speeds one hour apart. This suggests short-term persistence in wind speed. Partial autocorrelations decay with increasing lag and around 6-hours it diminishes. At this point the maximum time lag is selected as 5 hours.

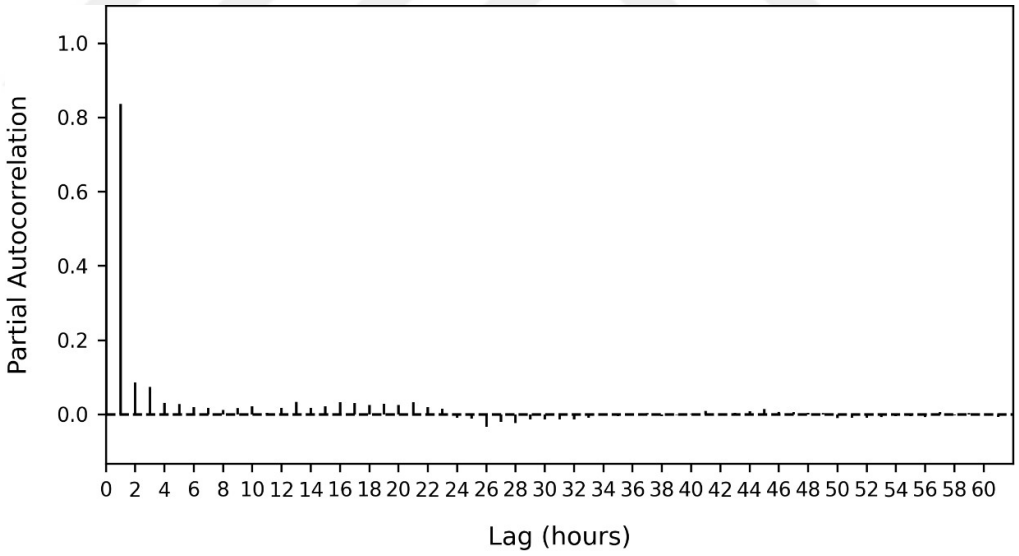

Figure 5.2 PACF of Standardized Hourly Wind Speed at MS18386 between 2014 and 2023

5.1.1.2 Sensitivity Analysis for Maximum Time Lag Selection

Hourly wind speed simulations are conducted using different maximum time lag values, and ACF is computed for each simulated dataset. Then, to compare ACF of observed hourly wind speeds with ACF of simulated hourly wind speeds with different maximum lag time, the absolute errors between them are calculated and plotted in Figure 5.3 to Figure 5.7. The y-axis in Figure 5.3 to Figure 5.7 (ACF Observed - ACF Simulated) represents the absolute difference between the observed hourly wind speed ACF and the simulated hourly wind speed ACF for different maximum time lags. Higher values indicate a greater discrepancy between the simulated and observed ACF, while lower values signify a better alignment. As the difference between the ACF of observed values and simulated values approach zero, the simulation more accurately captures the autocorrelation structure of the observed wind speed data. Large fluctuations and consistently high differences suggest simulation struggles to replicate the observed data. The ACF errors are visualized to analyze the impact of different maximum lag times on temporal dependence. This analysis is done to identify the most suitable maximum time lag value that produces results closest to the observed hourly wind speed autocorrelation values.

Analysis Figure 5.3 to Figure 5.7 reveals that when the maximum time lag is between 1 and 6 hours, the ACF differences are slightly higher in the first few hours. However, as time progresses, the simulated ACF values gradually converge toward the observed hourly wind speed ACF. Among these, a maximum time lag of 5 hours yields the best results, as it demonstrates the lowest error at initial lag hours and the most stable alignment with the observed ACF for late time lags. In contrast, when the maximum time lag ranges from 7 to 24 hours, the simulated ACF values become increasingly irregular and oscillatory. These fluctuations suggest that the simulations struggle to capture the observed ACF structure effectively, particularly for longer time lags. The deviation is especially pronounced beyond 15 hours, where the simulated ACF significantly diverges from the observed ACF, failing to preserve its temporal correlation.

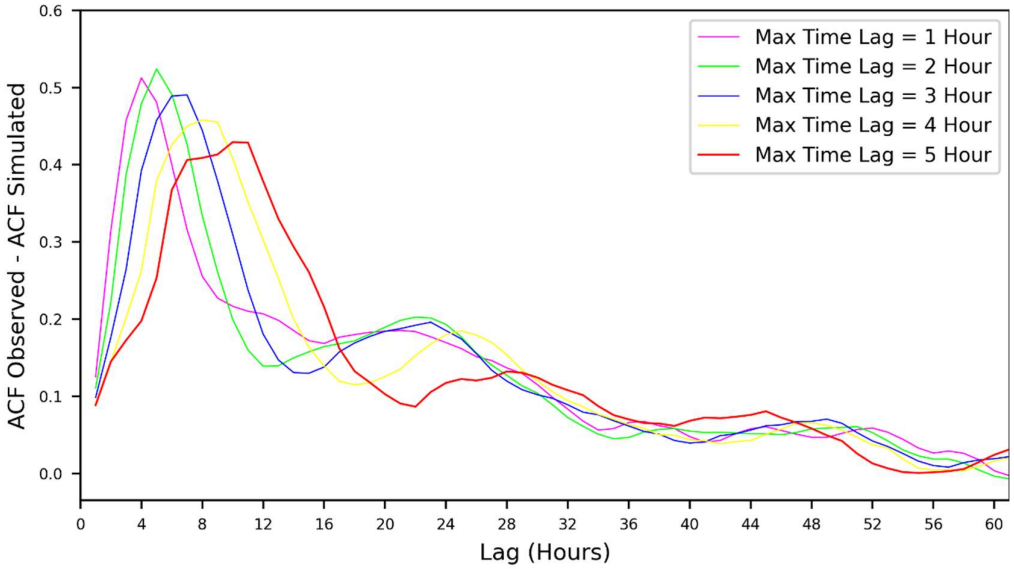

Figure 5.3 The error between ACF of Observed and Simulated Hourly Wind Speeds with maximum time lags of 1, 2, 3, 4, and 5 hours

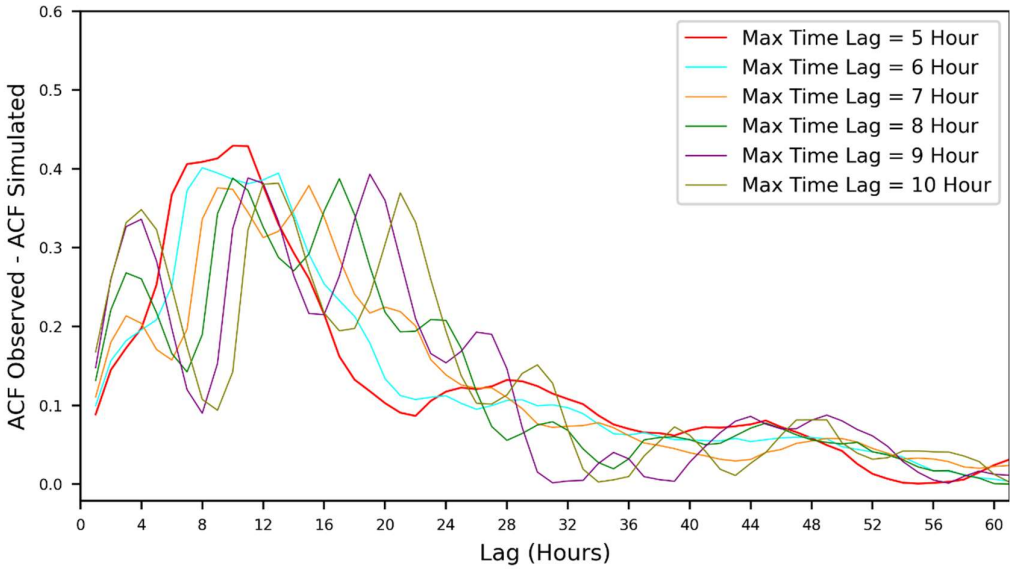

Figure 5.4 The error between ACF of Observed and Simulated Hourly Wind Speeds with maximum time lags of 5, 6, 7, 8, 9, and 10 hours

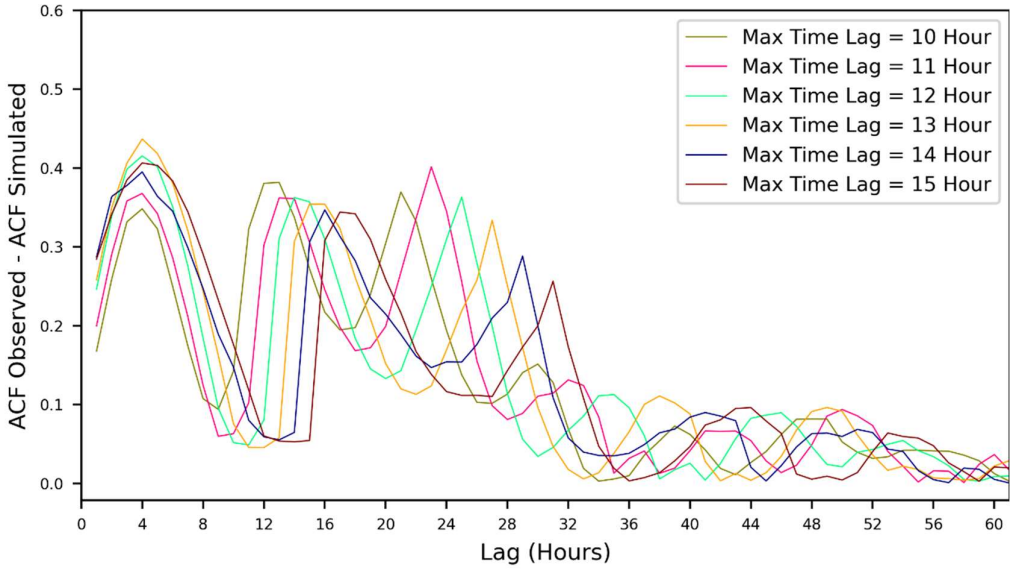

Figure 5.5 The error between ACF of Observed and Simulated Hourly Wind Speeds with maximum time lags of 10, 11, 12, 13, 14 and15 hours

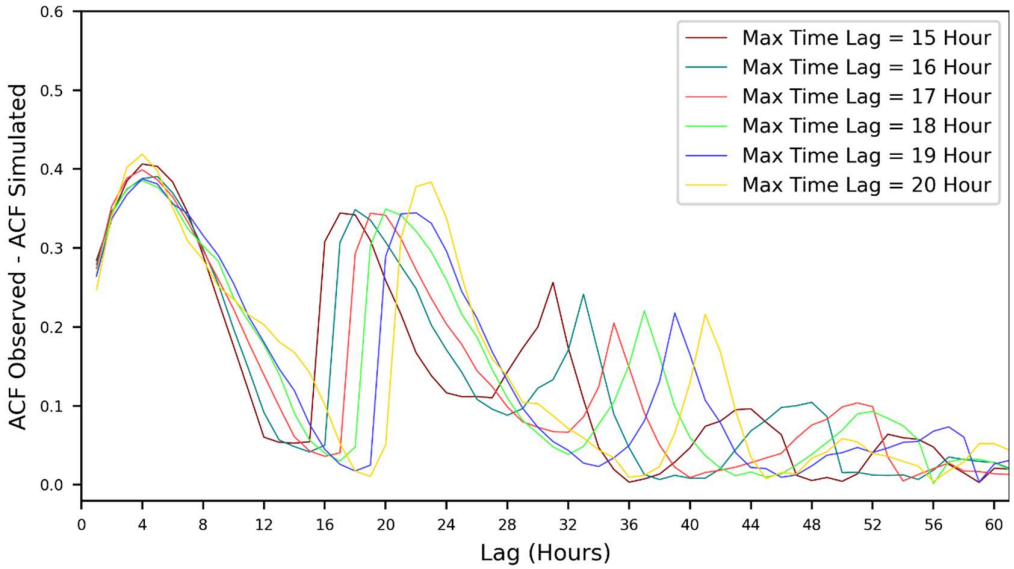

Figure 5.6 The error between ACF of Observed and Simulated Hourly Wind Speeds with maximum time lags of 15, 16, 17, 18, 19, and 20 hours

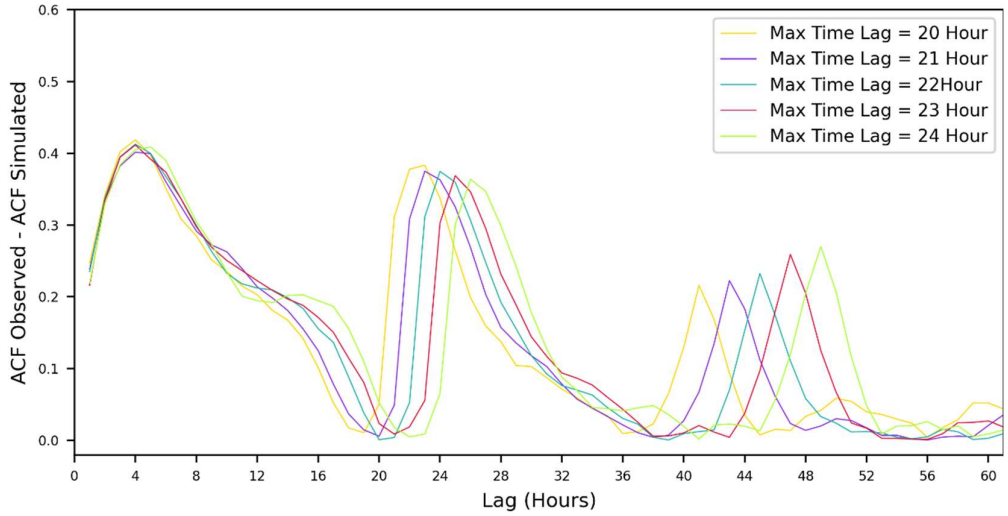

Figure 5.7 The error between ACF of Observed and Simulated Hourly Wind Speeds with maximum time lags of 20, 21, 22, 23, and 24 hours

Figure 5.3 and Figure 5.4 show that the autocorrelation values of the simulated hourly wind speeds which have a maximum time lag between 1 hour to 6 hours closely match the autocorrelation values of the observed hourly wind speeds, especially in the early lags. To facilitate a more precise comparison between the observed and simulated ACF values in the early lags, Table 5.1 presents the ACF values of simulated hourly wind speeds generated with maximum time lags of 1, 2, 3, 4, 5, and 6 hours, alongside the observed data's ACF values. ACF values are shown for the first 24 hours lag since after 24 hours lag all simulated hourly wind speeds (maximum time lags of 1, 2, 3, 4, 5, and 6 hours) ACF get close to each other as can be seen from Figure 5.3 and Figure 5.4.

Table 5.1 ACF of Simulated Hourly Wind Speeds for Maximum Time Lags up to 6 Hours

Max. Time Lag (Hours) / ACF Lag (Hours)	1	2	3	4	5	6	MS18386 Hourly Wind Speeds
0	1.00	1.00	1.00	1.00	1.00	1.00	1.00
1	0.76	0.77	0.78	0.79	0.79	0.78	0.88
2	0.45	0.55	0.59	0.62	0.62	0.61	0.77
3	0.20	0.27	0.39	0.45	0.48	0.47	0.65
4	0.02	0.06	0.14	0.27	0.34	0.34	0.53
5	-0.07	-0.11	-0.04	0.03	0.16	0.21	0.41
6	-0.10	-0.19	-0.19	-0.13	-0.07	0.05	0.30
7	-0.12	-0.23	-0.29	-0.25	-0.21	-0.18	0.20
8	-0.15	-0.23	-0.34	-0.35	-0.30	-0.29	0.11
9	-0.19	-0.22	-0.34	-0.42	-0.38	-0.36	0.04
10	-0.23	-0.21	-0.32	-0.42	-0.44	-0.40	-0.01
11	-0.26	-0.21	-0.29	-0.40	-0.48	-0.43	-0.05
12	-0.28	-0.21	-0.25	-0.37	-0.45	-0.46	-0.07
13	-0.27	-0.21	-0.22	-0.32	-0.40	-0.46	-0.07
14	-0.24	-0.20	-0.18	-0.25	-0.35	-0.40	-0.05
15	-0.19	-0.18	-0.15	-0.18	-0.28	-0.31	-0.02
16	-0.14	-0.13	-0.11	-0.11	-0.18	-0.22	0.03
17	-0.08	-0.07	-0.06	-0.02	-0.06	-0.13	0.10
18	0.00	0.01	0.01	0.06	0.05	-0.03	0.18
19	0.08	0.09	0.09	0.15	0.15	0.09	0.27
20	0.17	0.17	0.17	0.23	0.25	0.22	0.36
21	0.26	0.24	0.25	0.31	0.35	0.33	0.44
22	0.33	0.31	0.32	0.36	0.42	0.40	0.51
23	0.38	0.35	0.36	0.39	0.45	0.44	0.56
24	0.40	0.37	0.38	0.39	0.45	0.45	0.57

Based on Table 4.1, during the initial hours, the simulated hourly wind speeds using a maximum time lag of 5 hours yield the most accurate results, closely matching the observed hourly wind speeds. According to the findings from the sensitivity analysis, setting the maximum time lag to 5 hours appears to be the most effective approach for achieving an accurate representation of the observed wind speed ACF.

As a result of the analyses conducted above, the most suitable maximum time lag for this study has been determined as 5-hours. Hence, a maximum time lag of 5 hours is used in the optimization step of aLHS. From here on the simulated hourly wind speed generated using a 5-hour maximum time lag will be referred to as the simulated hourly wind speeds.

5.1.2 Autocorrelated Latin Hypercube Sampling (aLHS)

After determining the maximum lag time as 5 hours, the aLHS procedure is carried out. Then to preserve the autocorrelation structure, a reordering process is applied to the sampled data using the Powell optimization method where the semivariogram of the reordered data is matched to that of the observed data, by minimizing the total semivariance error across lags of 1 to 5 hours which is the maximum lag time. Although a maximum of 1,000,000 iterations is allowed, convergence is typically achieved within 20 to 40 iterations in this study. After the de-standardization step simulated hourly wind speed time series for a year is obtained.

5.1.3 Hourly Wind Speed Simulation Results

Using the methodology outlined in Section 3.1, 1,000 simulated hourly wind speeds for a year are generated. To evaluate the effectiveness of this approach, the statistical properties of these simulated wind speeds are compared with those observed hourly wind speeds recorded between 2014 and 2023. The following paragraphs present a detailed comparison of their statistical characteristics, highlighting the performance of the simulation methodology.

In Figure 5.8, the diurnal variation of the observed hourly wind speeds from 2014 to 2023 and the simulated hourly wind speeds are presented. The observed dataset consists of 83,521 hourly wind speed data (10×365×24-missing data). On the other hand, simulated data includes 1,000 separate one-year-long hourly wind speed series, resulting in a total of approximately 8,760,000 simulated hourly wind speed data (1,000×365×24). In Figure 5.9, out of 83,521 observed wind speed data points, 80,389 (96.25%) falls within the whisker range of the boxplot, while 3,132 values (3.75%) are considered outliers. Similarly, in the simulated dataset containing 8,760,000 values, 8,454,470 (96.51%) are within the whiskers, and 305,530 (3.49%) are outliers.

As can be seen from Figure 5.8, both datasets exhibit a clear diurnal pattern, with wind speeds increasing during the afternoon hours (approximately between 13:00 and 17:00). The median values and interquartile ranges of the simulated data are similar to those of the observed data, indicating that the simulation method effectively captures both the central tendency and variability. While the proportion of outliers in both datasets is approximately the same (3.75% for observed and 3.49% for simulated), the outlier values in the simulated dataset tend to be higher than those in the observed dataset. This is due to the sampling of extreme events with longer return periods, which are rarely or not observed in the historical dataset, but are sampled during 1,000 simulation cycles.

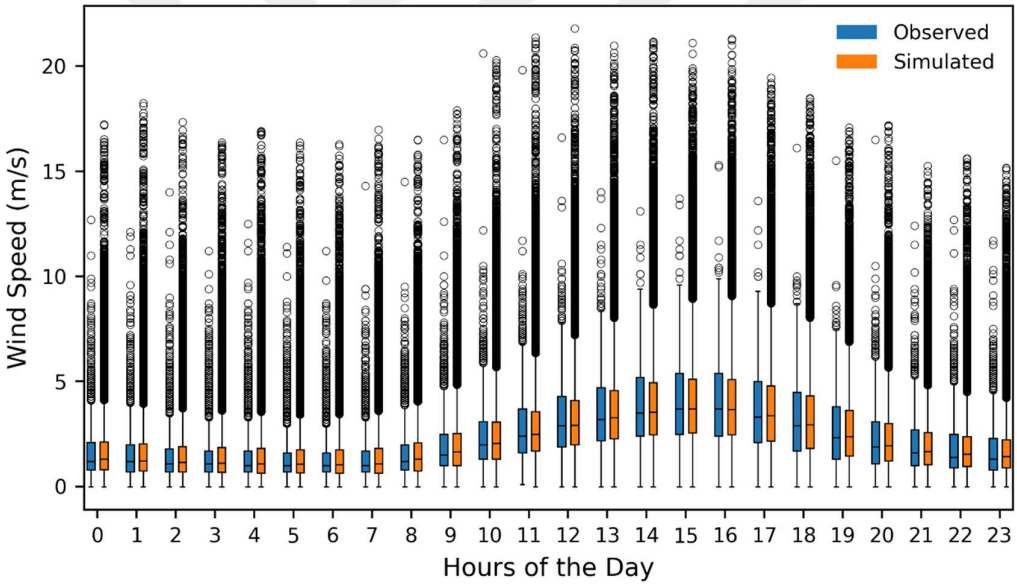

Figure 5.8 Diurnal Variation of Observed and Simulated Hourly Wind Speeds

In Figure 5.9, diurnal variation of standardized observed and simulated hourly wind speeds are presented. The standardized observed and standardized simulated hourly wind speeds do not exhibit a diurnal pattern, as the standardization removes the diurnal behavior. The distributions of both datasets appear centered around zero with similar interquartile ranges, indicating that the simulation method preserves the relative variability in wind speed. In Figure 5.10, 80,180 out of 83,521 observed values (95.98%) fall within the whisker range, leaving 3,341 values (4.02%) as

outliers. In the simulated dataset, 8,437,765 out of 8,760,000 values (96.32%) lie within the whiskers, with 322,235 (3.68%) classified as outliers.

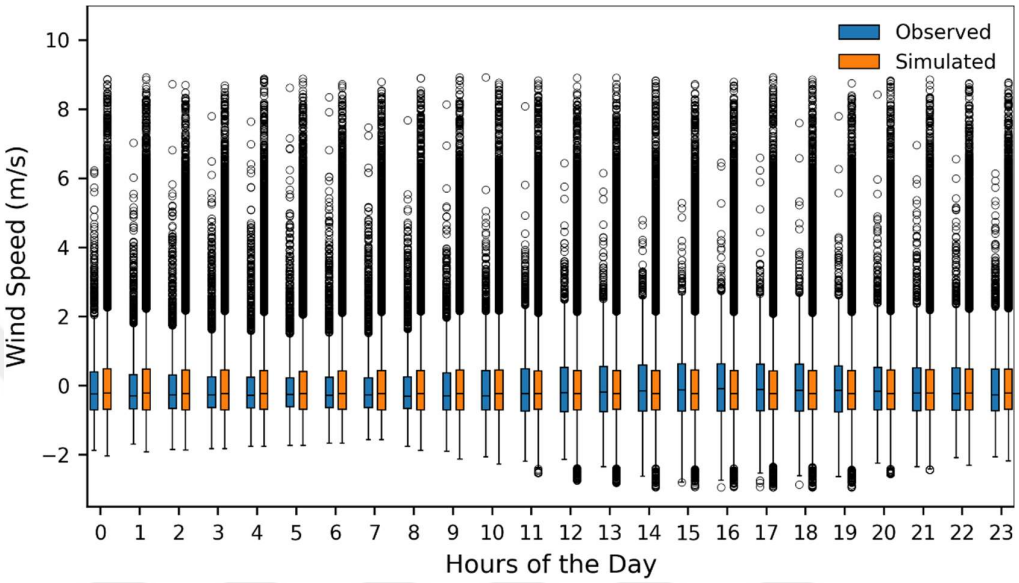

Figure 5.9 Diurnal Variation of Standardized Observed and Standardized Simulated Hourly Wind Speeds

Figure 5.10 compares the monthly distribution of observed (blue) and simulated (orange) hourly wind speeds. Overall, the simulated data successfully reproduces the seasonal trend observed in the historical dataset. The median values of the simulated wind speeds are generally close to those of the observed data, although some deviations are present—particularly in July and August, where the simulated medians are higher, and in November, where they are slightly lower. The observed data tends to show wider whisker ranges, indicating greater variability within the central distribution. Notably, although the proportion of outliers in both datasets (%2.70 for observed and % 3.06 for simulated) are similar, the outlier values in the simulated dataset are typically higher than those in the observed dataset. This may again be due to the sampling of extreme events with longer return periods, which are not or rarely observed in the historical dataset, but are sampled during 1,000 simulation cycles.

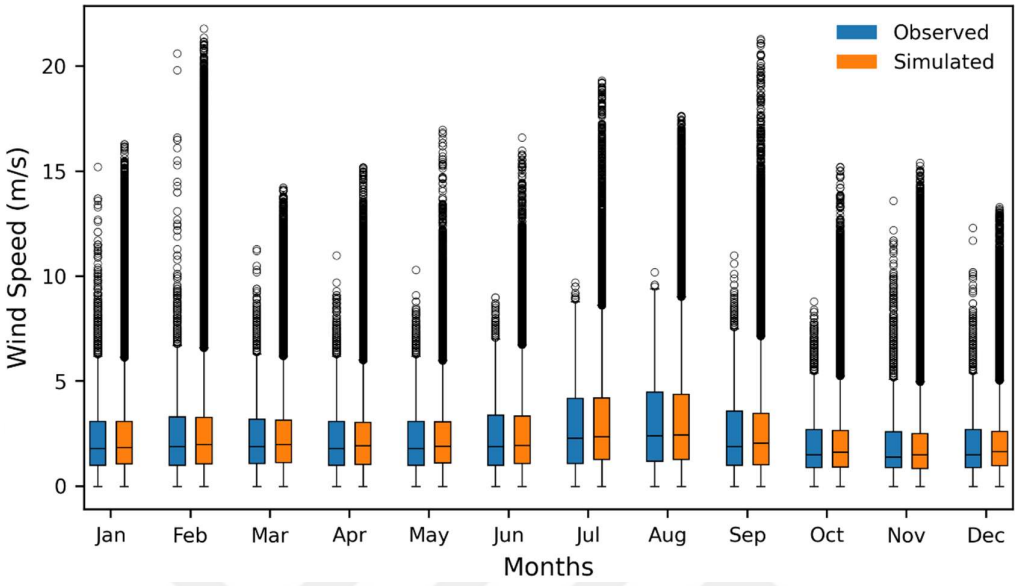

Figure 5.10 Monthly Variation of Observed and Simulated Hourly Wind Speeds

In Figure 5.11, monthly variation of standardized observed and simulated hourly wind speeds is presented. For both boxplots, the outliers are around 4%.

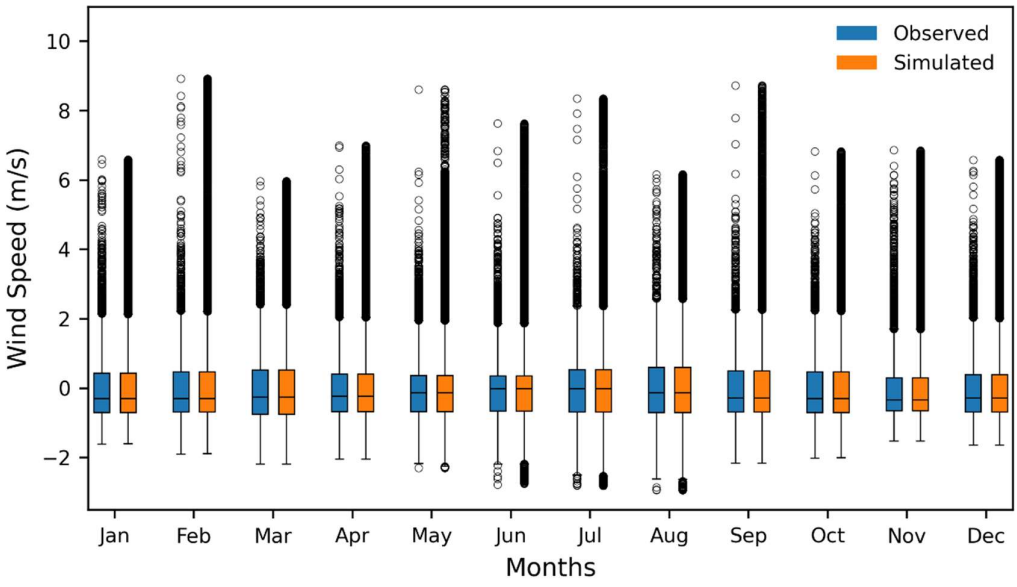

Figure 5.11 Monthly Variation of Standardized Observed and Standardized Simulated Hourly Wind Speeds

Figure 5.12 displays the CDFs of both observed and simulated hourly wind speeds. The black lines represent the CDFs of observed hourly wind speeds for each year between 2014 and 2023, while the green lines correspond to the CDFs of 1,000 simulated hourly wind speed time series, each representing a simulation year. The simulated CDFs closely follow the range and shape of the observed CDFs, indicating that the simulation method effectively reproduces the overall statistical distribution of the historical wind speed data. The agreement is particularly strong in the central part of the distribution, while minor deviations can be observed in the tails, especially at higher wind speed values. This suggests that the simulation model successfully captures the general probabilistic behavior of wind speeds, with slight differences likely due to the rare extreme events introduced during the sampling process.

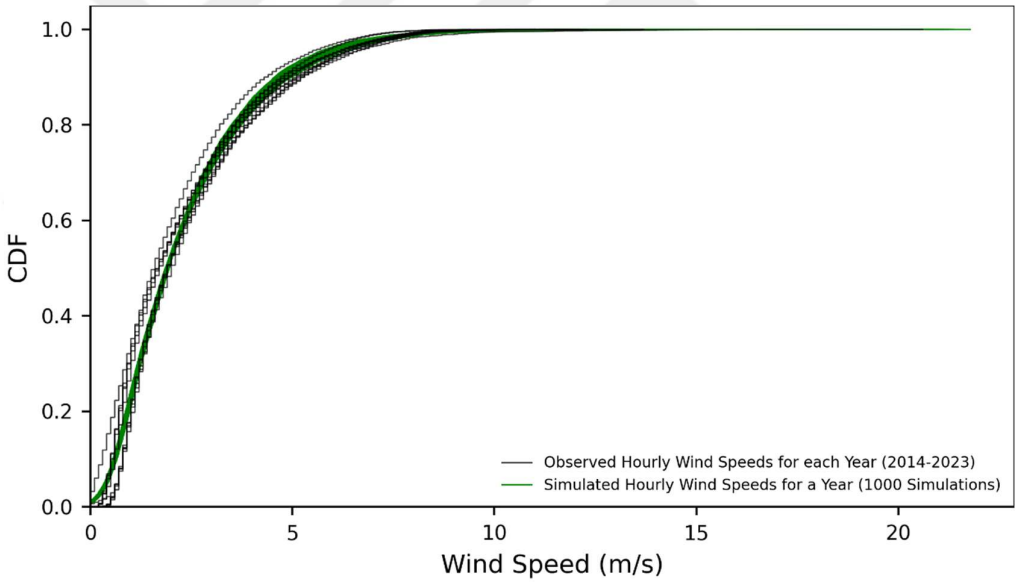

Figure 5.12 CDFs of Observed and Simulated Hourly Wind Speeds

Figure 5.13 presents the ACFs of observed and simulated hourly wind speeds up to a lag of 72 hours. The blue line represents the ACF calculated from the observed data spanning the years 2014 to 2023, while the orange line corresponds to the ACF computed from the 1,000 simulated hourly wind speed time series. Both curves exhibit a clear 24-hour periodicity, reflecting the diurnal nature of wind speed. The simulated ACF closely follows the observed ACF, particularly at larger lags,

indicating that the simulation method successfully captures the temporal dependency structure of wind speed. However, slight underestimations are observed in the simulated ACF at lower lags, suggesting a somewhat weaker short-term autocorrelation in the simulated data compared to the observed data.

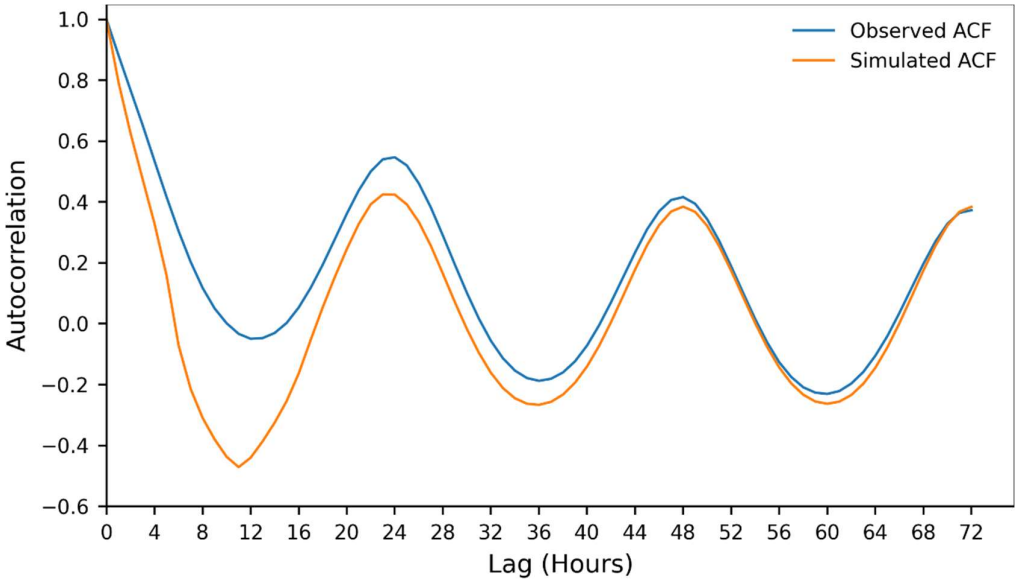

Figure 5.13 ACF of both Observed and Simulated Hourly Wind Speeds

5.2 Daily Revenue Optimization Model

The simulation outcomes of the WHHS annual revenue, reflecting uncertainties in electricity prices and wind speeds, are presented in two sections: Section 5.2.1 details the results for a WHHS with a wind farm of 50 MW installed capacity, while Section 5.2.2 outlines the outcomes for a WHHS with a wind farm of 250 MW installed capacity.

5.2.1 Daily Revenue Optimization Results of WHHS with a 50 MW Installed Capacity

In Figure 5.14 to Figure 5.26, the daily revenues for each year from 2012 to 2024 are presented, showcasing the optimized performance of a WHHS with a wind farm of 50 MW installed capacity under varying electricity price and wind speed conditions. For the years between 2014 and 2023, observed hourly wind speed data is available. Therefore, for these specific years, the daily revenues calculated using observed hourly wind speeds and the corresponding realized electricity prices are also included in Figures 5.16 to 5.25. These additional red lines represent the WHHS revenue that would have been obtained based on actual wind and price conditions. The average daily revenues (i.e., the average of 1,000 simulations) for each year from 2012 to 2024 are shown for a WHHS with a wind farm of 50 MW installed capacity on Figure 5.27.

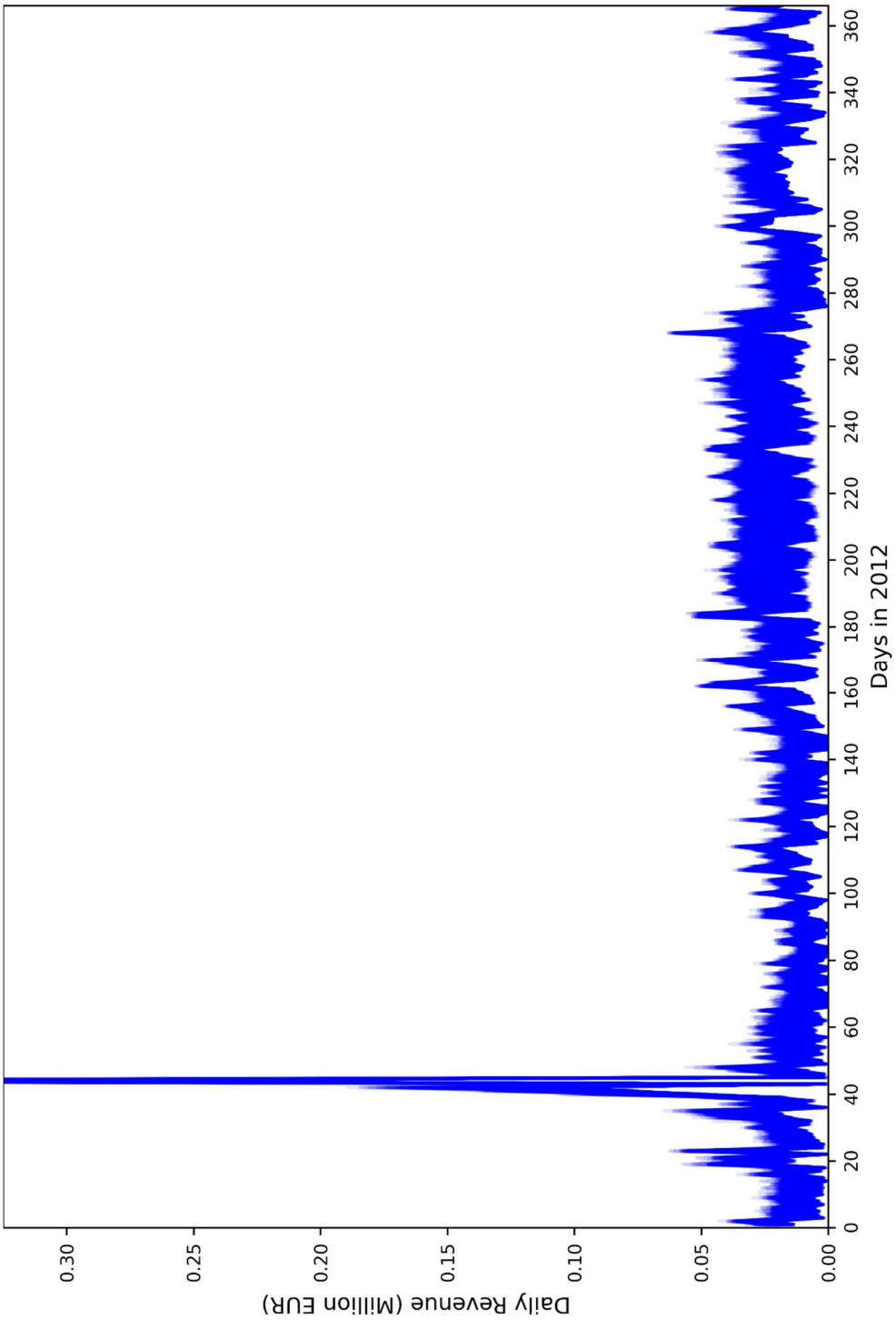

Figure 5.14 Optimized Daily Revenues for Realized Electricity Price Year 2012. In February 13, daily revenue reached approximately 0.62 million euros, which is not shown on the figure to enhance the representation in the rest of the days.

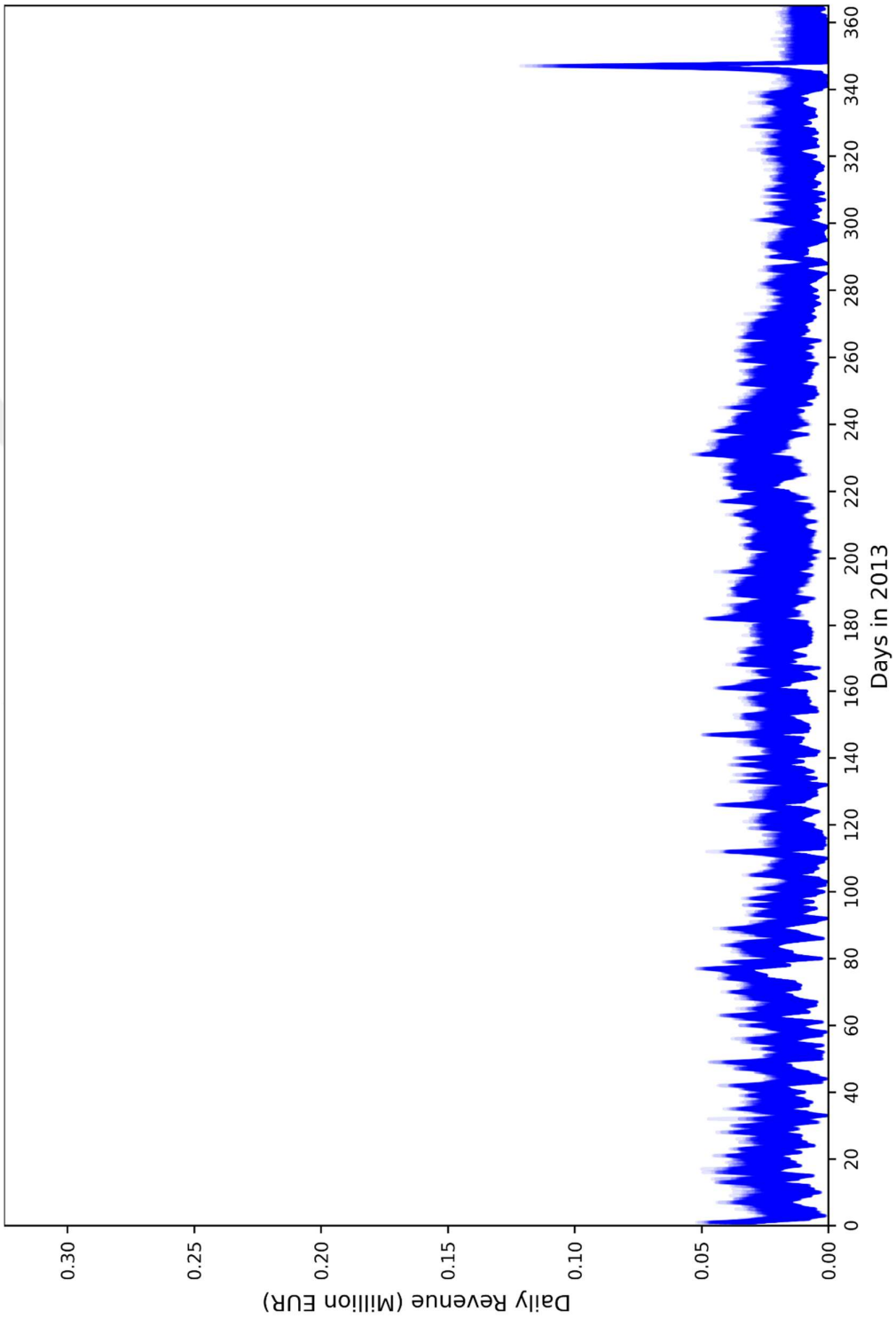

Figure 5.15 Optimized Daily Revenues for Realized Electricity Price Year 2013

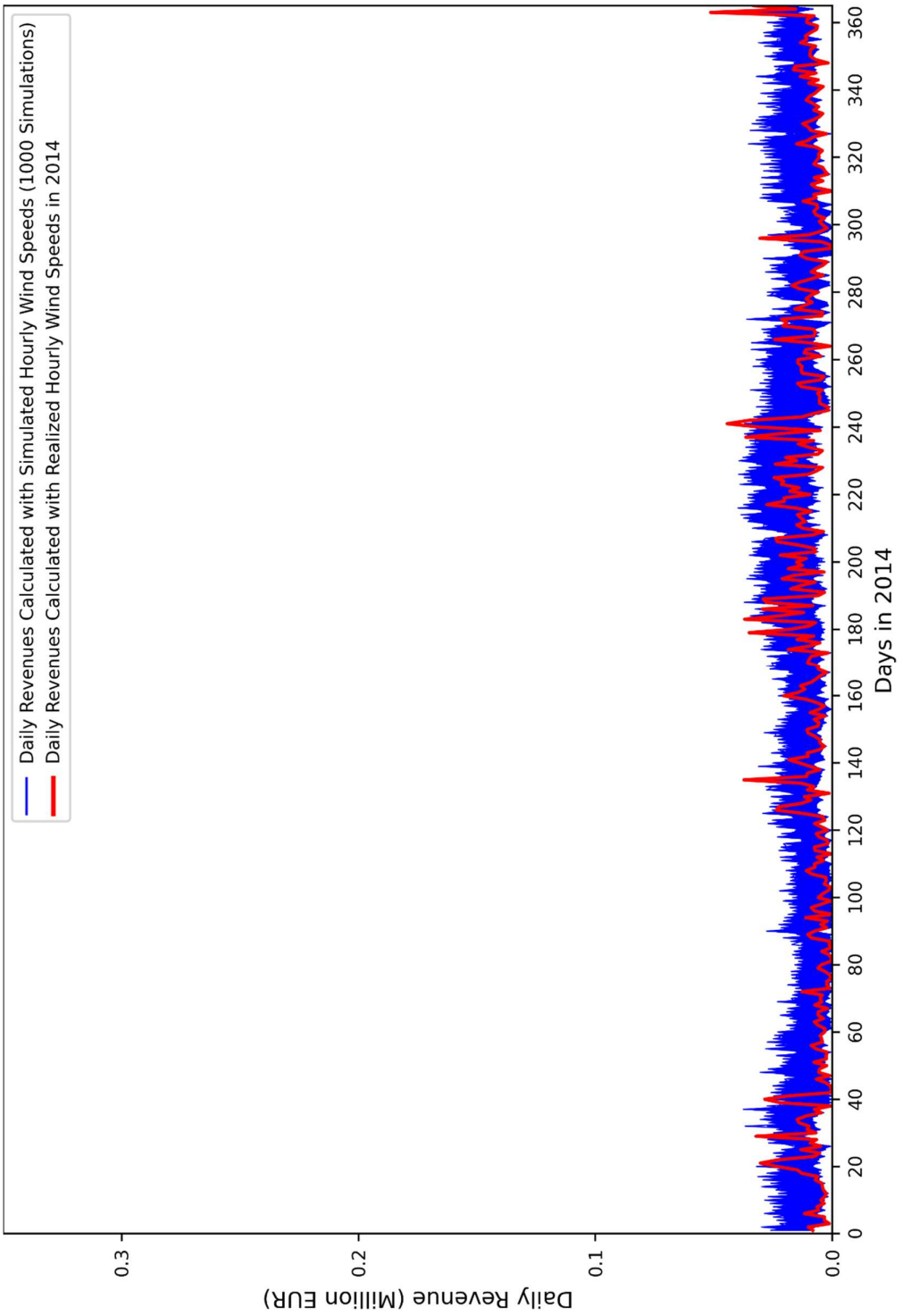

Figure 5.16 Optimized Daily Revenues for Realized Electricity Price Year 2014

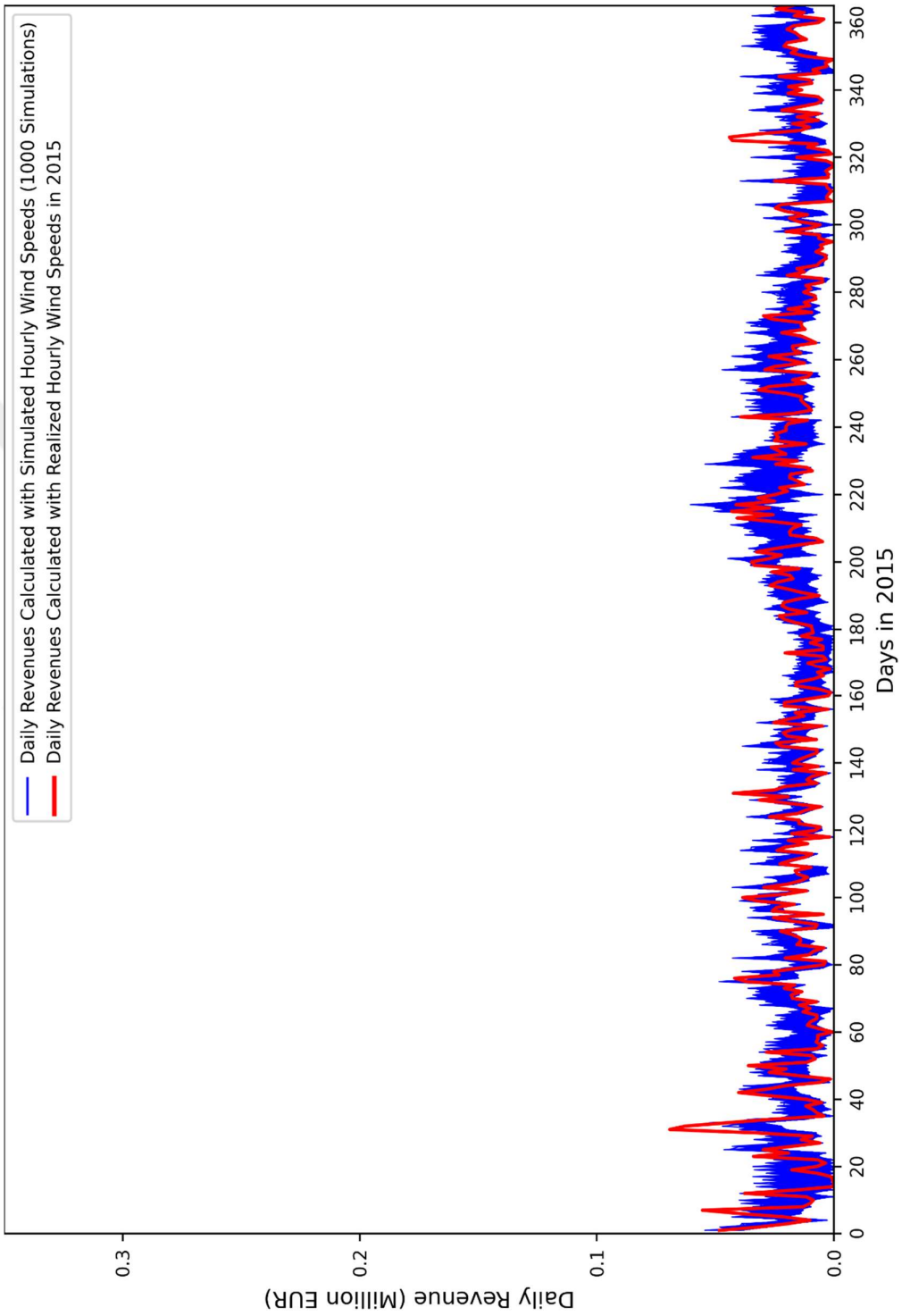

Figure 5.17 Optimized Daily Revenues for Realized Electricity Price Year 2015

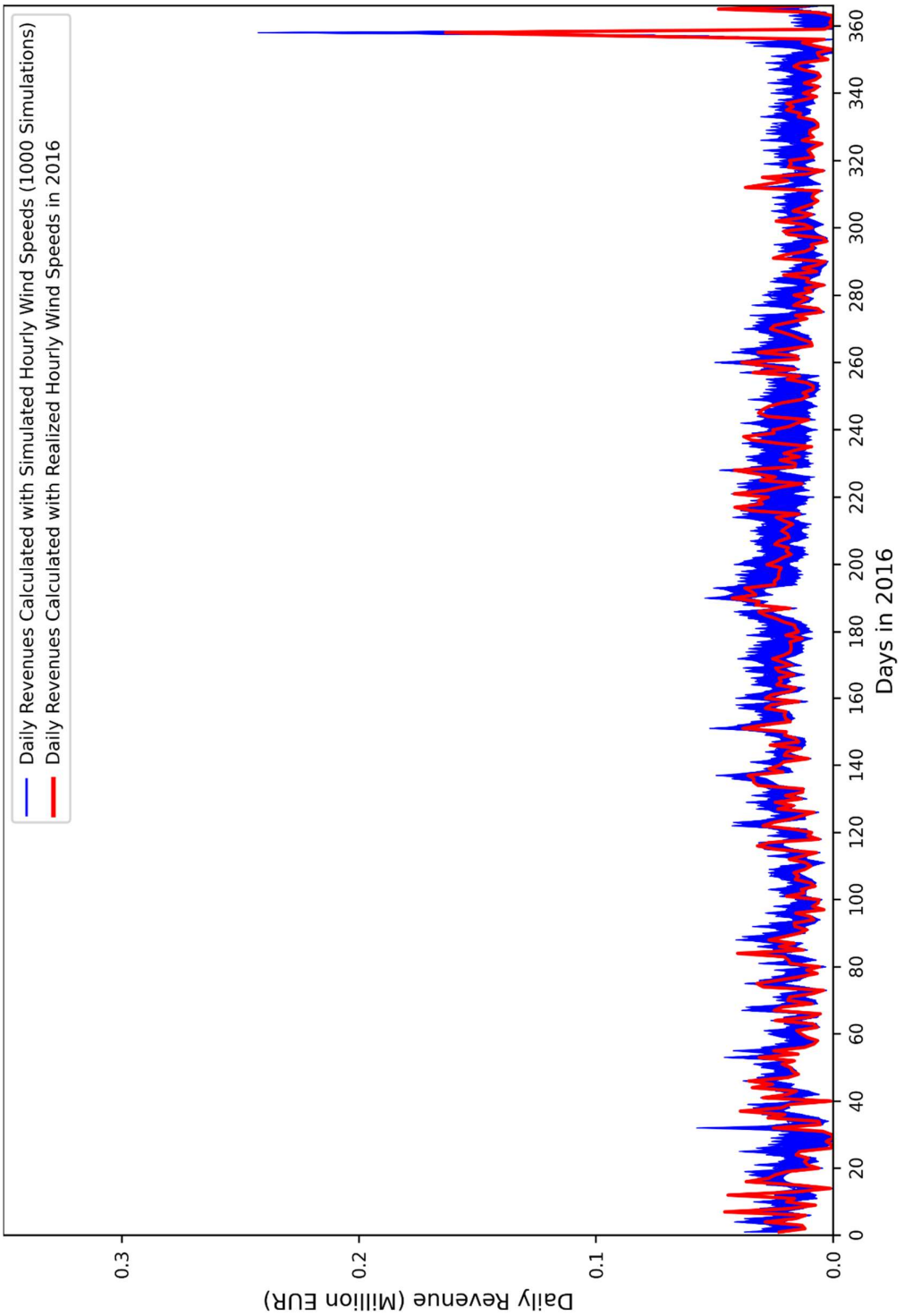

Figure 5.18 Optimized Daily Revenues for Realized Electricity Price Year 2016

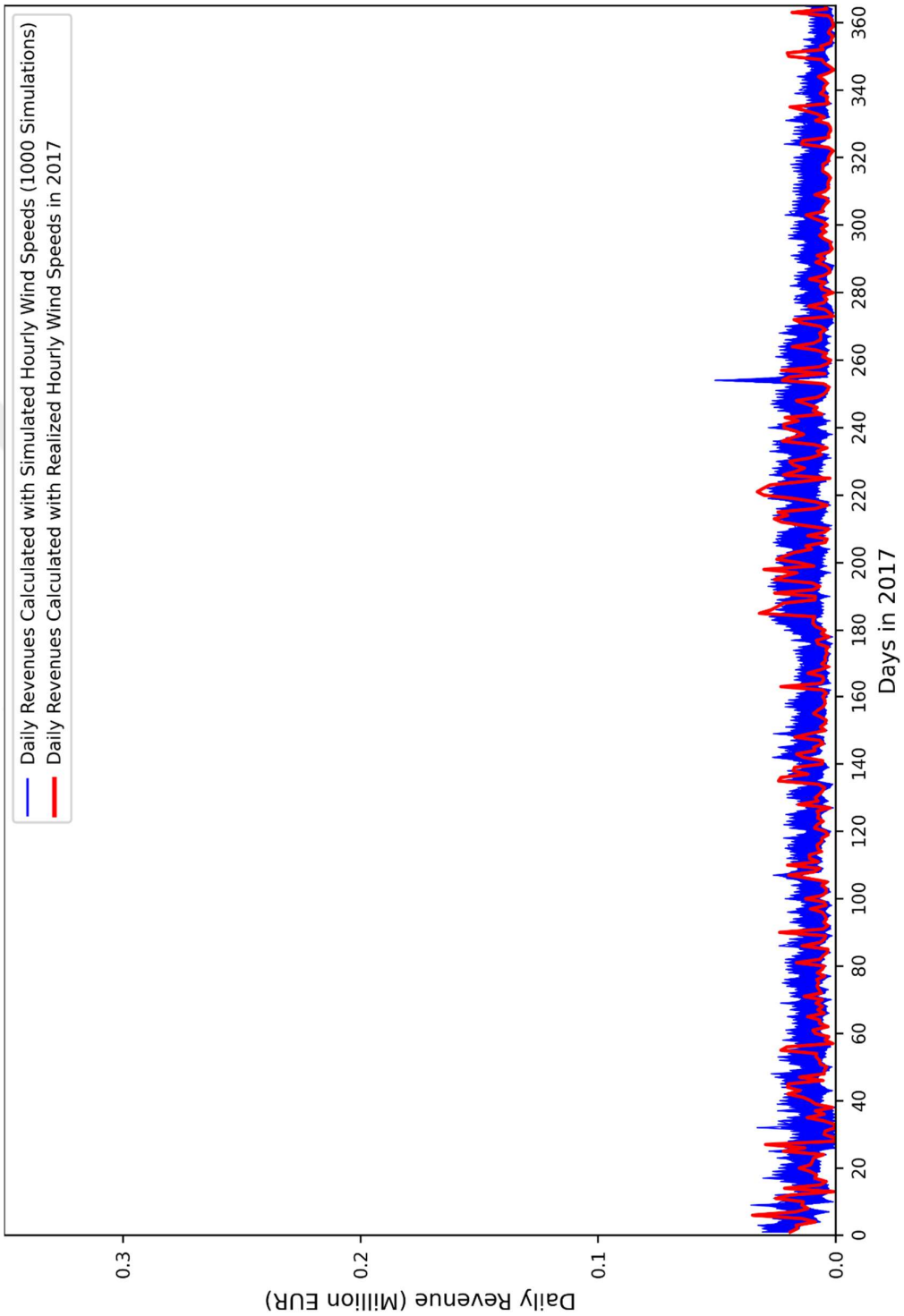

Figure 5.19 Optimized Daily Revenues for Realized Electricity Price Year 2017

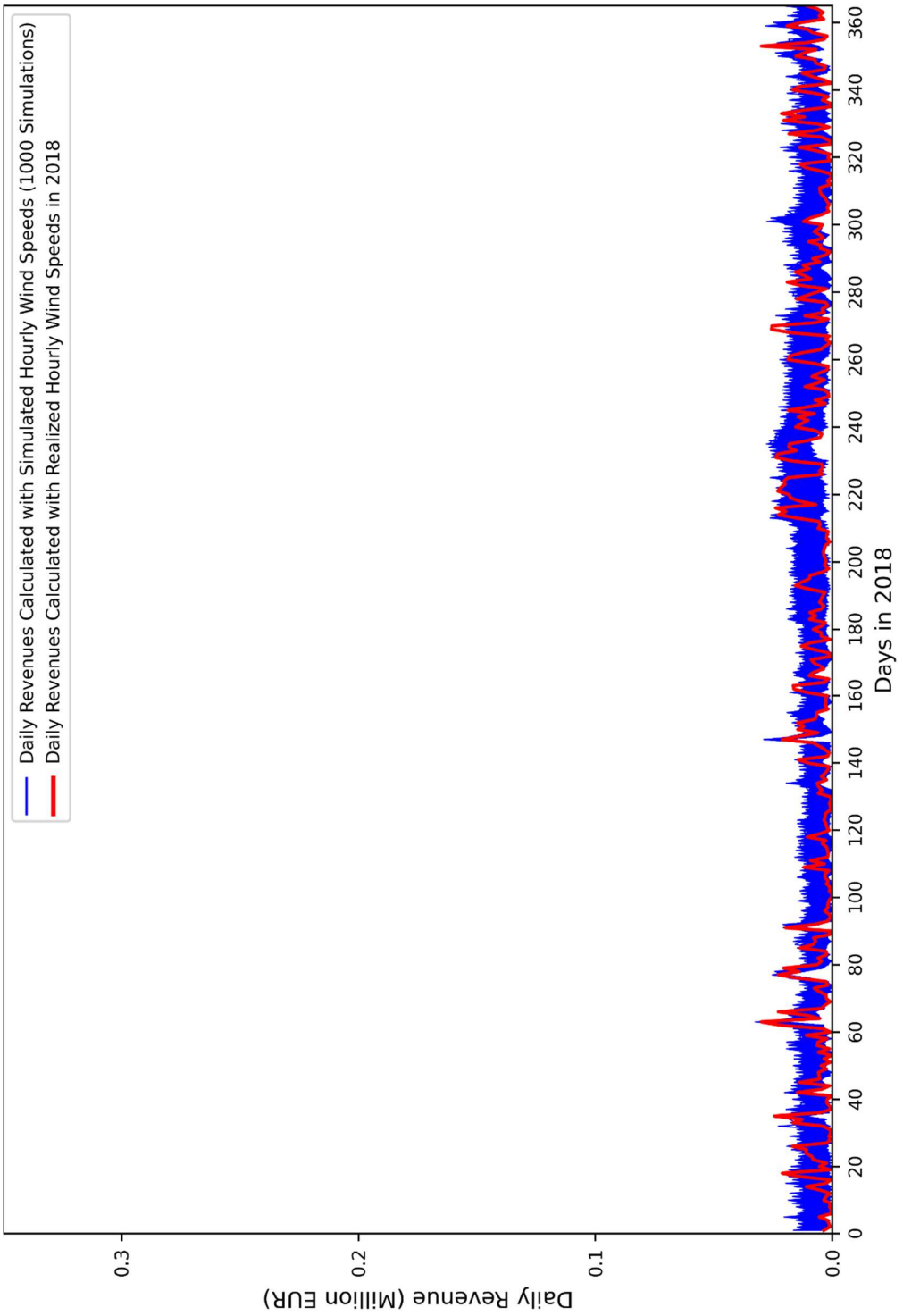

Figure 5.20 Optimized Daily Revenues for Realized Electricity Price Year 2018

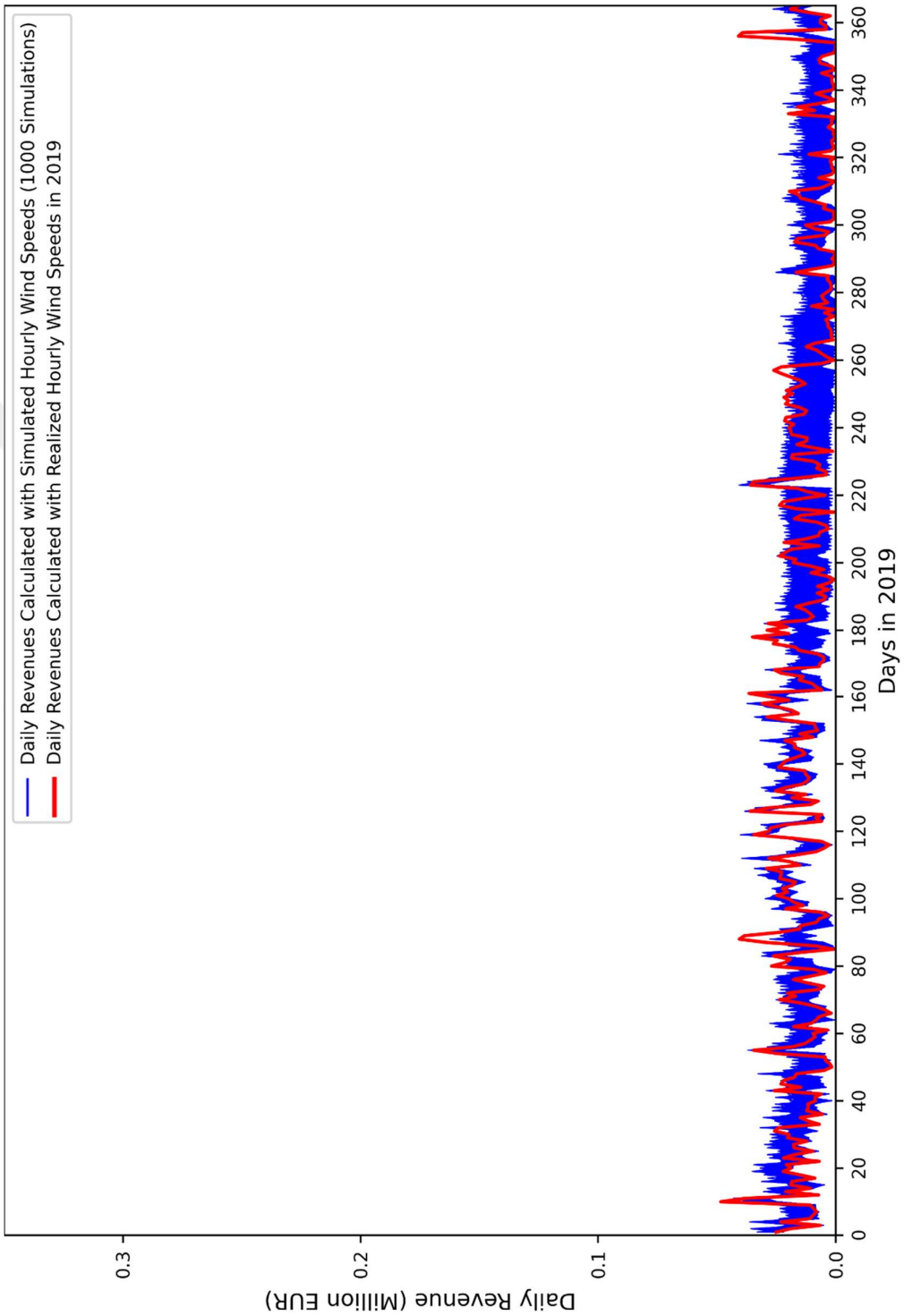

Figure 5.21 Optimized Daily Revenues for Realized Electricity Price Year 2019

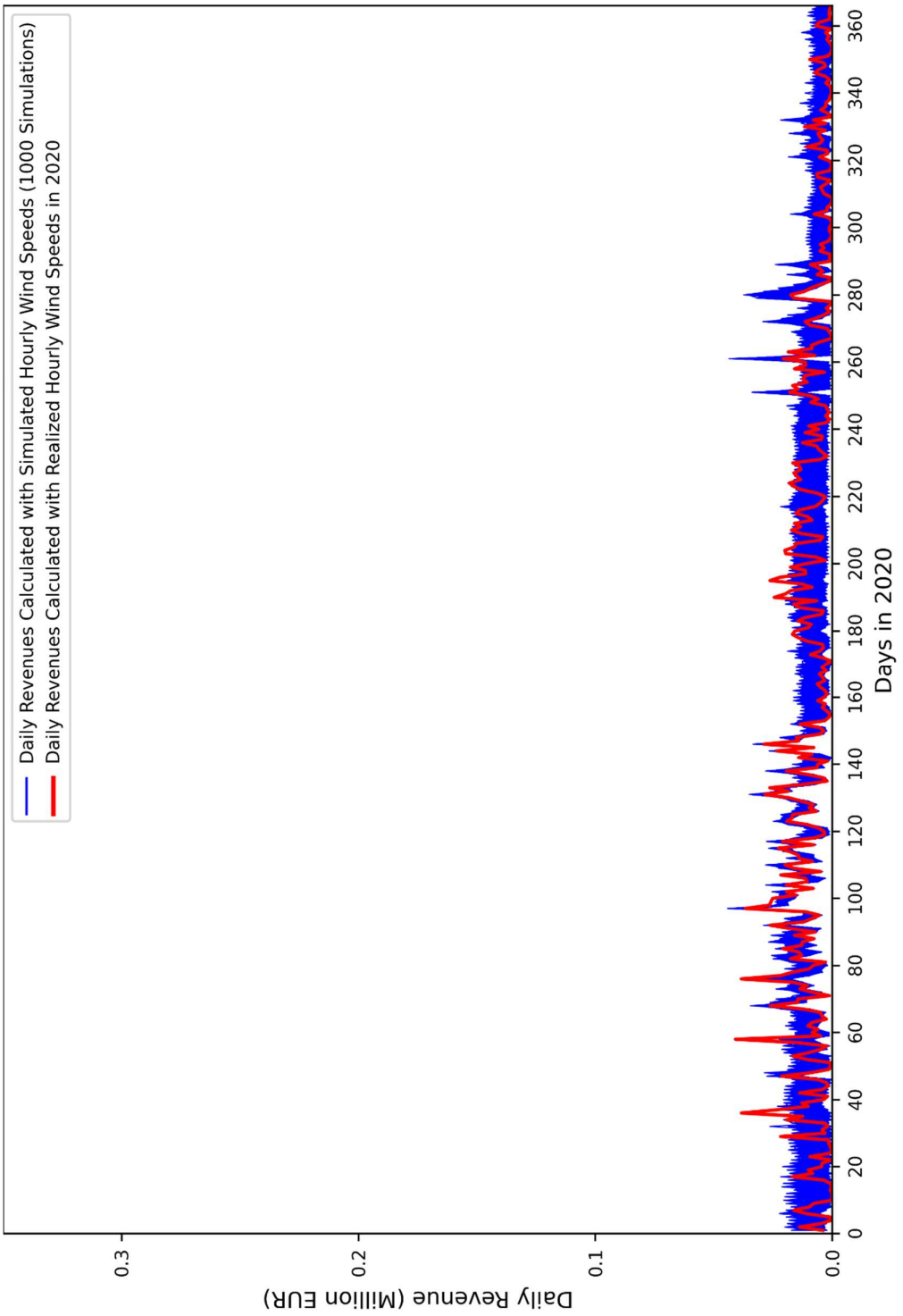

Figure 5.22 Optimized Daily Revenues for Realized Electricity Price Year 2020

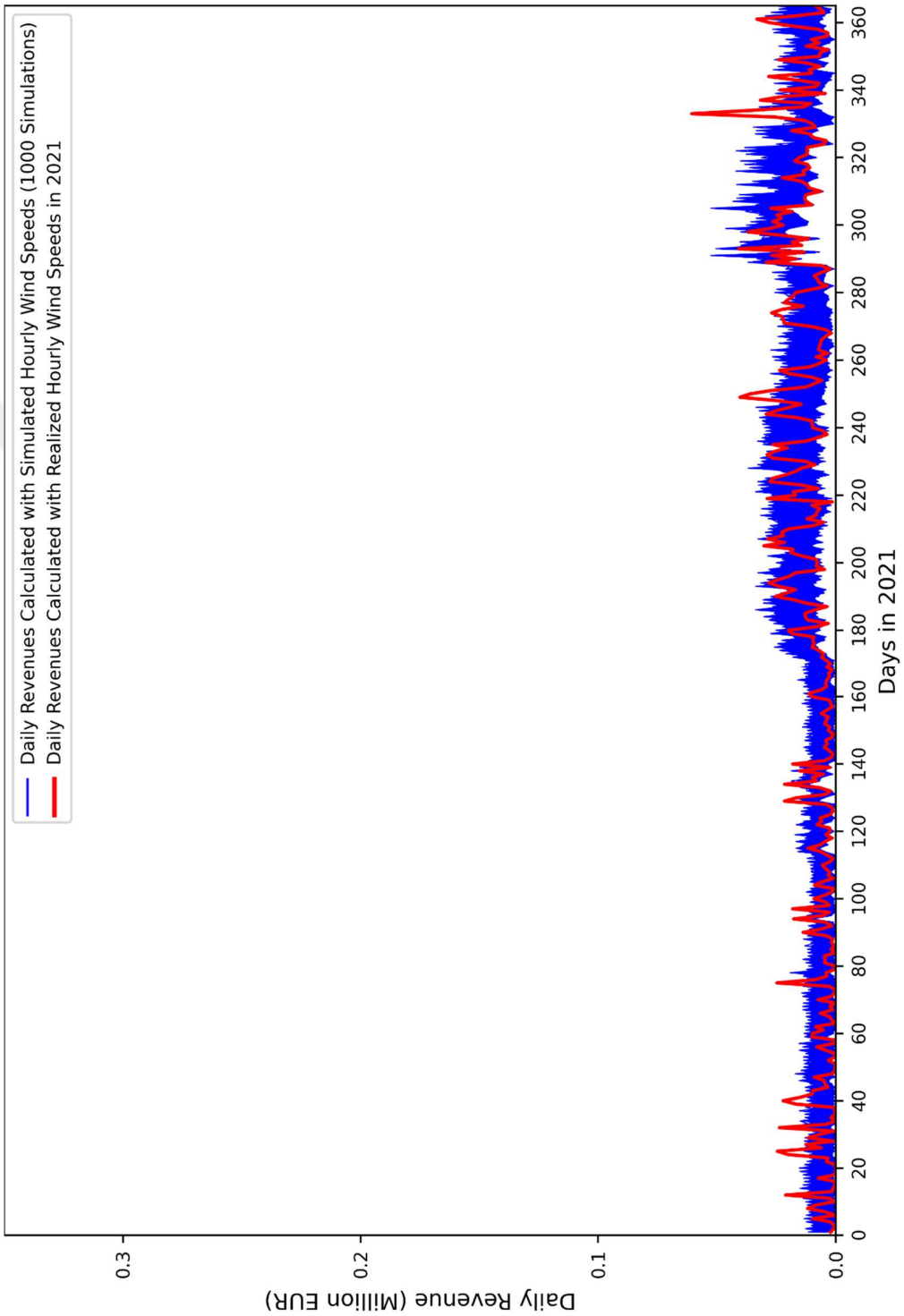

Figure 5.23 Optimized Daily Revenues for Realized Electricity Price Year 2021

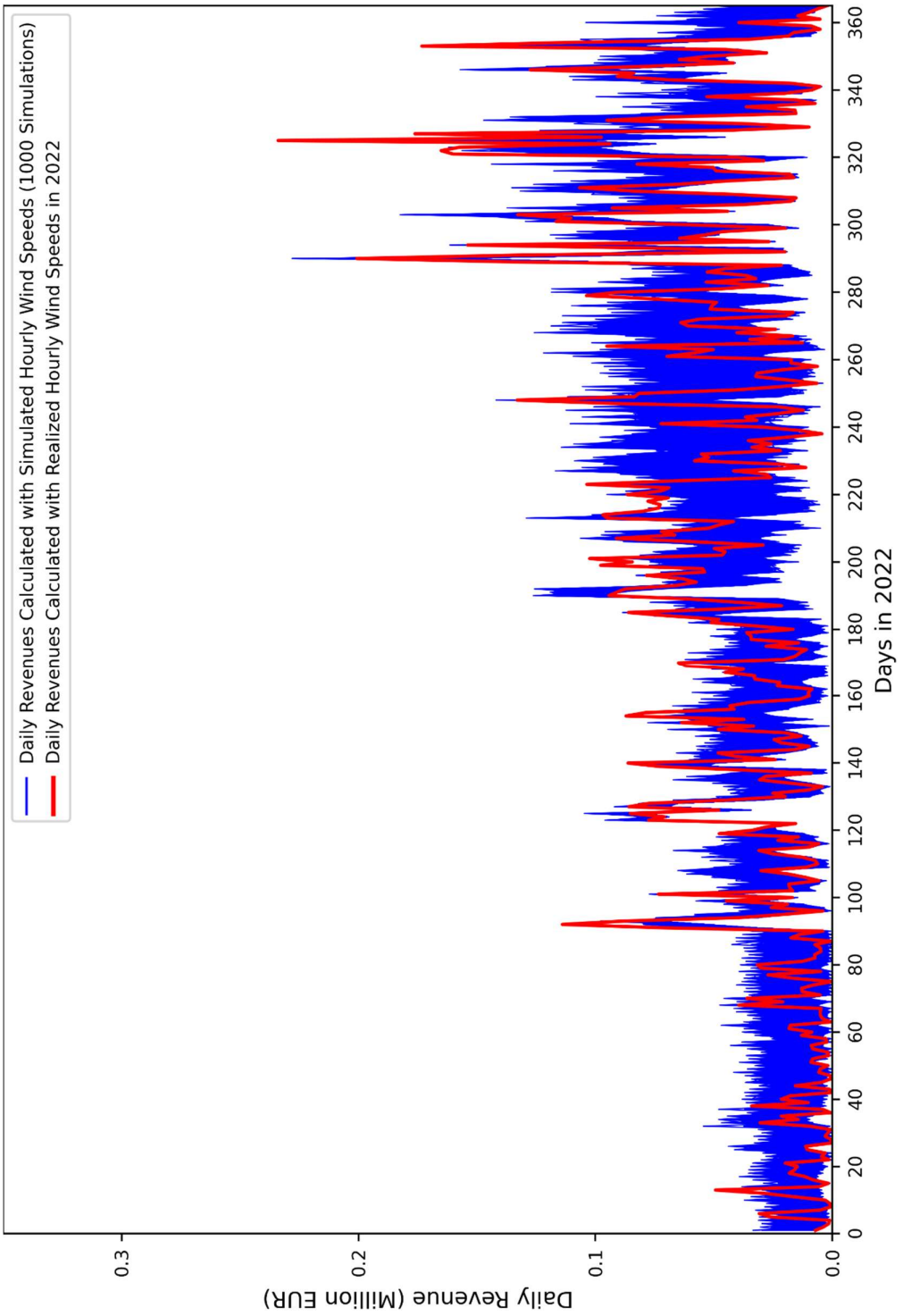

Figure 5.24 Optimized Daily Revenues for Realized Electricity Price Year 2022

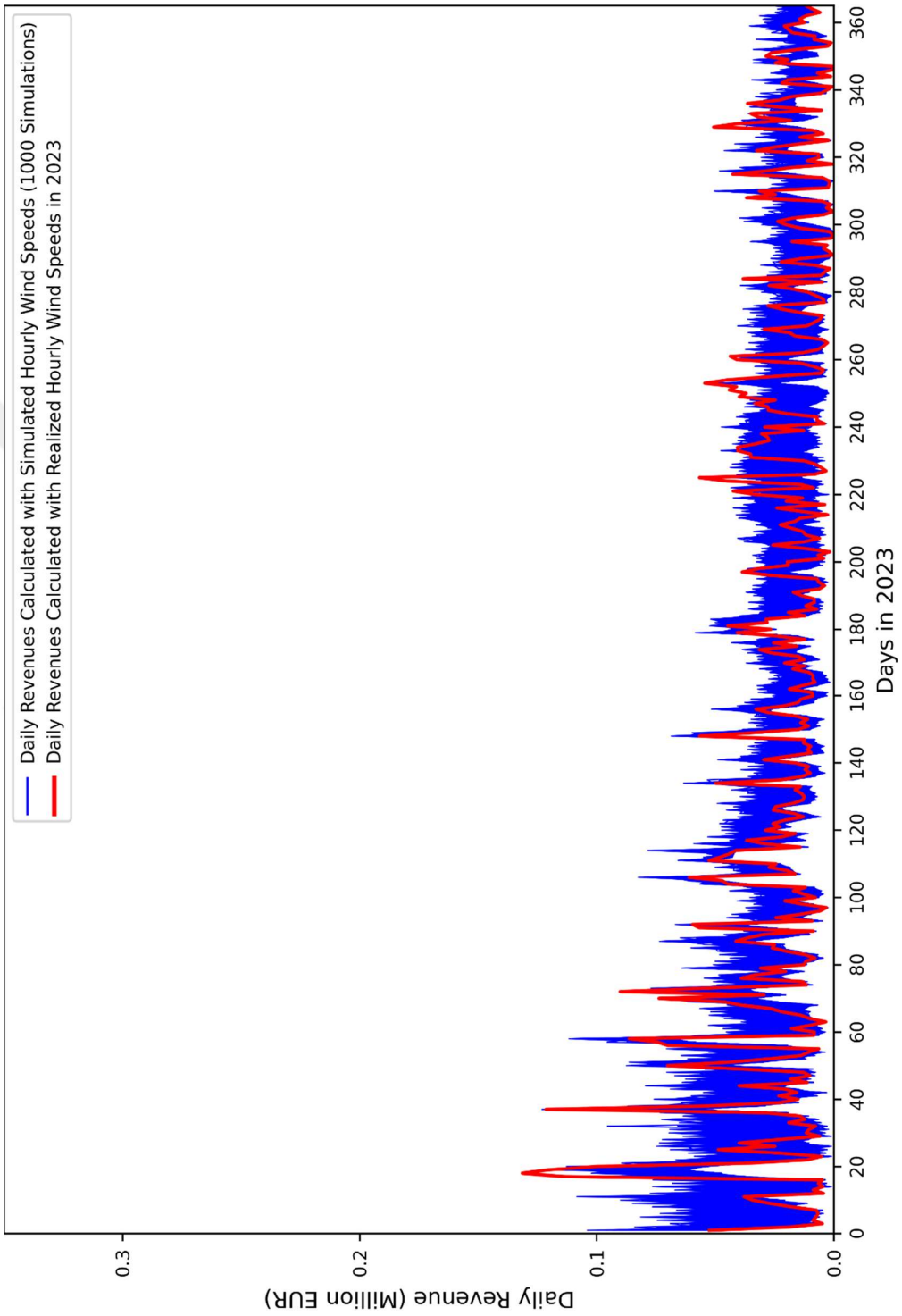

Figure 5.25 Optimized Daily Revenues for Realized Electricity Price Year 2023

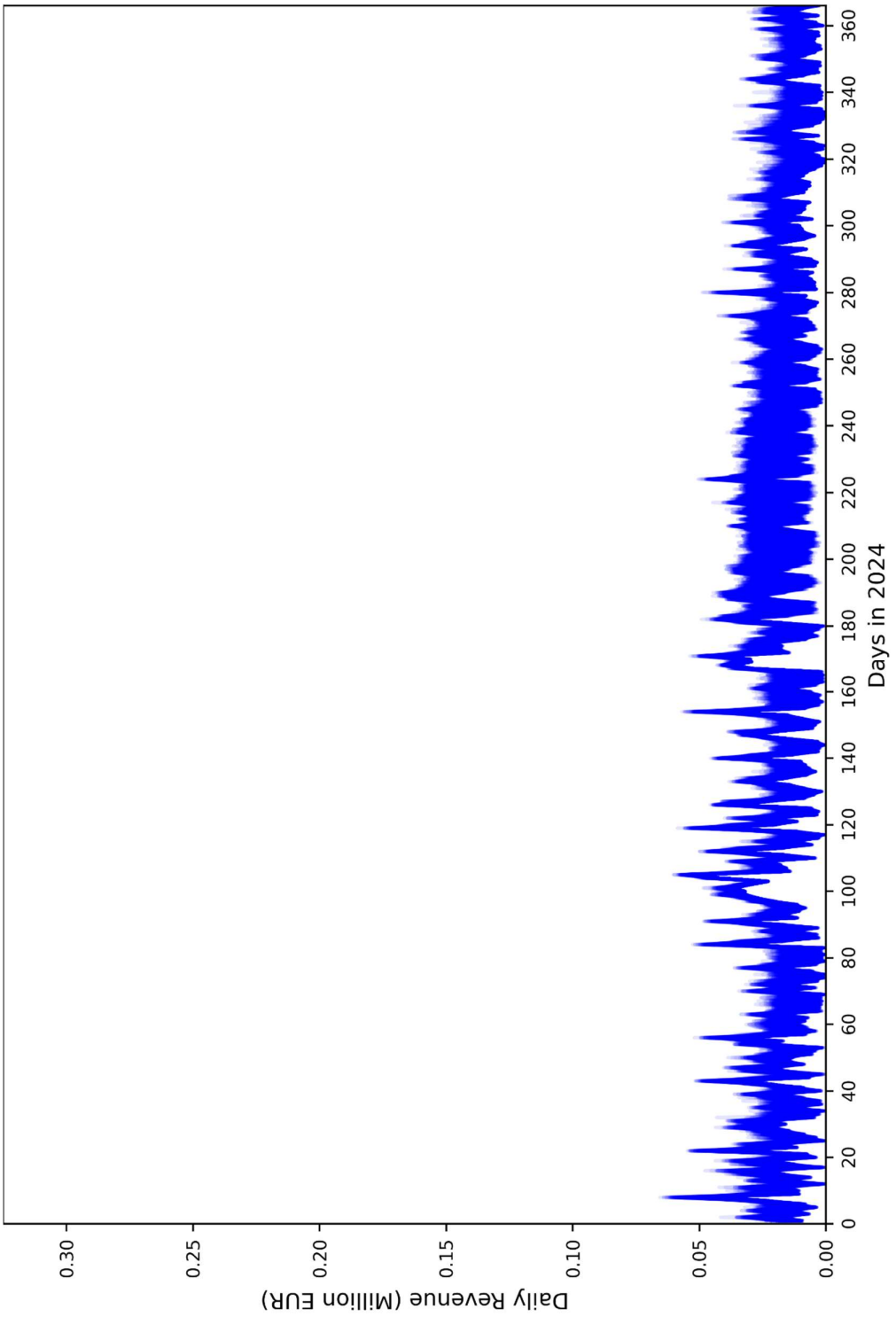

Figure 5.26 Optimized Daily Revenues for Realized Electricity Price Year 2024

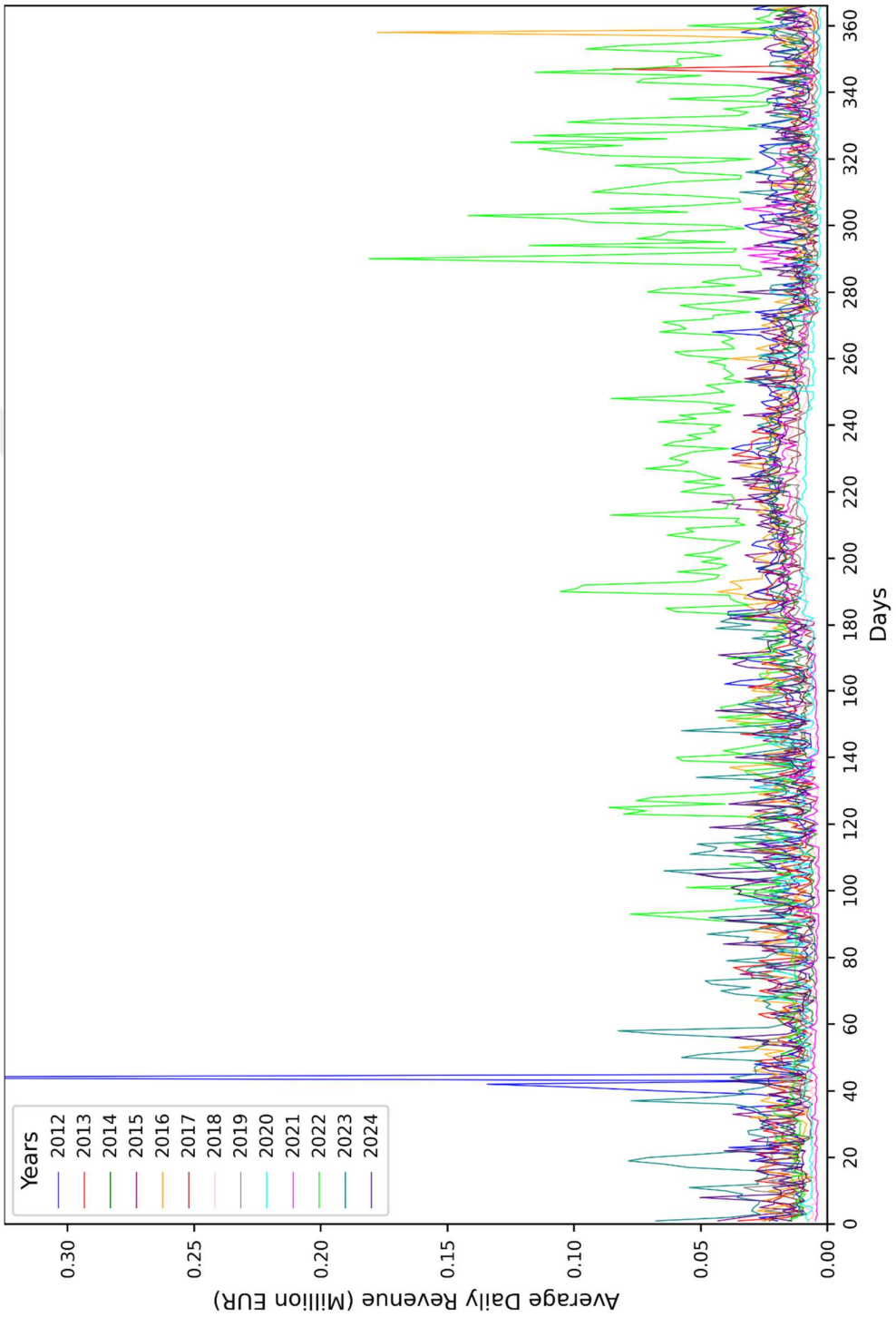

Figure 5.27 Optimized Average Daily Revenues for Realized Electricity Price Years.
In February 13, daily revenue reached approximately 0.62 million euros, which is not shown on the figure to enhance the representation in the rest of the days.

Monthly revenues from 2012 to 2024 are presented in Figure 5.28 to Figure 5.40. For the years between 2014 and 2023, observed hourly wind speed data is available. Therefore, for these specific years, the monthly revenues calculated using observed hourly wind speeds and the corresponding realized electricity prices are also included in Figures Figure 5.30 to Figure 5.39. These additional red lines represent the WHHS revenue that would have been obtained based on actual wind and price conditions. In most of these years, revenue in August is the highest with the highest variability. Variability in revenue from November to April is usually smaller than that of the rest of the year.

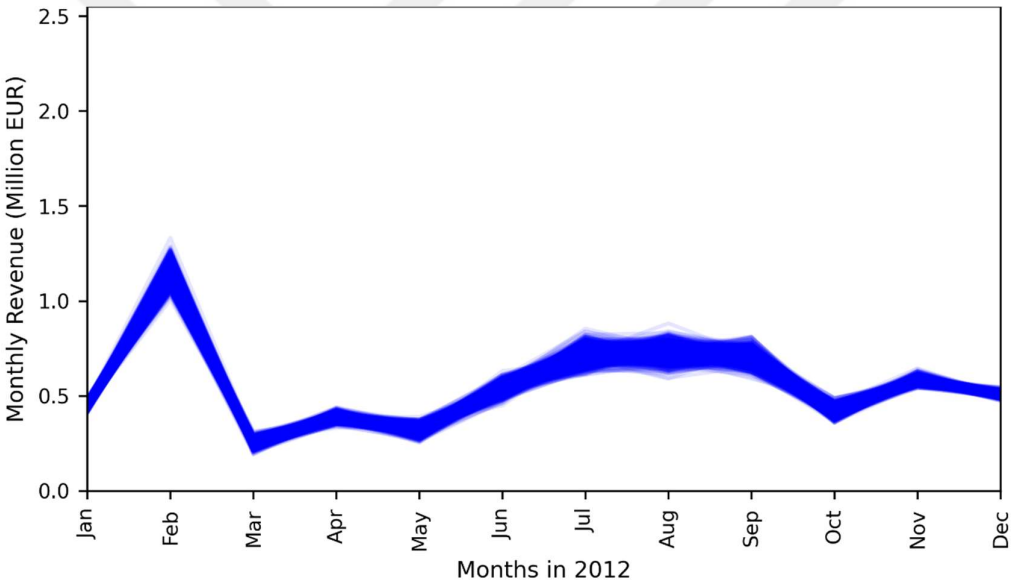

Figure 5.28 Optimized Monthly Revenues for Realized Electricity Price Year 2012

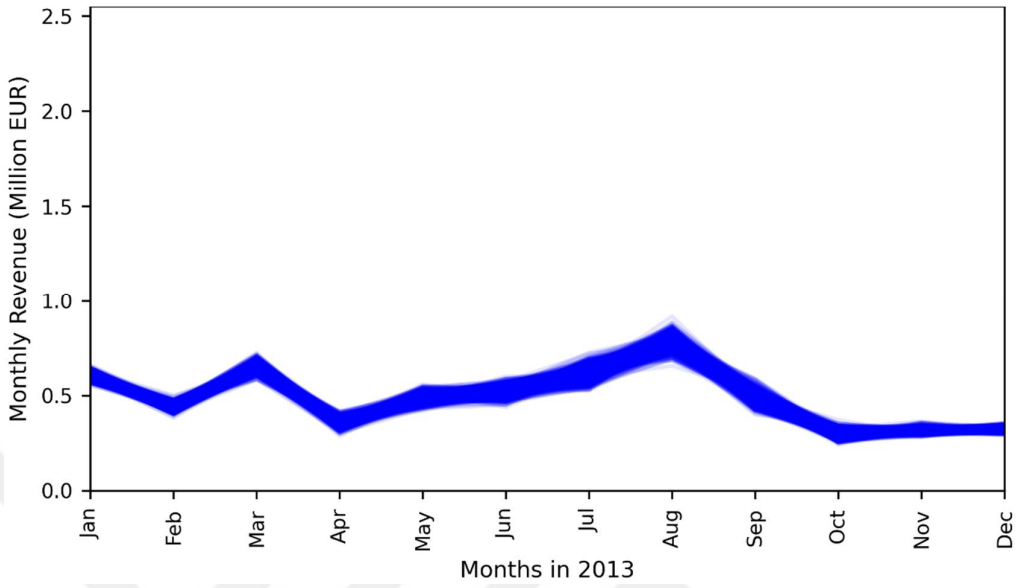

Figure 5.29 Optimized Monthly Revenues for Realized Electricity Price Year 2013

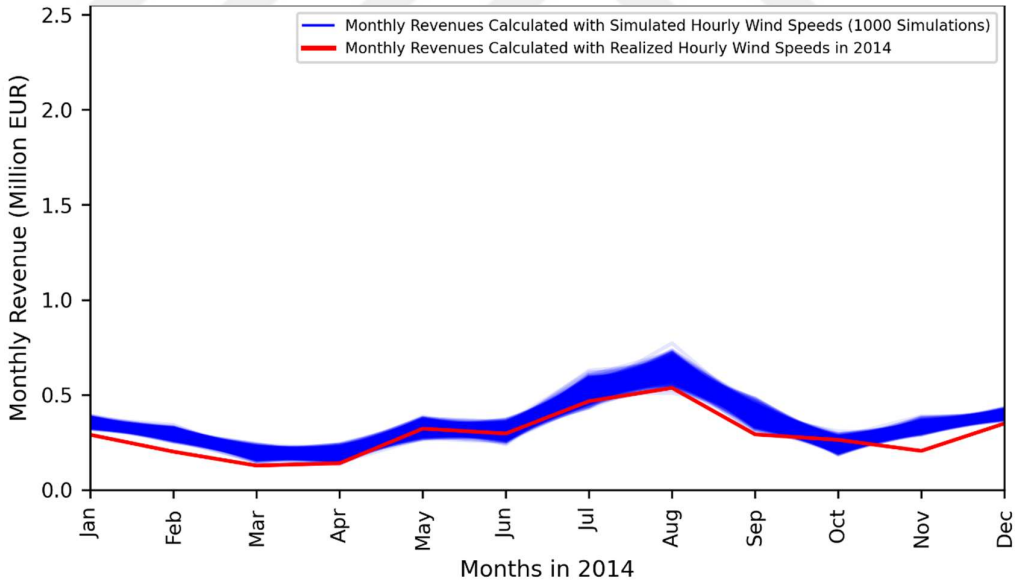

Figure 5.30 Optimized Monthly Revenues for Realized Electricity Price Year 2014

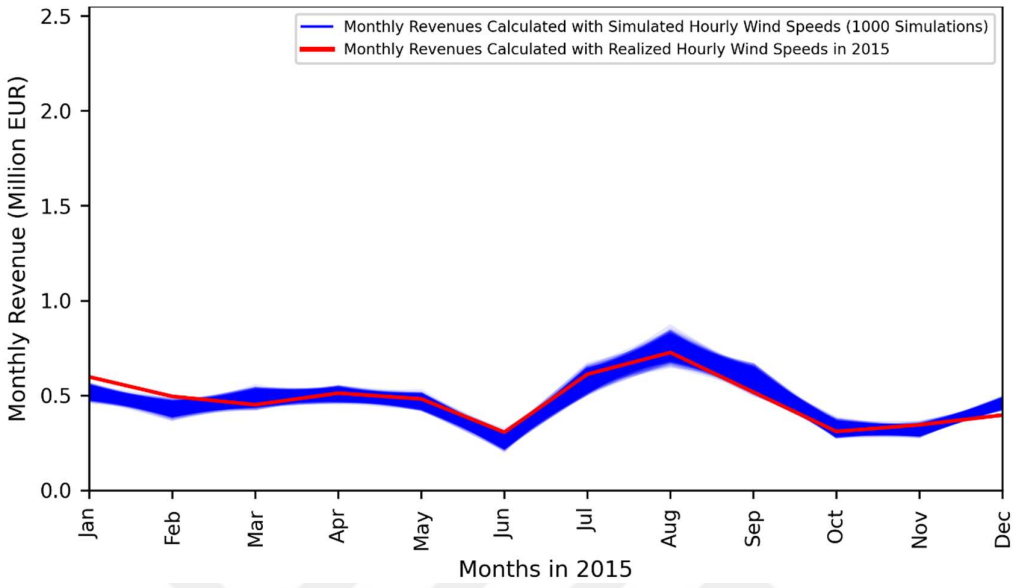

Figure 5.31 Optimized Monthly Revenues for Realized Electricity Price Year 2015

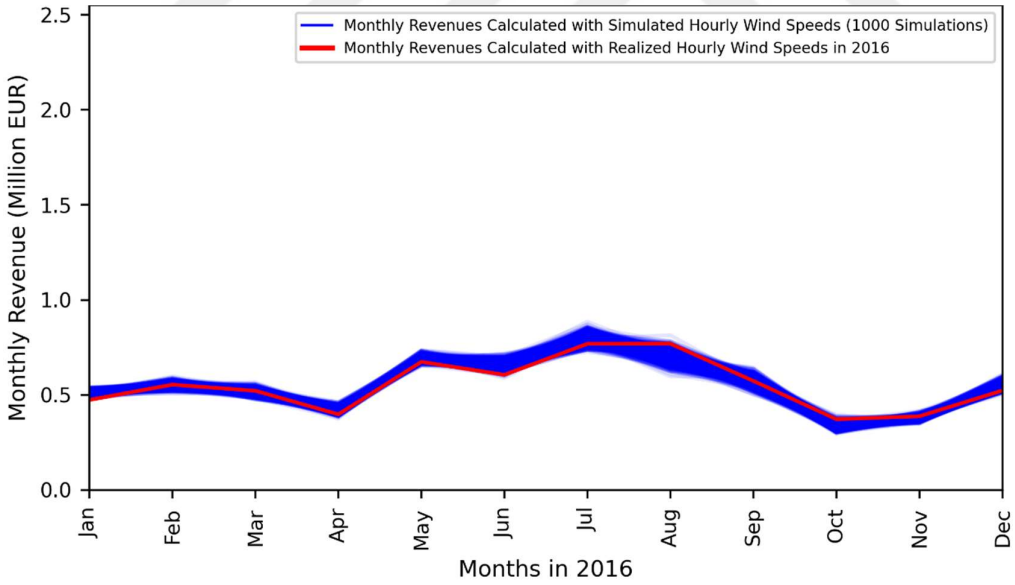

Figure 5.32 Optimized Monthly Revenues for Realized Electricity Price Year 2016

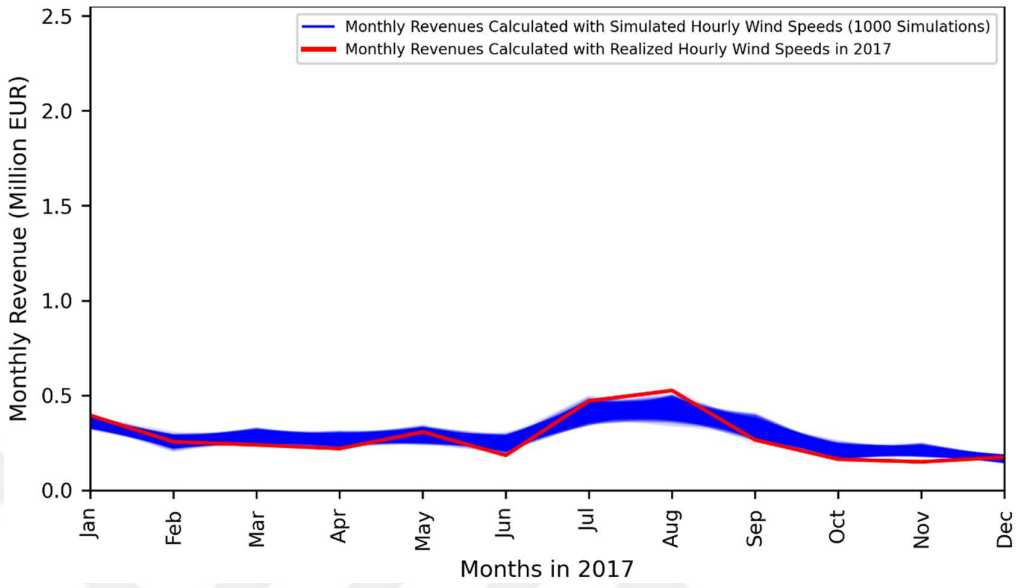

Figure 5.33 Optimized Monthly Revenues for Realized Electricity Price Years 2017

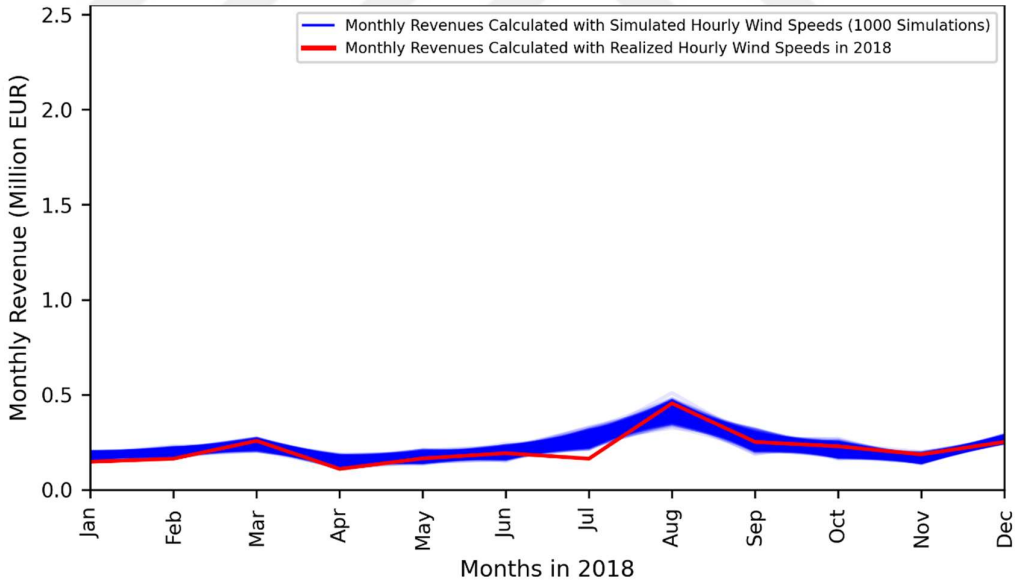

Figure 5.34 Optimized Monthly Revenues for Realized Electricity Price Year 2018

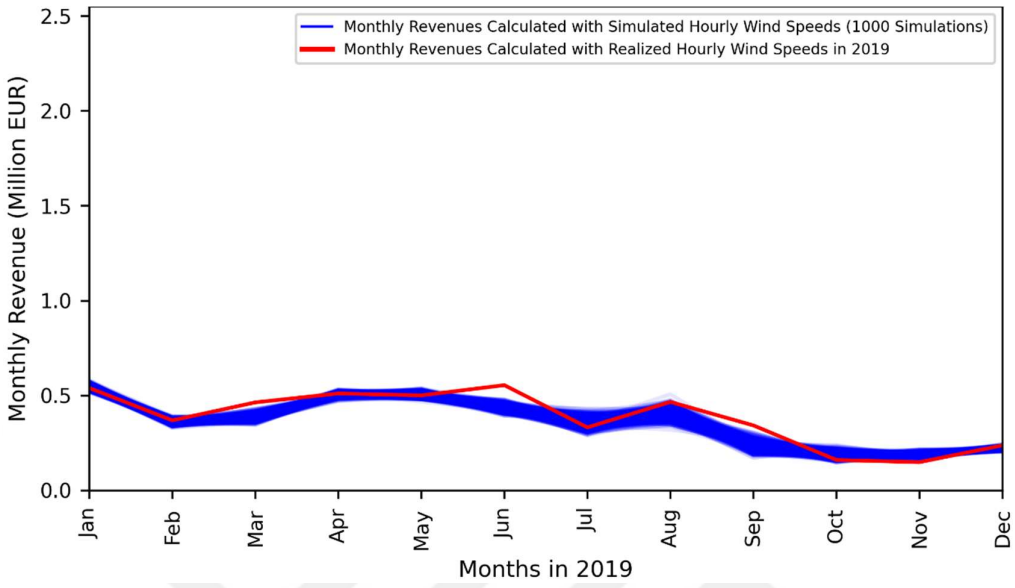

Figure 5.35 Optimized Monthly Revenues for Realized Electricity Price Year 2019

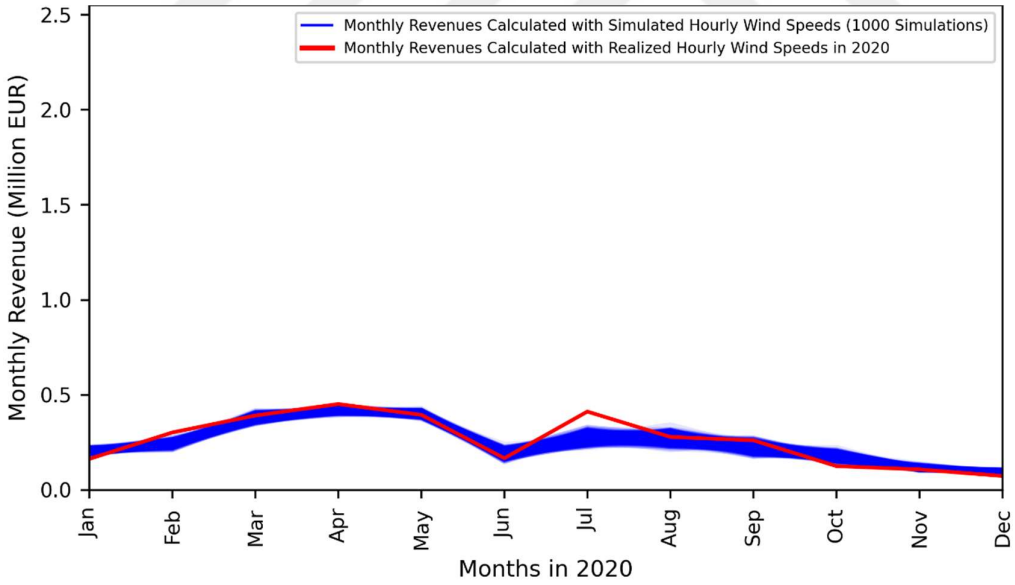

Figure 5.36 Optimized Monthly Revenues for Realized Electricity Price Year 2020

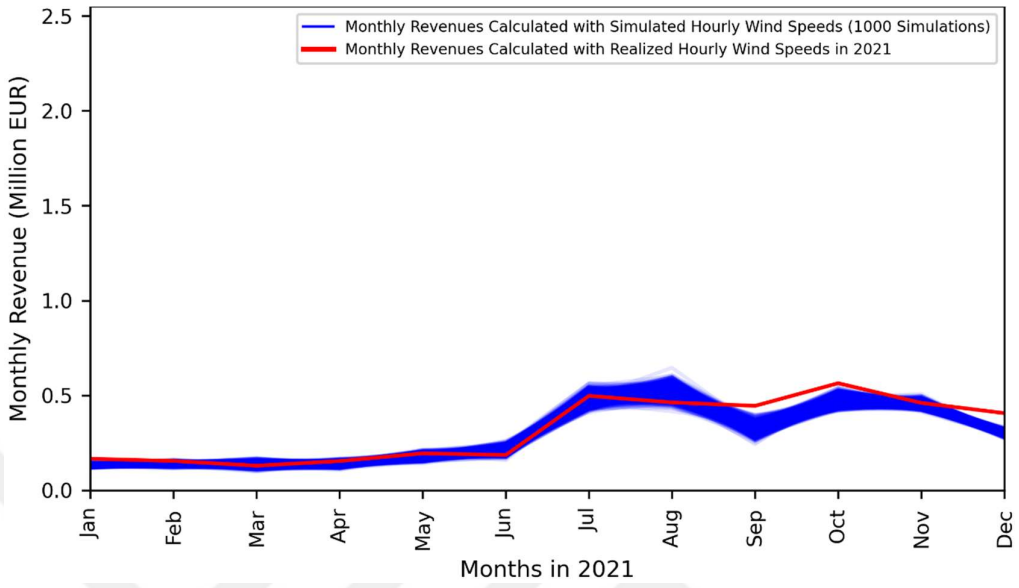

Figure 5.37 Optimized Monthly Revenues for Realized Electricity Price Year 2021

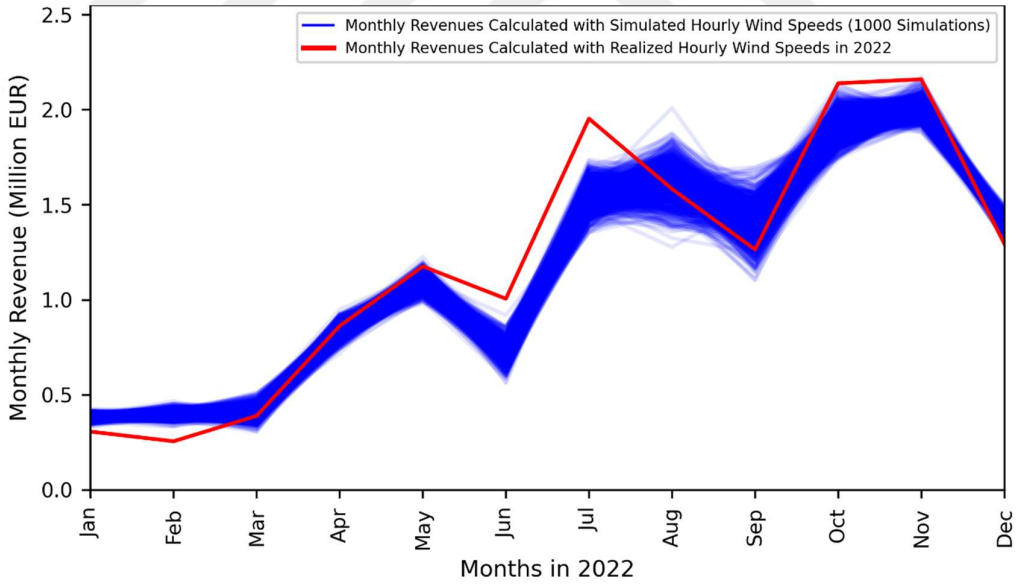

Figure 5.38 Optimized Monthly Revenues for Realized Electricity Price Year 2022

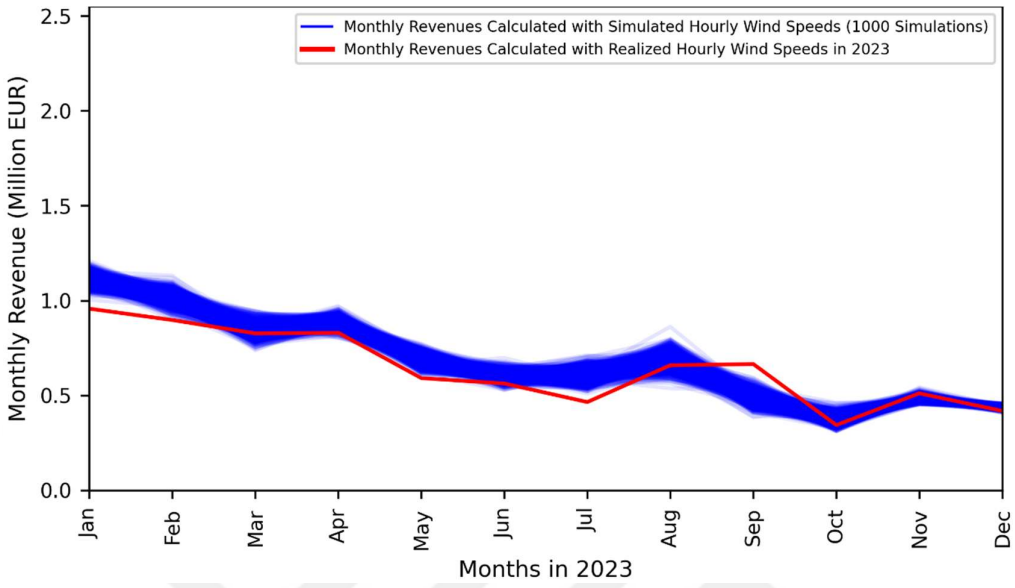

Figure 5.39 Optimized Monthly Revenues for Realized Electricity Price Year 2023

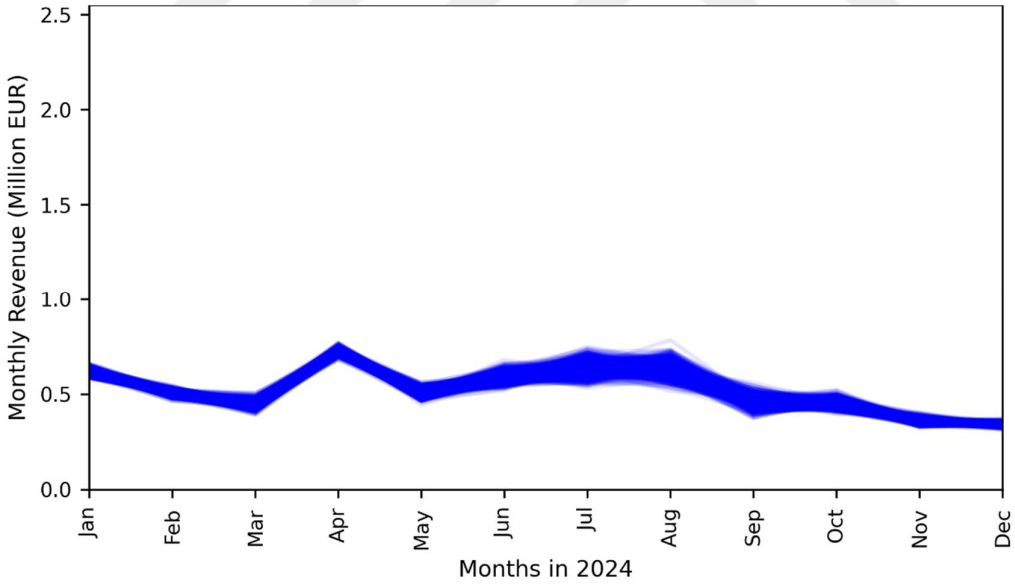

Figure 5.40 Optimized Monthly Revenues for Realized Electricity Price Year 2024

Figure 5.41, the average monthly revenues for each year from 2012 to 2024 are shown for a WHHS with wind farm of a 50 MW installed capacity. Each line

represents one year, calculated by averaging 1,000 monthly revenue trajectories from simulated wind speeds and optimized with that year's electricity prices.

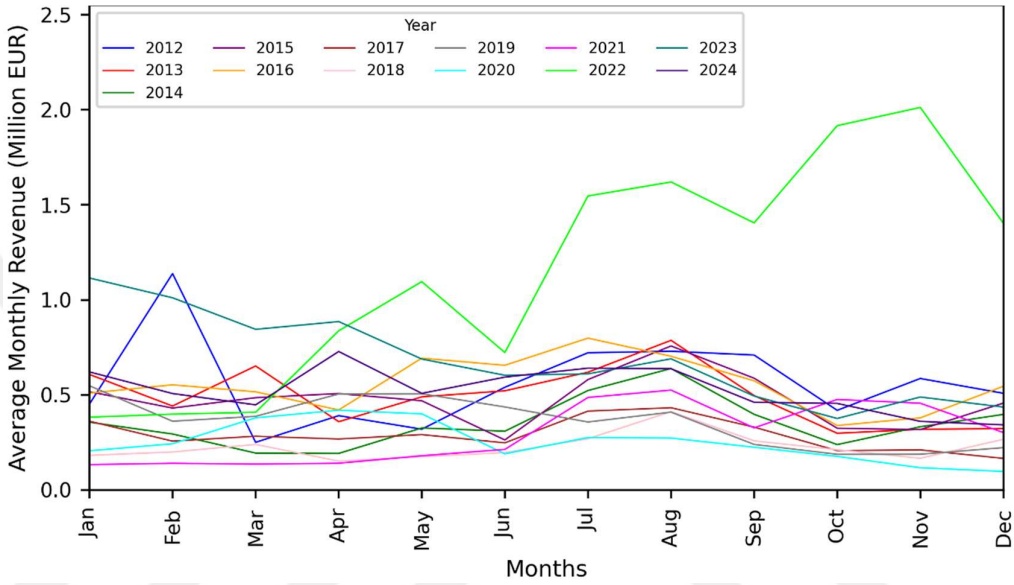

Figure 5.41 Optimized Average Monthly Revenues for Realized Electricity Price Years

In Figure 5.42, variation of annual revenues for each scenario year are plotted. In Figure 5.43 and Figure 5.44, variations of monthly revenues for each scenario year are plotted.

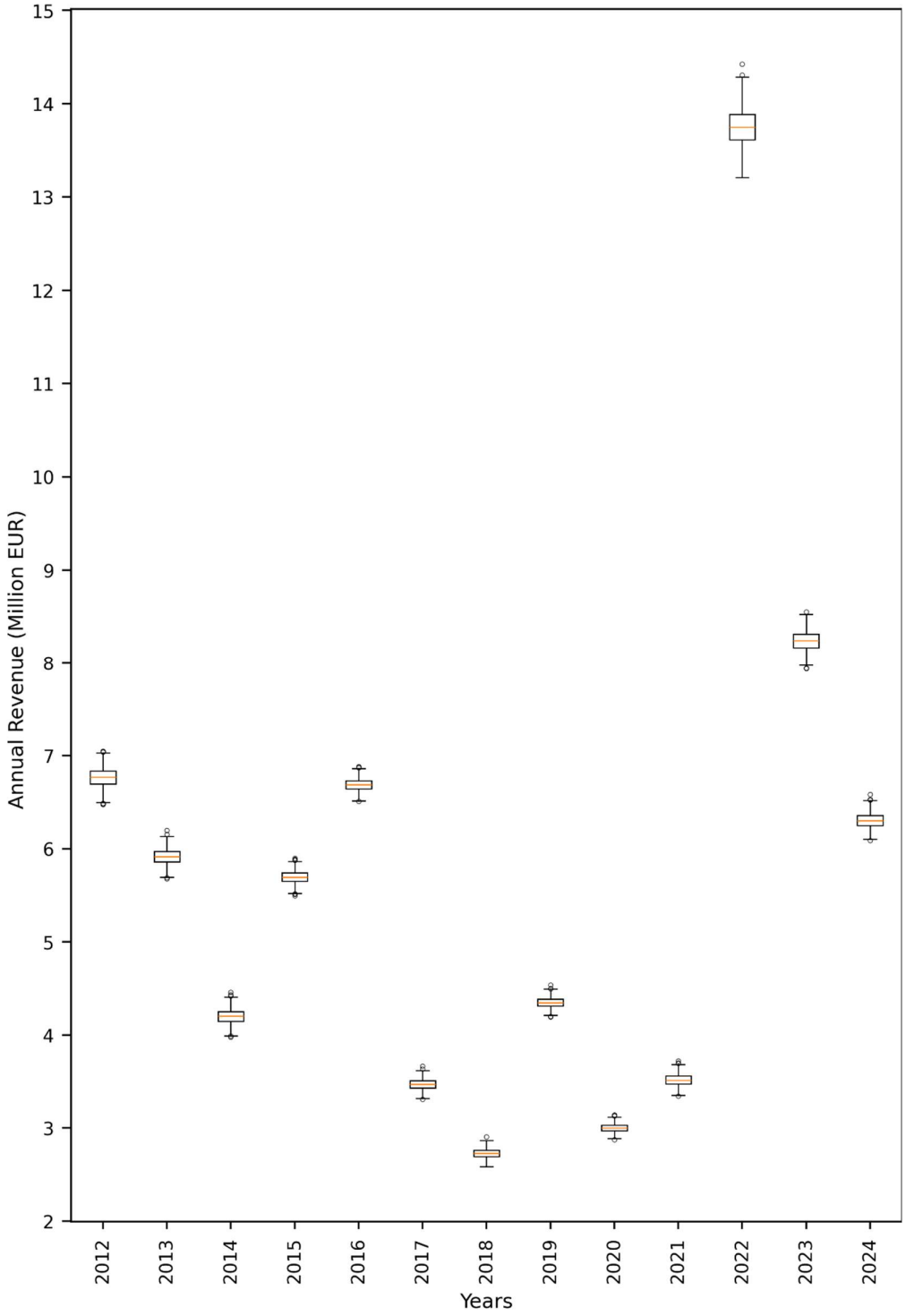

Figure 5.42 Variation of Annual Revenues for Realized Electricity Price Years

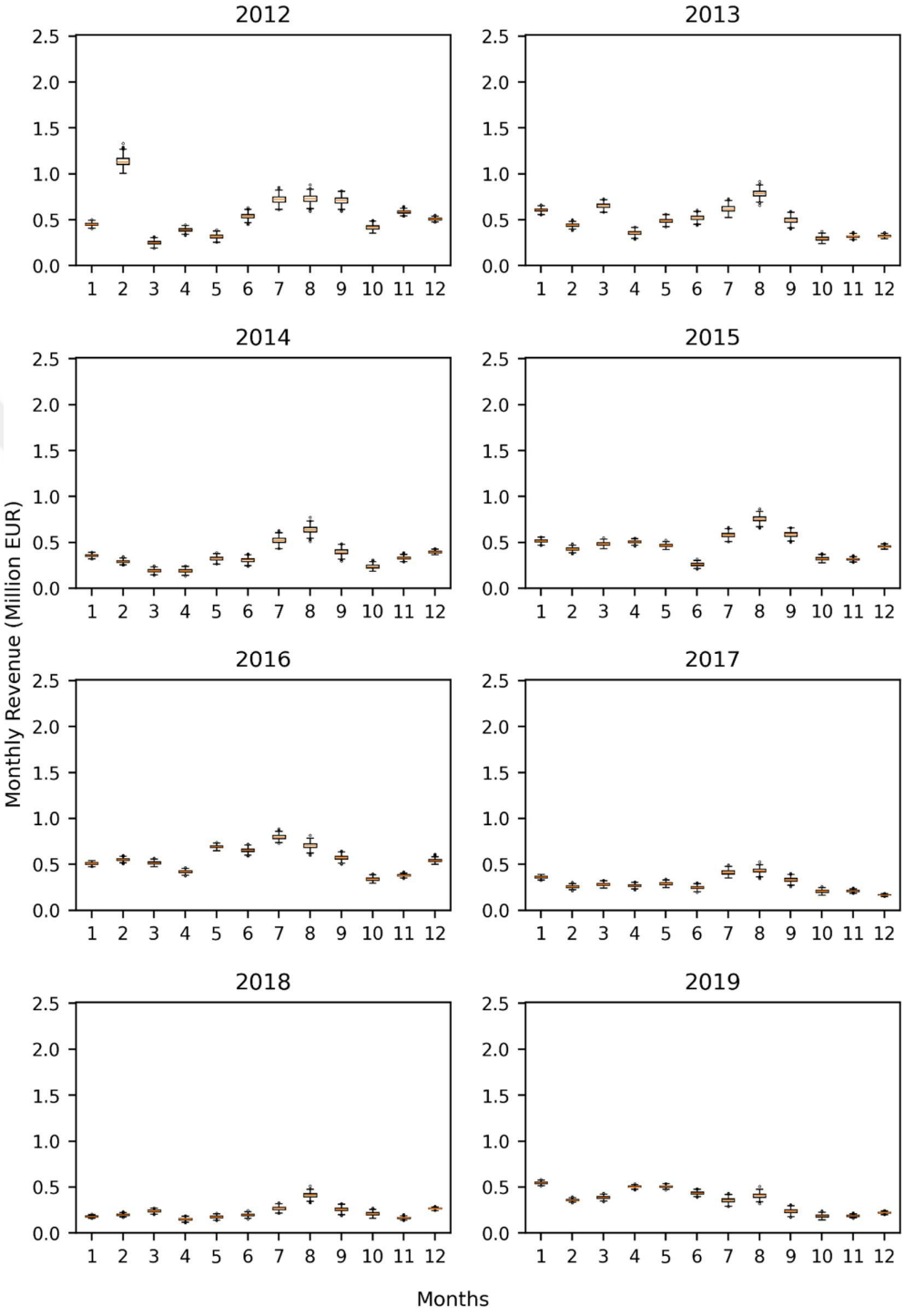

Figure 5.43 Variation of Monthly Revenues for Realized Electricity Price Years from 2012 to 2019

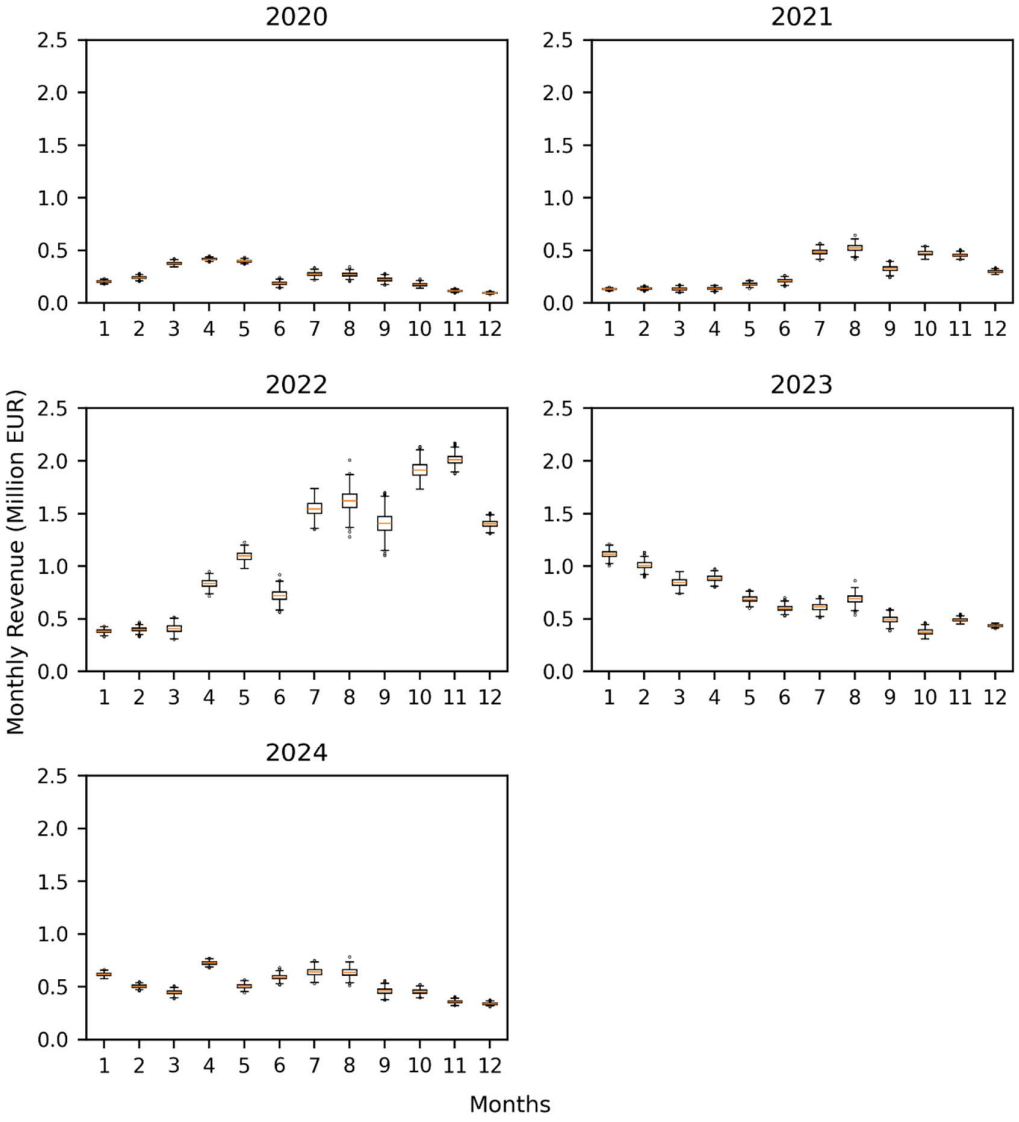

Figure 5.44 Variation of Monthly Revenues for Realized Electricity Price Years from 2020 to 2024

Figure 5.45 presents the distribution of annual revenues for the WHHS with a wind farm of 50 MW installed capacity for each scenario year (i.e., 2012–2024). For each year, 1,000 annual revenue values are computed using the same set of 1,000 simulated hourly wind speed time series. This allows isolating the impact of electricity price variability from that of wind speed uncertainty. Although the simulated wind speed data includes some extreme outliers (see Figure 5.8), the width

of the revenue distributions remains relatively narrow across all years. This suggests that the uncertainty resulting from wind speed variability has a limited influence on annual revenue. In contrast, the position of the PDFs shifts considerably along the x-axis from year to year, reflecting changes in electricity prices result in relatively large changes in annual revenues. These horizontal shifts demonstrate that electricity price variability is the dominant driver of revenue variation. Although wind speed simulations included some extreme outliers (see Figure 5.9and Figure 5.10), the effect of wind-related uncertainty is relatively smaller compared to that of electricity market fluctuations.

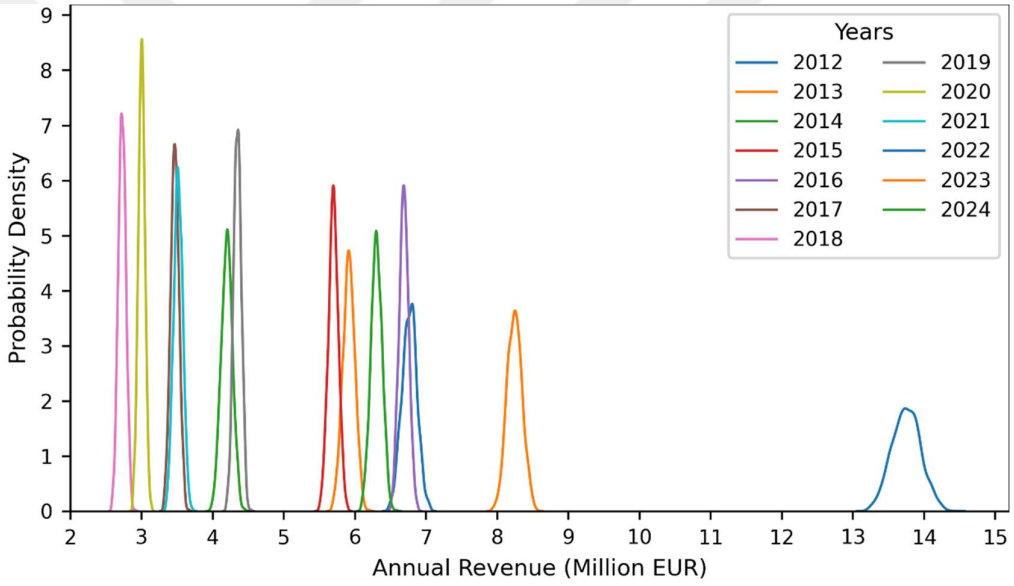

Figure 5.45 PDF of Annual Revenue for Realized Electricity Price Years

Change in annual revenue interquartile range (IQR) with respect to hourly electricity price IQR is given in Figure 5.46. Each data point represents one scenario year (i.e., 2012 to 2024) in Figure 5.46. There is a positive relationship between electricity price variability and revenue variability. In other words, as the hourly electricity price variability increases within a year, the corresponding uncertainty in the annual revenue, obtained through the optimization model with simulated wind data

increases. Notably, a particular year exhibits significantly higher price variability (~85 EUR) resulting in a substantial rise in revenue uncertainty (~0.27 million EUR), emphasizing how extreme market fluctuations can considerably amplify financial risk for WHHS.

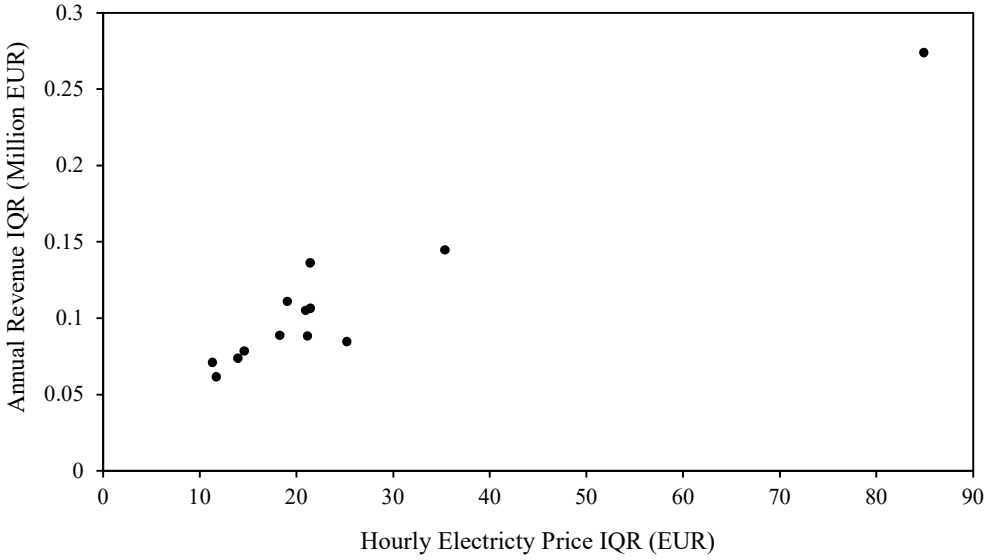

Figure 5.46 Change in Annual Revenue IQR with Hourly Electricity Price IQR

The change in annual revenue median with hourly electricity price median is given in Figure 5.47. Again, each data point represents one scenario year (i.e., 2012 to 2024) in Figure 5.47. As the median hourly electricity price increases, the corresponding median annual revenue increases as expected. A year with particularly high electricity prices (~130 EUR median price) clearly yields significantly higher median annual revenues (~14 million EUR), emphasizing the substantial influence of electricity market price levels on annual profitability.

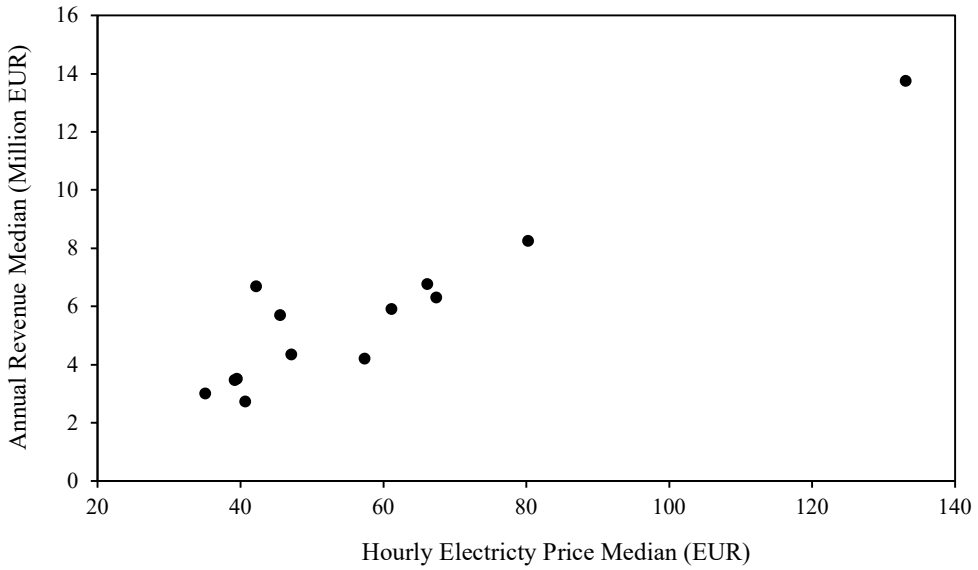

Figure 5.47 Change in Annual Revenue Median with Hourly Electricity Price Median

5.2.2 Daily Revenue Optimization Results of WHHS with a 250 MW Installed Capacity

In Figure 5.48 to Figure 5.60 the daily revenues for each year from 2012 to 2024 are presented, showcasing the optimized performance of a WHHS with a wind farm of 250 MW installed capacity under varying electricity price and wind speed conditions. For the years between 2014 and 2023, observed hourly wind speed data is available. Therefore, for these specific years, the daily revenues calculated using observed hourly wind speeds and the corresponding realized electricity prices are also included in Figures 5.50 to 5.59. These additional red lines represent the WHHS revenue that would have been obtained based on actual wind and price conditions. The average daily revenues (i.e., the average or 1,000 simulations) for each year from 2012 to 2024 are shown for a WHHS with a wind farm of 250 MW installed capacity on Figure 5.61.

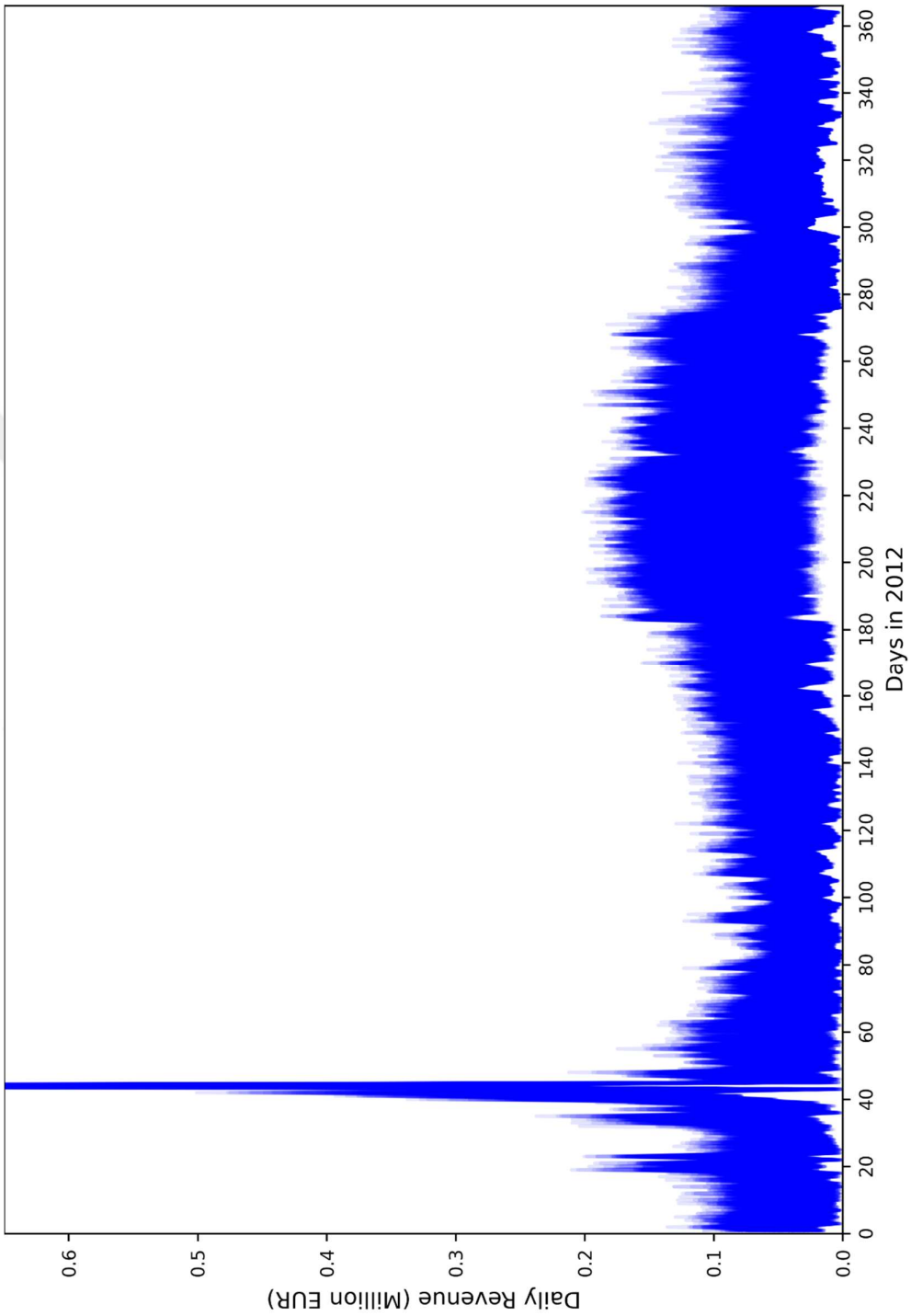

Figure 5.48 Optimized Daily Revenues for Realized Electricity Price Year 2012. In February 13, daily revenue reached approximately 1.51 million euros, which is not shown on the figure to enhance the representation in the rest of the days.

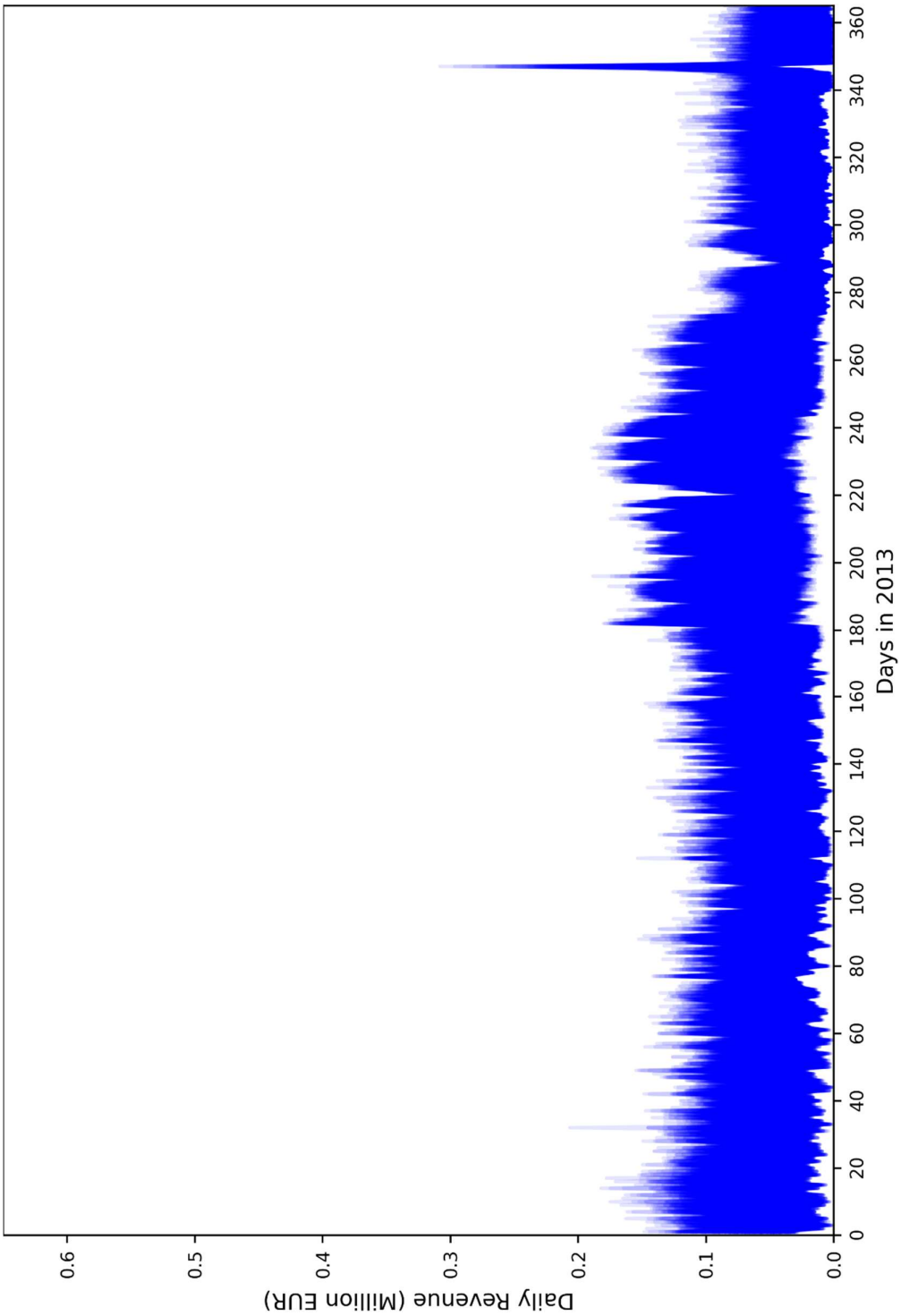

Figure 5.49 Optimized Daily Revenues for Realized Electricity Price Year 2013

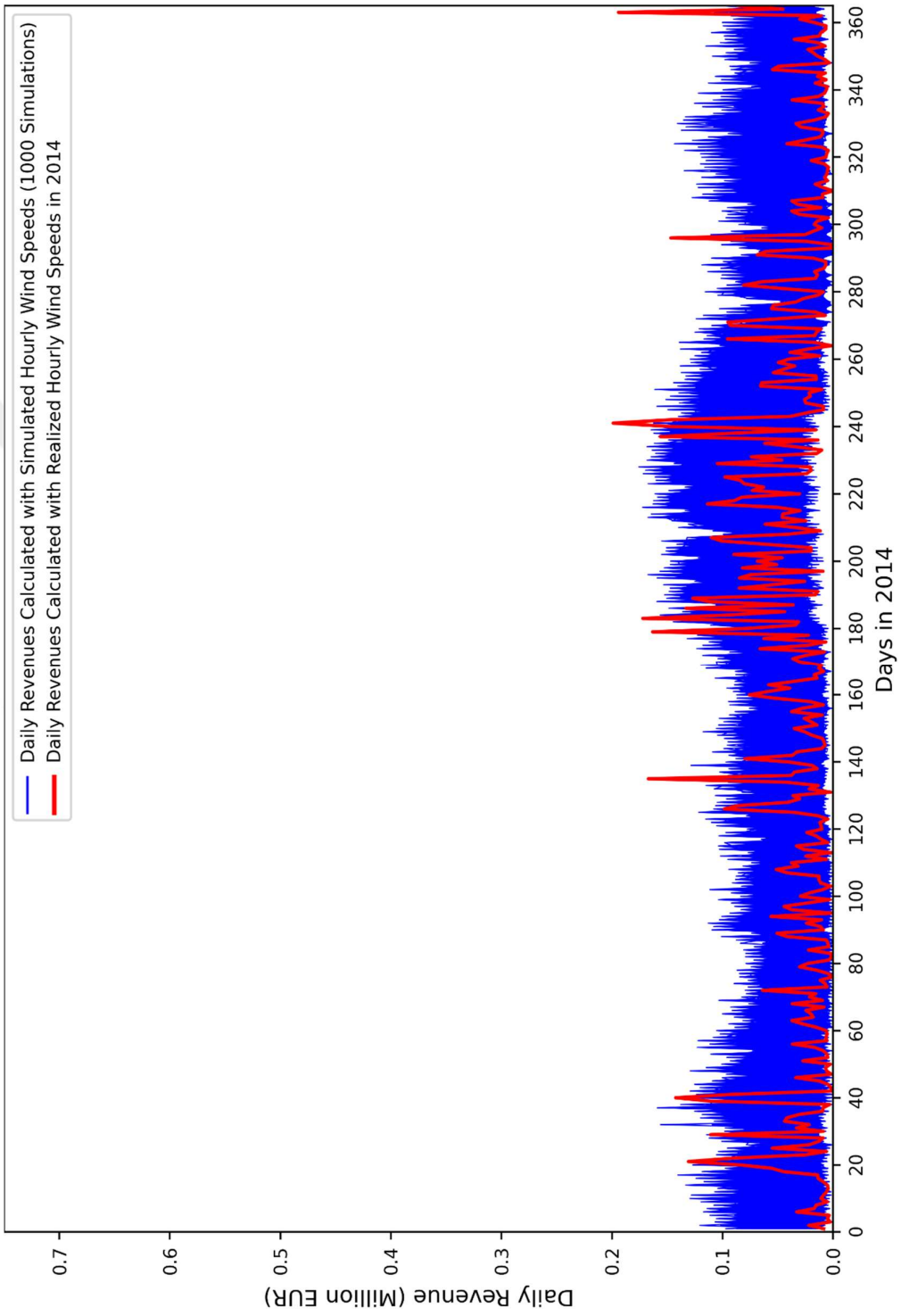

Figure 5.50 Optimized Daily Revenues for Realized Electricity Price Year 2014

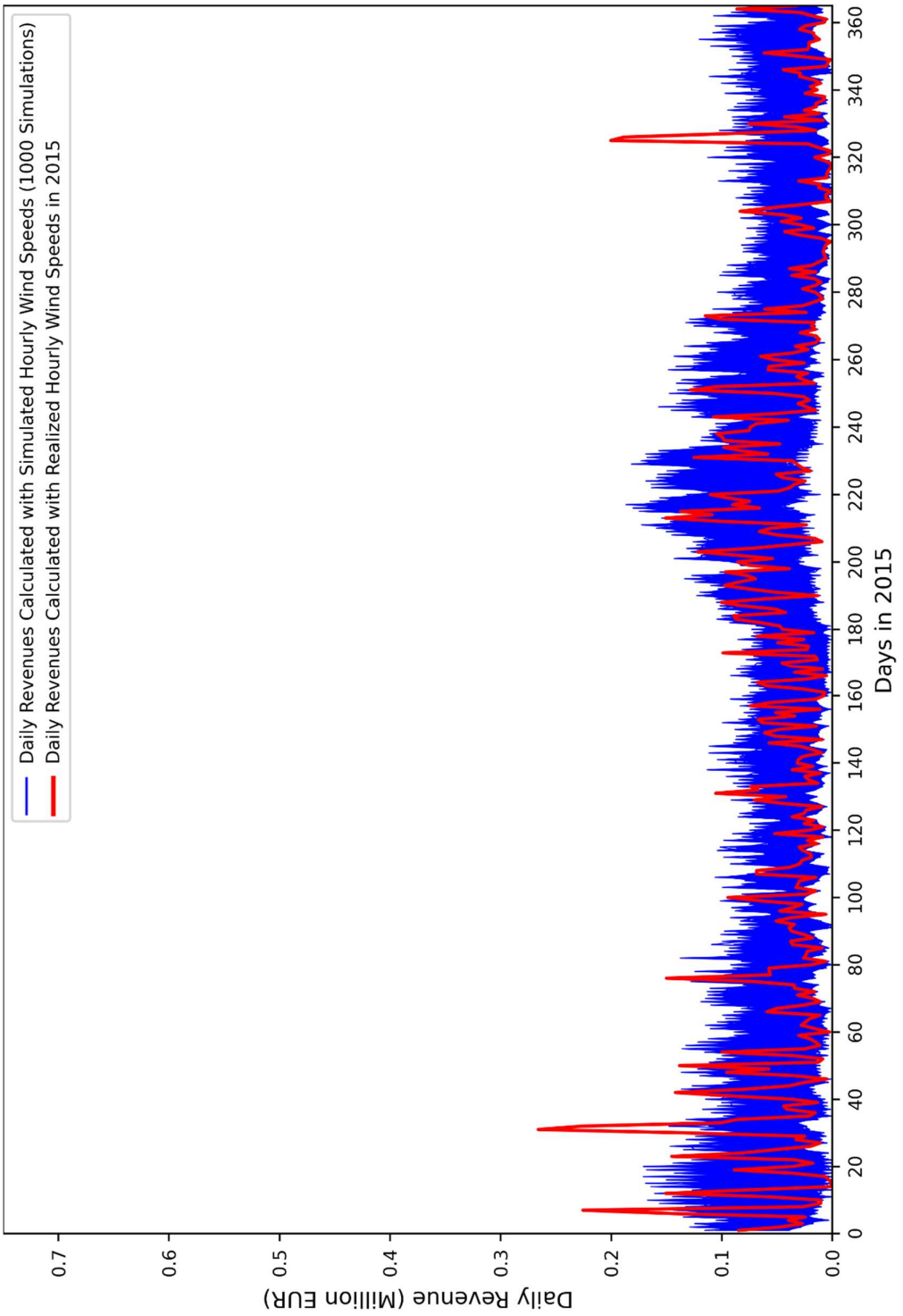

Figure 5.51 Optimized Daily Revenues for Realized Electricity Price Year 2015

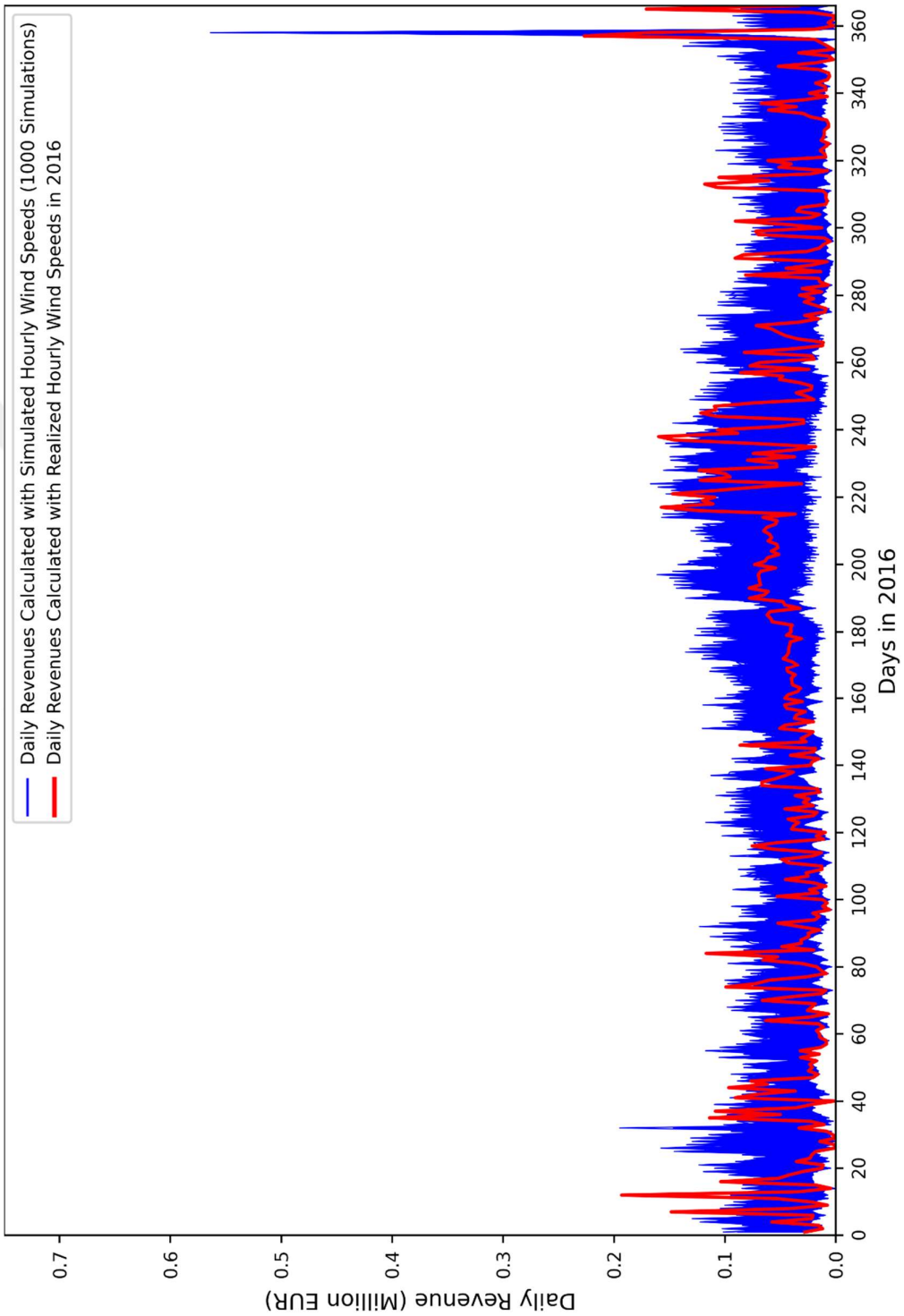

Figure 5.52 Optimized Daily Revenues for Realized Electricity Price Year 2016

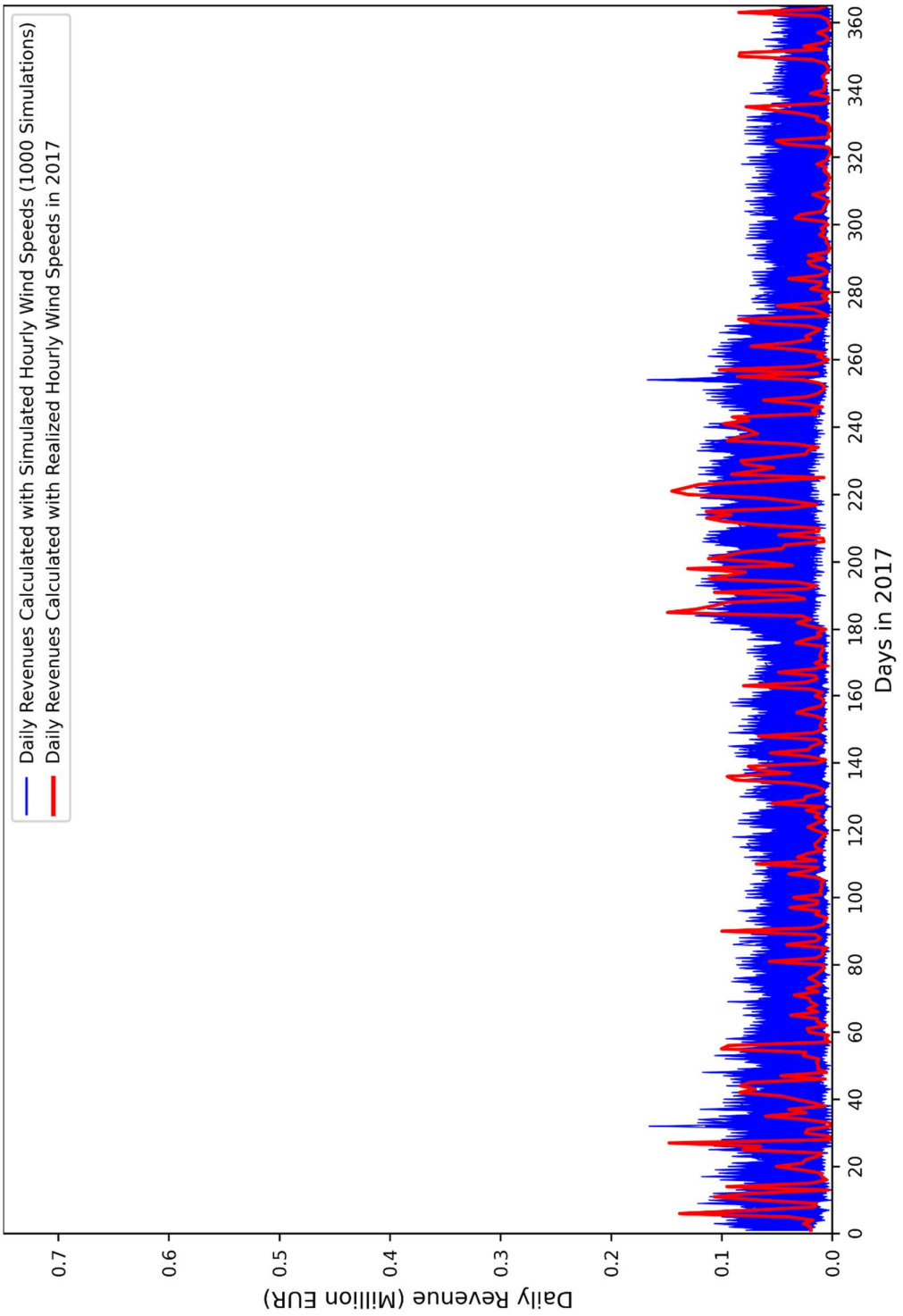

Figure 5.53 Optimized Daily Revenues for Realized Electricity Price Year 2017

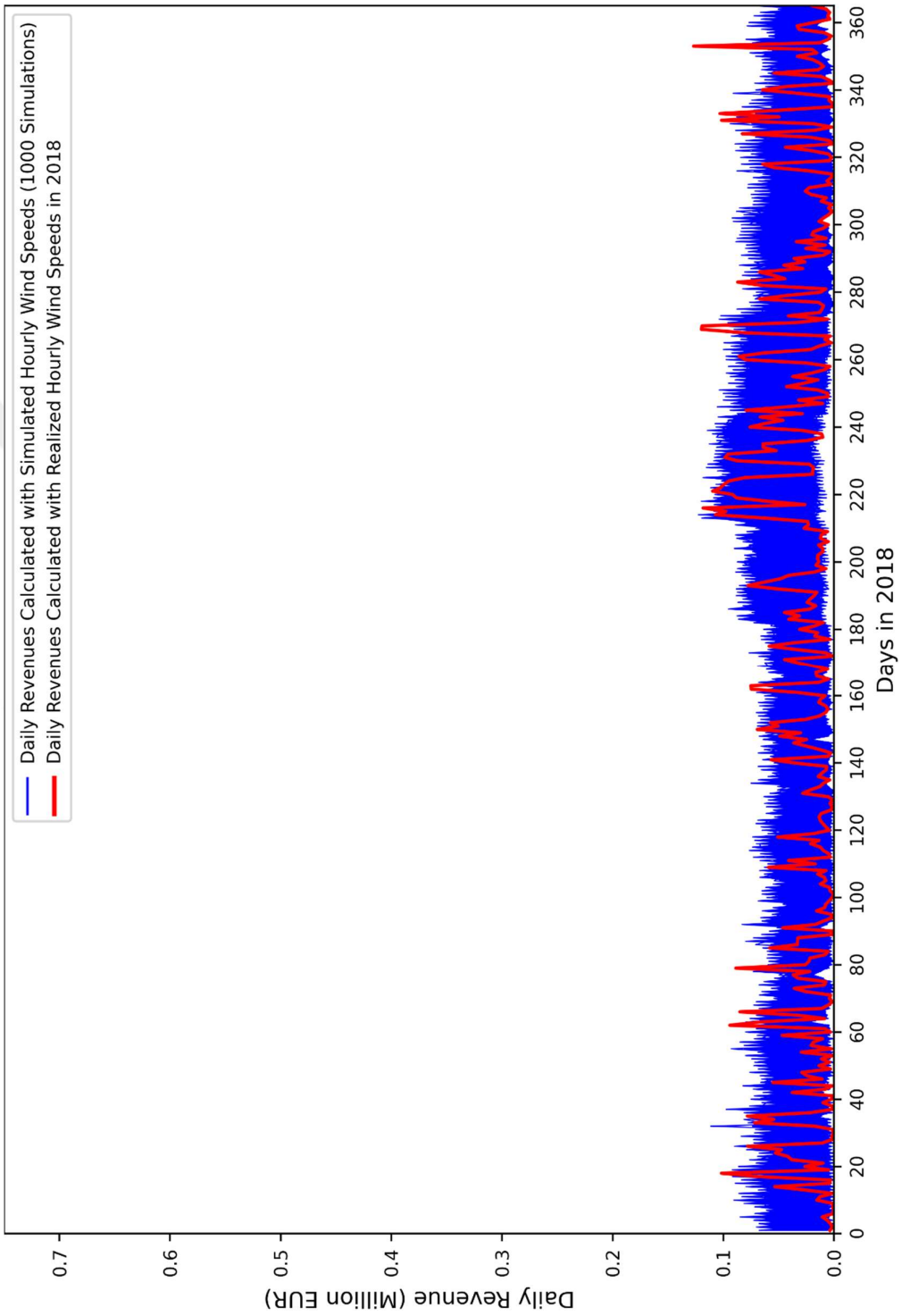

Figure 5.54 Optimized Daily Revenues for Realized Electricity Price Year 2018

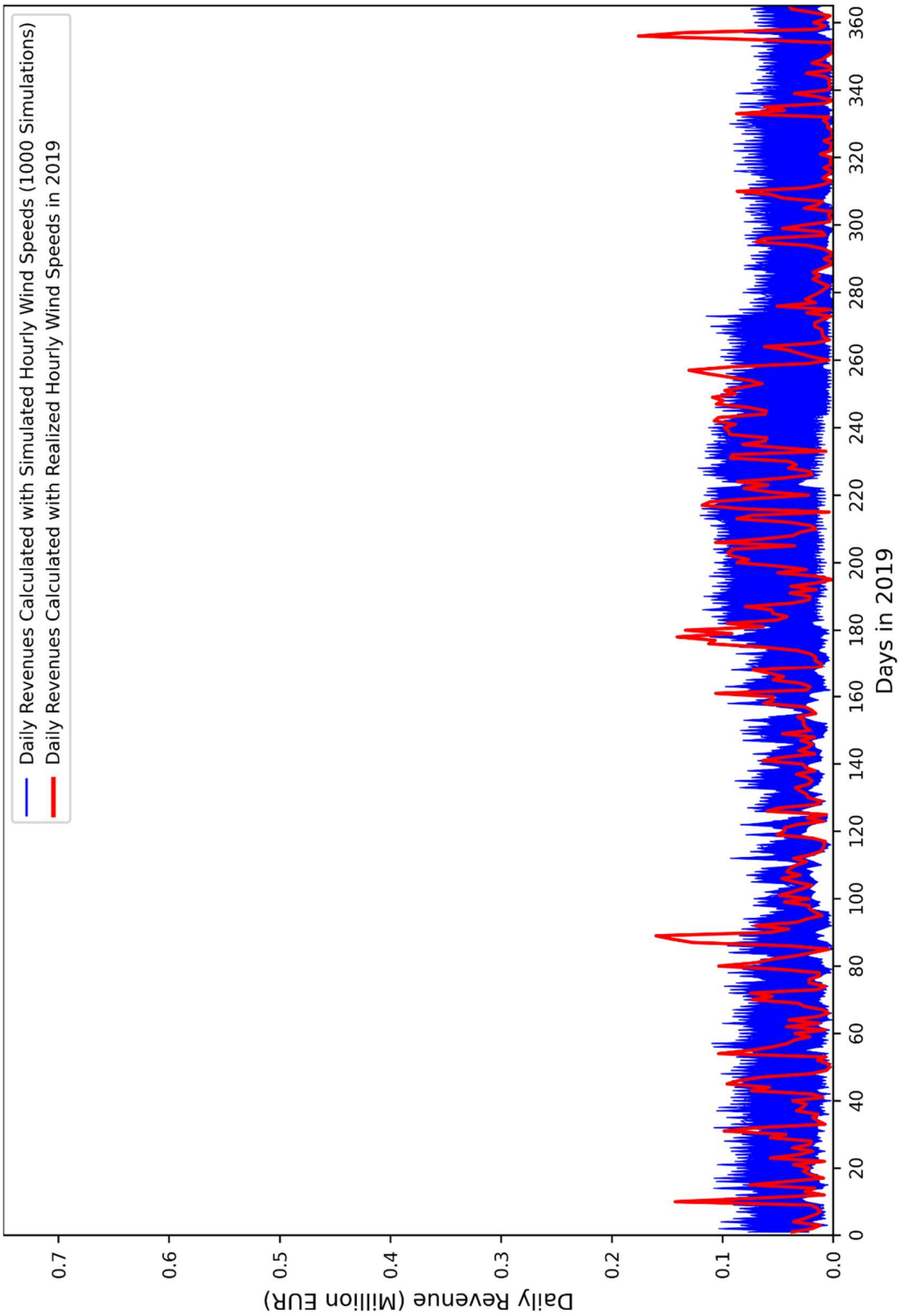

Figure 5.55 Optimized Daily Revenues for Realized Electricity Price Year 2019

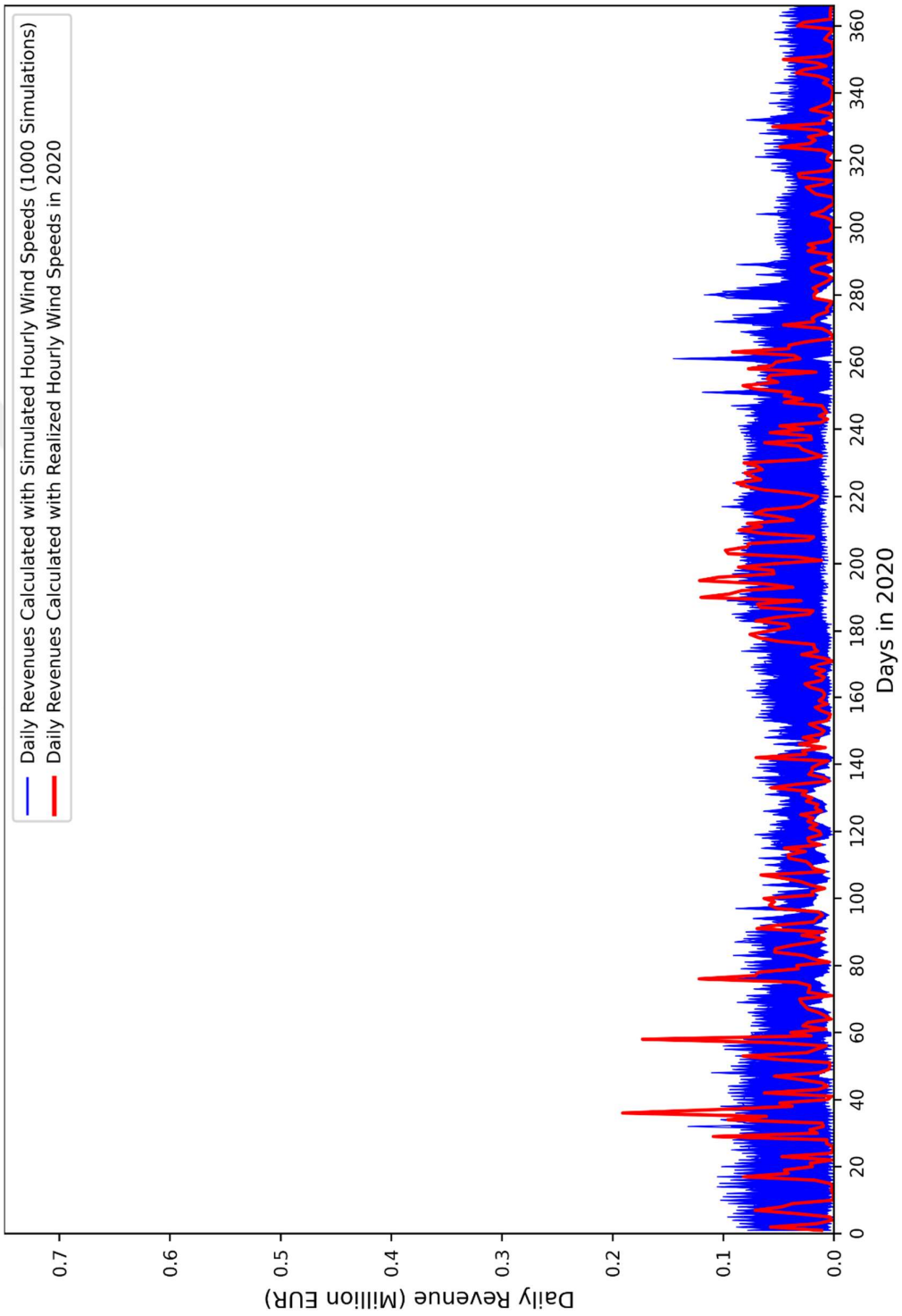

Figure 5.56 Optimized Daily Revenues for Realized Electricity Price Year 2020

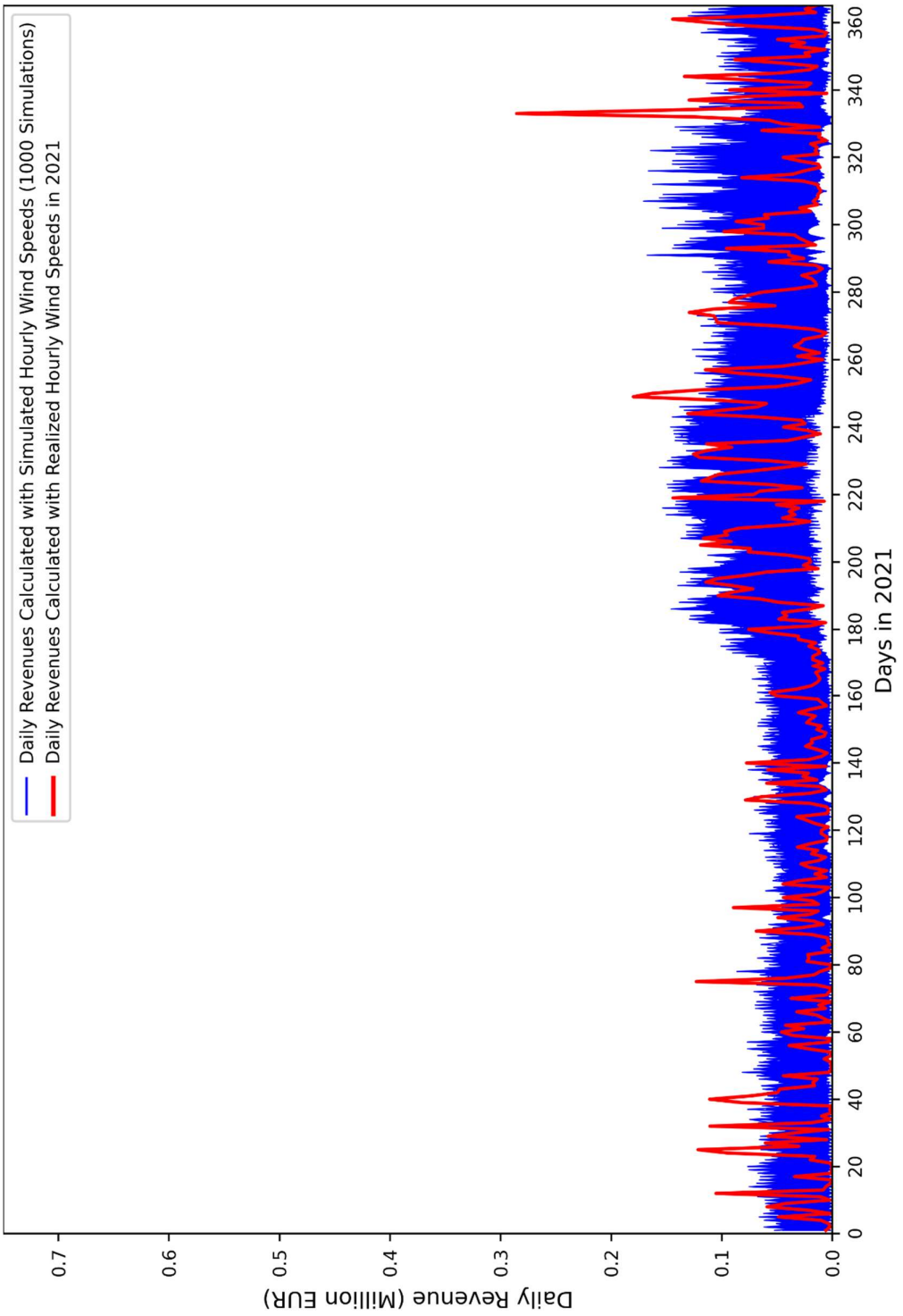

Figure 5.57 Optimized Daily Revenues for Realized Electricity Price Year 2021

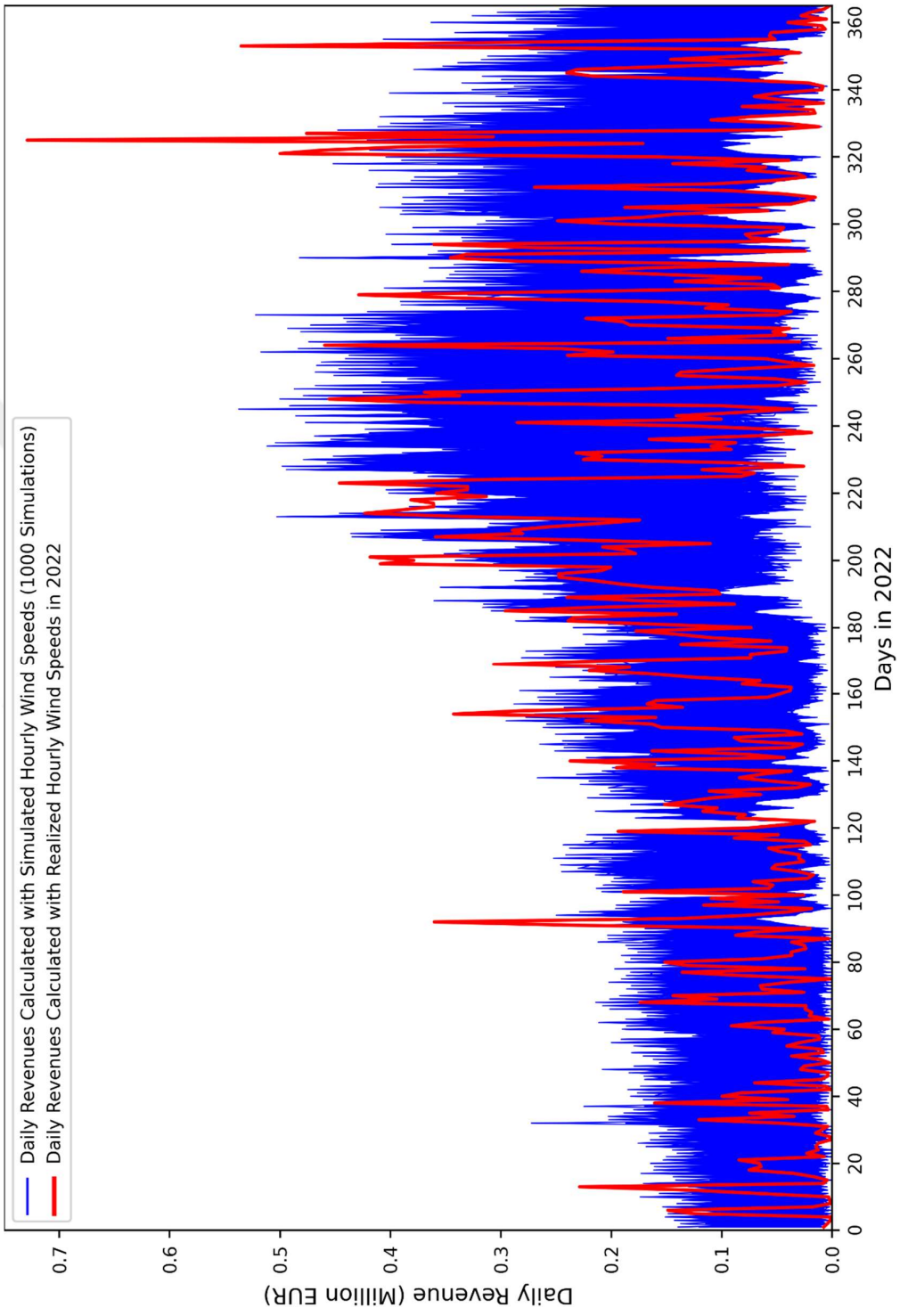

Figure 5.58 Optimized Daily Revenues for Realized Electricity Price Year 2022

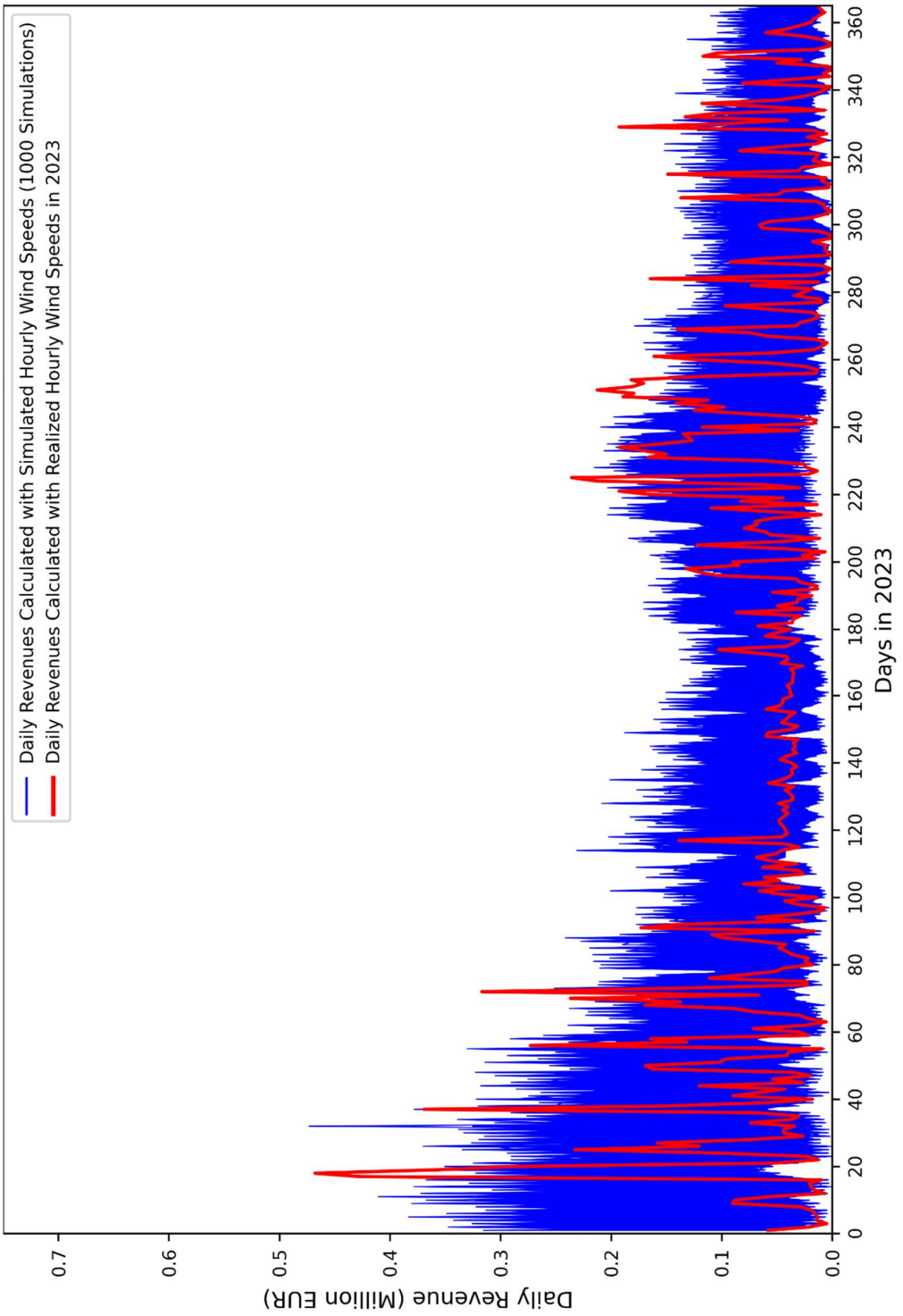

Figure 5.59 Optimized Daily Revenues for Realized Electricity Price Year 2023

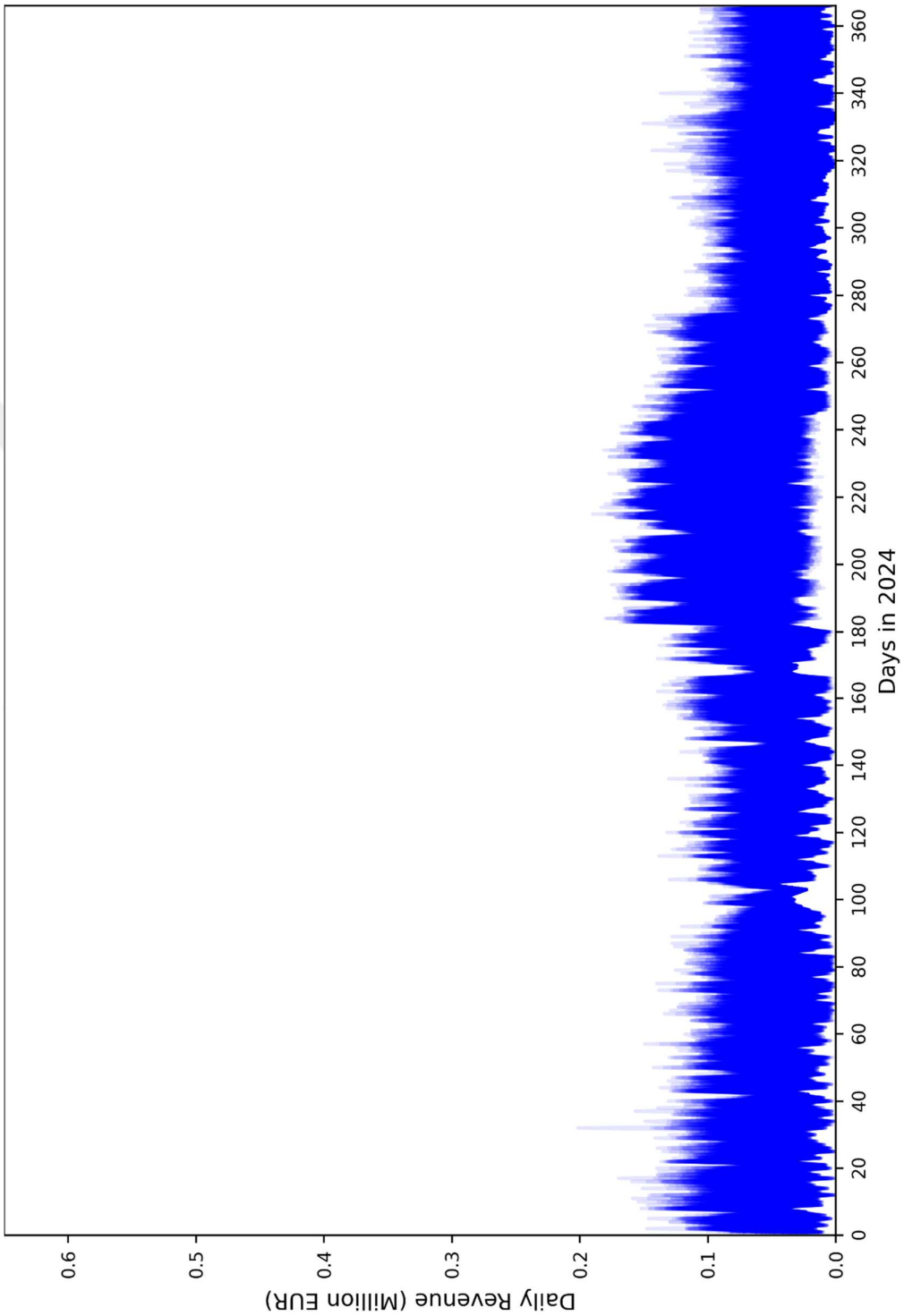

Figure 5.60 Optimized Daily Revenues for Realized Electricity Price Year 2024

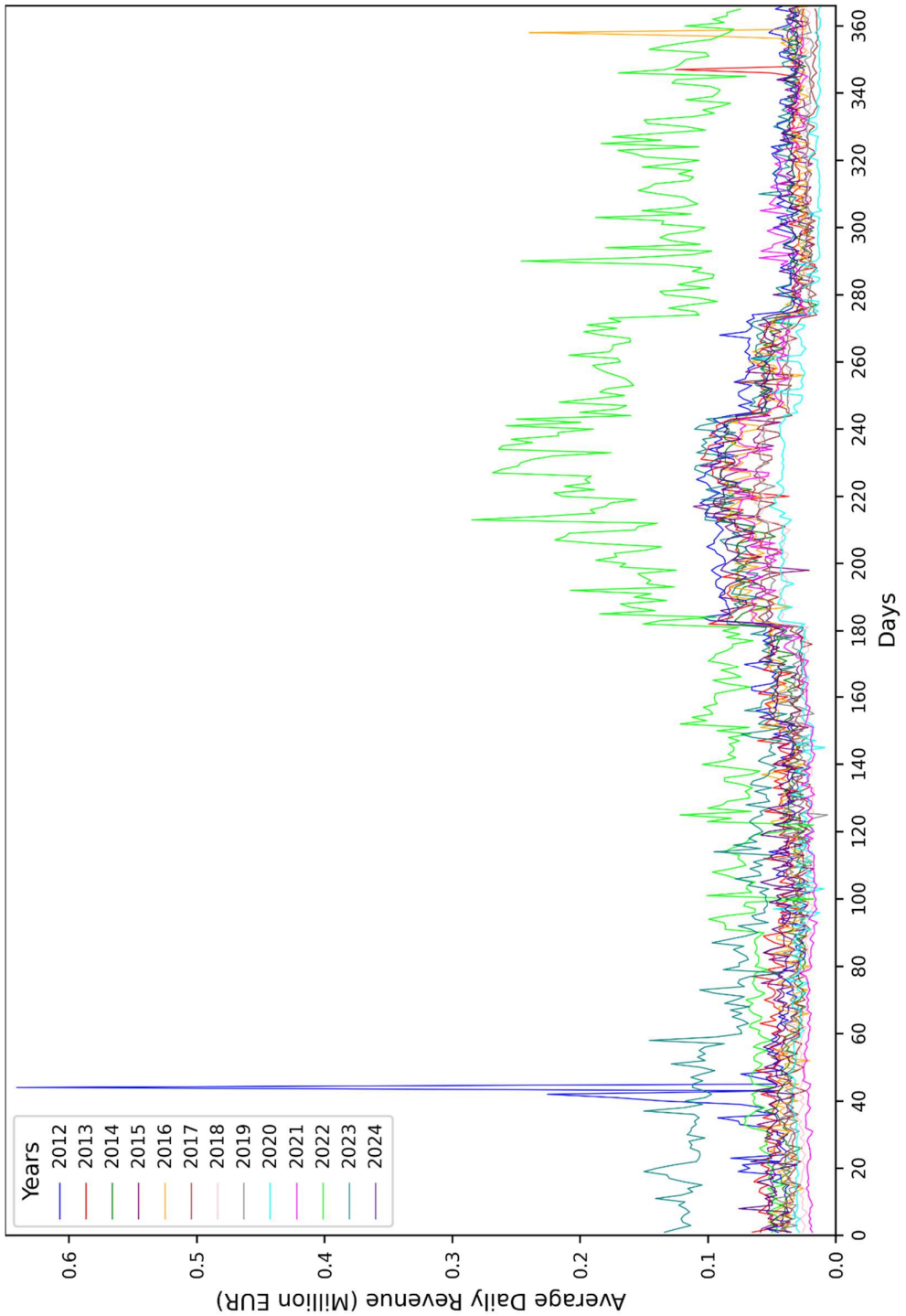

Figure 5.61 Optimized Average Daily Revenues for Realized Electricity Price Years

Monthly revenues from 2012 to 2024 are given in Figure 5.62 to Figure 5.74. For the years between 2014 and 2023, observed hourly wind speed data is available. Therefore, for these specific years, the monthly revenues calculated using observed hourly wind speeds and the corresponding realized electricity prices are also included in Figure 5.30 to Figure 5.73. These additional red lines represent the WHHS revenue that would have been obtained based on actual wind and price conditions. Similar to the 50 MW installed capacity case, under the 250 MW case, August typically exhibits the highest monthly revenue along with the highest variability. Variability in revenue from November to April is usually smaller than that of the rest of the year.

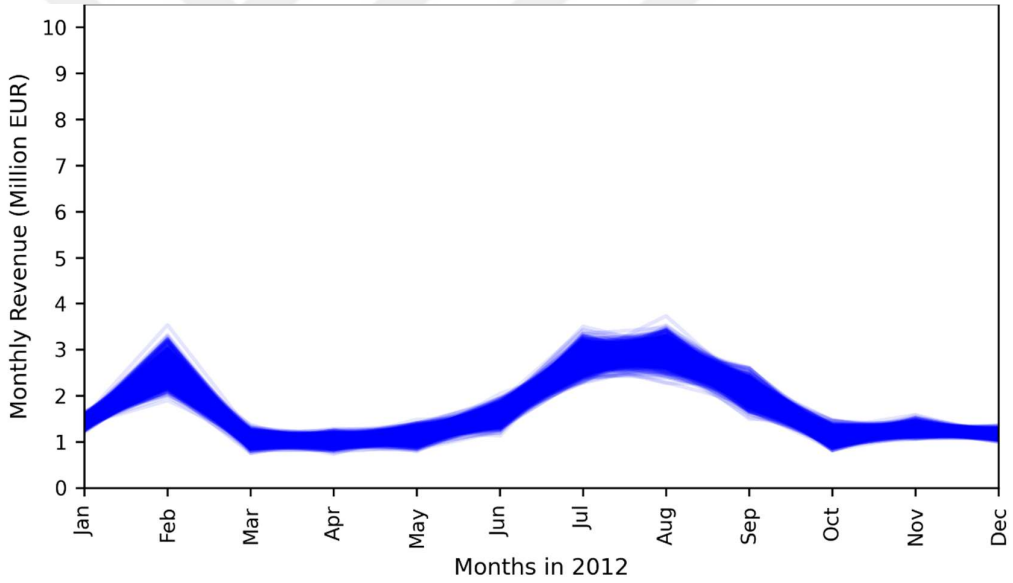

Figure 5.62 Optimized Monthly Revenues for Realized Electricity Price Year 2012

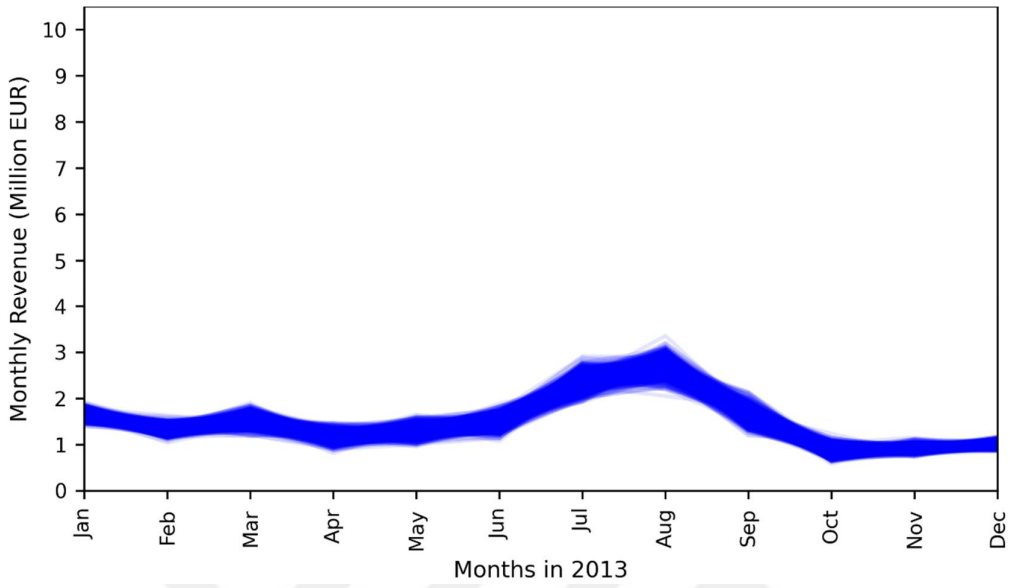

Figure 5.63 Optimized Monthly Revenues for Realized Electricity Price Year 2013

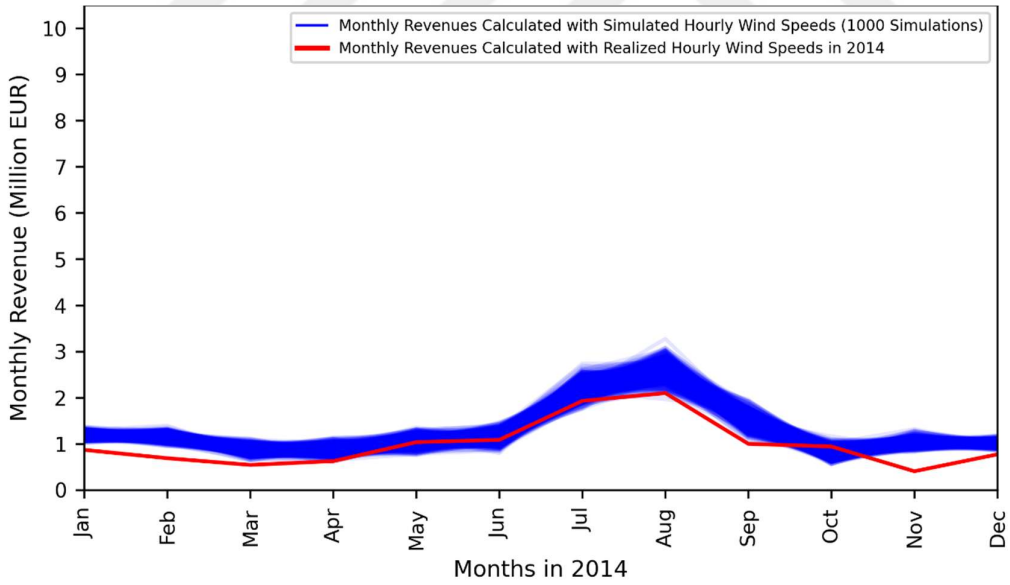

Figure 5.64 Optimized Monthly Revenues for Realized Electricity Price Year 2014

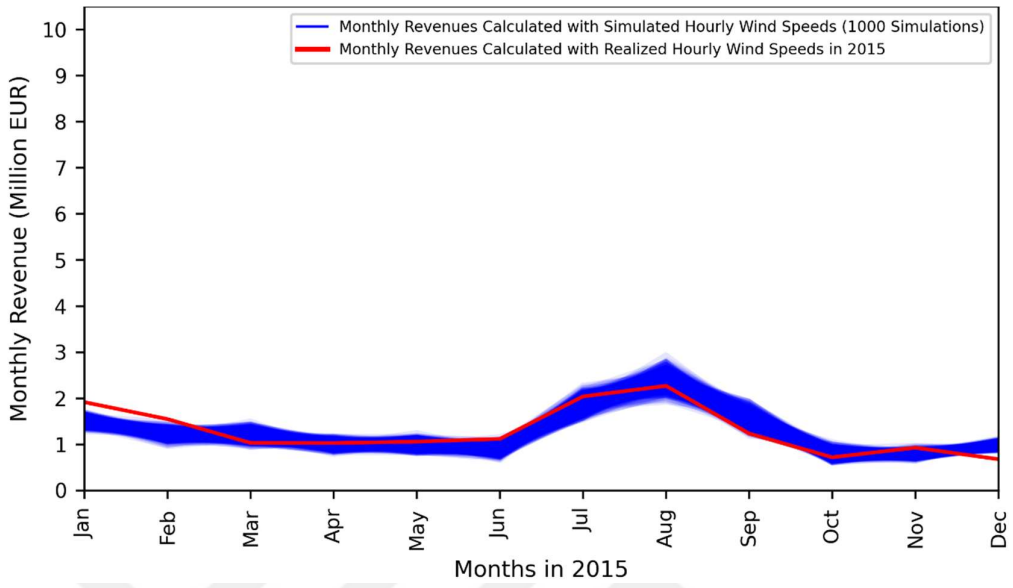

Figure 5.65 Optimized Monthly Revenues for Realized Electricity Price Year 2015

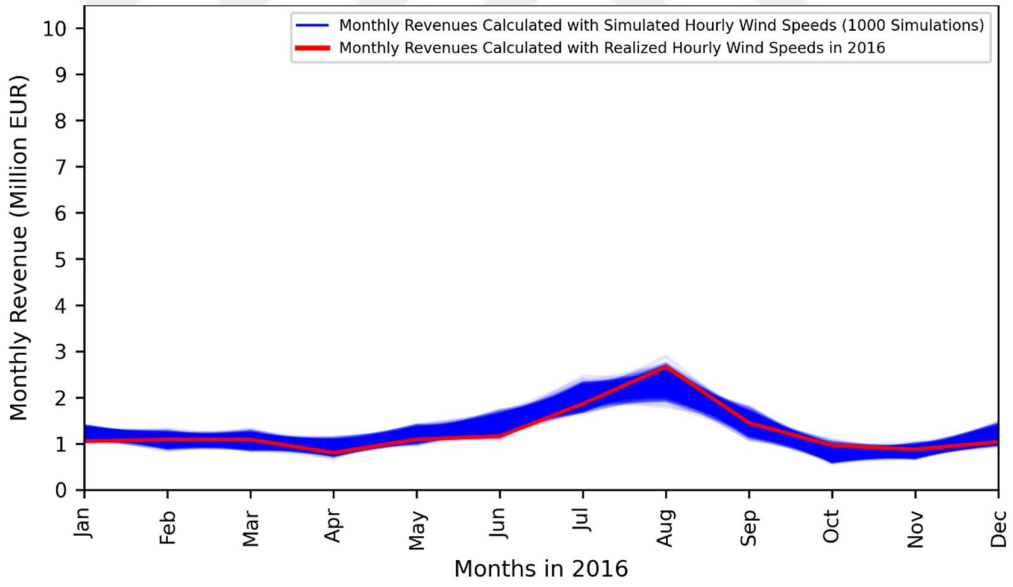

Figure 5.66 Optimized Monthly Revenues for Realized Electricity Price Year 2016

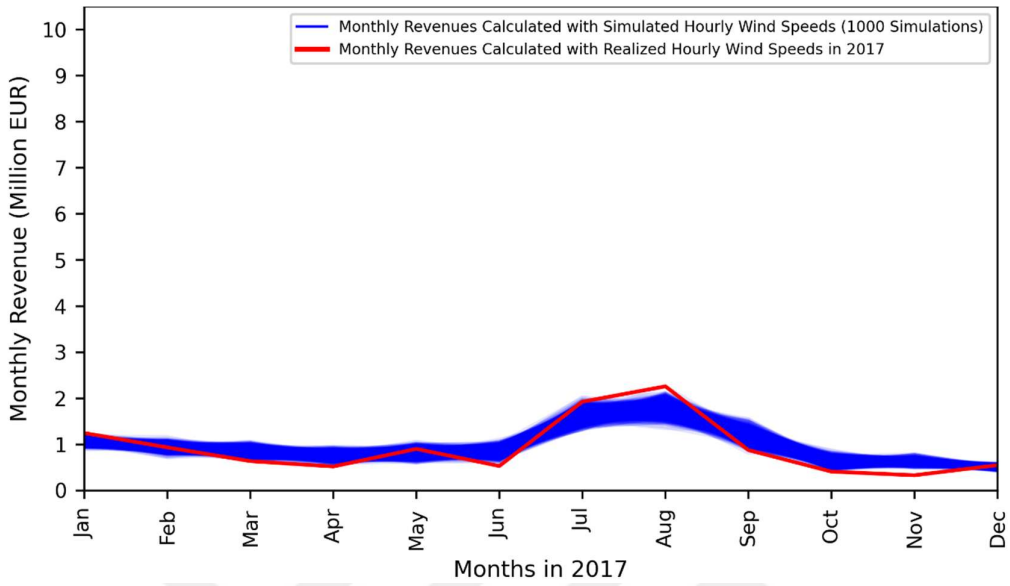

Figure 5.67 Optimized Monthly Revenues for Realized Electricity Price Year 2017

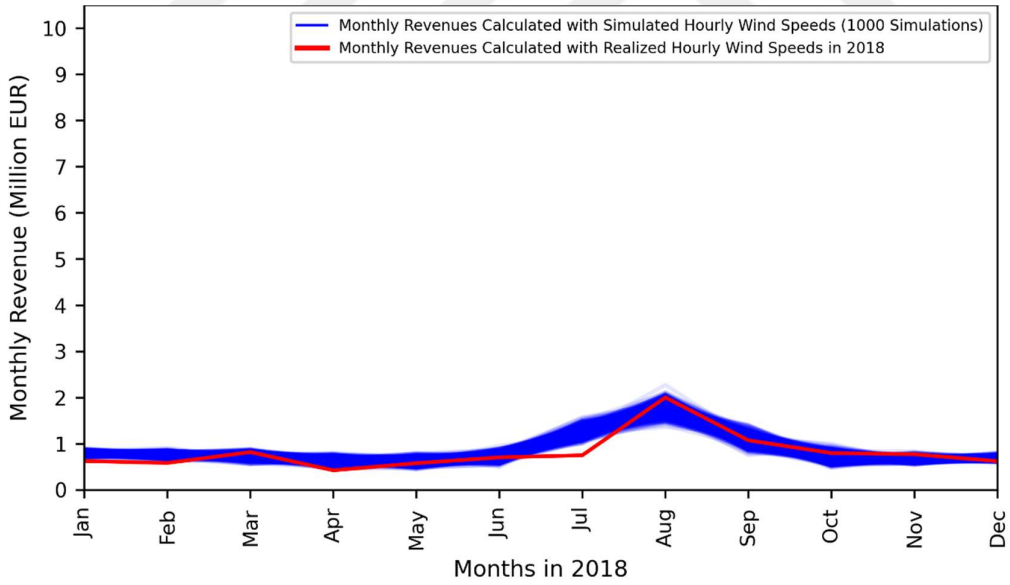

Figure 5.68 Optimized Monthly Revenues for Realized Electricity Price Year 2018

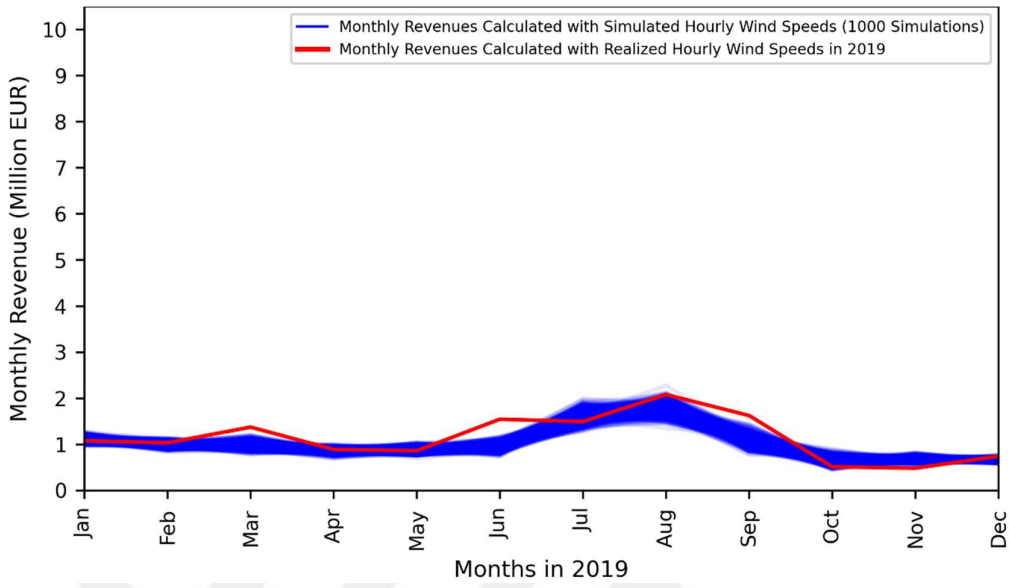

Figure 5.69 Optimized Monthly Revenues for Realized Electricity Price Year 2019

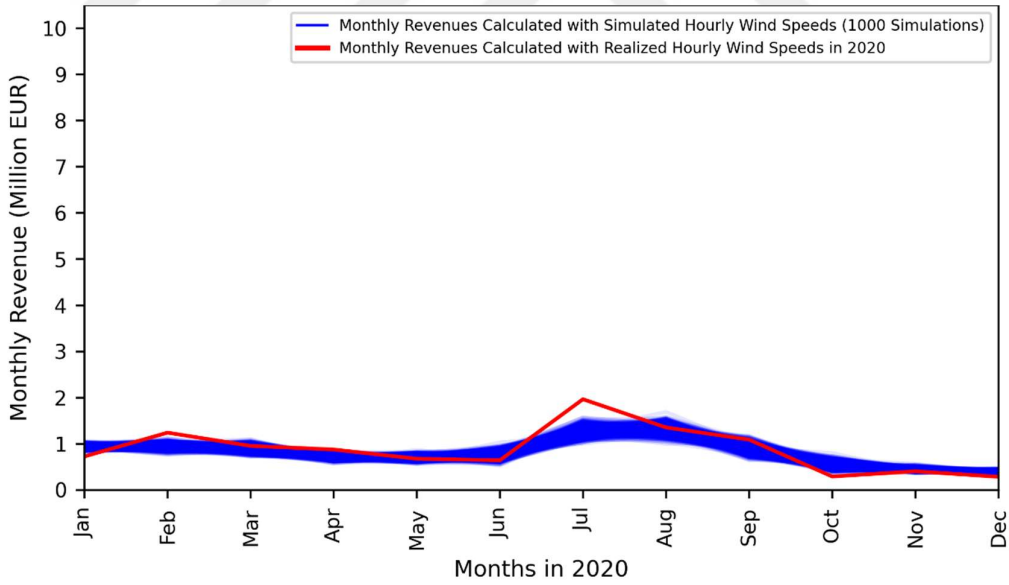

Figure 5.70 Optimized Monthly Revenues for Realized Electricity Price Year 2020

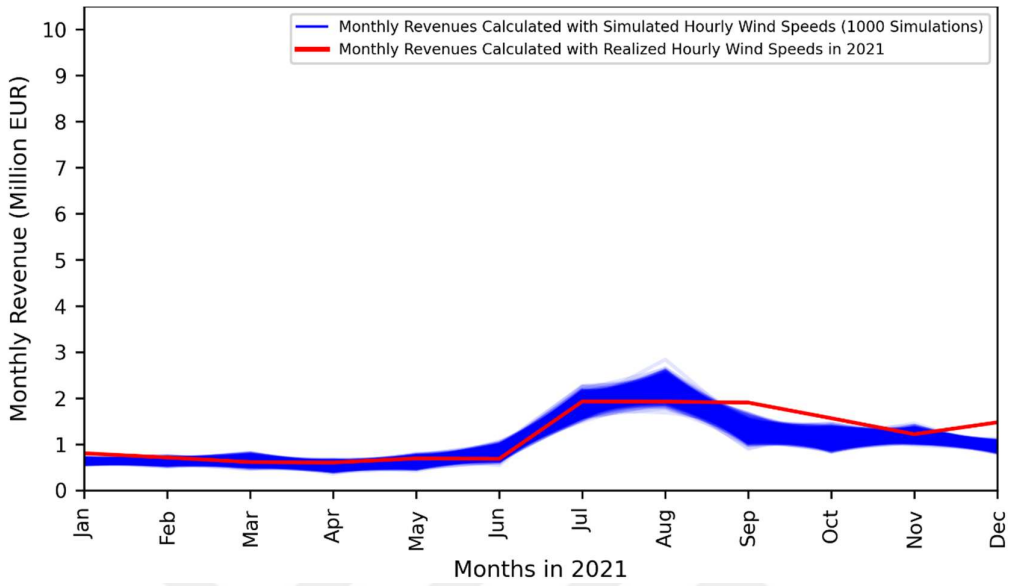

Figure 5.71 Optimized Monthly Revenues for Realized Electricity Price Year 2021

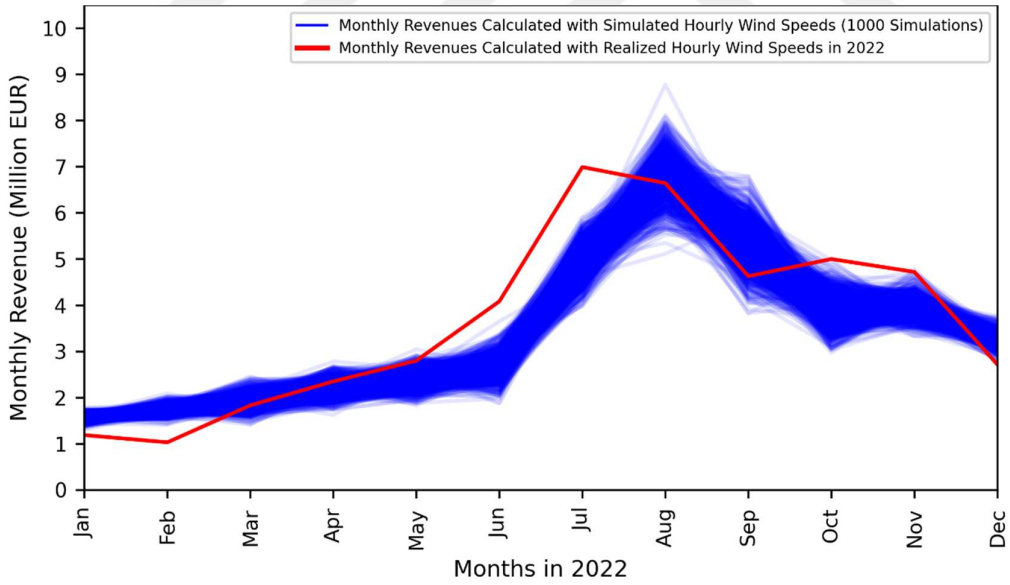

Figure 5.72 Optimized Monthly Revenues for Realized Electricity Price Year 2022

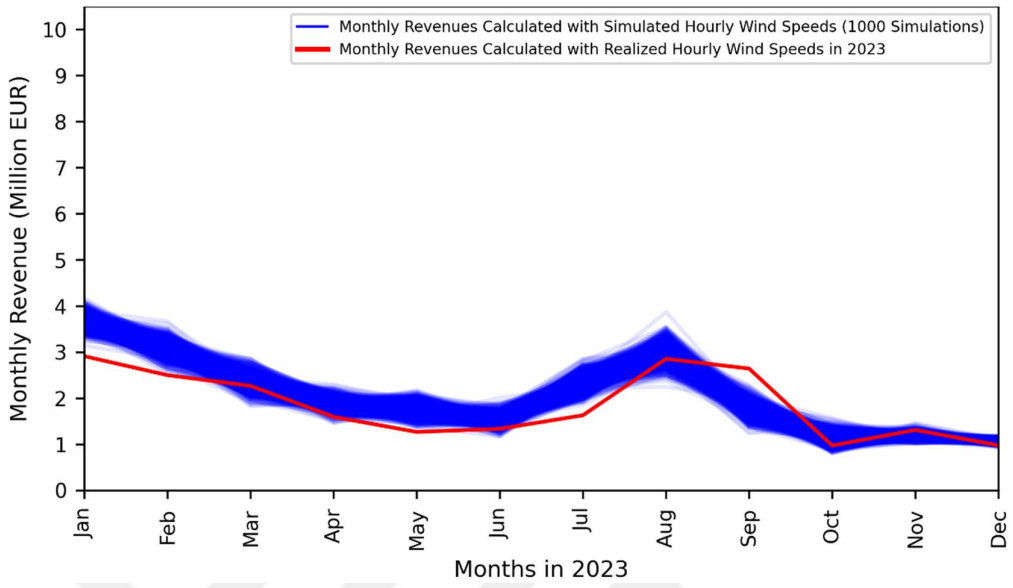

Figure 5.73 Optimized Monthly Revenues for Realized Electricity Price Year 2023

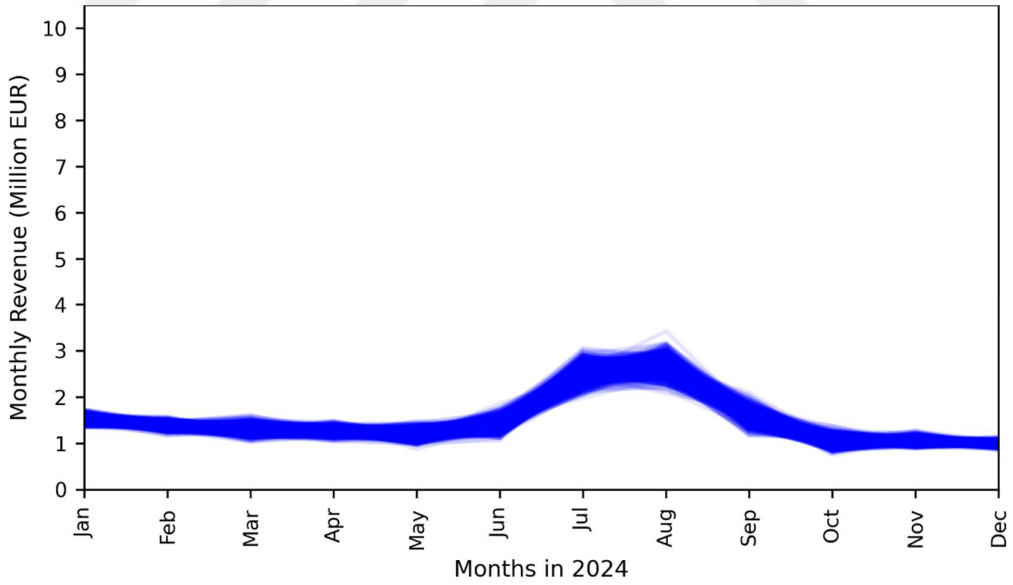

Figure 5.74 Optimized Monthly Revenues for Realized Electricity Price Year 2024

Figure 5.75, the average monthly revenues for each year from 2012 to 2024 are shown for a WHHS with a wind farm of 250 MW installed capacity. Each line

represents one year, calculated by averaging 1,000 monthly revenue trajectories from simulated wind speeds and optimized with that year's electricity prices.

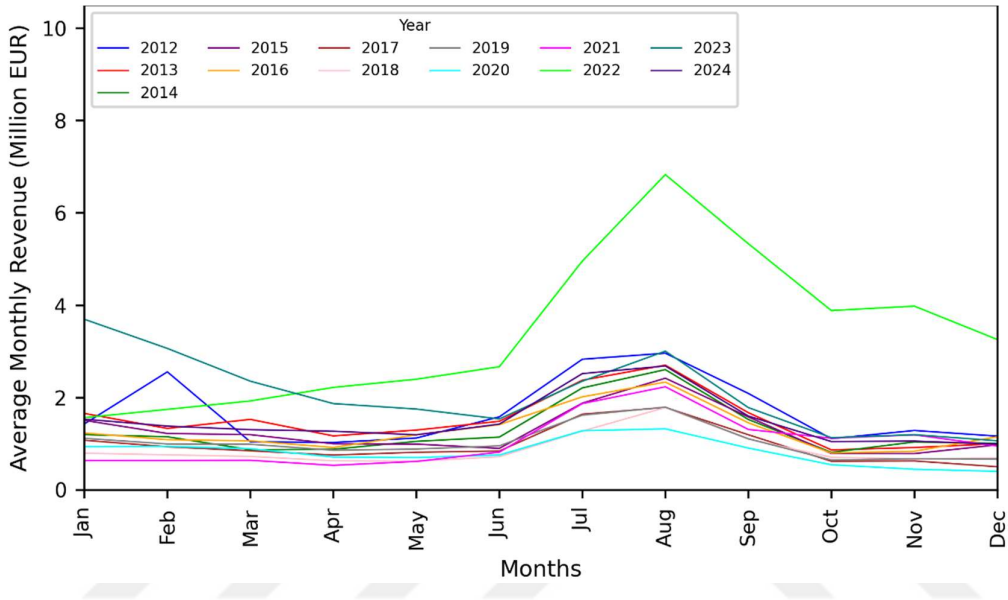

Figure 5.75 Optimized Average Monthly Revenues for Realized Electricity Price Years

In Figure 5.76, variation of annual revenues for each scenario year are plotted. In Figure 5.77 and Figure 5.78, variations of monthly revenues for each scenario year are plotted.

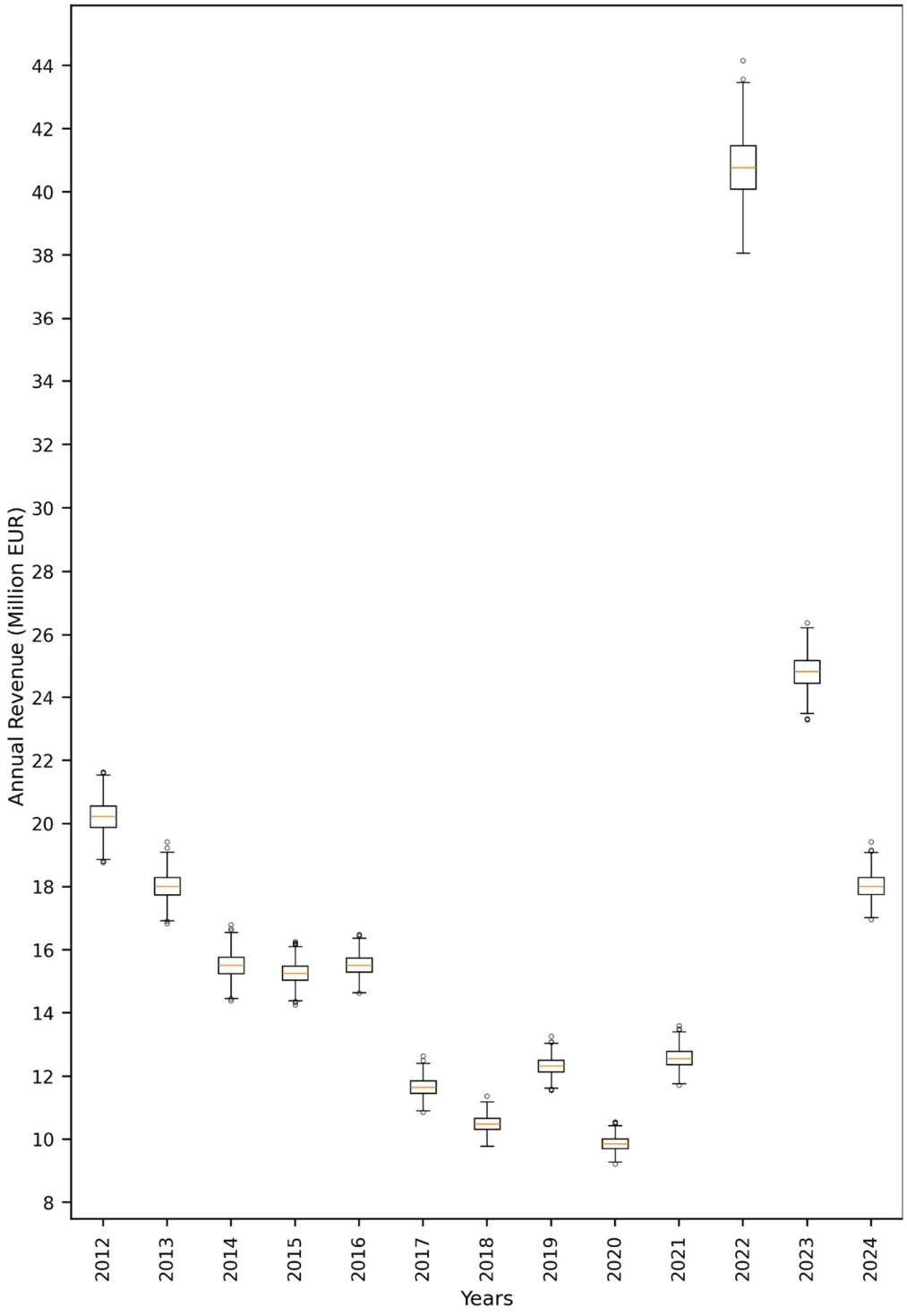

Figure 5.76 Variation of Annual Revenues for Realized Electricity Price Years

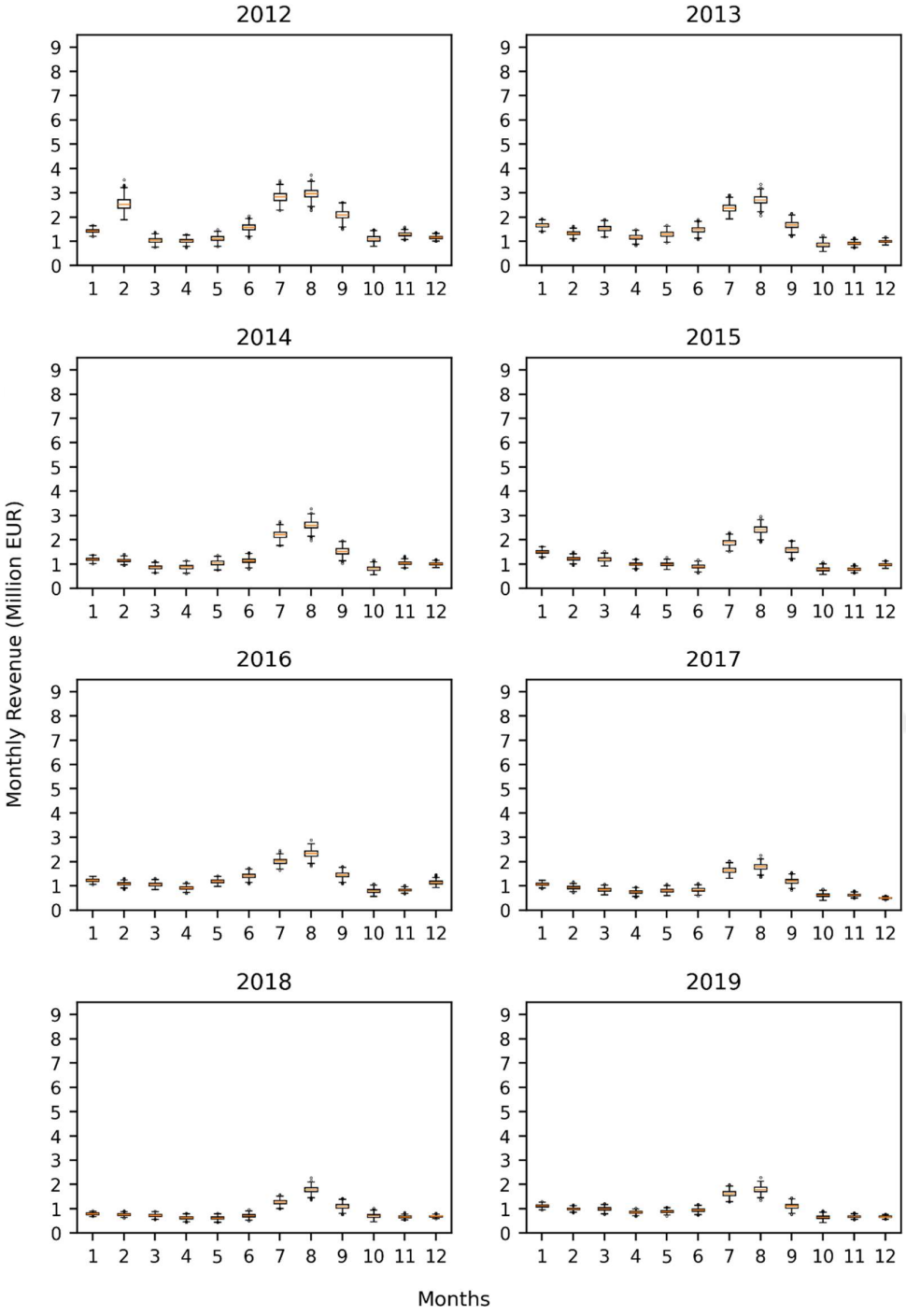

Figure 5.77 Variation of Monthly Revenues for Realized Electricity Price Years from 2012 to 2019

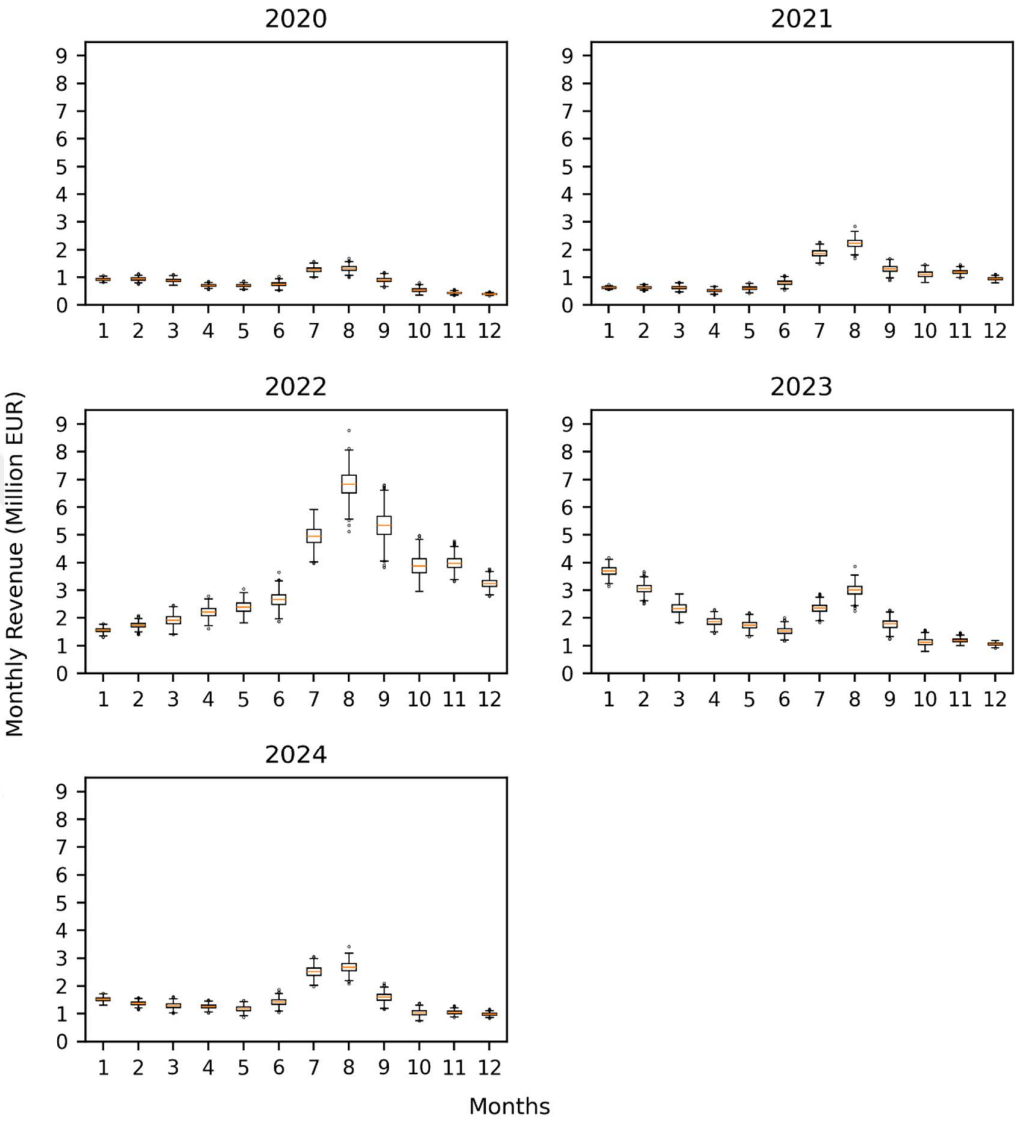

Figure 5.78 Variation of Monthly Revenues for Realized Electricity Price Years from 2020 to 2024

Figure 5.79 presents the distribution of annual revenues for the WHHS with a wind farm of 250 MW installed capacity for each scenario year (i.e., 2012–2024). For each year, 1,000 annual revenue values are computed using the same set of 1,000 simulated hourly wind speed time series. This allows isolating the impact of

electricity price variability from that of wind speed uncertainty. Although the simulated wind speed data includes some extreme outliers (see Figure 5.8), the width of the revenue distributions remains relatively narrow across all years. This suggests that the uncertainty resulting from wind speed variability has a limited influence on annual revenue. In contrast, the position of the PDFs shifts considerably along the x-axis from year to year, reflecting changes in electricity prices results in relatively large changes in annual revenues. Similar to the 50 MW installed capacity case, electricity price variability remains the dominant driver of revenue variation under the 250 MW case as well. Although wind speed simulations included some extreme outliers (see Figures 5.10 and 5.11), the effect of wind-related uncertainty is relatively smaller compared to that of electricity market fluctuations.

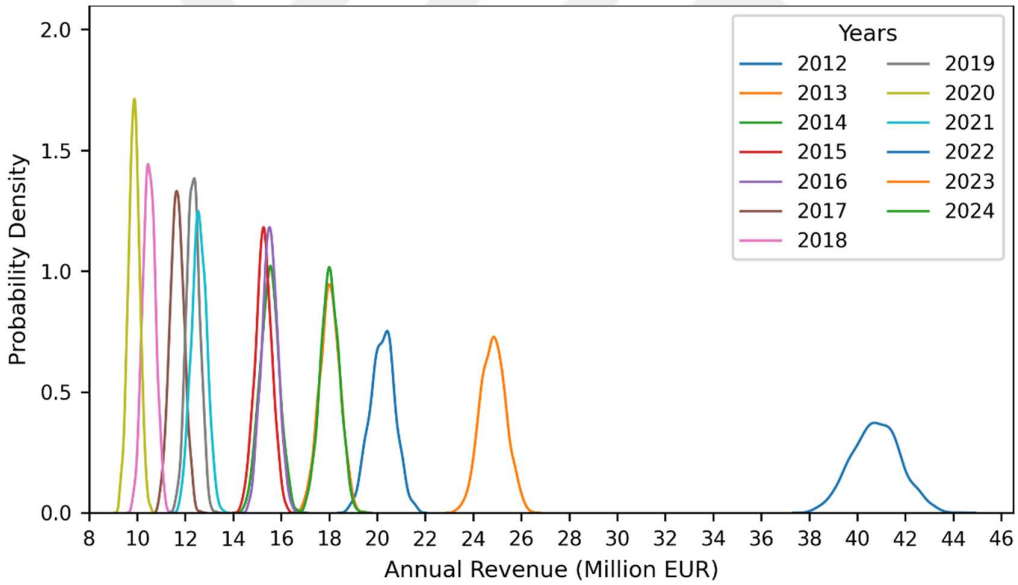

Figure 5.79 PDF of Annual Revenue for Realized Electricity Price Years

Change in annual revenue interquartile range (IQR) with respect to hourly electricity price IQR is given in Figure 5.80. Each data point represents one scenario year (i.e., 2012 to 2024) in Figure 5.80. There is a positive relationship between electricity price variability and revenue variability. In other words, as the hourly electricity

price variability increases within a year, the corresponding uncertainty in the annual revenue, obtained through the optimization model with simulated wind data increases. Notably, a particular year exhibits significantly higher price variability (~85 EUR) resulting in a substantial rise in revenue uncertainty (~1.37 million EUR), emphasizing how extreme market fluctuations can considerably amplify financial risk for WHHS. Notably, while the 50 MW installed capacity case exhibited an increase in revenue IQR of approximately 0.27 million EUR under a price IQR of ~85 EUR, the 250 MW case shows a much larger absolute increase of about 1.37 million EUR, illustrating how a higher installed capacity amplifies annual revenue uncertainty from market fluctuations.

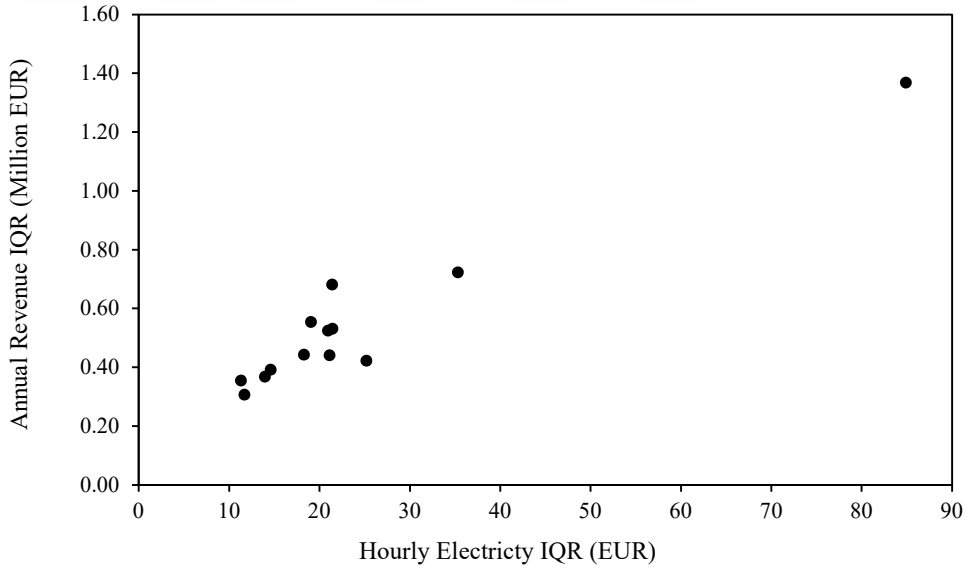

Figure 5.80 Change in Annual Revenue IQR with Hourly Electricity Price IQR

The change in annual revenue median with hourly electricity price median is given in Figure 5.81. Again, each data point represents one scenario year (i.e., 2012 to 2024) in Figure 5.81. As the median hourly electricity price increases, the corresponding median annual revenue increases as expected. A year with particularly high electricity prices (~130 EUR median price) clearly yields significantly higher

median annual revenues (~40 million EUR), emphasizing the substantial influence of electricity market price levels on annual profitability. By comparison, in the 50 MW case the same ~130 EUR median price corresponds to a median annual revenue of only about 14 million EUR, underscoring how increasing installed capacity amplifies revenue outcomes.

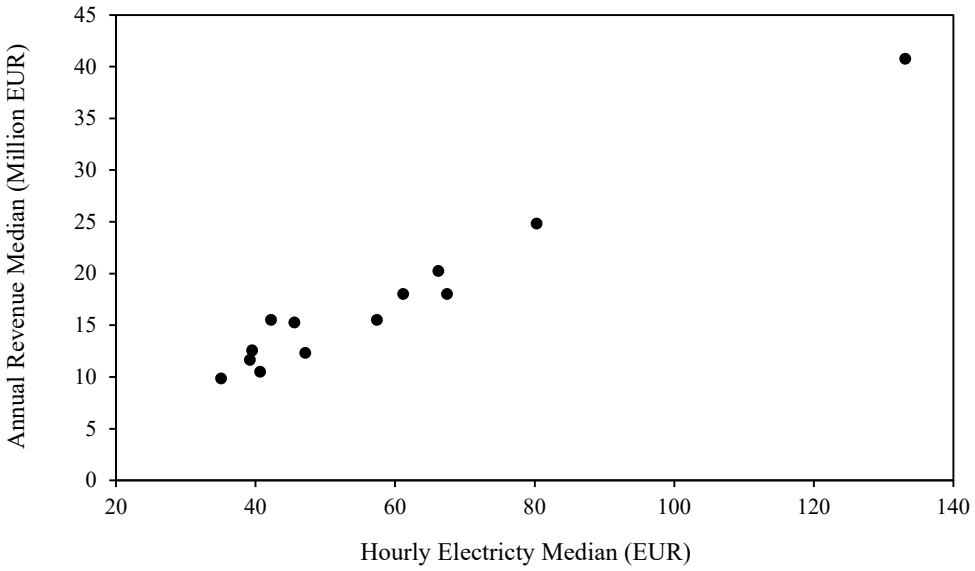

Figure 5.81 Change in Annual Revenue Median with Hourly Electricity Price Median

CHAPTER 6

CONCLUSION

This thesis examines the effect of uncertainty in wind speed on the revenue of a WHHS. To maximize yearly revenues, a daily revenue optimization model is employed, accounting for wind speed variability and electricity price fluctuations. Simulated wind speed time series are generated using the aLHS method to realistically reflect uncertainty in wind. Realized electricity price data from 2012 to 2024 are obtained from the Turkish electricity spot market and are used as scenarios to understand electricity price uncertainty, providing a robust representation of market variability. These datasets offer practical insight into optimizing hybrid systems under changing market conditions.

The significant findings of this thesis are given below:

- The analysis of PDFs of annual revenues for each scenario year from 2012 to 2024 (Figure 5.45) reveals that electricity price variability is the primary driver of revenue uncertainty in the WHHS. The PDFs shift significantly from year to year, reflecting substantial changes in annual revenue due to fluctuating electricity prices, while the width of the distributions—indicative of wind speed variability—remains relatively narrow. This suggests that, despite the inclusion of extreme wind speed outliers in the 1,000 simulated time series (Figure 5.8), wind speed uncertainty contributes less to revenue variability compared to electricity price fluctuations. For operators, this underscores the need to prioritize strategies that mitigate risks associated with electricity market volatility over those addressing wind speed unpredictability.

- A clear positive relationship between the IQR of hourly electricity prices and the IQR of annual revenues across the scenario years are observed (Figure 5.46). As electricity price variability increases, so does the uncertainty in annual revenue, with one year exhibiting exceptionally high price variability (~80 EUR) leading to a significant revenue uncertainty of approximately 0.28 million EUR. This finding highlight that, years with volatile electricity prices amplify financial risk, necessitating robust price forecasting and risk management strategies to stabilize WHHS revenue.

- A strong positive correlation between the median hourly electricity price and the median annual revenue is observed (Figure 5.47). Higher median electricity prices correspond to increased median revenues, with a notable outlier year (~130 EUR median price) yielding an annual revenue of approximately 15 million EUR. This indicates that the overall level of electricity prices in a given year significantly influences the profitability of the WHHS.

- The monthly revenue plots (Figure 5.28 to Figure 5.40) and their averages (Figure 5.41) reveal distinct seasonal patterns, with August consistently exhibiting the highest revenue and variability across most years, while November to April show lower variability. This aligns with seasonal wind speed trends (e.g., higher speeds in summer months like August, as seen in Figure 5.10). The variation of monthly revenues (Figure 5.43 and Figure 5.44) further supports this, showing broader spreads in the summer months. Operationally, this suggests that the WHHS could benefit from tailored strategies to capitalize on high revenue in summer months while managing lower variability in winter periods.

Some recommendations for future studies are listed below:

- A detailed economic study can be conducted to compare the initial investment, operational costs, and long-term returns of WHHS with other renewable energy systems, such as solar-hydro or wind-solar hybrids. A life-cycle assessment could also be included to evaluate which system offers the best value and sustainability over time.

- The model can be extended to include inflows (e.g., rainfall, river contributions) and outflows (e.g., evaporation, irrigation needs), reflecting an open-system approach. The WHHS simulation could be made more representative of real-world conditions.

- In this thesis, realized electricity prices serve to examine how fluctuations in electricity prices affect WHHS revenue. Instead of relying solely on realized electricity price data, future studies can use simulated electricity prices to capture future price uncertainty. This approach enables researchers to explore a broader range of scenarios, including extreme price spikes or potential future market conditions not reflected in historical data. By incorporating simulated electricity prices, researchers may gain a deeper understanding of the risks and opportunities arising from price volatility.

REFERENCES

Akenerji. (2005). *Çınarcık HES Gerekçe Raporu*.

Bhattacharya, S. (2019). *Design of Foundations for Offshore Wind Turbines*. Wiley. https://doi.org/10.1002/9781119128137

Blakers, A., Stocks, M., Lu, B., & Cheng, C. (2021). A review of pumped hydro energy storage. *Progress in Energy*, *3*(2). https://doi.org/10.1088/2516-1083/abeb5b

Borovkov, A. A. (1999). *Mathematical Statistics*. Gordon and Breach Science Publishers.

Brett, A. C., & Tuller, S. E. (1991). The Autocorrelation of Hourly Wind Speed Observations. *Journal of Applied Meteorology*, *30*(6), 823–833. https://doi.org/10.1175/1520-0450(1991)030<0823:TAOHWS>2.0.CO;2

Brown, B. G., Katz, R. W., & Murphy, A. H. (1984). Time Series Models to Simulate and Forecast Wind Speed and Wind Power. *Journal of Climate and Applied Meteorology*, *23*(8), 1184–1195. https://doi.org/10.1175/1520-0450(1984)023<1184:TSMTSA>2.0.CO;2

Castronuovo, E. D., & Lopes, J. A. P. (2004). On the Optimization of the Daily Operation of a Wind-Hydro Power Plant. *IEEE Transactions on Power Systems*, *19*(3), 1599–1606. https://doi.org/10.1109/TPWRS.2004.831707

Chen, H., Cong, T. N., Yang, W., Tan, C., Li, Y., & Ding, Y. (2009). Progress in electrical energy storage system: A critical review. *Progress in Natural Science*, *19*(3), 291–312. https://doi.org/10.1016/j.pnsc.2008.07.014

Cruz, P., Pousinho, H. M. I., Melício, R., & Mendes, V. M. F. (2014). Optimal Coordination on Wind-Pumped-Hydro Operation. *Procedia Technology*, *17*, 445–451. https://doi.org/10.1016/j.protcy.2014.10.253

Deane, J. P., Ó Gallachóir, B. P., & McKeogh, E. J. (2010). Techno-economic review of existing and new pumped hydro energy storage plant. *Renewable and Sustainable Energy Reviews*, *14*(4), 1293–1302. https://doi.org/10.1016/j.rser.2009.11.015

Díaz-González, F., Sumper, A., Gomis-Bellmunt, O., & Villafáfila-Robles, R. (2012). A review of energy storage technologies for wind power applications. *Renewable and Sustainable Energy Reviews*, *16*(4), 2154–2171. https://doi.org/10.1016/j.rser.2012.01.029

Dickey, D. A., & Fuller, W. A. (1979). Distribution of the Estimators for Autoregressive Time Series With a Unit Root. *Journal of the American Statistical Association*, *74*(366), 427. https://doi.org/10.2307/2286348

Dinçer, A. E., & Bozkuş, Z. (2016). Investigation of Waterhammer Problems in Wind-Hydro Hybrid Power Plants. *Arabian Journal for Science and Engineering*, *41*(12), 4787–4798. https://doi.org/10.1007/s13369-016-2142-2

Dursun, B., & Alboyaci, B. (2010). The contribution of wind-hydro pumped storage systems in meeting Turkey's electric energy demand. *Renewable and Sustainable Energy Reviews*, *14*(7), 1979–1988. https://doi.org/10.1016/j.rser.2010.03.030

Dursun, B., Alboyaci, B., & Gokcol, C. (2011). Optimal wind-hydro solution for the Marmara region of Turkey to meet electricity demand. *Energy*, *36*(2), 864–872. https://doi.org/10.1016/j.energy.2010.12.028

Dutta, S., & Gandomi, A. H. (2020). Design of experiments for uncertainty quantification based on polynomial chaos expansion metamodels. In *Handbook of Probabilistic Models* (pp. 369–381). Elsevier. https://doi.org/10.1016/B978-0-12-816514-0.00015-1

EMRA. (2024). *Electricity Market Sector Report*.

EPIAS TRANSPARENCY PLATFORM . (n.d.). EPİAS.

Ercan, E. (2020). *DEVELOPING OPTIMUM OPERATION STRATEGIES FOR WIND-HYDRO HYBRID SYSTEMS* [Master's thesis]. Middle East Technical University.

Ercan, E., & Kentel, E. (2022). Optimum daily operation of a wind-hydro hybrid system. *Journal of Energy Storage*, *50*, 104540. https://doi.org/10.1016/j.est.2022.104540

Eroğlu, M., & Finger, M. (Eds.). (2021). *The Regulation of Turkish Network Industries*. Springer International Publishing. https://doi.org/10.1007/978-3-030-81720-6

Fulton, B. J., Petigura, E. A., Blunt, S., & Sinukoff, E. (2018). RadVel: The Radial Velocity Modeling Toolkit. *Publications of the Astronomical Society of the Pacific*, *130*(986), 044504. https://doi.org/10.1088/1538-3873/aaaaa8

GE. (2010). *2.5 MW Wind Turbine Series*.

Graça Gomes, J., Telhada, J., Xu, H., Sá da Costa, A., & Zhao, C. (2021). Optimal operation scheduling of a pump hydro storage system coupled with a wind farm. *IET Renewable Power Generation*, *15*(1), 173–192. https://doi.org/10.1049/rpg2.12014

Hino, T., & Lejeune, A. (2012). Pumped Storage Hydropower Developments. *Comprehensive Renewable Energy*, 405–434. https://doi.org/10.1016/B978-0-08-087872-0.00616-8

Hosseini-Firouz, M. (2013). Optimal offering strategy considering the risk management for wind power producers in electricity market. *International Journal of Electrical Power & Energy Systems*, *49*, 359–368. https://doi.org/10.1016/j.ijepes.2013.01.015

Hunt, J. D., Zakeri, B., Lopes, R., Barbosa, P. S. F., Nascimento, A., Castro, N. J. de, Brandão, R., Schneider, P. S., & Wada, Y. (2020). Existing and new arrangements of pumped-hydro storage plants. *Renewable and Sustainable Energy Reviews*, *129*. https://doi.org/10.1016/j.rser.2020.109914

IEA. (2024). *World Energy Statistics and Balances*.

IRENA. (2024). *Renewable energy statistics 2024*. www.irena.org

Janssen, H. (2013). Monte-Carlo based uncertainty analysis: Sampling efficiency and sampling convergence. *Reliability Engineering and System Safety*, *109*, 123–132. https://doi.org/10.1016/j.ress.2012.08.003

Justus, C. G., & Mikhail, A. (1976). Height variation of wind speed and wind distributions statistics. *Geophysical Research Letters*, *3*(5), 261–264. https://doi.org/10.1029/GL003i005p00261

Korpaas, M., Holen, A. T., & Hildrum, R. (2003). Operation and sizing of energy storage for wind power plants in a market system. *International Journal of Electrical Power & Energy Systems*, *25*(8), 599–606. https://doi.org/10.1016/S0142-0615(03)00016-4

Kose, F., & Kaya, M. N. (2013). Analysis on meeting the electric energy demand of an active plant with a wind-hydro hybrid power station in Konya, Turkey: Konya water treatment plant. *Renewable Energy*, *55*, 196–201. https://doi.org/10.1016/j.renene.2012.12.047

Lamb, W. F., Wiedmann, T., Pongratz, J., Andrew, R., Crippa, M., Olivier, J. G. J., Wiedenhofer, D., Mattioli, G., Khourdajie, A. Al, House, J., Pachauri, S., Figueroa, M., Saheb, Y., Slade, R., Hubacek, K., Sun, L., Ribeiro, S. K., Khennas, S., de la Rue du Can, S., … Minx, J. (2021). A review of trends and drivers of greenhouse gas emissions by sector from 1990 to 2018. *Environmental Research Letters*, *16*(7), 073005. https://doi.org/10.1088/1748-9326/abee4e

Le, V. H., & Vargas, R. (2024). An autocorrelated conditioned Latin hypercube method for temporal or spatial sampling and predictions. *Computers and Geosciences*, *184*. https://doi.org/10.1016/j.cageo.2024.105539

Li, S. H. (2018). Effect of disjunct sampling on calibration of design wind speed. *Journal of Wind Engineering and Industrial Aerodynamics*, *183*, 283–294. https://doi.org/10.1016/j.jweia.2018.11.016

Luo, X., Wang, J., Dooner, M., & Clarke, J. (2015). Overview of current development in electrical energy storage technologies and the application potential in power system operation. *Applied Energy*, *137*, 511–536. https://doi.org/10.1016/j.apenergy.2014.09.081

Ma, X.-Y., Sun, Y.-Z., & Fang, H.-L. (2013). Scenario Generation of Wind Power Based on Statistical Uncertainty and Variability. *IEEE Transactions on Sustainable Energy*, *4*(4), 894–904. https://doi.org/10.1109/TSTE.2013.2256807

Madlener, R., & Specht, J. M. (2020). An Exploratory Economic Analysis of Underground Pumped-Storage Hydro Power Plants in Abandoned Deep Coal Mines. *Energies*, *13*(21). https://doi.org/10.3390/en13215634

Manwell, J. F., McGowan, J. G., & Rogers, A. L. (2009). *Wind Energy Explained*. Wiley. https://doi.org/10.1002/9781119994367

McCoy, A., Musial, W., Hammond, R., Hernando, D. M., Duffy, P., Beiter, P., Pérez, P., Baranowski, R., Reber, G., & Spitsen, P. (2024). *OFFSHORE WIND MARKET REPORT 2024 EDITION*. https://www.nrel.gov/docs/fy24osti/90525.pdf

Minasny, B., & McBratney, A. B. (2006). A conditioned Latin hypercube method for sampling in the presence of ancillary information. *Computers and Geosciences*, *32*(9), 1378–1388. https://doi.org/10.1016/j.cageo.2005.12.009

Moghimi Ghadikolaei, H., Ahmadi, A., Aghaei, J., & Najafi, M. (2012). Risk constrained self-scheduling of hydro/wind units for short term electricity markets considering intermittency and uncertainty. *Renewable and Sustainable Energy Reviews*, *16*(7), 4734–4743. https://doi.org/10.1016/j.rser.2012.04.019

Morales, J. M., Conejo, A. J., & Perez-Ruiz, J. (2010). Short-Term Trading for a Wind Power Producer. *IEEE Transactions on Power Systems*, *25*(1), 554–564. https://doi.org/10.1109/TPWRS.2009.2036810

Nakanishi, K. M., Fujii, K., & Todo, S. (2020). Sequential minimal optimization for quantum-classical hybrid algorithms. *Physical Review Research*, *2*(4), 043158. https://doi.org/10.1103/PhysRevResearch.2.043158

Olauson, J. (2018). ERA5: The new champion of wind power modelling? *Renewable Energy*, *126*, 322–331. https://doi.org/10.1016/j.renene.2018.03.056

Pinson, P., Chevallier, C., & Kariniotakis, G. N. (2007). Trading Wind Generation From Short-Term Probabilistic Forecasts of Wind Power. *IEEE Transactions on Power Systems*, *22*(3), 1148–1156. https://doi.org/10.1109/TPWRS.2007.901117

Pinson, P., Madsen, H., Nielsen, H. Aa., Papaefthymiou, G., & Klöckl, B. (2009). From probabilistic forecasts to statistical scenarios of short-term wind power production. *Wind Energy*, *12*(1), 51–62. https://doi.org/10.1002/we.284

Poggi, P., Muselli, M., Notton, G., Cristofari, C., & Louche, A. (2003). Forecasting and simulating wind speed in Corsica by using an autoregressive model. *Energy Conversion and Management*, *44*(20), 3177–3196. https://doi.org/10.1016/S0196-8904(03)00108-0

Ramírez, P., & Carta, J. A. (2005). Influence of the data sampling interval in the estimation of the parameters of the Weibull wind speed probability density distribution: A case study. *Energy Conversion and Management*, *46*(15–16), 2419–2438. https://doi.org/10.1016/j.enconman.2004.11.004

Romero, J., Babbush, R., McClean, J. R., Hempel, C., Love, P. J., & Aspuru-Guzik, A. (2018). Strategies for quantum computing molecular energies using the unitary coupled cluster ansatz. *Quantum Science and Technology*, *4*(1), 014008. https://doi.org/10.1088/2058-9565/aad3e4

Tong, W. (2010). *Wind Power Generation and Wind Turbine Design*. WIT Press.

Wiser, R., Millstein, D., Hoen, B., Bolinger, M., Gorman, W., Rand, J., Barbose, G., Cheyette, A., Darghouth, N., Jeong, S., Kemp, J., O'Shaughnessy, E., Paulos, B., & Seel, J. (2024). *LAND-BASED WIND MARKET REPORT 2024 EDITION*.

Yang, C.-J., & Jackson, R. B. (2011). Opportunities and barriers to pumped-hydro energy storage in the United States. *Renewable and Sustainable Energy Reviews*, *15*(1), 839–844. https://doi.org/10.1016/j.rser.2010.09.020

Yarıcı, M. (2018). *Day Ahead Market*. World Energy Council Turkish National Committee.

Yule, G. U. (1927). VII. On a method of investigating periodicities disturbed series, with special reference to Wolfer's sunspot numbers. *Philosophical Transactions of the Royal Society of London. Series A, Containing Papers of a Mathematical or Physical Character*, *226*(636–646), 267–298. https://doi.org/10.1098/rsta.1927.0007

Zhao, K., Wang, J., & Qiu, L. (2024). Approval and progress analysis of pumped storage power stations in Central China during the 14th five-year plan period. *Journal of Energy Storage*, *102*. https://doi.org/10.1016/j.est.2024.114104

APPENDICES

A. Daily Revenue Optimization Model

In this study, the same optimization model used in Ercan (2020) is used. Thus, the mathematical formulation and following explanations are taken from Ercan (2020).

Mathematical Formulation

The daily schedule of the WHHS that maximizes the net revenue of the day can be obtained from the solution of the following optimization problem modified by Ercan (2020) from the formulation developed by Cruz et al.(2014):

$$\text{Max. } Z = \sum_{t=0}^{23} \lambda_t p_t \tag{6-1}$$

s.t.

$$p_t = p_t^{\text{wdirect}} + p_t^{\text{hydro}} - p_t^{\text{fgrid}} \tag{6-2}$$

$$p_t^{\text{wdirect}} + p_t^{\text{hydro}} \leq \left(p_{max}^{w} + p_{max}^{\text{hydro}}\right) y_t \quad \forall y_t \tag{6-3}$$

$$p_t^{\text{fgrid}} \leq p_{max}^{\text{fgrid}} (1 - y_t) \quad \forall y_t \tag{6-4}$$

$$p_t^{w} = p_t^{\text{wdirect}} + p_t^{\text{wpump}} \tag{6-5}$$

$$p_t^{\text{pump}} = p_t^{\text{wpump}} + p_t^{\text{fgrid}} \tag{6-6}$$

$$0 \leq p_t^{w} \leq p_{max}^{w} \tag{6-7}$$

$$0 \leq p_t^{\text{hydro}} \leq p_{max}^{\text{hydro}}(1 - x_t) \quad \forall x_t \tag{6-8}$$

$$0 \leq p_t^{\text{pump}} \leq p_{max}^{\text{pump}} x_t \quad \forall x_t \tag{6-9}$$

$$p_t^{\text{hydro}} \leq \min\{(E_t - E_{min})\eta_{\text{hydro}},\ p_{max}^{\text{hydro}}\} \tag{6-10}$$

$$p_t^{\text{pump}} \leq \min\left\{(E_{max} - E_t)\frac{1}{\eta_{\text{pump}}},\ p_{max}^{\text{pump}}\right\} \tag{6-11}$$

$$E_{t+1} = E_t + \eta_{\text{pump}} p_{t+1}^{\text{pump}} - \frac{1}{\eta_{\text{hydro}}} p_{t+1}^{\text{hydro}} \quad t = 0,1,\ldots,22 \tag{6-12}$$

$$E_0 = E_{\text{initial}} + \eta_{\text{pump}} p_0^{\text{pump}} - \frac{1}{\eta_{\text{hydro}}} p_0^{\text{hydro}} \tag{6-13}$$

$$E_{min} \leq E_t \leq E_{max} \tag{6-14}$$

$$y_t \in \{0,1\} \tag{6-15}$$

$$x_t \in \{0,1\} \tag{6-16}$$

$$p_t^{\text{hydro}},\ p_t^{\text{wdirect}},\ p_t^{\text{fgrid}},\ p_t^{\text{wpump}},\ p_t^{\text{pump}},\ p_t^{W},\ E_t \geq 0 \tag{6-17}$$

Where the set is:

$t \in \{0,1,2,\ldots,23$ the duration of each interval, hour;

where the variables are:

p_t the energy output injected into the grid minus energy bought from the grid in t;

λ_t the electricity price in t;

p_t^{wdirect} the energy output of wind turbines that is sold directly to the grid in t;

p_t^{hydro} the energy output of the hydro turbine that is sold directly to the grid in t;

p_t^{fgrid} the energy bought from the grid in t;

p_t^{w} the wind energy that is generated in t;

p_t^{wpump} the energy that is generated by wind turbines and is used by the pump in t;

p_t^{pump} the energy that is used for pumping in t;

E_t the energy stored in the upper reservoir at the end of t;

y_t the binary variable that represents the buying or selling mode of the system in t where $y_t = 0$ is the buying mode, and $y_t = 1$ is the selling mode;

x_t the binary variable that represents the turbine or pump modes in t where $x_t = 0$ is the turbine mode, and $y_t = 1$ is the pump mode;

and the corresponding parameters are:

p_{max}^{w} the maximum energy that can be generated by the wind turbines in an hour;

p_{max}^{hydro} the maximum energy that can be generated by the hydro turbine in an hour;

p_{max}^{fgrid} the maximum energy that can be bought from the grid in an hour;

p_{max}^{pump} the maximum energy that can be used as pumping input in an hour;

E_{min} the minimum energy level in the upper reservoir;

E_{max} the maximum energy level that can be stored in the upper reservoir;

η_{hydro} the efficiency for the turbine mode;

η_{pump} the efficiency for the pump mode;

E_{initial} the initial energy in the upper reservoir.

Equation (6-1) is the objective function of the optimization problem. It aims to maximize the revenue of one day. Equation (6-2) defines the net energy sold to the grid, which is the energy sold minus the energy bought. When p_t^{wdirect} and p_t^{hydro} are positive values, p_t^{fgrid}cannot be a positive value. Because selling and buying energy from the grid at the same time is illogical and not allowed. This is achieved by Equations (6-3) and (6-4). If y_t equals one, the system sells energy to the grid in t; if it equals zero, the system buys energy from the grid in t. The wind energy that is generated in t p_t^w , can be sold directly to the grid or used to pump the water to the upper reservoir. This is defined in Equation (6-5). The energy that is used for pumping in t p_t^{pump}, can be supplied by wind turbines or can be bought from the grid. Equation (6-6) presents this constraint. The wind energy that is generated in t p_t^w, has a minimum value of zero, and its upper bound cannot exceed p_{max}^w as defined in Equation (6-7). The energy output of the hydro turbine in t p_t^{hydro}, and the energy used for pumping in t p_t^{pump} cannot be larger than their maximum installed capacities. Also, they cannot be positive values at the same hour since it is not possible to run the pump and the turbine at the same time. These limitations are defined in Equations (6-8) and (6-9).

The energy output of the hydro turbine in t p_t^{hydro} is limited by two components in Equation (6-10). In the first component, $E_t - E_{min}$ represents the energy in the upper

reservoir that can be used to generate energy by the hydro turbine. When it is multiplied by η_{hydro}, it becomes the energy output of the hydro turbine. The second component is the maximum capacity of the hydro turbine. So, p_t^{hydro} is restricted to be at most the minimum of these two terms.

The energy that is used for pumping in t p_t^{pump} is limited by two components in Equation (6-11). In the first component, $E_{max} - E_t$ represents the available empty energy storage that can be filled by the water. When it is divided by η_{pump}, it becomes the pumping energy input. The second component is the maximum energy input for the pump. So, p_t^{pump} is restricted to be at most the minimum of these two terms.

The energy balance of the upper reservoir is defined in Equation (6-12). The energy stored in the upper reservoir at the end of $t + 1$ is composed of three components. The first component is the stored energy from the previous hour. The second component is the energy used for pumping the water from the lower reservoir to the upper reservoir in $t + 1$. The third component is the energy spend to run the hydro turbine to generate electricity in $t + 1$. So, E_{t+1} equals the summation of the first two components minus the third component. For the first hour, $t = 0$, the energy stored in the upper reservoir is initialized based on the starting energy storage in the upper reservoir E_{-1}. Lastly, E_t must be between E_{min} and E_{max}, and that is defined in Equation (6-14).

Except binary variables, y_t and x_t, units of all decision variables (p_t, p_t^{wdirect}, p_t^{hydro}, p_t^{fgrid}, p_t^{wpump}, p_t^{pump}, p_t^w, E_t) are MWh. Units of all parameters (p_{max}^{hydro}, p_{min}^{hydro}, p_{max}^{pump}, p_{min}^{pump}, p_{max}^w, p_{min}^w, p_{max}^{fgrid}, E_{initial}, E_{max}, E_{min}) are MWh, except a few ones. The unit of λ_t is TL/MWh, and η_{hydro} and η_{pump} are unitless.

The optimization model involves three assumptions. First, head losses in the piping system of WHHS are not included explicitly. They are assumed to be included in the efficiency values of the turbine and pump modes. Second, there is no inflow to or outflow from the reservoir. So, the system is assumed to be a closed-loop system.

Third, the cost of pumping operation is assumed to be the same value as the electricity price at that hour (Cruz et al., 2014).

The following modifications to the mathematical formulation suggested by Cruz et al. (2014) are carried out in this study:

- The energy that is generated by the wind turbines is allowed to be used for pumping and direct selling, and stored in two different variables (see Equation (6-5)).
- The energy that is used for pumping is allowed to be obtained from wind turbines and grid, and stored in two different variables (see Equation (6-6)).
- To prevent buying and selling at the same time in each hour, a binary variable is defined (see Equations (6-3) and (6-4)).
- Considering the minimum and maximum water levels in the upper reservoir, water can be pumped or released from the upper reservoir, and the energy stored in the upper reservoir is updated (see Equations (6-10) and (6-11)).
- Equations (13) and (14) in Cruz et al. (2014) are not used since they are satisfied by Equations (6-10) and (6-11).
- In Cruz et al. (2014), the final energy level of the upper reservoir is taken as a fixed value. However, in our study, we used the reservoir level of the last hour of the previous day.

The formulated optimization problem is a mixed-integer linear programming problem since two of the decision variables (i.e., x_i and y_i) are restricted to binary values. To solve the optimization problem, a code is written in Python. The code uses Coinor branch and cut solver which is developed by Forrest, Ralphs, Vigerske, LouHafer, Kristjansson, Jpfasano, EdwinStraver, Lubin, Santos, Rlougee and Saltzman (2018). To apply this solver in Python, Google OR-Tools library is included in the code.

B. Daily Revenue Optimization Model Parameters

The optimization model has eight parameters, which are the maximum energy that can be generated by wind turbines in an hour, the maximum energy that can be generated by the hydro turbine in an hour, the maximum energy that can be bought from the grid in an hour, the maximum energy that can be consumed by the pump in an hour, the minimum energy level in the upper reservoir, the maximum energy level that can be stored in the upper reservoir, the efficiency for the turbine mode and the efficiency for the pump mode. The maximum energy that can be generated by the wind turbines p_{max}^{w} in an hour equals to the available hourly wind energy. Its calculation is explained in Section 4.4.

Currently, the installed capacity of the hydro turbine in the Uluabat Hydropower Plant is 100 MW (Akenerji, 2005). Same installed capacity is sued by changing the hydro turbine with a hydro pump-turbine. So, for this case study, the system can work either as a hydro turbine or a pump. Thus, the maximum energy that can be generated by the hydro turbine in an hour p_{max}^{hydro} and the maximum energy that can be consumed by pumping in an hour p_{max}^{pump} equal to 100 MWh.

The maximum energy that can be bought from the grid in an hour is not limited. Thus, this parameter equals positive infinity. The schematic view of Çınarcık Dam, Uluabat Hydropower Plant, and Lake Uluabat are shown in Figure 6.1. The minimum energy level in the upper reservoir and the maximum energy level that can be stored in the upper reservoir is computed based on the elevation-area curve of the dam by using the following expression:

$$E_p = 2.778 \times 10^{-10}\, \rho g h V \tag{6.18}$$

where E_p is the potential energy of the fluid in MWh, V is the volume of the fluid in m^3, ρ is the density of the fluid in kg/m^3, g is the acceleration due to gravity in m/s^2, h is the height of the fluid in m. The minimum energy level in the upper

reservoir E_{min}, and the maximum energy level that can be stored in the upper reservoir E_{max} are computed as 138233.8 MWh and 298624.1 MWh, respectively. The initial energy level E_{initial} is fixed to E_{min}, 138233.8 MWh.

The efficiency of the turbine mode and the efficiency of the pump mode are assumed as 0.88 and 0.85, respectively, based on the study by Cruz et al. (2014).

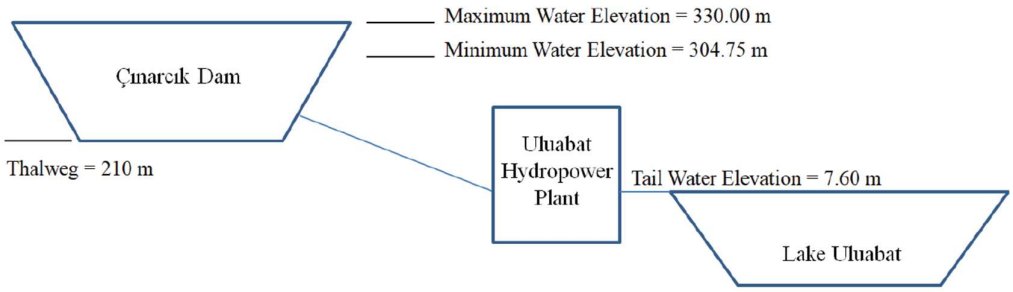

Figure 6.1 The Schematic View of Çınarcık Dam, Uluabat Hydropower Plant and Lake Uluabat (Ercan, 2020)

C. R Script for Stationarity Test of Observed Hourly Wind Speeds

```
# Load required packages
library(tseries)
library(xts)
library(fUnitRoots)
library(writexl)  # For writing results to Excel

# Load data from file
wind_data <- read.csv2(file = "path/MS18386_(2014_2023).csv",
                       sep = ";",
                       header = TRUE,
                       na.strings = "")

# Rename columns
colnames(wind_data) <- c("Date", "Wind_Speed")

# Convert Date column to time series format
wind_data$Date <- as.POSIXct(wind_data$Date, format = "%d.%m.%Y %H:%M", tz = "UTC")

# Remove missing values from the entire data frame
wind_data <- na.omit(wind_data)

# Convert Wind_Speed column to numeric format
wind_data$Wind_Speed <- as.numeric(wind_data$Wind_Speed)

# Define frequency values (daily, weekly, monthly, yearly)
frequencies <- c(daily = 24, weekly = 24*7, monthly = 24*30, yearly = 24*365.25)
frequency_names <- names(frequencies)

# Define lag values (1 to 12)
lag_values <- 1:6

# Define test types (including tseries::adf.test as "stationary")
test_types <- c("tseries_stationary", "funit_nc", "funit_c", "funit_ct")

# Create an empty data frame to store results
results_table <- data.frame(
  Frequency = character(),
  Lag = integer(),
  Test_Type = character(),
  ADF_Statistic = numeric(),
  ADF_pvalue = numeric(),
  stringsAsFactors = FALSE
)

# Loop through frequencies, lags, and test types to run ADF tests
for (freq_idx in seq_along(frequencies)) {
  freq <- frequencies[freq_idx]
  freq_name <- frequency_names[freq_idx]
```

```
# Loop through frequencies, lags, and test types to run ADF tests
for (freq_idx in seq_along(frequencies)) {
  freq <- frequencies[freq_idx]
  freq_name <- frequency_names[freq_idx]

  # Create time series object
  wind_ts <- ts(wind_data$Wind_Speed, frequency = freq)

  for (lag in lag_values) {
    for (type in test_types) {
      # Run appropriate ADF test based on type
      if (type == "tseries_stationary") {
        adf_result <- adf.test(wind_ts, alternative = "stationary", k =
        test_label <- "tseries: Stationary"
      } else if (type == "funit_nc") {
        adf_result <- adfTest(wind_ts, lags = lag, type = "nc")
        test_label <- "fUnitRoots: No Constant"
      } else if (type == "funit_c") {
        adf_result <- adfTest(wind_ts, lags = lag, type = "c")
        test_label <- "fUnitRoots: Constant"
      } else if (type == "funit_ct") {
        adf_result <- adfTest(wind_ts, lags = lag, type = "ct")
        test_label <- "fUnitRoots: Constant+Trend"
      }

      # Extract statistic and p-value
      if (type == "tseries_stationary") {
        statistic <- adf_result$statistic
        p_value <- adf_result$p.value
      } else {
        statistic <- adf_result@test$statistic
        p_value <- adf_result@test$p.value
      }

      # Add results to the table
      results_table <- rbind(results_table, data.frame(
        Frequency = freq_name,
        Lag = lag,
        Test_Type = test_label,
        ADF_Statistic = statistic,
        ADF_pvalue = p_value,
        stringsAsFactors = FALSE
      ))
    }
  }
}

# Display results in console (optional)
print("ADF Test Results:")
print(results_table)

# Save results to an Excel file
write_xlsx(results_table, "path/adf_test_results.xlsx")

# Notification
cat("ADF test results have been saved to 'adf_test_results.xlsx'.\n")
```

D. ADF Stationarity Test Results of Observed Hourly Wind Speeds

Table 6-1 Stationarity Test Results for Observed Hourly Wind Speeds (lag=1 hour)

Frequency	Lag	Test Type	Statistic	P value
daily	1	tseries: Stationary	-73.72	0.01
daily	1	fUnitRoots: No Constant	-42.79	0.01
daily	1	fUnitRoots: Constant	-73.51	0.01
daily	1	fUnitRoots: Constant+Trend	-73.72	0.01
weekly	1	tseries: Stationary	-73.72	0.01
weekly	1	fUnitRoots: No Constant	-42.79	0.01
weekly	1	fUnitRoots: Constant	-73.51	0.01
weekly	1	fUnitRoots: Constant+Trend	-73.72	0.01
monthly	1	tseries: Stationary	-73.72	0.01
monthly	1	fUnitRoots: No Constant	-42.79	0.01
monthly	1	fUnitRoots: Constant	-73.51	0.01
monthly	1	fUnitRoots: Constant+Trend	-73.72	0.01
yearly	1	tseries: Stationary	-73.72	0.01
yearly	1	fUnitRoots: No Constant	-42.79	0.01
yearly	1	fUnitRoots: Constant	-73.51	0.01
yearly	1	fUnitRoots: Constant+Trend	-73.72	0.01

Table 6-2 Stationarity Test Results for Observed Hourly Wind Speeds (lag=2 hour)

Frequency	Lag	Test Type	Statistic	P value
daily	2	tseries: Stationary	-76.13	0.01
daily	2	fUnitRoots: No Constant	-43.21	0.01
daily	2	fUnitRoots: Constant	-75.91	0.01
daily	2	fUnitRoots: Constant+Trend	-76.13	0.01
weekly	2	tseries: Stationary	-76.13	0.01
weekly	2	fUnitRoots: No Constant	-43.21	0.01
weekly	2	fUnitRoots: Constant	-75.91	0.01
weekly	2	fUnitRoots: Constant+Trend	-76.13	0.01
monthly	2	tseries: Stationary	-76.13	0.01
monthly	2	fUnitRoots: No Constant	-43.21	0.01
monthly	2	fUnitRoots: Constant	-75.91	0.01
monthly	2	fUnitRoots: Constant+Trend	-76.13	0.01
yearly	2	tseries: Stationary	-76.13	0.01
yearly	2	fUnitRoots: No Constant	-43.21	0.01
yearly	2	fUnitRoots: Constant	-75.91	0.01
yearly	2	fUnitRoots: Constant+Trend	-76.13	0.01

Table 6-3 Stationarity Test Results for Observed Hourly Wind Speeds (lag=2 hour)

Frequency	Lag	Test Type	Statistic	P value
daily	3	tseries: Stationary	-80.81	0.01
daily	3	fUnitRoots: No Constant	-44.69	0.01
daily	3	fUnitRoots: Constant	-80.55	0.01
daily	3	fUnitRoots: Constant+Trend	-80.81	0.01
weekly	3	tseries: Stationary	-80.81	0.01
weekly	3	fUnitRoots: No Constant	-44.69	0.01
weekly	3	fUnitRoots: Constant	-80.55	0.01
weekly	3	fUnitRoots: Constant+Trend	-80.81	0.01
monthly	3	tseries: Stationary	-80.81	0.01
monthly	3	fUnitRoots: No Constant	-44.69	0.01
monthly	3	fUnitRoots: Constant	-80.55	0.01
monthly	3	fUnitRoots: Constant+Trend	-80.81	0.01
yearly	3	tseries: Stationary	-80.81	0.01
yearly	3	fUnitRoots: No Constant	-44.69	0.01
yearly	3	fUnitRoots: Constant	-80.55	0.01
yearly	3	fUnitRoots: Constant+Trend	-80.81	0.01

Table 6-4 Stationarity Test Results for Observed Hourly Wind Speeds (lag=4 hour)

Frequency	Lag	Test Type	Statistic	P value
daily	4	tseries: Stationary	-83.64	0.01
daily	4	fUnitRoots: No Constant	-44.97	0.01
daily	4	fUnitRoots: Constant	-83.36	0.01
daily	4	fUnitRoots: Constant+Trend	-83.64	0.01
weekly	4	tseries: Stationary	-83.64	0.01
weekly	4	fUnitRoots: No Constant	-44.97	0.01
weekly	4	fUnitRoots: Constant	-83.36	0.01
weekly	4	fUnitRoots: Constant+Trend	-83.64	0.01
monthly	4	tseries: Stationary	-83.64	0.01
monthly	4	fUnitRoots: No Constant	-44.97	0.01
monthly	4	fUnitRoots: Constant	-83.36	0.01
monthly	4	fUnitRoots: Constant+Trend	-83.64	0.01
yearly	4	tseries: Stationary	-83.64	0.01
yearly	4	fUnitRoots: No Constant	-44.97	0.01
yearly	4	fUnitRoots: Constant	-83.36	0.01
yearly	4	fUnitRoots: Constant+Trend	-83.64	0.01

Table 6-5 Stationarity Test Results for Observed Hourly Wind Speeds (lag=5 hour)

Frequency	Lag	Test Type	Statistic	P value
daily	5	tseries: Stationary	-85.14	0.01
daily	5	fUnitRoots: No Constant	-44.43	0.01
daily	5	fUnitRoots: Constant	-84.82	0.01
daily	5	fUnitRoots: Constant+Trend	-85.14	0.01
weekly	5	tseries: Stationary	-85.14	0.01
weekly	5	fUnitRoots: No Constant	-44.43	0.01
weekly	5	fUnitRoots: Constant	-84.82	0.01
weekly	5	fUnitRoots: Constant+Trend	-85.14	0.01
monthly	5	tseries: Stationary	-85.14	0.01
monthly	5	fUnitRoots: No Constant	-44.43	0.01
monthly	5	fUnitRoots: Constant	-84.82	0.01
monthly	5	fUnitRoots: Constant+Trend	-85.14	0.01
yearly	5	tseries: Stationary	-85.14	0.01
yearly	5	fUnitRoots: No Constant	-44.43	0.01
yearly	5	fUnitRoots: Constant	-84.82	0.01
yearly	5	fUnitRoots: Constant+Trend	-85.14	0.01

Table 6-6 Stationarity Test Results for Observed Hourly Wind Speeds (lag=6 hour)

Frequency	Lag	Test Type	Statistic	P value
daily	6	tseries: Stationary	-84.41	0.01
daily	6	fUnitRoots: No Constant	-42.74	0.01
daily	6	fUnitRoots: Constant	-84.07	0.01
daily	6	fUnitRoots: Constant+Trend	-84.41	0.01
weekly	6	tseries: Stationary	-84.41	0.01
weekly	6	fUnitRoots: No Constant	-42.74	0.01
weekly	6	fUnitRoots: Constant	-84.07	0.01
weekly	6	fUnitRoots: Constant+Trend	-84.41	0.01
monthly	6	tseries: Stationary	-84.41	0.01
monthly	6	fUnitRoots: No Constant	-42.74	0.01
monthly	6	fUnitRoots: Constant	-84.07	0.01
monthly	6	fUnitRoots: Constant+Trend	-84.41	0.01
yearly	6	tseries: Stationary	-84.41	0.01
yearly	6	fUnitRoots: No Constant	-42.74	0.01
yearly	6	fUnitRoots: Constant	-84.07	0.01
yearly	6	fUnitRoots: Constant+Trend	-84.41	0.01